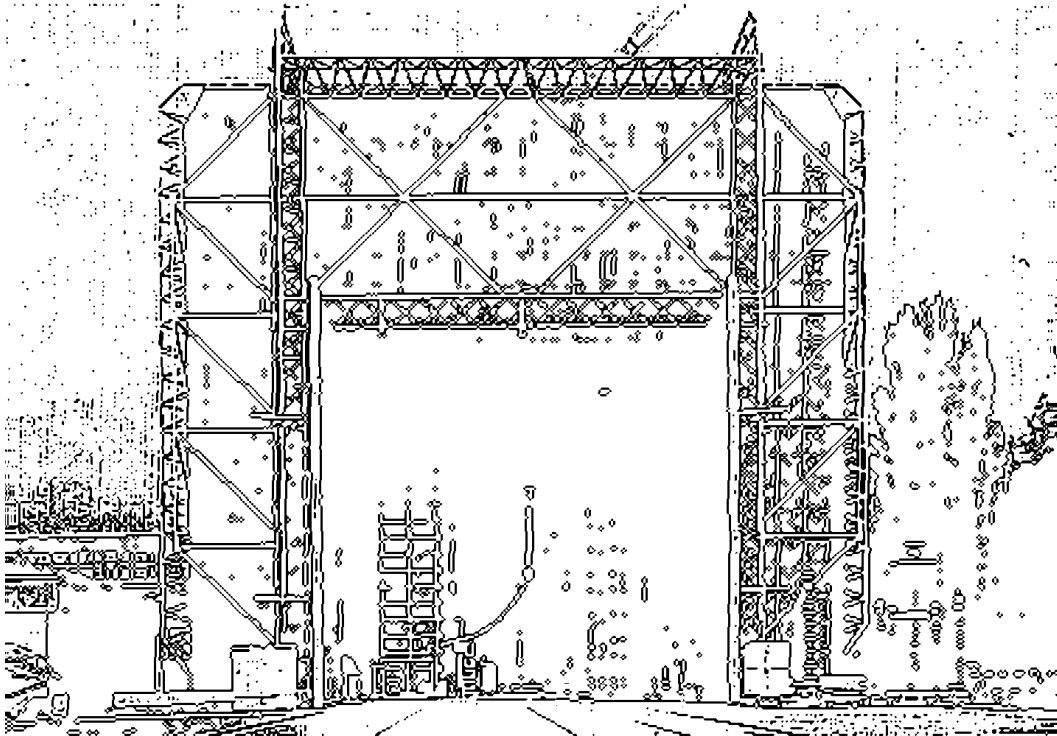


TECHNISCHE UNIVERSITÄT GRAZ

DISSERTATION



INSTITUT FÜR HOCHSPANNUNGSTECHNIK
UND SYSTEMMANAGEMENT

PARTIAL DISCHARGE INCEPTION VOLTAGE CHARACTERISTICS OF MINERAL OIL

Dissertation

zur Erlangung des Grades eines
Doktors der technischen Wissenschaften

von

M.Eng. Norasage Pattanadech

1. Begutachter: Em.-Prof. Dipl.-Ing. Dr. techn. Dr. h.c. Michael Muhr
2. Begutachter: Prof. Dr. Rainer Haller, University of West Bohemia in Pilsen, Czech Republic

**Institut für Hochspannungstechnik und Systemmanagement
Technische Universität Graz**

Partial discharge inception voltage characteristics of mineral oil
Teilentladungs-Einsatzspannung in Mineralöl

Important Note: Measurement data and results are basically valid for the investigated samples only. Due to possible variability in the material composition and sample preparation process, materials can differ strongly from the ones tested within this work.

Abstract

Partial discharge (PD) testing and analysis is one of the most widely useful tools applied for evaluating of the integrity of insulation. Partial discharge inception voltage (PDIV) measurement is always performed with PD testing. However, the conception of PDIV and PD especially for liquid insulation is not understood distinctly. In 1993, IEC has issued PDIV test procedure for insulating liquids experimented by using the needle - sphere electrode. This standard has been questioned about the sensitivity and validity of the test results. Therefore, an in-depth knowledge of PDIV and PD for the dielectric liquids has to be researched and developed consistently. The scope of this research, the electrode configurations and mineral oil conditions which affect the PDIV value were investigated. Moreover, the influence of PDIV test methods on PDIV value was also examined. SEM and EDX test techniques were utilized to analyze the erosion of the tested electrodes. Then, an alternative electrode for PDIV test experiment and an alternative PDIV test method have been proposed. Furthermore, the preliminary arcing test for the mineral oil was studied as well. **Various types of electrode configurations** were employed to investigate the effect of electrode configurations on the PDIV value. The 10 μm , 20 μm , and 40 μm tip radius needles with the needle length of 25 mm and 45 mm were used as a high voltage electrode, while the plane electrode with diameter of 50 mm and 75 mm as well as the sphere electrode with the diameter of 12.7 mm, 25.4 mm, 50.8 mm and 76.2 mm were used as a grounded electrode respectively. Mineral oil, Nynas nytro 4000x was used for all research work. The 10 μm tip radius tungsten needle -75 mm dia. brass plane electrode produced the lowest PDIV value compared with other electrode configurations. In addition, PD activity and PD pulse current were measured and analyzed at the PDIV level. **The mineral conditions** with water content 4-40 ppm were experimented under room temperature until 90°C. At room temperature, it was found that the degree of water contents influenced more or less on PDIV values. However, at higher temperatures, the PDIV values of the mineral oil with different water contents were relatively the same. The weakness of PDIV measurement according to IEC was studied. The combine PDIV test procedure was established and verified. The combine PDIV test provided lower PDIV values and also lower charge quantities with lower repetition rate of PD activities. Normal and weibull distributions were used to describe the test data. The 10 μm tip radius tungsten needle - 75 mm dia. brass plane electrode with the gap distance of 50 mm has been proposed as **an alternative electrode for PDIV test experiment** and the PDIV combine test method has been proposed as **an alternative PDIV test method**. The **preliminary arcing test** demonstrated the effect of arcing electrode configurations on arcing voltage and arcing current. Normal and weibull distributions were proved that they can be used to describe the arcing test data. The effect of arcing current density on the arcing by-product was explained. The erosion of arcing rods and plane electrodes was examined. Additionally, the significant degradation of the mineral oil after arcing test such as oil color was clearly observed.

Keywords: Partial discharge inception voltage (PDIV), Partial discharge (PD), mineral oil, arcing test

Kurzfassung

Teilentladungsmessungen (PD - partial discharge) und deren Analyse ist ein nützliches Werkzeug zur Bewertung von Isolationssystemen. Im Rahmen einer TE-Untersuchung wird häufig die TE-Einsatzspannung (PDIV- partial discharge inception voltage) durchgeführt. Allerdings sind noch nicht alle Phänomene der TE-Messung im Zusammenhang mit einem flüssigen Isoliermaterial verstanden und untersucht. Im Jahr 1993 hat IEC ein PDIV Testverfahren für Isolierflüssigkeiten mit einer Nadel-Kugel-Elektrodenanordnung durchgeführt. Die Testergebnisse dieser Norm wurden jedoch bezüglich ihrer Empfindlichkeit und Aussagekraft der Elektrodenanordnung in Frage gestellt. Daher ist eine tiefgreifende Forschung im Bereich der Teilentladungsmessung unumgänglich und sollte konsequent fortgesetzt werden. Im Rahmen dieser Forschungsarbeit wurden **die Auswirkung unterschiedlichen Elektroden-Konfigurationen** sowie **die Auswirkung verschiedener Mineralölbedingungen** (Feuchte, Temperatur) auf die PDIV untersucht. Darüber hinaus wurde der Einfluss von verschiedenen PDIV Testverfahren auf die Höhe des PDIV Wertes untersucht. Zur Analyse der Erosion an den getesteten Elektroden wurden die Testverfahren SEM (Scanning Electron Microscope) und EDX (Energy Dispersive X-Ray) eingesetzt. Im Anschluss wurden eine neue Elektrodenanordnung sowie eine neue Methode zu PDIV-Messung vorgeschlagen. Zusätzlich zu den Teilentladungsuntersuchungen wurden Lichtbogen-Untersuchungen für Stab-Platte-Anordnungen in Mineralöl durchgeführt. Wie erwähnt wurden verschiedene Arten von Elektroden-Anordnungen eingesetzt, um die Auswirkung der Elektroden-Konfigurationen auf der PDIV Wert zu untersuchen. Als Hochspannungselektrode wurden Nadeln mit einem Spitzenradius von 10 µm, 20 µm und 40µm und einer Länge von 25 mm und 45 mm verwendet. Als Erdelektrode wurden zwei ebene Elektroden mit einem Durchmesser von 50 mm und 75 mm verwendet. Zusätzlich wurden Untersuchungen mit Kugelelektroden mit den Durchmessern von 12,7 mm, 25,4 mm, 50,8 mm und 76,2 mm durchgeführt. Für die in dieser Arbeit durchgeführten Untersuchungen wurde das Mineralöl Nynas Nytro 4000X verwendet. Es stellte sich heraus, dass die Spitze-Platte-Anordnung mit einem Spitzenradius von 10 µm und einem Plattendurchmesser von 75 mm die niedrigste TE-Einsatzspannung hatte. Es wurden die TE-Aktivität und der TE-Strom in bezug auf die TE-Einsatzspannung gemessen und analysiert. Untersucht wurden die PDIV und die genannten TE-Eigenschaften bei unterschiedlichen Feuchtwerten (4-40 ppm) und verschiedenen Temperaturen (Raumtemperatur bis 90°C). Es stellte sich heraus, dass der Feuchtegrad des Mineralöles bei Raumtemperatur einen signifikanten Einfluss auf die TE-Einsatzspannung hat. Im Gegensatz dazu ist der Einfluss der Feuchte bei höheren Temperaturen nicht mehr gegeben, hier sind die TE-Einsatzwerte sehr ähnlich. Weiters wurde die PDIV-Messung nach IEC auf ihre Schwächen untersucht. Es wurde eine „Combine Testmethod“ als zweite Testmethode eingeführt und verifiziert. Die „Combine-Testmethod“ lieferte im Vergleich zur Methode nach IEC niedrigere PDIV-Werte sowie eine geringere Ladungshöhen bei weniger TE-Ereignissen. Als **Alternative zur IEC-Elektrodenanordnung** wird **eine Spitze-Platte-Anordnung mit einem Spitzenradius (Wolframnadel) von 10 µm und einer Plattenelektrode mit einem Durchmesser von 75 mm** vorgeschlagen. Weiters wird **die „Combine Testmethod“** **wird als alternative Testmethode** empfohlen. Der Lichtbogentest demonstrierte die Auswirkung von unterschiedlichen Elektrodenanordnungen auf die Lichtbogen Spannung und den Lichtbogenstrom. Der Effekt der Lichtbogenstromdichte und ihr Zusammenhang mit entstehenden Nebenprodukten wurde erklärt. Bei der Analyse der Ergebnisse wurde gezeigt, dass die Normalverteilung und die Weibullverteilung zur Beschreibung der Daten verwendet

werden kann. Weiters wurden die an den Elektroden entstehenden Erosion untersucht. Zusätzlich wurde die durch die Versuche verursachte Zersetzung des Mineralöles genau beobachtet.

Schlüsselwörter: Teilentladungseinsatzspannung, Teilentladung, Mineralöl, Lichtbogentest

EIDESSTATTLICHE ERKLÄRUNG

Ich erkläre an Eides statt, dass ich die vorliegende Arbeit selbstständig verfasst, andere als die angegebenen Quellen/Hilfsmittel nicht benutzt und die den benutzten Quellen wörtlich und inhaltlich entnommenen Stellen als solche kenntlich gemacht habe.

Graz, am ...Dezember 2013...

.....
Norasage Pattanadech

STATUTORY DECLARATION

I declare that I have authored this thesis independently, that I have not used other than the declared sources/ resources and that I have explicitly marked all material which has been quoted either literally or by content from the used sources.

Graz,...December 2013.....

.....
Norasage Pattanadech

Acknowledgement

First of all I would like to express my deepest gratitude to my supervisor, Em.Univ.-Prof. Dipl.-Ing. Dr.techn. Dr.h.c. Michael Muhr for his guidance, encouraging, enthusiasm, and patience. Without his professional support, the achievement of this work would not have been possible. Moreover, I am extremely grateful for Prof. Dr. Rainer Haller for serving as the second supervisor and also for amendments to this thesis.

My appreciation is extended to my colleagues especially Bettina Wieser, DI Julia Podesser, Dipl.-Ing. Dr.techn. Robert Eberhardt for mineral oil preparation and testing guidances and for solving many technical problems during the experiment as well. Mr. Fari Pratomosiwi, Mr. Ahmad Azhari Kemma and Mr. T. Ferdinand Sipahutar for practically performing of some parts of laboratory work. Special thanks go to Dipl.-Ing. Dr.tech Thomas Judendorfer, Dipl.-Ing. Dr.tech Jürgen Fabian, DI Markus Lerchbacher, DI Thomas Berg, DI Angelika Straka, DI Rainer Reischenbacher, DI Andreas Zlodnjak, DI Christian Auer and DI Jürgen Flesch, for providing a greatly work atmosphere.

For PD measurement, I wish to convey my deeply gratitude to Dipl.-Ing. Dr.tech Werner Lick, Dipl.-Ing. Dr.tech. Priv.-Doz. Robert Schwarz, Univ.-Doz. Dipl.-Ing. Dr.tech Christof Sumereder for many helps and numerous invaluable discussion. Furthermore, I would like to thank Ao.Univ.-Prof. Dipl.-Ing. Dr.techn. Rudolf Woschitz for assistance with laboratory equipment and his guidance about arcing test and also continuous helps. Additionally, I wish to express my gratitude to Ao.Univ.-Prof.Dipl.-Ing. Dr.techn. Stephan Pack and Mrs. Karin Wukounig for many supports.

I would like to give special thanks to all staffs in the workshop of high voltage and system management institute, Mr. Anton Schriebl, Mr. Matthias Kainz, Mr. Gerald Muster, and Mr. Markus Rappold.

Special thanks are also given to Asst. Prof. Dr. Onjira Sitthisak, Dr. Preechar Karin Mr.Chakkrapong Chaiburi and Dr. Ming Dong for thesis organization, fruitful discussion especially for thermodynamic aspect of heated mineral oil and so on.

Special thanks for every very beautiful pictures prepared by Mr. Pethai Nimsanong. He supports also for electric field simulation and distribution analysis. I would like to thank all of my students in King Mongkut's Institute of Technology Ladkrabang such as Mr. Punyavee Chaisiri, Mr. Nitthanakorn Suraporn, Mr. Piyapon Tuethong, Mr. Banyat Leelachariyakul and so on. For simulation and calculation programs, I would like to thank computer service center, King Mongkut's Institute of Technology Ladkrabang, Thailand.

Financial support for attending conferences by high voltage and system management institute, Technical Universität Graz and financial support for my scholarship from royal Thai government scholarship, Thailand are also acknowledged. I wish to thank for all of coordinators for my scholarship especially Miss. Pornpit Somwong from coordinating center for Thai government science and technology scholarship students and Mrs. Parichat

Luepaiboolphan from royal Thai embassy Vienna who are always kind and considerate Thai students in Austria. Part of financial support for this project from BAUR company, I wish like to thank Mr. Martin Baur. As a non-native English speaker, I very much appreciated the amendments by Mr. Nicholas Mazza.

My special thanks appertain to Assoc. Prof. Dr. Samruay Sangkasaad for encouraging to deeply study in high voltage engineering.

Finally, my greatest gratitude must go to my parents with their love, greatest motivation and constant supports with enormous patience, this work will be achievement.

Content

1	Introduction	1
2	The objectives and outline of this dissertation	2
2.1	Purposes of this study.....	2
2.2	Outcomes of this dissertation.....	2
2.3	Outline of this dissertation.....	3
3	Overviews of mineral oils	4
3.1	Insulation: a backbone of transformers for supporting the modern society.....	4
3.2	Mineral oil: one of an irreplaceable insulation system of power transformers for the next few ten years.....	6
3.3	Mineral oil testing and investigation.....	8
3.4	State of research on PDIV in liquid insulation under AC voltage and arcing test of the mineral oils.....	9
4	Theory	11
4.1	Mineral oils.....	11
4.1.1	Mineral oil structure.....	11
4.1.2	Mineral oil characteristics.....	16
4.1.3	Dielectric property of mineral oils.....	20
4.1.4	Factors influence on mineral oil characteristics.....	29
4.1.5	Mineral oil testing.....	37
4.2	Partial discharge in mineral oils.....	41
4.2.1	PD definition.....	41
4.2.2	PD in mineral oils.....	41
4.2.3	PD sources in mineral oils.....	44
4.2.4	Predischage or streamer mechanism in mineral oils.....	44
4.2.5	PD measurement techniques.....	49
4.2.6	PD pulse current measurement.....	52
4.3	Partial discharge inception voltage.....	54
4.3.1	PDIV definition.....	55
4.3.2	Partial discharge inception mechanism.....	56
4.3.3	Electrode configuration for PDIV measurement.....	58
4.3.4	PDIV measurement.....	62
4.3.5	Factors influencing PDIV and PD activity.....	63
4.4	Arcing.....	66

4.4.1 Arcing definition	66
4.4.2 Breakdown in mineral oils.....	66
4.4.3 Breakdown testing of mineral oils.....	69
4.4.4 Arcing in mineral oils.....	71
4.4.5 Arcing test	75
4.5 Erosion Analysis	76
4.5.1 Erosion of the electrode used for electrical testing of mineral oils.....	76
4.5.2 Scanning electron microscope and energy dispersive X- ray for erosion analysis	78
4.6 Statistic for test result analysis.....	82
5 Experiment test set up	85
5.1 Electrode systems and test specimen for PDIV experiment	85
5.1.1 Electrode systems for PDIV experiment	85
5.1.2 Test cells for PDIV experiment	88
5.1.3 Mineral oil preparation for PDIV experiment	90
5.2 PDIV test set up	92
5.2.1 Test circuit for PDIV measurement.....	92
5.2.2 Test circuit for PDIV experiment with different PDIV test circuits	93
5.3 Electrode systems and test specimen for arcing experiment.....	94
5.3.1 Electrode systems for arcing experiment	94
5.3.2 Mineral oil preparation for arcing experiment	95
5.4 Arcing test circuit set up	96
5.5 SEM and EDX analysis.....	97
5.6 Electric field simulation	97
6 Experiment test procedure	99
6.1 PDIV test procedure.....	99
6.1.1 PDIV standard test method (M1): IEC test method	99
6.1.2 Combine PDIV test method with 100 pC charge detection (M2 and M3).....	100
6.1.3 Combine PDIV test method with the first PD pulse current detection (M4 and M5)	101
6.1.4 Up and down PDIV test method with 100 pC charge detection (M6)	102
6.2 PD activity measurement	103
6.3 PD pulse current measurement.....	103
6.4 Arcing test procedure	103
7 Test results	105
7.1 Electric field simulation	105
7.1.1 Electric field patterns of the electrode systems with different tip radius needles for preliminary PDIV test.....	105
7.1.2 Electric field patterns of the electrode systems with different tip radius needles and different grounded electrode types and dimensions	106

7.1.3 Electric field patterns of the electrode systems with different needle lengths	109
7.1.4 Electric field patterns of the electrode systems with different tip diameter rods and different gap distances	111
7.2 PDIV characteristics of the mineral oil	113
7.2.1 Preliminary PDIV experiment	113
7.2.2 Effect of PDIV test methods on PDIV characteristics	122
7.2.3 Effect of grounded electrodes on PDIV and PD characteristics	128
7.2.4 Effect of needle lengths on PDIV and PD characteristics	142
7.2.5 Effect of water contents and temperatures of the mineral oil on PDIV and PD characteristics	150
7.2.6 Effect of PDIV test circuits on PDIV and PD characteristics	160
7.3 Breakdown voltage characteristic of the mineral oil	164
7.4 PD pulse current	165
7.4.1 PD pulse train characteristics from preliminary PDIV test	165
7.4.2 PD pulse characteristics	166
7.5 Preliminary arcing experiment	174
7.5.1 Arcing voltage and arcing current experiment	174
7.5.2 Arcing current pulse train	177
7.5.3 Physical appearance of the mineral oil after arcing test	180
7.6 SEM and EDX experiment	182
7.6.1 SEM and EDX analysis for PDIV electrode systems	182
7.6.2 SEM and EDX analysis for arcing electrode systems	186
8 Discussion and Conclusion	192

8.1 Effect of electrode configuration on PDIV and PD characteristics of the mineral oil	192
8.2 PD and breakdown mechanism of the mineral oil under PDIV test according to IEC 61294 tested by a needle-plane and a needle-sphere electrode	193
8.3 PDIV and breakdown voltage relationship of the mineral oil tested by the needle-plane electrodes	198
8.4 Effect of PDIV test methods on PDIV characteristics of the mineral oil	202
8.5 Effect of needle lengths on PDIV and PD characteristics of the mineral oil	202
8.6 Effect of water contents and temperatures on PDIV and PD characteristics of the mineral oil	203
8.7 PD pulse current behaviors of the mineral oil under PDIV experiment	205
8.8 Effect of electrode configurations on arcing test characteristic of the mineral oil	206
8.9 SEM and EDX analysis	206
8.10 Conclusion	207
8.11 Resumee	210

9	Summary	212
9.1	Summary	212
9.2	Further research recommendation	214
	List of Figures	215
	List of Tables	224
	References	227
	Appendices	244
A	List of publications	244
B	Investigated material.....	246
C	High water content mineral oil preparation.....	247
D	Temperature control of the mineral oil.....	249
E	Summarized lists of equipment.....	251

Glossary

PD	Partial Discharge
PDIV	Partial Discharge Inception Voltage
CIGRE'	Conseil International des Grands Réseaux Électriques
AC	Alternating Current
IEC	International Electrotechnical Commission
SEM	Scanning Electron Microscope
EDX	Energy Dispersive X-Ray
OECD	Organization for Economic Co-operation and Development
IEO	Independent Evaluation Office
DGA	Dissolved Gas Analysis
PCB	Polychlorinated Biphenyls
DDF	Dielectric Dissipation Factor
DC	Direct Current
DBDS	Dibenzyl Disulphide
ASTM	American Society for Testing and Materials
VDE	Verband der Elektrotechnik
ISO	International Organization for Standardization
FEM	Finite Element Method
BD	Breakdown Voltage
PDF	Probability Density Function
CDF	Cumulative Density Function
IEEE	Institute of Electrical and Electronics Engineers
EDS	Energy Dispersive Spectroscopy
SE	Secondary Electron
BSE	Backscattered Electron
AD	Anderson-Darling statistic

Symbols and constants

D	Electric flux density (C/m ²)
E	Electric field strength (V/m)
ε	Permittivity (F/m)
ε_0	Permittivity of free space = 8.854×10^{-12} F/m
ε_r	Relative permittivity (dimensionless)
C	Capacitance (F)
C_0	Capacitance with vacuum as the dielectric (F)
P	Polarization (C/m ²)
χ	Dielectric susceptibility (dimensionless)
ε'_r	Real part of the complex permittivity (dimensionless)
ε''_r	Imaginary part of the complex permittivity (dimensionless)
I, i	Electric current (A)
V, v	Electric potential (V)
I_r	A resistive component current (A)
I_c	A capacitive component current (A)
ω	Angular velocity (rad/s)
$\tan \delta$	Dielectric loss (dimensionless)
σ	Conductivity ($\Omega \cdot m$) ⁻¹
ρ	Resistivity ($\Omega \cdot m$)
J	Current density (A/m ²)
Q, q	Charge (C)
N	Concentration of charge carrier (kg/m ³)
μ_m	Ionic mobility (C/Pm)
η	Viscosity (P)

r_0	Radius of ion (m)
N_+	Concentration of positive ion (kg/m ³)
N_-	Concentration of negative ion (kg/m ³)
μ_{m+}	Mobility of positive ion (C/Pm)
μ_{m-}	Mobility of negative ion (C/Pm)
W_s	Solubility of water in oil (mg/kg)
T	Temperature (Kelvin)
W_{abs}	Absolute water content (mg/kg)
$W_{rel}(\%)$	Relative water content (dimensionless)
D_{rel}	Relative oil dissolved air density (dimensionless)
V_{25}	Percent gas solubility (by volume) under standard condition 25°C
V_t	Percent gas solubility (by volume) under test condition
r	Radius of curvature at the apex of needle (μm)
a	Distance between the middle point of the needle tip and the plane electrode (mm)
g	Gap distance of the electrode (mm)
F_e	Force between plate electrodes (N)
ϵ_{liq}	Relative permittivity of liquid (dimensionless)
r_p	Particle radius (m)
ϵ_p	Relative permittivity of particle (dimensionless)
E_0	Electric field in liquid in the absence of the bubble (V/m)
E_b	Electric field in a spherical gas bubble (V/m)
V_p	Critical applied voltage (kV)
H	Hardness (kg/cm ²)

U_{PDIV}	Mean value partial discharge inception voltage (kV)
σ_u	Voltage standard deviation (kV)
Q_{IEC}	Average apparent charge, PD charge (pC)
I_p	Peak current (mA)
U_{ARC}	Mean value arcing voltage (kV)
I_{ARC}	Mean value arcing current (mA)
σ_i	Current standard deviation (mA)
J_{ARC}	Mean value arcing current density (A/cm^2)

1 Introduction

Mineral oil is one of the most important dielectric liquids used for high voltage equipment especially transformers. The mineral oil has been used since the first commercial liquid-insulated transformer was produced [1]. Currently, alternative dielectric fluids are widely used in a variety of transformer applications. However, the mineral oil still plays an important role for an insulation for high voltage apparatus especially for power transformers and instrument transformers [2]. Transformers are expected to reliably and efficiently operate for about 40 years. The reliability and efficiency of using transformer strongly depend on the integrity of an insulation system especially mineral oil and cellulose. In addition, life of the insulation system often coincides with life of the electrical apparatus hosting the system [3]. To assure that the insulation operates in good conditions, their quality has to be monitored and examined regularly. Many test techniques for oil and cellulose verifying have been developed and proved for many ten years. Partial discharge(PD) testing and analysis are accepted as one of powerful tools to aid assessment of insulation condition of high voltage apparatus [4]. The existence or increment of the PD activity is the signal of the beginning state of the dielectric degradation [5]. Moreover, partial discharge inception voltage (PDIV) is an alternatively important indicator for representing the integrity of the insulation. PDIV test results may be used to describe the insulating liquid characteristic subjected to locally high electric field stress. PDIV value of insulating liquids can be applied for quality control, product development, condition monitoring and so on. Currently, only the standard IEC 61294 is available for PDIV measurement of liquid insulations. However, there are still some questions about the validity and sensitivity of this PDIV measurement technique [6]. Unfortunately, there is lack of study for PDIV measurement for dielectric liquids under AC voltage especially for the mineral oil. There are few research groups who research on PDIV, however, the cross comparison among results from different research groups is a difficult task to perform as reported by CIGRÉ [2]. In addition, the findings and conclusions of many research groups focusing on liquid insulations cannot be reconciled and also produce a general theory for liquid dielectrics [7]. Therefore, the knowledge of PDIV of liquid insulation is still obscure.

This research work was designed to study the PDIV characteristics of the mineral oil tested by the needle - plane electrode systems and to preliminary study of arcing test of the mineral oil. Mineral oil with various oil conditions was investigated under AC voltage with different kinds of electrode configurations. A conventional PD test technique as well as a nonconventional PD measurement of the mineral oil was performed. The results will provide a better understanding of PDIV, PD and arcing characteristics of the mineral oil. Moreover, the finding will suggest an alternative electrode system with an alternative PDIV measurement technique for the mineral oil characteristic testing.

2 The objectives and outline of this dissertation

2.1 Purposes of this study

The purposes of this study are as follows:

- investigating PDIV and PD characteristics of the mineral oil tested by various electrode systems,
- examining the possibility of using the needle - plane electrode systems for PDIV measurement of the mineral oil,
- introducing a new electrode configuration for PDIV measurement of the mineral oil,
- investigating the influence of PDIV test methods on PDIV value measured by the needle - plane electrode configuration,
- investigating the influence of mineral oil conditions on PDIV value tested by the needle - plane electrode configuration,
- studying PD characteristics of mineral oil measured by both a conventional PD measurement technique (IEC 60270) and a nonconventional PD measurement technique (PD pulse current measurement),
- investigating the preliminary arcing test for the mineral oil.

2.2 Outcomes of this dissertation

The results of this study will provide as following:

- enhancement the knowledge of PDIV and PD characteristics of the mineral oil with various oil conditions tested by a needle - plane and a needle - sphere electrode configuration,

-
- a better understanding of PDIV and PD measurement techniques of the mineral oil,
 - a new electrode configuration for PDIV measurement of the mineral oil which will be proposed as an alternative PDIV measuring system,
 - elevating the knowledge of the arcing phenomena and it will be the fundamental information for the further research of arcing in the mineral oil.

2.3 Outline of this dissertation

This dissertation is composed of 9 chapters. After gives an introduction in **chapter 1** and the objectives as well as the outline of this dissertation in **chapter 2**,

Chapter 3 provides the overviews of mineral oils.

Chapter 4 dedicates to the basics principles of mineral oils, the background of PD and PDIV as well as arcing test of mineral oils. Basic knowledge for scanning electron microscopic (SEM) and energy dispersive X - ray (EDX) are also introduced in this chapter.

In **chapter 5** the experiment test set up for PDIV, PD and arcing test are described.

The test experiment procedures are delineated in **chapter 6**.

The experiment results are illustrated in **chapter 7** and discussed as well as concluded in **chapter 8**.

Finally summarizes and recommended topics of further research are depicted in **chapter 9**.

3 Overviews of mineral oils

3.1 Insulation: a backbone of transformers for supporting the modern society

A Transformer is one of the key elements in the electrical power system. Transformers transfer electrical energy from the generating plant to the customer. These transformers play more and more important roles in the transmission grid for support the continually increase energy demand, including electrical energy of the modern society as can be seen in Fig. 3.1 [8]. By 2040, it is estimated that global electricity demand will be about 80 percent higher than today [9]. Generally, transformers consist of two or more insulated windings on a common iron core. The construction of the transformer depends upon the application. Technology for design and production of transformers have been continually developed as reported in [10]. The choices of material selection for transformer producing rely strongly on the advancement of the material innovation. Up to now, the oil–cellulose system is an irreplaceable insulation system for the transformer industries especially for the power transformers.

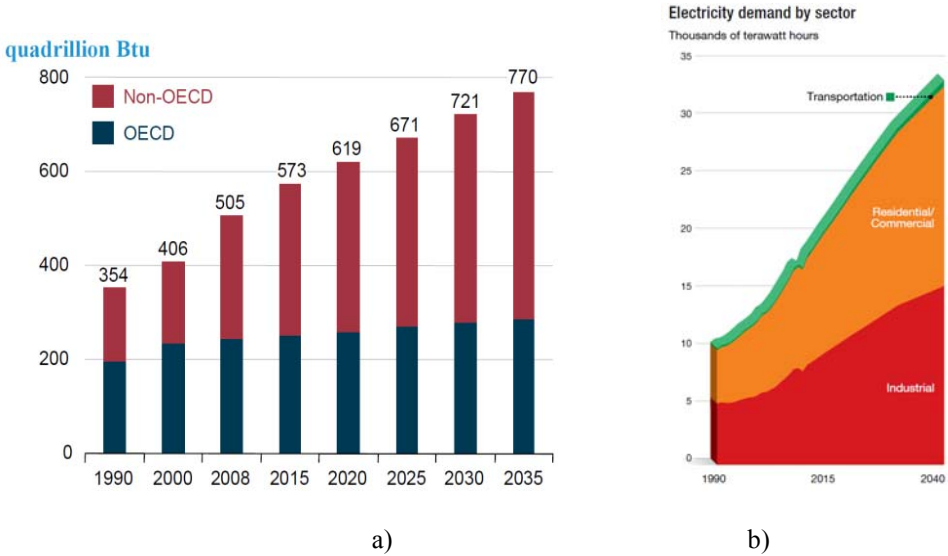


Figure 3.1: Energy and electrical consumptions for the next twenty years

a) world energy consumption 1990- 2035[adapted from [8]] b) Electricity demand by sector 1990-2040 [adapted from [9]]

Note: Current OECD member countries (as of September 1, 2010) are the United States, Canada, Mexico, Austria, Belgium, Chile, Czech Republic, Denmark, Finland, France, Germany, Greece, Hungary, Iceland, Ireland, Italy, Luxembourg, the Netherlands, Norway, Poland, Portugal, Slovakia, Slovenia, Spain, Sweden, Switzerland, Turkey, the United Kingdom, Japan, South Korea, Australia, and New Zealand. Israel became a member on September 7, 2010, and Estonia became a member on December 9, 2010, but neither country's membership is reflected in IEO 2011.

Transformers are generally very reliable equipment with expected service lives of 40 years or more [11]. However, it is very difficult to avoid the failure of transformers especially for the transformers operating for a certain duration. The statistical failure of the transformers and failure types of the power transformers illustrate in Fig. 3.2. The malfunction of transformers may lead to the power shortage or power blackout which may strongly impact on the society both social aspect and economic aspect. Examples of power blackout consequence can be found in [12]. Besides, the in-service failure of a transformer is potentially dangerous to utility personnel through explosions and fire. It causes also a potentially damaging to the environment through oil leakage which is costly to repair or replace and may result in significant loss of revenue.

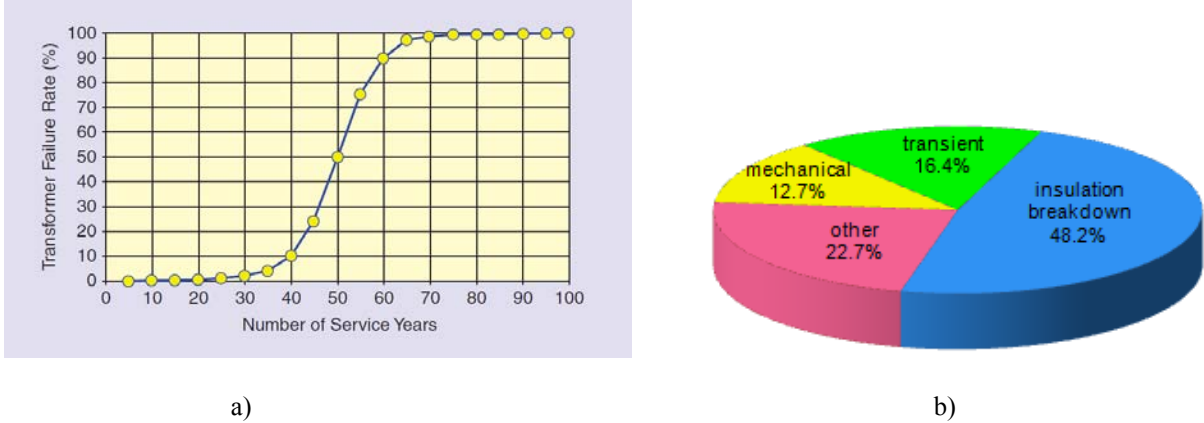


Figure 3.2: Failure causes for transformers

a) failure statistic of the transformers [adated from [13]] b) failure initiating causes for power transformers (1979 survey) [adapted from [14]]

From the failure statistic, it confirms that to keep the availability of the transformers, the insulation system needs to be monitored and performed maintenance. Currently, a large number of tests can be applied to examine the characteristics of insulation for the transformers. Each technique gives information about the condition of separate components or subcomponents of the transformers. To select the test methods for examining the insulation system, the selected test experiments should provide the information directly about the insulation used under the practical conditions. The testing engineers should deeply understand the details before applying the testing techniques or standards.

3.2 Mineral oil: one of an irreplaceable insulation system of power transformers for the next few ten years

Considering the power transformer insulations, the cellulose and mineral oil are the predominant insulation due to the high reliability, reasonable life time if good maintenance and relatively low price compared with other insulation systems. Cellulose is used in various forms as a solid insulation material. Insulation made from pure kraft cellulose provides outstanding oil impregnation characteristics, thus excellent performance in electric fields and has good geometric stability in oil [15]. Without suitable oil-cellulose impregnated process, which is elaborate and time consuming, cellulose materials are not much good dielectric. This is due to their hygroscopic characteristic. Furthermore, the excellent cooling characteristic of the mineral oil is required to maintain the possible low temperature in the transformers. Operating the transformer at higher temperatures is not a preferred condition for the cellulose material as well as the liquid insulation. The life time of the transformer will decrease drastically when the transformer is run over the specified temperature. Celluloses, including paper and pressboard are functioning as barrier systems in order to subdivide the oil channels into a narrow gap. This insulation construction can prevent the triggering of discharge which improves the dielectric strength of the insulating liquid. This construction also provides a good mechanical property to withstand mechanic force, especially from surge or short circuit inside the transformer. Cellulose materials should provide high dielectric strength, good dielectric and mechanic properties, low power factor and dielectric constant as well as excellent oil absorption [16].

Mineral oils provide a high breakdown strength, an excellent cooling material including an ability of arc extinguishing and self-healing. Recently, alternative liquids have been introduced. They give the chance for biodegradation and higher fire and flammable points. However, it needs a huge effort and time to prove the insulation integrity characteristics and the compatibility of alternative liquids with cellulose material and other metal parts inside the transformers. Many test procedures and diagnosis techniques have been developed for verifying these alternative insulating liquids. Fortunately, some testing and diagnosis techniques can be adapted from that of mineral oil test techniques. The application of alternative liquids compared with that of mineral oils for a variety of transformer types is shown in Table 3.1. Another important point for using alternative oils is cost – effectiveness. It has been reported that the cost of a 3 phase, 50 kVA, 11 kV/430 volt transformer using the ester liquid (Midel 7131) was approximately five times higher than using the BS 148 mineral oil as insulating material. The price of Midel 7131 and BS 148 mineral oil per liter was 1.88 pound and 0.32 pound respectively [17]. Moreover, A.C.M. Wilson compared the ratio of oil prices at that time as depicted in Table 3.2. Whereas, the approximately insulating liquid prices in this year (2013) obtained from the transformer factory is 0.9 -1.6 euro/ kilogram for mineral oil, 2.5 - 4.5 euro/ kilogram for natural ester and, 3 - 5 euro/ kilogram for synthetic ester. The oil prices depend on the amount and oil quality e.g. oil with inhibitor or without inhibitor.

Table 3.1: Use of insulating liquids[2]

Transformer type	Mineral oil	Silicone fluid	Synthetic ester	Vegetable oil (natural ester)
Power transformers	A	X	B	B
Traction transformers	A	A	A	X
Distribution transformers	A	A	A	A
Instrument transformers	A	X	X	X

(Symbol: A = Largely used, B = Used but less common, X = Currently not used)

Table 3.2: Relative cost of insulating liquids[18]

Type of liquid	Cost (relative)
Petroleum oils	1
Synthetic hydrocarbons	2-3
Askarels	8
Halogenated hydrocarbons(other than askarel)	10-40
Silicones	10
Organic ester	4-8
Phosphate ester	6

3.3 Mineral oil testing and investigation

The quality of insulation oil plays an important role in the performance of the oil filled transformers which are expected to function reliably and efficiently for many years [19]. To assure that the mineral oil operates in good conditions, the oil quality has to be examined regularly. Concurrently, the good maintenance of the whole transformer insulation needs to be continuously performed.

A large number of tests can be applied to examine the characteristics of the mineral oil used in the electrical equipment, such as the breakdown voltage test, viscosity test, water content measurement and so on. IEC introduces the test lists that are considered sufficient to determine whether the conditions of oil are adequate for continued operation [20]. Selection of the mineral oil test method should provide the information directly about the insulation used under the practical conditions. The testing engineers should deeply understand the details before applying the testing standard.

Furthermore, mineral oil investigation is a crucial task to elevate a better understanding of the transformer insulation integrity. The information obtained from the oil insulation investigation explains not only the oil characteristics, such as breakdown voltage, but the cellulose characteristics, such as the analysis results of furanic compounds also.

Research in mineral oils has been done in different aspects, such as:

- mineral oil and mineral oil- cellulose degradation as reported in [21-25],
- Dissolved gas analysis (DGA) and artificial techniques applied for DGA as reported in [26-29],
- mineral oil characteristics compared with alternative oils as reported in [30-34],
- streamer or prebreakdown mechanism and characteristic as reported in [35-40],
- nano dielectric application for insulation characteristic improvement as reported in [41-47].

Moreover, other aspects about transformer oil characteristics, such as corrosive sulphur and electricification, have been investigated as shown in [48-53].

PD measurement is one of the most important techniques for mineral oil investigation. PD testing and analysis have proven to be the most effective way to evidence the presence of local degradation mechanisms [4]. IEC introduces the PD test technique, conventional PD measurement, for high voltage equipment [54]. In general, PDIV value of the mineral oil can be used to characterize the liquid insulation characteristics especially under high electric field stress. PDIV value also can be used to alarm as the first step of mineral oil degradation.

3.4 State of research on PDIV in liquid insulation under AC voltage and arcing test of the mineral oils

PDIV testing including PD measurement is one of the test techniques used to verify oil characteristics. PDIV test result is used to describe the behavior and the ability of the insulating liquids to prevent or suppress PDs when the liquids are submitted to high electrical stress. PDIV value can be applied for the purpose of quality assurance, specification, product development and condition monitoring of the insulating liquids. Based on the momentary knowledge, PDIV in liquids is considered to be mostly related to their chemistry and relatively little affected by the liquid conditions. Generally, PDIV testing provides some advantages compared to a traditional electrical characteristic testing of liquid dielectrics for example PDIV test is virtually nondestructive test, therefore the PDIV test can be performed a large number of testing on the single sample of the liquids. Moreover, the PDIV testing is easier to perform than breakdown voltage test. IEC 61294 proposes PDIV test technique as one of a test method to examine the insulating liquid characteristics [55]. However, the test results achieved from this PDIV test technique are still questioned about the validity and sensitivity [6,56-58]. Recently, the effort to improve the PD and PDIV measurement in liquid insulation has been discussed and carried out continually. Additionally, new concepts for PDIV measurement of the insulation liquids have been proposed as in [2,59-60]. However, the PDIV research topic including other relevant topics is strongly needed to profoundly and steadily investigate. Unfortunately, there is lack of study for PDIV measurement for dielectric liquids especially for the mineral oils. Much work has been done towards understanding the prebreakdown or PD phenomena in liquids under impulse voltages because there are more convenient experimental conditions for their observation. In other word; the prebreakdown mechanism of liquid dielectrics under AC field is difficult to research, therefore some aspects of prebreakdown phenomena still fails to explain[61]. In general, the findings and conclusions of many research groups cannot be reconciled and so produce a general theory applicable to liquids, as the independent data are at variance and sometimes contradictory [7]. Moreover, there is also lack of research for arcing test of the mineral oils. The state of PDIV in liquid research and arcing test investigation under AC field, up to now, can be concluded as following:

1. A lack of PDIV under AC voltage research work includes the arcing test of the mineral oil. Therefore, this research work focuses on the PDIV measurement of the mineral oil under AC voltage and the preliminary arcing test. This work concentrates only on the investigations of the PDIV of the mineral oil experimented with various needle tip radii, 10 μ m, 20 μ m, and 40 μ m as high voltage electrode and various kind of plane and sphere electrodes as the grounded electrode with the plane diameter of 50 and 75 mm and the sphere diameter of 12.7 mm, 25.4 mm, 50.8 mm, and 76.2 mm respectively. In addition, the PDIV of the mineral oil with different water contents and temperatures are also investigated. Furthermore, the arcing phenomena under rod-plane electrodes are introduced in this work.
2. The validity of IEC standard for PDIV measurement method including the definition of PDIV [6,56-58,62].
3. The requirement of a new electrode system which can give more sensitivity than the needle-sphere electrode configuration [59].

-
4. Even though, some groups have been researching on PDIV, the cross comparison among results from different research groups is a difficult task to perform due to the following reasons [2]:
 - Needle tip radii are varying without any accurate specification, from 3 μm to 100 μm mentioned by CIGRÉ [2], however, the smaller tip radius needles such as 2 μm tip radius and smaller sizes had been used to investigated PDIV such reported in [63].
 - Various oil gap distances are used, from 20 mm to 50 mm mentioned also by CIGRÉ [2], nevertheless, for the smaller gap distances such as 15 mm have been researched[58].
 - Two types of electrode systems, needle - plane or needle - sphere electrode configuration, make the field distribution varying across the gap [2].
 - The maximum PD value which is defined as the condition of PDIV existence, from 10 pC to 100pC [2]. Besides, Pompili et al. had compared the PDIV values obtained from different PDIV definitions which the maximum amplitude of PD was between 20 pC - 200 pC [58].
 - Different definitions of PDIV and PDIV test methods. It is obviously that PDIV strongly depends on the PDIV definition and PDIV test method [6,64].
 5. No experiment results were reported on some important parameters such as the erosion of the needle after using for PDIV test under AC field. Furthermore, the degradation of the mineral oils after PDIV testing is still unknown.

This research work was designed to study the PDIV of the mineral oil tested by the needle - plane electrode system compared with other electrode configurations. Moreover, the influence of mineral oil conditions was also investigated. Furthermore, the possibility to use the needle - plane electrode systems for PDIV measurement of mineral oil tested by a conventional and nonconventional PD test techniques was evaluated. Additionally, the preliminary arcing test of the mineral oil was carried out. The results will provide a better understanding of PDIV, PD and arcing characteristics of the mineral oil and also give an alternative PDIV measurement technique with a new electrode configuration.

4 Theory

This chapter describes the basic knowledge of mineral oils. The overviews of PD, PDIV and arcing test of the mineral oils including the fundamental knowledge of SEM and EDX analysis are provided in this chapter.

4.1 Mineral oils

4.1.1 Mineral oil structure

Mineral oils are complex mixtures of hydrocarbons either occurring naturally or derived from crude oils. Basically, mineral oils consist of paraffins, naphthenes, aromatic compound and a small amount of olefins. Furthermore, small quantities of organic compounds such as sulfur, nitrogen and oxygen which are present in the mineral oils are also important. These atoms which are not carbon or hydrogen in oil molecules are called “heteroatoms” which have an important effect on oil characteristics [1,65-69]. The proportion of the basic constituents of mineral oils is depicted in Table 4.1.

Table 4.1: Mineral oil composition

Component	% of composition [67,70]	General formula	Example of chemical compound
Paraffins	40-60	C_nH_{2n+2} [71-74]	CH_4 (methane) ¹⁾
Naphthenes	30-50	C_nH_{2n} [1, 71-75]	C_3H_6 (cyclopropane)
Aromatics	5-20	C_nH_n [71,76], C_nH_{2n-6} [70,77]	C_6H_6 (benzene) ¹⁾
Olefins	1	C_nH_{2n} [72-75]	C_2H_4 (ethylene) ¹⁾

Note: 1. The general formula of naphthenes and olefins is the same.

2. ¹⁾ means the simplest molecule of these compounds.

4.1.1.1 Paraffins

Paraffins (also known as alkanes or saturated aliphatic hydrocarbon) are saturated hydrocarbons in which their molecules contain the maximum number of hydrogen atoms. Therefore, paraffin molecules cannot be supplemented by other atoms [72]. Paraffins have the general formula C_nH_{2n+2} where n is the number of carbon atoms in the paraffinic molecule and $n \geq 1$. All of carbon atoms in the chain are connected by single covalent bonds [75]. The simplest paraffin molecule is that of methane (CH_4), which is symmetrical and has a dipole moment of zero. Paraffins are either a nonpolar or weakly polar. They are soluble in nonpolar or weakly polar solvents and are insoluble in water and other highly polar solvents [75]. Because of their non-polar molecule characteristic which having fairly weak intermolecular forces, paraffins have relatively low boiling points. The boiling point increases with the increasing of the number of atoms in the hydrocarbon molecules [73]. Moreover, paraffins are stable and quite unreactive at an ordinary condition. At high temperatures they can burn completely in the presence of excess oxygen or air to yield CO_2 or H_2O as products [75]. Basically, paraffin structures can either be straight or branched chain as described below [69].

4.1.1.1.1 N-paraffins

Paraffinic molecular structure which contains continuous or straight - chain is called “normal paraffins”, “n - paraffins” or “n - alkanes”. N - paraffins exhibit smooth and graded variation in physical properties. They are also inert to strong acids, bases and oxidizing agents [75]. N - paraffins form wax on cooling which impedes the oil flow at low temperature [1,66].

4.1.1.1.2 Iso-paraffins

Branched chain paraffins which are saturated hydrocarbons with alkyl substituent or a side branch from the main chain are known as “iso - paraffins” or “iso - alkanes”. These molecule structures are possible when $n \geq 4$ [68, 75]. Generally, a branched chain isomer has a lower boiling point than a straight - chain isomer and the more numerous the branches, the lower its boiling point. Considering butanes which gives a good example to clarify these characteristics, butanes (C_4H_{10}) have two molecular structures which are n - butane and iso - butane. N - butane has four carbons joined in a continuous chain while iso - butane has a branched carbon chain. Boiling and melting characteristics of n- butane and iso - butane are shown in Table 4. 2. The molecular structures of n - paraffin and iso-paraffin are illustrated in Table 4.3.

Table 4.2: N- butane and isobutane characteristic comparison [adapted from [71]]

Butane	Structural formula	Boiling point	Melting point
N -butane	$CH_3CH_2CH_2CH_3$	-0.4 °C	-139 °C
Iso - butane	CH_3CHCH_3 or $(CH_3)_3CH$ CH_3	-10.2 °C	-160.9 °C

4.1.1.2 Naphthenes

Naphthenes (also known as “cycloparaffins”, “cycloalkanes”, or “saturated alicyclic hydrocarbon”) consist of combinations of one or more ring - like structures of five, six or seven rings of singly bonded carbon atoms. Such molecular structures have a possible propensity towards some molecular charges asymmetry. Two or more of these ring structures can be fused together. Naphthenes may have one or more linear or branched alkane chains (alkyl) attached [1]. The general formula of naphthenes is C_nH_{2n} where n is the number of carbon atom in the naphthenic molecule which $n \geq 3$ for rings without substituent groups [75]. The most common naphthenes are methyl-, and dimethyl- substituent cyclopentane and cyclohexane [75]. Naphthenes have great low temperature properties and better solubility than n - paraffins [69]. They are less viscous and do not have the wax type constituent which reduces their fluidity at low temperatures [70]. They have also good gas - absorbing properties [77]. Therefore, naphthenic oils are general preferred to use as dielectrics [70,77]. The molecular structures of naphthenes are delineated in Table 4.3.

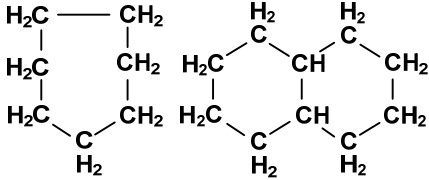
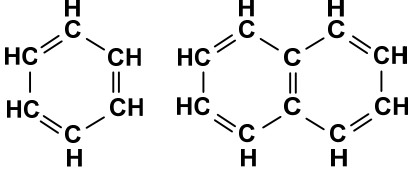

4.1.1.3 Aromatics

Aromatic hydrocarbons (Arenes) are unsaturated cyclic compounds. These compounds contain carbon atoms that can potentially bond to additional atoms [74,75]. Aromatic hydrocarbons contain one or more ring - like structures of carbon atoms, normally six, but with carbon - carbon double bonds. Two or more of these rings may be fused together [1,75]. At least, two different general formulae of aromatic hydrocarbons have been proposed such as C_nH_n in [71,76] and C_nH_{2n-6} in [70,77] where n is the number of carbon atom in the aromatic molecule. The simplest aromatic hydrocarbon is benzene, C_6H_6 [68-75]. Aromatic hydrocarbons may be divided into two forms: the monoaromatic and the polyaromatic hydrocarbons. Aromatic components allow the oil to have a good performance with oxidation (the radicals will be destroyed by production of phenols) and good gas properties due to they have a strong capacity of gas absorption [77]. Aromatic hydrocarbons are generally nonpolar. They are not soluble in water, but can dissolve in organic solvents such as diethyl ether and carbon tetrachloride [68]. The molecular structures of aromatic hydrocarbons are depicted in Table 4.3. The effect of compositions on mineral oil characteristics is represented in Table 4.4.

4.1.1.4 Olefins

Olefins (also called alkenes) are unsaturated hydrocarbons which have the general formula C_nH_{2n} , with $n \geq 2$ where n is the number of carbon atom in the olefinic molecule. The general formula of olefin is the same as naphthene and the simplest molecule of this compound is C_2H_4 (ethylene) [72-75]. Structural isomer of olefins can exist when $n \geq 4$ [75]. Because of containing a single $C=C$ double bond, olefins are highly reactive. Olefins are characterized by their higher reactivity compared to paraffinic hydrocarbons. They can easily react with inexpensive reagents such as water, oxygen, hydrochloric acid, and chlorine to form valuable chemicals [68]. The molecular structures of olefinic hydrocarbons are portrayed in Table 4.3.

Table 4.3: Molecular structures of hydrocarbon components [adapted from [67]]

Component	Example of molecular structure
Paraffins	N- paraffin: $\dots\text{CH}_2-\text{CH}_2-\text{CH}_2-\text{CH}_2-\text{CH}_2\dots$
	Iso-paraffin: $\begin{array}{ccccccc} & & \dots\text{CH}_2 & & & & \\ & & & & & & \\ \dots\text{CH}_2 & - & \text{CH} & - & \text{CH}_2 & - & \text{CH} & - & \text{CH}_2\dots \\ & & & & & & & & \\ & & & & & & \text{CH} & - & \text{CH}_2\dots \\ & & & & & & & & \\ & & & & & & \dots\text{CH}_2 & & \end{array}$
Naphthenes	
Aromatics	
Olefins	$\begin{array}{c} \dots\text{CH}_2-\text{CH}=\text{CH}-\text{CH}-\text{CH}_2\dots \\ \\ \dots\text{CH}_2 \\ \text{CH}_2-\text{CH}=\text{CH}-\text{CH}_2 \\ \quad \quad \quad \quad \quad \\ \text{CH}_2-\text{CH}_2-\text{CH}_2 \end{array}$
<p>Examples of hydrocarbon molecules (ball and stick models)</p> <p>n- butane (C₄H₁₀) isobutane(C₄H₁₀) cyclopropane (C₃H₆) benzene(C₆H₆) ethylene (C₂H₄)</p> 	

Note: a white ball represents a hydrogen atom and a black ball for a carbon atom.

Table 4.4: Effect of compositions on mineral oil properties [adapted from [78]]

Property	N- paraffins	Iso - paraffins	Naphthenes	Aromatics
Viscosity index	Very high	High	Low	Low
Pour point	High	Low	Low	Low
Oxidative stability	Good	Good	Average	Average/poor
Responsible to antioxidants	Good	Good	Good	Some poor
Volatility	Good	Good/average	Average	Poor

4.1.1.5 Mineral oil molecule

In general, the insulating oils contain a certain percentage of paraffinic, naphthenic and aromatic hydrocarbons. However, it is possible that some molecules may be only paraffinic, paraffinic and naphthenic, or paraffinic and aromatic components [1,69]. The amount of the paraffinic, naphthenic, and aromatic constituents in the oil can be designated as percentage of the number of carbon atoms associated with these structures. The molecular structures of mineral oils may be illustrated in Fig. 4.1. The exact shape of the oil molecule is difficult to identified, however, it can be assumed that the molecular structure would tend to be a rather compact quasi - spherical shape with paraffinic chain structures protruding from the main body [1]. This is because the existence of ring structures, both aromatic and naphthenic, in most insulating oils. Because the mineral oil is a very complex mixture of hydrocarbons, their properties may vary significantly from one batch to another. The characteristics of the mineral oil depend strongly on their structures. Basically, the aromatic species have a dominant effect on the chemical behavior of the mineral oil because of their unsaturated compound characteristics. Unfortunately, aromatic components show a greater tendency to form sludge and vanish than paraffinic or naphthenic derivatives. Aromatic components have also a negative effect on impulse breakdown and streaming charging properties. Besides, aromatic hydrocarbons have a higher density than naphthenes and paraffinic hydrocarbons for a given molecular weight. The density and molecular weight of the component affect the thermal conductivity, specific heat and expansion coefficient of the mineral oil. Considering the physical characteristics of the mineral oil, paraffins and naphthenes have some influences on the physical properties due to the large amounts of such components existing in the mineral oil, although these characteristics are also influenced greatly by the aromatic contents [1,18, 78-79].

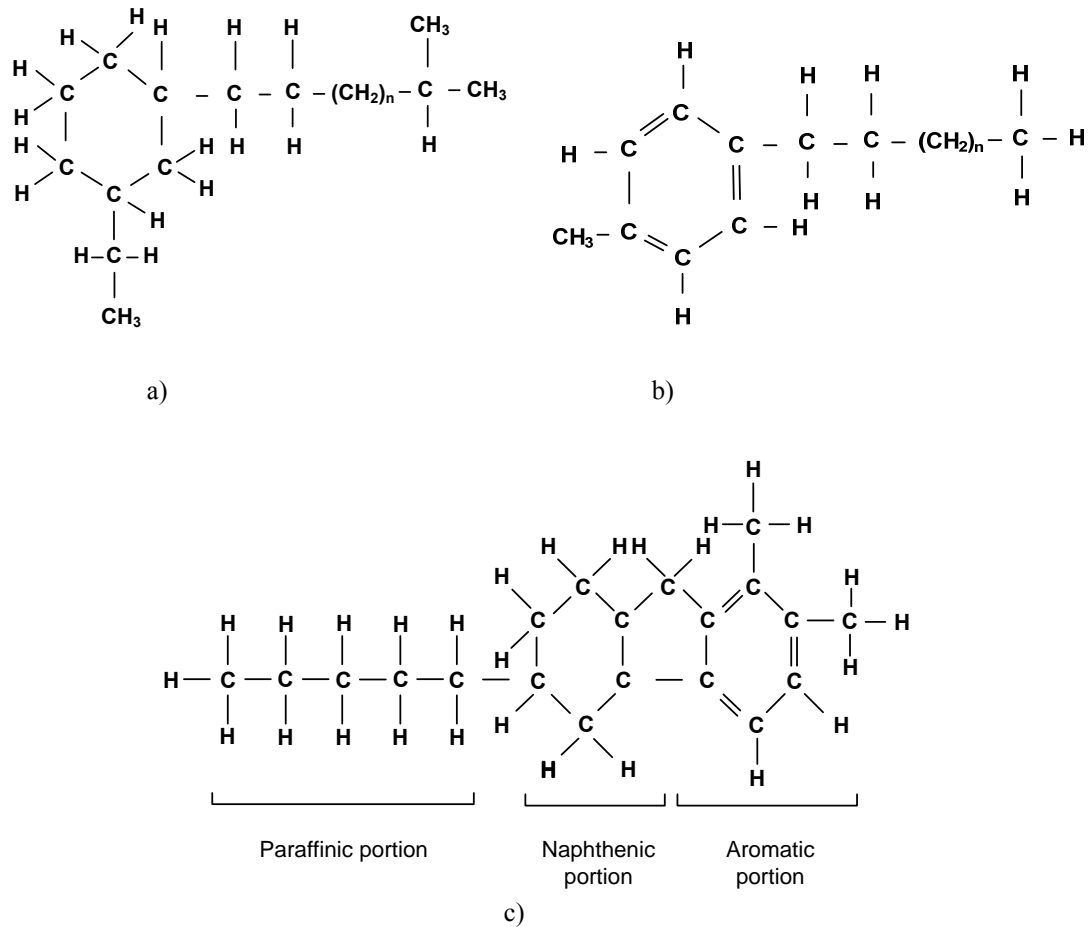


Figure 4.1: A possible molecular structure of the mineral oils

a) cyclohexane with paraffin chains[80] b) aromatics with paraffin chains[80] c) paraffinic, naphthenic and aromatic compound chains[1]

4.1.2 Mineral oil characteristics

Mineral oils or transformer oils have been proposed as a transformer insulating and cooling medium for about 120 years ago. The word “mineral oil” in this dissertation has the same meaning as “transformer oil”. The early transformer oils were paraffinic based oils. However, they were replaced with naphthenic oils because of the high pour point of paraffinic based oils. Then, it was found that the naphthenic oils had a tendency to produce sludge. A lot of efforts, then, devoted to ameliorate the mineral oil characteristics. Besides, a world shortage of required grade naphthenic crude oils was predicted. Generally, naphthenic crude oils have represented only 5% - 10% of the world total production. Therefore, the paraffinic oils are reconsidered and elevated their characteristics [81-82]. Up to now, mineral oil characteristics have been improved dramatically. Fig. 4.2 a) illustrates the mineral oil demand used in a transformer per kV rating of transformer. This picture gives a good explanation about the quality improvement of the mineral oils. The development of mineral oil characteristics is very important to the transformer industries in which the energy output of the transformers continuously growing as shown in Fig. 4.2 b).

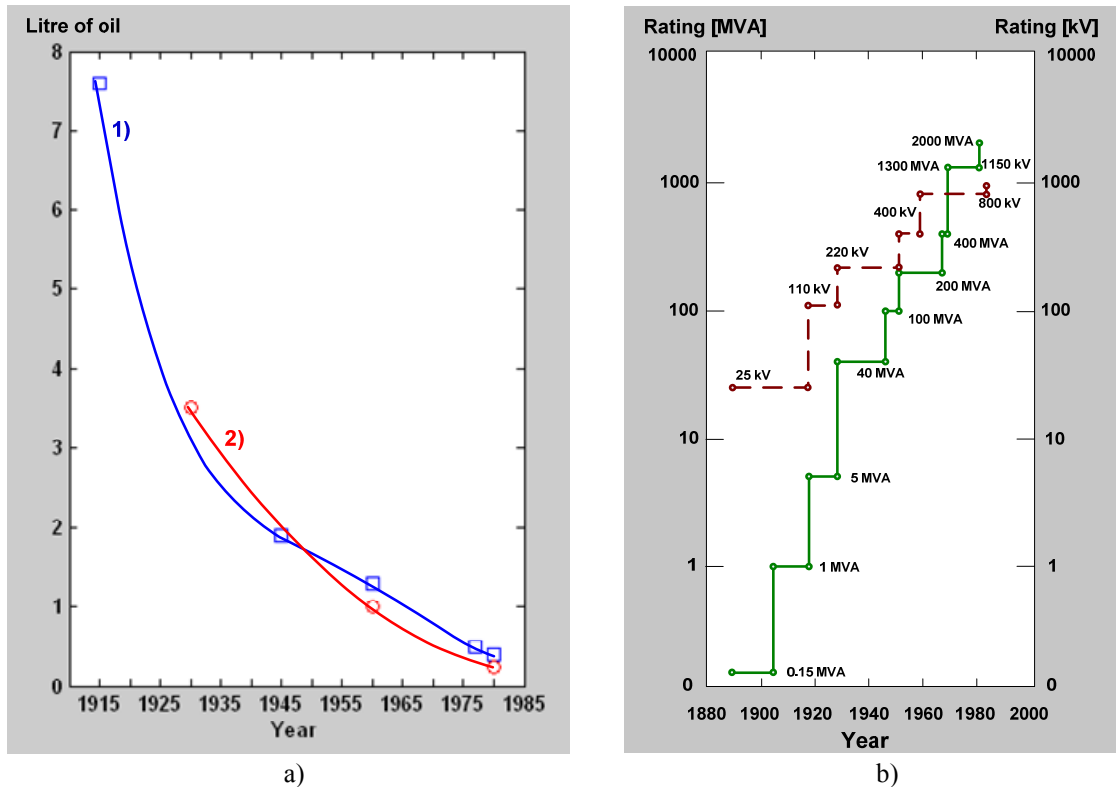


Figure 4.2: Development of mineral oil characteristics and the increasing of transformer capacity

a) quantity of oils used to insulate a transformer per kVA rating of transformer [curve 1 adapted from [83], curve 2 adapted from [84]] b) development of rated voltage and power of transformers[10]

As a rule, mineral oils have to perform multi functions such as dielectric, coolant, and arc-quencher. To accomplish their multiroles, IEC 60422 recommends that the mineral oils need principally to possess certain properties [20] as followings:

- high dielectric strength to withstand the electric stress during operation service,
- low viscosity to maintain a good ability of mineral oil circulation and heat dissipation,
- acceptable low- temperature properties to functionally operate in the expected lowest temperature at the installation place,
- resistance to oxidation to reliably operate with longevity service life.

Furthermore, from the point of views of the manufacturers, the high flash point is an important factor that has to take into account for selecting the mineral oils. Moreover, the hot issues that attract transformer manufacturings, the customers and also the researchers are about the environment and ecology effect of the insulating liquids. Biodegradability and higher flash point of alternative insulating liquids such as synthetic and natural ester are widely discussed and investigated with deeply interesting. However, the usage of alternative oils is only introduced for the distribution transformers. Generally, one can divide the mineral oil characteristics into three parts as physical, chemical and electrical characteristics. However, the distinctions are not simple and clear cut in many cases [70]. The important physical, chemical and electrical characteristics are summarized in Table 4.5- Table 4.7 respectively.

Table 4.5: Physical characteristics of mineral oils

Property	Definition
1. Color and appearance	The color of the mineral oil is determined in transmitted light and is expressed by a numerical value, between 0.5 (lightest) to 8 (darkness), based on comparison with a series of color standard [20, 85-86].
2. Density	The density is the mass of the mineral oil per unit volume [19]. Density may be useful for type identification and evaluation of the mineral oil's suitability [82].
3. Viscosity	The viscosity is the property that describes the mineral oil resistance to flow. It is very important to dissipate of heat of the mineral oil in service.
4. Flash point	The flash point is the lowest temperature at which the mineral oil releases enough gases to make the gas mixtures above the mineral oil surface to ignite momentarily when a flame is applied to it under controlled conditions of temperature, time and flame size [1,18].
5. Fire point	The fire point is the lowest temperature at which the mineral oil releases sufficient vapors continue to be formed to sustain a fire for a specified time [18].
6. Pour point	The lowest temperature at which the mineral oil is capable to flow [85].
7. Interfacial tension	The interfacial tension is the strength of the interface between the mineral oil and water [19].

Table 4.6: Chemical characteristics of mineral oils

Property	Definition
1. Water content	The amount of water which is usually present in the mineral oil as free moisture, in soluble, emulsion or dissolved form in the mineral oil [1].
2. Acidity	The amount of acidic constituents or contaminants in the mineral oil as a result of oxidation or contamination [1,20].
3. Corosive sulphur	The quantities of elemental sulphurs are in the mineral oil [19].
4. Sediment and sludge	Sediment is the soluble material including insoluble oxidation or degradation products of solid and liquid insulating materials presented in the mineral oil. Sludge is a polymerized degradation product of solid or liquid insulating materials [20]. Sludge is composed of high - molecular weight molecules resulting from oxidation, which are no longer soluble in oil and have precipitated [1].
5. Particle count	The amount of particles in the mineral oil with diffent sizes. The particles are classified in six classes, according to their sizes [1].
6. Oxidation stability	The ability of mineral oil to withstand oxidation under thermal stress and under the presence of oxygen and a copper catalyst [20].
7. Polychlorinated biphenyls (PCBs)	PCBs are a family of synthetic chlorinated aromatic hydrocarbon, which have good thermal, electrical and excellent chemical stability but negative environment impact [20, 84].
8. Compatibility	The compatibility of unused mineral oils to mix with the oil in service.

Table 4.7: Electrical characteristics of mineral oils

Property	Definition
1. Permittivity	Permittivity is defined as the ratio of capacitance of a given set-up with a specific material (in this case the specific material should refer to the mineral oil) to the capacitance with the same set – up using vacuum or air as a dielectric [87].
2. Dielectric dissipation factor (DDF)	DDF is a value to show a dielectric loss in the mineral oil when it is used in an alternating electric field by which the energy is dissipated as heat [88].
3. Power factor	Power factor is defined as the cosine of the phase angle between a sinusoidal potential applied to the mineral oil and the resulting current [19].
4. Resistivity	The ability of the mineral oil to resist the conduct of an electrical current. Therefore, a very high resistivity of the mineral oil is expected.
5. AC breakdown voltage	The minimum AC voltage at which electrical breakdown occurs in a specified gap of the mineral oil. AC breakdown voltage represents the ability of the mineral oil to withstand AC voltage stress [1,84].
6. Impulse breakdown voltage	The voltage at which electrical breakdown occurs in the mineral oil under a specific shaped transient voltage wave in a highly divergent field geometry [19]. This value represents the ability of the mineral oil to withstand transient voltage stress in highly divergent field [1].

4.1.3 Dielectric property of mineral oils

4.1.3.1 Permittivity

Consider the electric field in a dielectric material, the relationship between electric field strength, E (V/m) and dielectric flux density, D (C/m²) can be expressed as

$$D = \epsilon E = \epsilon_0 \epsilon_r E \tag{4.1}$$

Where ϵ is the permittivity of the dielectric material (F/m), ϵ_0 represents the permittivity in free space (8.854×10^{-12} F/m) and ϵ_r is the relative permittivity or the dielectric constant of the material (dimensionless).

Generally, ϵ_r is defined as a ratio of the capacitance, C (F), of a given configuration of electrode with a specific material as a dielectric to the capacitance, C_0 (F) with the same configuration with vacuum (or air for the most practical propose) as the dielectric [87,89].

$$\epsilon_r = C / C_0 \tag{4.2}$$

After inserting the dielectric between electrodes, the dielectric material responds to the applied electric field by redistribution their charge positions. Positive charges are attracted toward the negative electrode and negative charges are attracted toward the positive electrode. The displacement of charges which creates electric dipoles is the polarization characteristic of the dielectric material. The electric field within the polarized dielectric causes the decrease of the total electric field between the electrodes which also decreases the voltage between them, obviously observed in case of the voltage supply is removed, thereby increasing the capacitance of the electrode system. The effect of dielectric material on the changed capacitance of the electrode is due to the polarization phenomena of the dielectric under electric field as shown in Fig. 4.3.

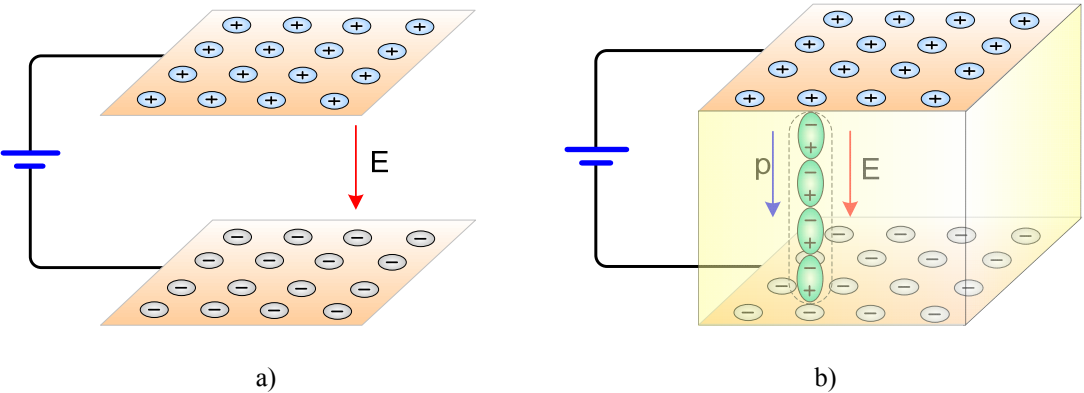


Figure 4.3: Polarization phenomena

a) vacuum as a dielectric b) polarization process

The polarization P (C/m^2) is defined as the quantity indicating the electric moment per unit volume induced in the material by the applied field. The magnitude of P is directly proportion to the field, if the field is not very high to cause the insulation degradation [90].

$$P = (\epsilon_r - 1)\epsilon_0 E = \chi\epsilon_0 E \quad (4.3)$$

Where $\chi = \epsilon_r - 1$ is called dielectric susceptibility of the medium. χ presents the ability of the material to response to electric field. P will have the same dimension as D [91].

Equation (4.1) can be rewritten as

$$D = \epsilon_0 E + P \quad (4.4)$$

In general, ϵ_r can be presented as a complex dielectric constant when the dielectric undergoes the alternating field. A complex dielectric constant can be written as

$$\epsilon_r = \epsilon_r' - j\epsilon_r'' \quad (4.5)$$

Where ϵ_r' represents the real part of the complex permittivity or the real value of the dielectric constant. This value is associated with the stored energy in the material and ϵ_r'' illustrates the imagine part which relates to the dielectric loss of the material. The meaning of the real and imaginary parts of the complex dielectric constant can be readily explained by considering the capacitive circuit as depicted in Fig. 4.4. The current i which flows after an alternating voltage v is applied across the electrodes, may be calculated as follows [91].

$$i = j\omega\epsilon_r C_0 v = j\omega(\epsilon_r' - j\epsilon_r'')C_0 v \quad (4.6)$$

$$i = \omega\epsilon_r'' C_0 v + j\omega\epsilon_r' C_0 v = I_r + I_c \quad (4.7)$$

Where: I_r represents a resistive component of current I and I_c represents a capacitive component of current I .

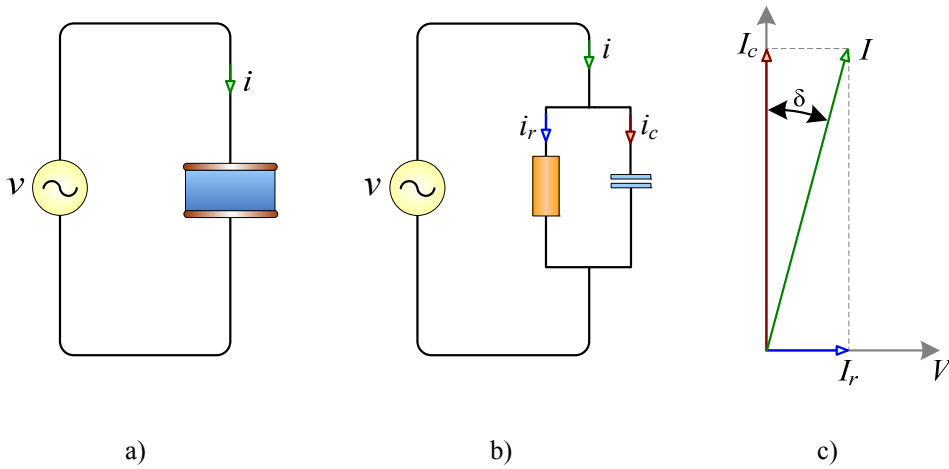


Figure 4.4: A circuit of a dielectric

a) and b) circuit diagram c) phasor diagram

The dielectric constant of liquids depends on the molecular structure, molecular weight and density. Normally, the polar dielectrics which have permanent dipoles have high relative permittivity such as highly purified water ($\epsilon_r = 80$). The dielectric constant of nonpolar dielectrics or relatively nonpolar dielectric liquids is relatively low compared with that of polar dielectrics for example the relative permittivity of mineral oil is about 2.2. The dielectric constant rests also upon frequency and temperature. P. J. Harrop reported that ϵ'_r varied only slowly with variables such as temperature and pressure whereas ϵ''_r varied sharply with these variables [92].

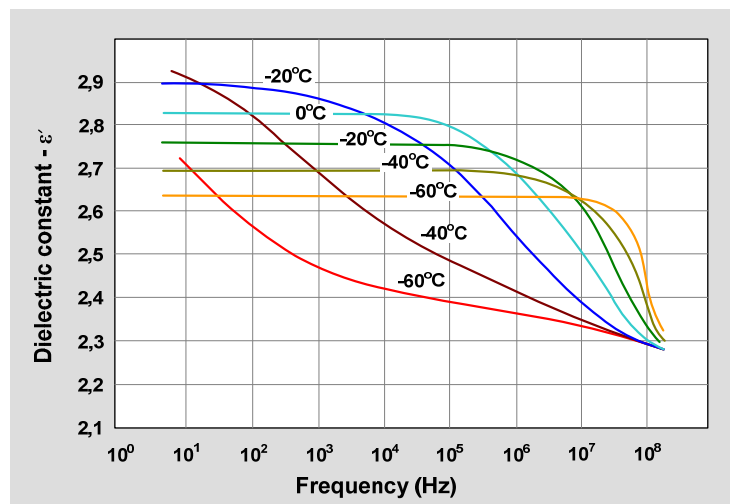


Figure 4.5: Dielectric constant as a function of frequency and temperature of a transformer oil [adapted from [1]]

Polarization in insulating materials

Polarization in insulating materials is fundamental phenomenon of interaction of the charges of dielectrics under the applied external electric field. Polarization phenomena play a significant role in the conducting and loss of liquid dielectrics. The main polarization mechanisms will be explained below.

Electronic Polarization (also called optical polarization) is caused by the displacement of the electron cloud with respect to the positive nucleus due to the external electric field. This displacement is quite small because the applied electric field is normally quite weak compared to the intra - atomic field at the electron due to the nucleus. This polarization takes place in about 10^{-14} seconds. It is responsible for the refraction of light and does not cause electric losses [90, 93-94].

Atomic Polarization is also known as ionic polarization or vibrational polarization. The electric field causes the atoms or ions of a poly atomic molecule to be displaced relative to each other. The electric field can also distort the arrangement of atomic nuclei and the normal lattice vibration. This polarization cannot occur at such high frequency as electronic polarization because of markedly slow in movement of the heavy nuclei compared to that of electron. Generally, the magnitude of atomic polarization is quite small about one – tenth of that of electronic polarization [90, 93-94].

Orientation Polarization takes place only in materials consisting of molecules or particles having a naturally permanent dipole. However, their dipoles normally rotate freely or are

randomly oriented. Therefore, there is no net polarization. When the materials are under the electric field, the dipoles of molecules or particles are reoriented toward the direction of the field [90, 93-94].

Hopping polarization explains the phenomena that the localized charges such as ions and vacancies, or electrons and holes can jump from one site to the neighboring site for a short time, and then becoming trapped in the localized state. For example, a negative charged particle can hop from its site to another site by leaving a positive charge in the former site and creating a negative charge in a new site. This phenomenon forms a dipole [94].

Space charge polarization, or interfacial polarization, is created by the separation of mobile positively and negatively charged particles under the external applied electric field. The mobile charge carriers may be injected from electrical contacts or may be trapped in the bulk or at the interfaces and so on. When the space charge is formed, the original electric field distribution will be distorted which has an effect on the average dielectric constant. The space charge can be also formed from the interfaces between layers of different permittivities under the electric field [90,93-94]. Fig. 4.6 represents the polarization mechanisms.

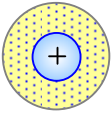
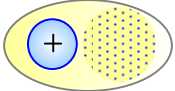

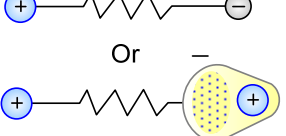
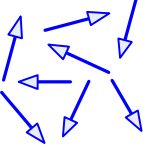
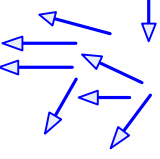
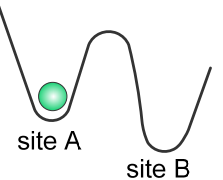
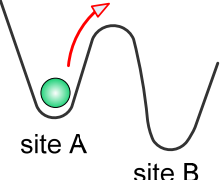
Polarization Type	No E field	With E field
Electronic Polarization		
Atomic Polarization		
Orientation Polarization		
Hopping Polarization		

Figure 4.6: Different kinds of polarization mechanisms [adapted from [94]]

Time to perform the polarization is different depending on the polarization type. This time constant rests upon the frequency of the applied voltage and the molecular structure of the

liquids. The response of polarization of the dielectric liquid under the high frequency electric field which may lag behind the electric force is called relaxation. This relaxation time is caused by the friction resistance of the liquids to the change in molecular orientation. Under alternating voltage, the dipoles or charges must change their direction every half cycle. Moreover, the temperature has also an effect on the polarization time. Therefore, the degree of the overall polarization relies on the time variation of the electric field. The relationship between polarization types and their time constants is presented in Fig. 4.7.

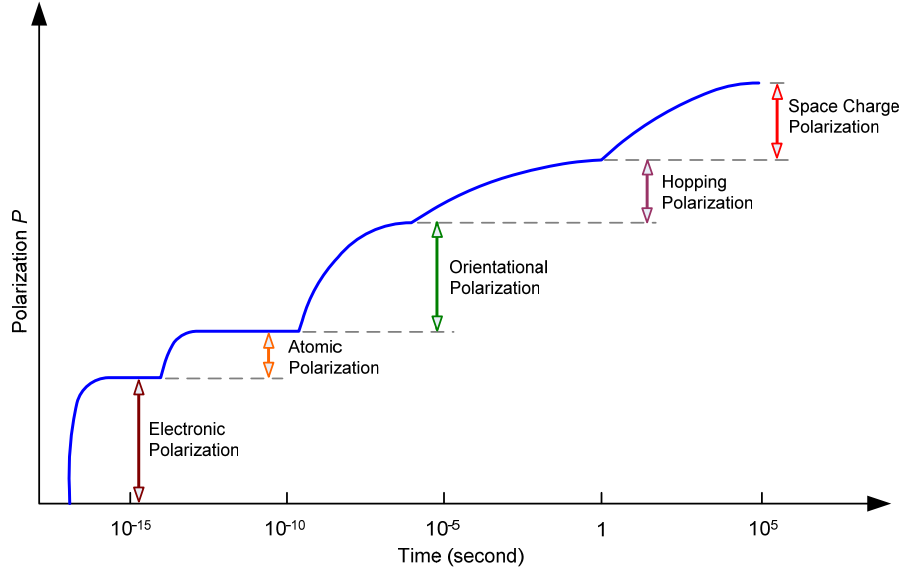


Figure 4.7: Variation of different types of polarization with relaxation time under a step-function electric field [adapted from [94]]

4.1.3.2 Dielectric dissipation factor

The heating in dielectrics subjected to an alternating voltage was observed and studied to develop the theory of dielectric loss. The study showed that the examined dielectric loss was a direct consequence of an energy loss current component in the dielectric originating from a lagging phase shift of the charging current vector behind the applied voltage. If the liquid represented a nearly perfect dielectric, the angle different, δ , between current I and I_c as shown in Fig. 4.4 cannot be detected i.e. current I lags behind voltage V 90 degree. Practically, the liquid dielectric is not perfect, the phase angle different, δ , can be found when the dielectric is under sufficiently low values of an alternative electric field [1].

The dielectric loss or dissipation factor ($\tan \delta$) is defined by equation (4.8)

$$\tan \delta = \text{energy dissipated per cycle} / \text{energy stored per cycle} = I_r / I_c \quad (4.8)$$

The dielectric loss can be written in the term of relative permittivity

$$\tan \delta = \varepsilon_r'' / \varepsilon_r' \quad (4.9)$$

Therefore, ε_r'' is also called the dielectric loss factor. This value describes the energy losses in the liquid dielectrics due to electronic, atomic and orientation polarization. In addition,

dielectric losses in liquid dielectrics can be generated from the movement of ionic charge carriers. Dielectric loss or dielectric dissipation depends on the frequency and amplitude of the applied electric field, the molecular structure and also the temperature.

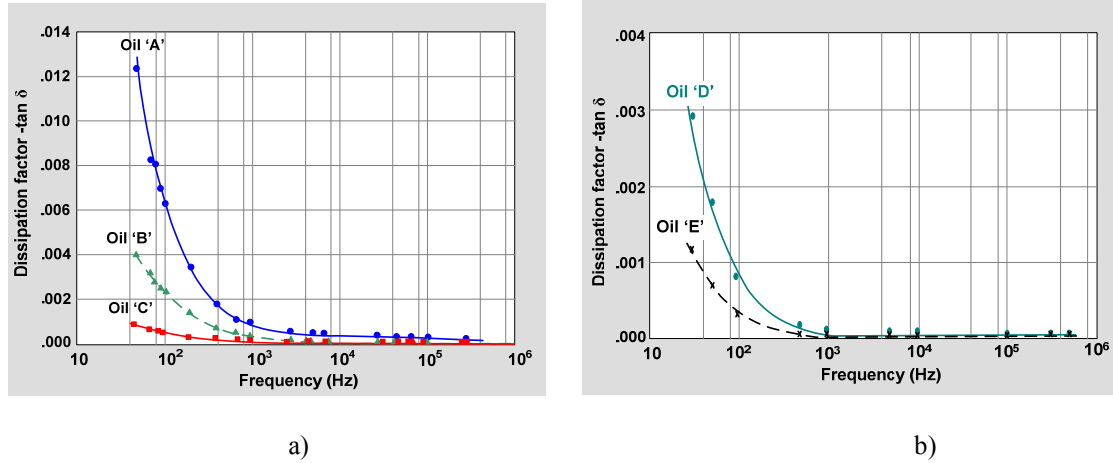


Figure 4.8: Dissipation factor against frequency at 90°C

a) three mineral oils with different aromatic contents at approximately equal viscosities b) two mineral oils with approximately equal aromatic contents but different viscosities [adapted from [1]]

4.1.3.3 Conductivity

Conductivity, σ (ohm. m)⁻¹, of the dielectric material describes the property of the material to permit the flow of electrical current through its volume. Conductivity is the reciprocal of the resistivity, ρ (ohm. m).

$$\sigma = 1/\rho \quad (4.10)$$

Conductivity can be expressed in the term of current density, J (A/m²), as

$$J = \sigma E + \varepsilon_0 \varepsilon_r \partial E / \partial t \quad (4.11)$$

J is defined as current per unit area of dielectrics caused by the electric field E , σE represents the conduction current density and $\varepsilon_0 \varepsilon_r \partial E / \partial t$ is the displacement current density. E and J are the vector quantities.

The conduction mechanism in a dielectric liquid is strongly affected by the degree of its purity. Many kinds of mobile charges such as free ions, space charges or charge particles are generated in the mineral oil. Mobile charges can be generated by the dissociating molecules of the liquids or by the electrolytic impurities contained within the liquids and so on. The movement of charge carriers existed in the mineral oils or caused by double layers, space charge particles and so on as shown in Fig. 4.9 causes the current flow through the insulating liquids.

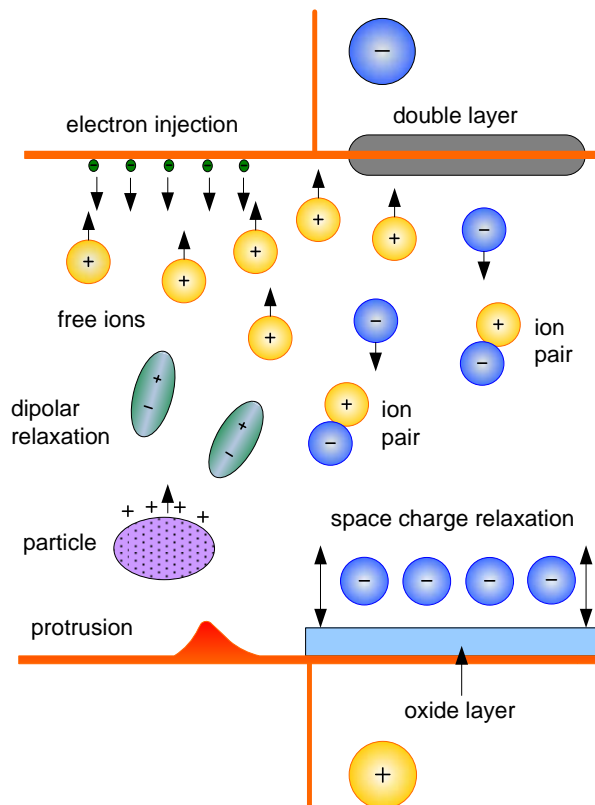


Figure 4.9: Conduction mechanism in dielectric liquids [adapted from [95]]

In practice, when the insulating liquid is subjected to a sufficient electric field, for example, a few kV/cm, the conduction current can be observed. In general, the relationship between the current density and the applied electric field strength is illustrated in Fig. 4.10 a). At first, when the dielectric is subjected to the electric field strength, the current density of the insulating is proportional to the electric field (region I) which represents the ohmic behavior of dielectrics. Then, the applied voltage is raised, the electric field strength is higher and the current density (ionic current) seems to saturate. This electric field causes an extraction of ions from the bulk of liquids. In this case (region II), the dissociation rate determines the current density. The higher electric field will increase the current density rapidly in region III. Finally, the increase of electric field strength leads to breakdown of the dielectric liquid (region IV) [95]. The experiment test results tested by the needle-plane electrode system to measure the conduction current under DC electric field are illustrated in Fig. 4.10 b).

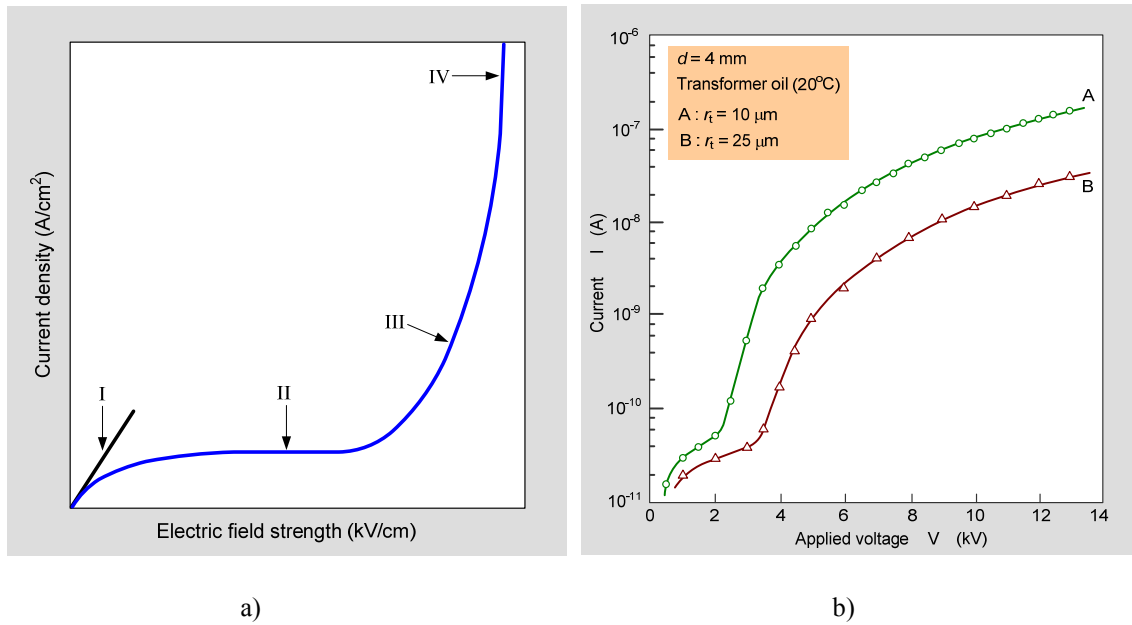


Figure 4.10: Conduction current

a) conduction phenomena in dielectric liquids [adapted from [95]] b) conduction currents from experiment, r_t is the needle tip radius of the needle - plane electrode [adapted from [96]]

DC conductivity is also a function of time for which the voltage is applied as shown in Fig. 4.11. The DC conductivity is very high at the first (region I) which is determined by dipole orientation. In region II, the conductivity is dominated by the movement of free charge carriers under the influence of the applied electric field. In region III, the space charges are developed in front of the electrode and in region IV the steady ion currents due to dissociation takes place.

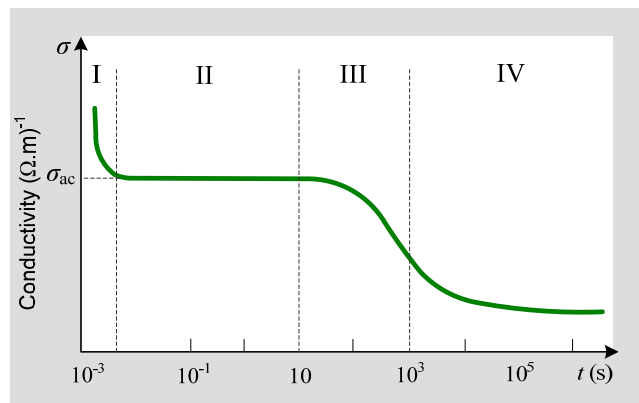


Figure 4.11: DC conductivity of an insulating oil respected to the time of applied voltage [adapted from [97]]

Under DC electric field, the conduction current will be observed. Furthermore, both current types arise when the dielectric material is subjected to AC electric field. Generally, the AC conductivity arising from the movement of mobile charge carriers consisting of mobile ions is called ionic conduction. Moreover, electrons or holes may cause the same phenomena as ions; this phenomenon is called electronic conduction [95]. The generation of electron/ion or electron/ hole pairs can be explained by the energy band theory. Electrons can move from the valence band to the conduction band after they are excited with enough energy.

AC conductivity can be calculated from this equation

$$\sigma = qN\mu_m \quad (4.12)$$

Where σ is AC conductivity, q represents the charge of ions, N is the concentrate of charge carriers involved with each one transporting a charge, q , and μ_m is the ionic mobility of the insulating liquids.

$$\mu_m = q / 6\pi\eta r_0 \quad (4.13)$$

Where η is the viscosity of the mineral oil and the ion shape may be approximated as sphere with radius of r_0 .

Hence, the conductivity, σ , can be rewritten as

$$\sigma = q^2 N / 6\pi\eta r_0 \quad (4.14)$$

Because both positive and negative ions contribute to the conductivity of dielectrics so the conductivity can be expressed as

$$\sigma = q[N_+\mu_{m+} + N_-\mu_{m-}] \quad (4.15)$$

Where N_+ and N_- are the concentrations of the positive and negative ions, μ_{m+} and μ_{m-} is the mobility of the positive and negative ions respectively. Moreover, the AC field causes also the separation of the opposite charged ions. This condition leads to a proportional rise in the ion concentrations, N_+ and N_- , with the field, as a result rise in the conductivity. The ionic concentrations, N_+ and N_- , are increased considerably with temperature because more dissociations of the impurity are activated at high temperature. Obviously, the conductivity of the mineral oil depends on ion concentrations which are strong relatively with the temperature. A rise in temperature causes a reduction on mineral oil viscosity which resists to the movement of ions. Besides, the higher temperature increases in number of ions as a consequence of an enhance dissociation rate. Fig. 4.12 illustrates the relationship between ion concentration and temperature of 3 different mineral oils; the mineral oil A has more aromatic contents than mineral oil B and the mineral oil C is the paraffinic oil.

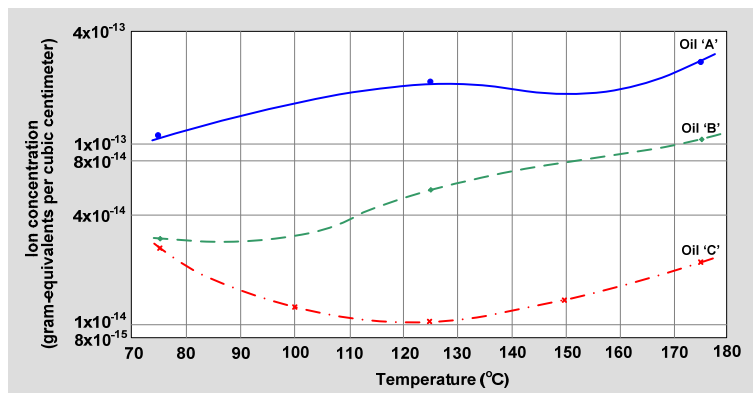


Figure 4.12: Ion concentration and temperature relationship at 1 kHz of the mineral oils with the approximately equivalent viscosity [adapted from [1]]

It can be seen that the ion content is higher for the more aromatic oils. The rising of temperatures increases the ionic contents for all oils except at the initial temperature of the paraffinic oil C. This may be caused by a remnant dipole loss which is reduced at the higher temperatures [1]. The conductivity has considerably effect on the loss of dielectric insulation. $\tan \delta$ can be written in term of conductivity as

$$\tan \delta = \sigma / \omega \epsilon_0 \epsilon'_r \quad (4.16)$$

and
$$\tan \delta = q[(N_+ \mu_{m+} + N_- \mu_{m-}) / \omega \epsilon_0 \epsilon'_r] \quad (4.17)$$

4.1.4 Factors influence on mineral oil characteristics

4.1.4.1 Water content

Water is one of important factors that reduce the electrical strength of the mineral oils. Water distributes not only in the oil but the majority of water is in the paper as well. The presence of water in cellulose materials has a dramatically negative effect on the electrical and mechanical strengths of the cellulose insulation. The water content of insulating oils influences also the ageing tendency of the liquids and solid insulation [16,20,85,98]. Water in the mineral oil in the high voltage equipment especially in the power transformer is caused by three sources [98-99]; the first is the residual moisture after manufacture. New transformers obtained from the factory have approximately 0.4 -1% water by weight in the cellulose insulation [98]. The acceptance of water content in the celluloses is about less than 0.5-1% depending on customer's and manufacturer's requirements [20]. The second, water exits in the mineral oil at the service time by the engrossing of moisture from the atmosphere. Degradation of cellulose and oil during service produces water more or less 0.1% per year [20].

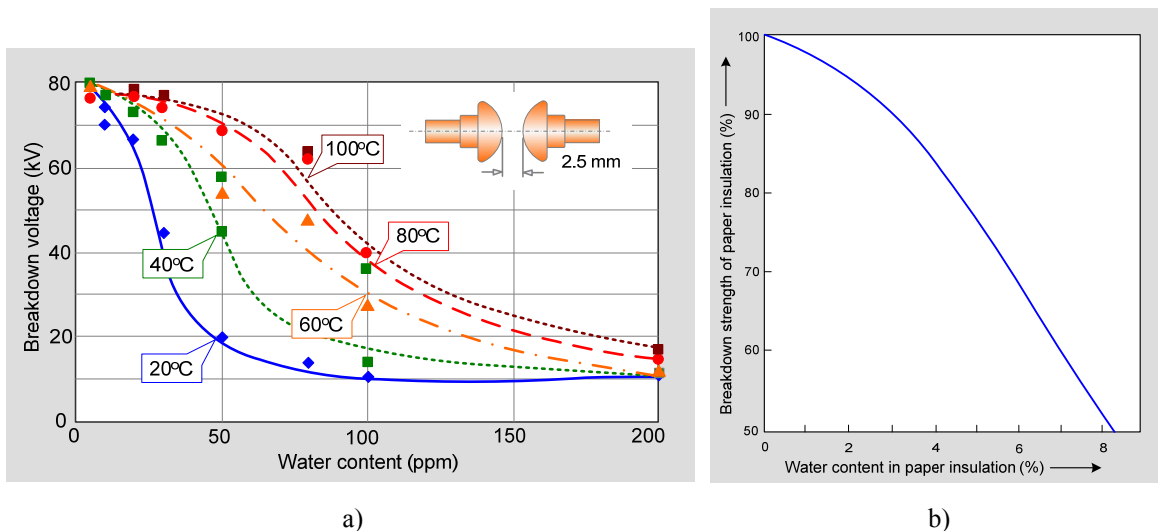


Figure 4.13: Influence of water content in the mineral oil

a) breakdown voltage of insulation oil with different water contents relative to temperatures [adapted from [16]] b) breakdown strength of paper insulation with different water contents [adapted from [80]]

The third, water can be present in oils in a dissolved form, as a tiny droplets mixed with the oil (emulsion) or in a free state at the bottom of the container holding the oil [86]. The solubility of water in oil, W_s (mg/kg), depends on temperature, the oil structure and the condition of oil [20]. The existence of polar compounds in severely aged liquids is considered to affect the water solubility characteristic because the water molecules may be captured by hydrogen bonds with carboxyl groupings [100].

The temperature dependence of the solubility of water in insulating liquids is described by

$$W_s = W_{oil} e^{(-B/T)} \quad (4.18)$$

Where W_{oil} and B are the material constant. T is the temperature of oil (Kelvin). The absolute water content, W_{abs} (mg/ kg), is not contingent with temperature, type of oil and oil condition. The water content in oil is directly proportional to the relative water concentration (relative saturation) up to the saturation level. According to IEC 60422 the saturate water content in unused oil can be expressed as

$$\log W_s = 7.0895 - 1567/T = F - (G/T) \quad (4.19)$$

The constant values (F and G) used to estimate the saturation solubility of water in oil have been also proposed by other reserchers for example F and G may be as 7.42 and 1670 or 7.3 with 1630 respectively [101]. The relationship between the saturate water content of the unused mineral oil and the aged mineral oil with acidity of 0.3 mg KOH/g is depicted in Fig. 4.14. Besides, ratio of the absolute water content to the water solubility is defined as the relative water content, W_{rel} (%) as

$$W_{rel}(\%) = W_{abs} / W_s \quad (4.20)$$

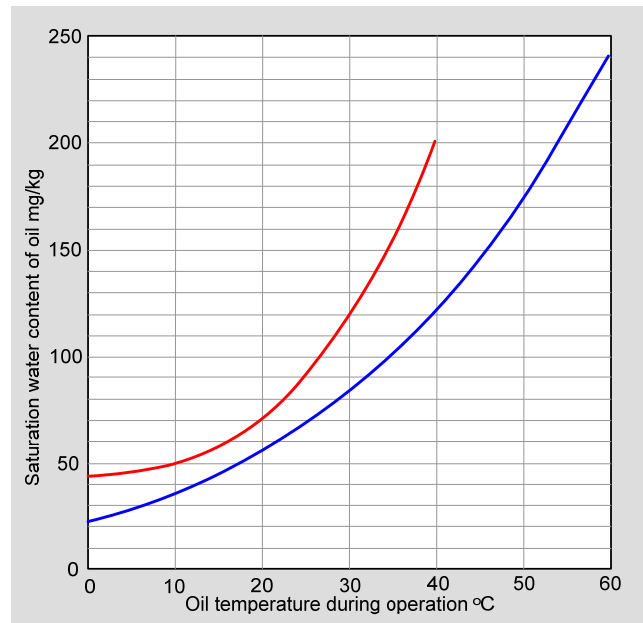


Figure 4.14: Relationship between the saturation water content and the oil temperature [adapted from [20]]

where the red line is the typical saturation water content in oxidized oil with acidity of 0.3 mg KOH/g, the blue line is the saturation water content in unused oil.

4.1.4.2 Temperature

Temperature is one of the most importance factors which greatly effect on the mineral oil characteristics. Generally, the most transformers operate in the range of 20°C to 80°C [102]. The maximum top oil at 90°C can found under the operating condition of the transformers [103]. The variations in temperature of the mineral oils can influence several parameters such as viscosity, conductivity, resistivity, surface tension of mineral oils. As mentioned in the section 4.1.3.3, high temperature causes a decrease in viscosity and then increases in the mobility of the ions as a consequence in a higher conductivity and losses in dielectrics. Fig. 4.15 represents the effect of the temperature on the viscosity and conductivity of the mineral oils. This figure also exhibits the effect of oil motion which generally causes the exaggeration of conductivity.

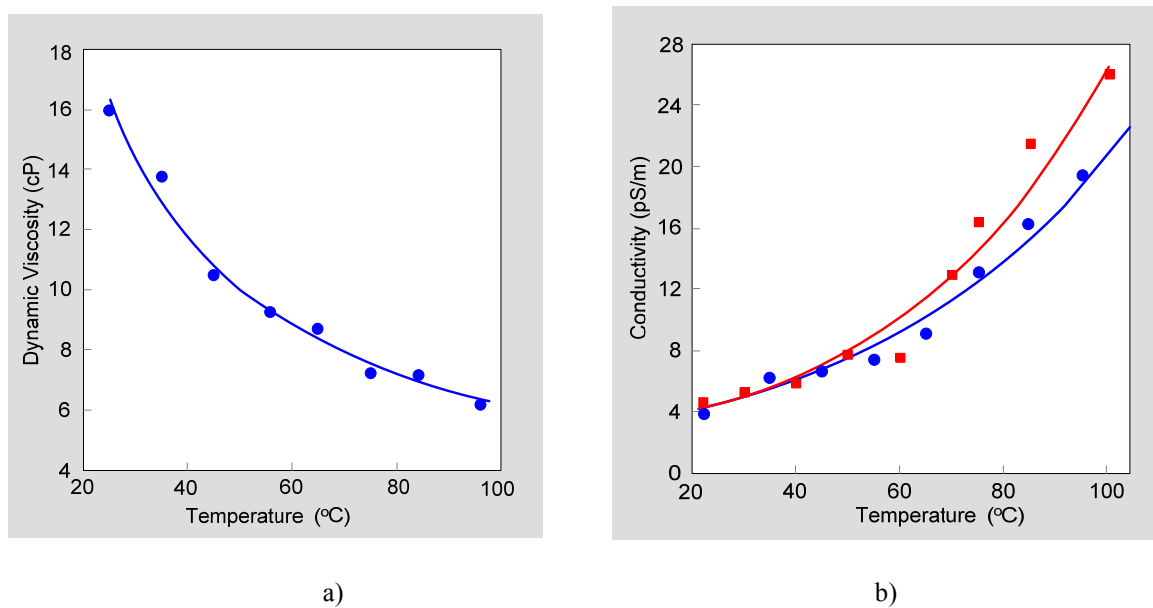


Figure 4.15: Temperature effect on

a) viscosity b) conductivity of the mineral oil with (squares) and without (circles) flow [adapted from [102]].

Temperature has also an effect on the breakdown characteristic of the mineral oil. It is quite complicate to analyze the effect of temperature on the mineral oil because other factors such as the oil viscosity have also a strong effect on the breakdown voltage. The test results from different experiments which examined the temperature dependence of the breakdown voltage are illustrated in Fig. 4.16.

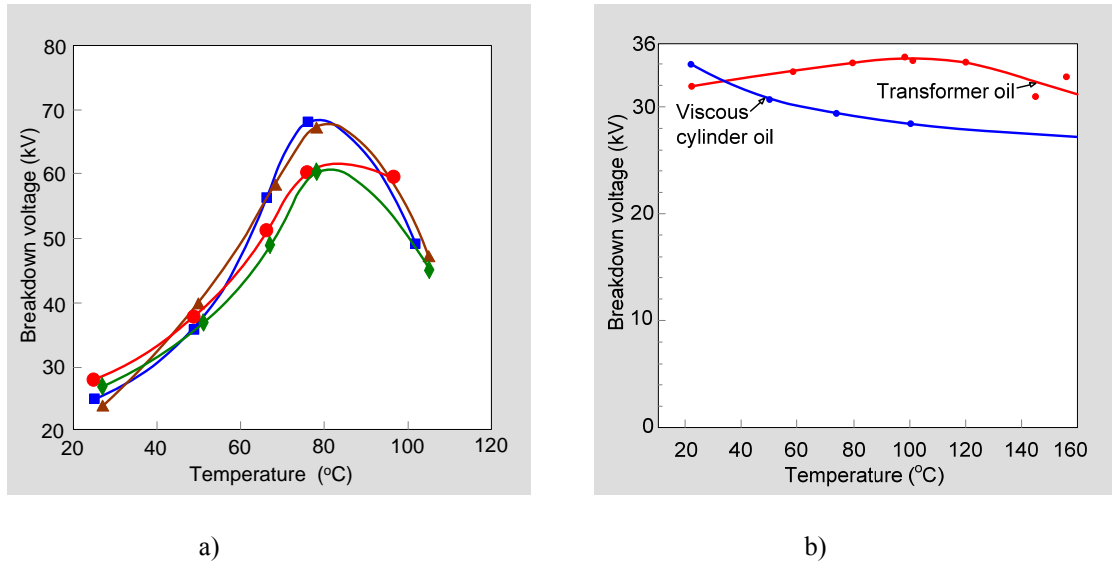


Figure 4.16: Temperature effect on breakdown characteristic of the mineral oil

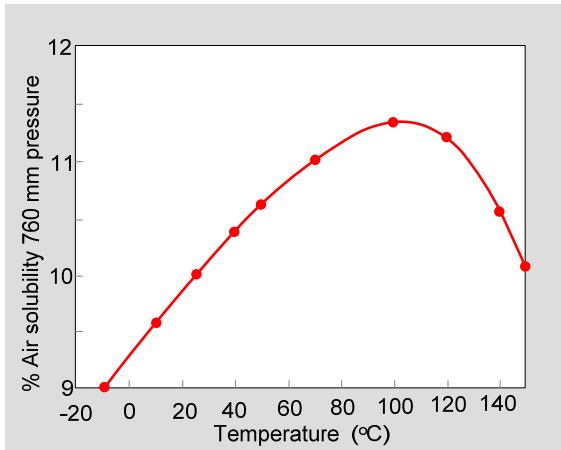
a) temperature effect on breakdown of the mineral oil Voltesso 35 with different oil flow rates, red line for no oil movement, blue line for oil movement with 25 ml/s, brown line for oil movement with 50 ml/s, green line for oil movement with 65 ml/s [adapted from [102]], b) temperature effect on breakdown of the mineral oil with different viscosities, red line for low viscosity oil and blue line for high viscosity oil [adapted from [104]]

The explanation about the increasing of breakdown voltage with increase of temperature has been proposed by F. M. Clark. He described that the dielectric breakdown strength depended on the solubility of air in the mineral oil which increased with the increasing of temperature until the temperature reached the boiling point; the breakdown strength would decrease. He proposed the term of relative oil-dissolved air density, D_{rel} (dimensionless) as in (4.21) which directly relates to the temperature.

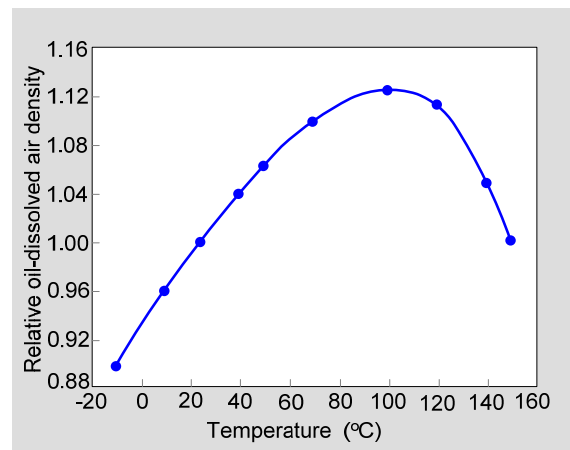
$$D_{rel} = V_t / V_{25} \quad (4.21)$$

Where V_{25} is the percentage of gas solubility (by volume) in the liquid tested under the standard condition, 25°C and 760 mm pressure, V_t is the percentage gas solubility (by volume) in the liquid under the specially selected condition.

The relationship between the solubility of air and temperature and the correlation between the relative oil - dissolved air density and temperature, including the relationship of the relative oil - dissolved air density with dielectric breakdown strength of the mineral oil are illustrated in Fig. 4.17- Fig. 4.18 respectively.



a)



b)

Figure 4.17: Temperature effect on air solubility

a) effect of temperature on the solubility of air in the mineral oil b) relative oil -dissolved air density in the mineral oil as a function of temperature [adapted from [104]]

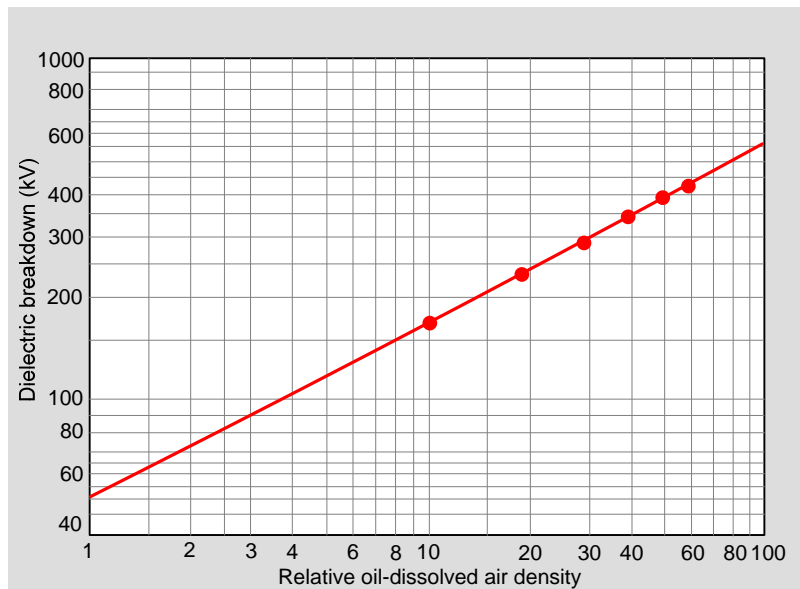


Figure 4.18: Relationship between dielectric breakdown and the relative oil – dissolved air density of the mineral oil [adapted from [104]]

The concept of air including water solubility relating to temperature and breakdown voltage is also clarified with the breakdown strength of the mineral oil with different water contents under AC voltage and impulse voltage as demonstrated in Fig. 4.19.

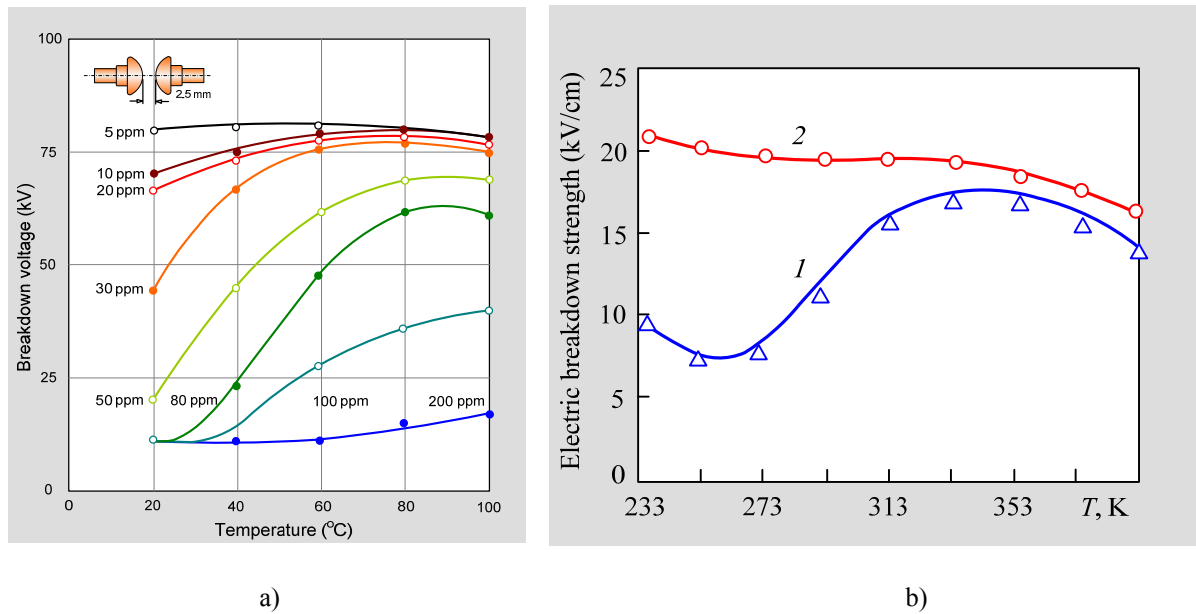


Figure 4.19: Relationship between breakdown strength of the mineral oil with different water contents and temperatures

a) under AC voltage [adapted from [16]] b) under impulse voltage: the blue line is the transformer oil in service and the red line is the dehumidified transformer oil [adapted from [105]]

4.1.4.3 Oxidation

Oxidation is one of the most important factors relating to the aging of the mineral oil. Oxidation cannot be eliminated but can be mitigated by incorporating inhibitors. Oxygen and temperature are the main parameters for oxidation process. While the metal such as copper and iron, acts as oxidation catalysts [18,84,98]. Without oxygen the mineral oil will not oxidize. However, the mineral oil contains a small amount of air even after degassing. In general, oxygen is present or ingresses in the mineral oil from the environment. The oxidation process occurs in several steps and produces by-products which compose of radicals, alcohols, water, aldehydes, ketones, sludge and so on [98]. The existence of sediment and sludge may change the electrical properties of the mineral oil. With increasing amounts of polar ageing by-product, the mineral oil becomes much oxidized and the water solubility characteristics of the mineral oil will increase as shown in Fig. 4.14 [20]. The important products of oxidation are acids, water, and sludge [18]. Acids and water lead to accelerate the degradation of celluloses and also may be responsible for the corrosion of metal parts in transformers [18,20]. Sludge deposited on windings and in cooler ducts decreases the heat transfer ability of the mineral oil and leads to increase the mineral oil temperature and oxidation rate. The elevated temperature affects the rate of oxidation which approximately doubles for each 7 - 10 °C rise [18]. The escalated temperature reduces sharply the insulating integrity of insulation materials and the transformer service life at the end. To maintain the oxidation stability, inhibitors are used; however, the oxidation inhibitors become depleted with the service time of the transformer.

4.1.4.4 Corrosive sulphur

Mineral oils principally consist of hydrocarbon compounds and contain small amount of sulfur and nitrogen as well as oxygen compounds [106-108]. Sulfur compounds in mineral oils may range from 0.001 to 0.5%. Generally, the organic sulfur compounds are composed of dibenzyl disulphide (DBDS), thiophenes, disulfides and polysulfides thioesters, and mercaptans [108]. Most sulfur compounds cause corrosion of conductors, acceleration the sludge formation, and degradation of the mineral oil. However, there are a few sulfur compounds which are beneficial to the mineral oil which act as retardants in the oxidation process of the insulating liquids [48]. Most corrosive sulfur oils consist of DBDS which is always found with a significant amount in the corrosive oils [109]. Moreover, there are free DBDS corrosive oils by which a relevant amount of disulfides and mercaptans can be detected when such oils become corrosive [49,110]. Corrosive sulfur causes the formation of substances that are insoluble in oil, precipitate as sludge or form copper sulfide [49]. In general, DBDS reacts with the copper conductors to form copper sulphide on the surfaces of these conductors and on the paper insulation used for wrapping the conductors [109]. Besides, copper particles moving in the mineral oil as the brownian motion caused by thermal gradient may enter and become trapped in the paper fiber and paper surfaces. When these copper particles contact with the corrosive sulphur oil, the copper sulphide will be formed at the insulation papers[49]. After formation, the copper sulphide seems to start deposite on the innermost paper layer adjacent to the conductors and sometimes directly on the conductors. The presence of conductive compounds causes an increase of dielectric dissipation factor which relates to the increased conductivity of the oils. A decrease of the interfacial tension is also often associated to the formation of conductive compounds [111]. The increase of dielectric losses for the mineral oils is mainly due to the soluble fraction of copper (ionic form of copper which is accounted for mobility charge carriers in the oil), whereas suspended copper forms or particles, do not affect considerably dielectric losses [111]. The forming of copper sulphide on the paper wrapped conductors changes the insulating paper partially conductive. Therefore, the dielectric losses within the insulating paper increase which lead to thermal instability and eventually to a thermo - electric breakdown of the insulating system [49]. Furthermore, the forming of copper sulphide can initiate a conductive bridge between two adjacent conductors which leads to breakdown finally. T. Amimoto reported that the deposition rate of copper sulfide was proportional to the DBDS concentration. Nevertheless, the incubation period before onset of the copper-sulfide deposition was inversely proportional to the DBDS concentration [112].

Temperature strongly influences the copper sulphide formation because most chemical reaction rates are temperature dependent. From the laboratory investigation pointed out in [109], the formation of copper sulphide took place in the temperature ranges of 80°C to 150°C. This related to the field data of transformer failures that the preference local sites of the copper sulfide formation on the copper conductors or on the insulation papers were at the overheating points such as the regions in the vicinity of the top portions of the windings where the temperature was highest, or in the zone of insufficient cooling windings [49]. Additionally, F. Scatiggio et al. reported that the corrosiveness of the mineral oil depended on the oil types. They found that the naphtenic oil was very sensitive to become the corrosive oil, while the iso-paraffinic had the lowest probability of being corrosive oil. The paraffinic oil had a little bit higher sensitive to become corrosive than did the iso - paraffinic oil [108]. CIGRE' reported that the paper or cellulose types may not an importance factor on the copper sulphide formation. Even though, standard kraft celluloses or papers especially made from

unbleached softwood celluloses may contain the small amounts of sulfur in the lignin parts of celluloses. The test results showed that there was no measurable evidence that the sulphur in celluloses was extracted to the oil under thermal stress at 120°C for 2 weeks [109]. This result was analogous with the test results reported in [113]. Besides, oxygen content has an effect on the copper sulphide formation especially low oxygen content worsens the copper sulphide formation than high oxygen content [109]. The switching operations of on load tap change cause also the extensive copper sulphide formation [109]. The mineral oil should undergo corrosion test whether the oil is corrosive or not as well as the experiment for evaluating the corrosiveness degree. Several corrosive sulfur mitigations can be performed, for example using metal surface passivators or replacing of the corrosive oil with a new non corrosive oil. The metal passivators can provide a film cover the copper conductors to protect the surfaces. However, after depletion or reduction in some degree of metal passivators, the insulating reverts back to a corrosive state.

4.1.4.5 Particles and other contaminants

Generally, the mineral oil characteristic depends on many factors such as molecular structure, temperature, water content and so on. Particles or contaminants and water have a harmful effect on the breakdown characteristic of the mineral oils. The moisture level in oil, the concentration, size, shape and type of the particles have directly effect on the breakdown strength of the insulating liquids. In addition, particles in suspension affect the breakdown strength distributions [114-115]. Examples of failure transformers attributed to the particles have been reported by CIGRE' [116]. Different types of particles can exist in transformers. However, copper, iron, carbon particles and cellulose particles are normally found. Metallic particles such as copper and iron are generated from the electrodes when breakdown occurs. These metallic particles can be from the manufacturing operation as well. A carbonization of the mineral oil is also generated from an arcing especially from the diverter switches. The chemical decomposition of molecules containing carbon during breakdown of the mineral oil may be classified as the semiconducting particles. Insulating particles such as cellulose, dust and fiber are found. Furthermore, contaminants may be from the mineral oil refining process, shipping process, storage process and so on [95,114,117]. According to F.Carraz et al., conducting particles had an harmful effect on the mineral oil electric strength more than insulating particles. The effect of particles on the reducing of breakdown voltage may be explained by the weakest link assumption by which the weak link are the conductive particles formed by particle absorbing water. Conducting particles can collect charges by contacting the electrodes and then a charge can transfer to such conducting particles. In case of non-conducting particles, water molecule can combine with these particles. Then, they can be charged to a lesser degree with longer charging time as well. These charged particles will form the conductive weak link in the mineral oil. The charged particles can produce a discharge at electrodes. Finally, the weak link can be developed to breakdown of the mineral oil [118-120]. F. Carraz et al. have also reported that the breakdown strength increased with decreasing concentration of particles by which the larger particle sizes, the more deleterious effect was. Besides, breakdown always occurred when the particle was in contact with the positive electrode [120]. The effect of a carbonization was reported by M. Krin et al. They reported that such carbonization reduced the breakdown strength of the mineral oil, however, it caused the rising of PDIV after the mineral oil underwent an accelerating ageing [117]. The effect of particles on impulse voltage strength was investigated by L.E. Lundgaard et al. They reported that only metal particles would be harmful the impulse breakdown strength

[121]. The combine effect of moisture and particles on breakdown voltage was studied by Kamal. He have illustrated that the breakdown field strength of the mineral oil at room temperature reduced due to the present of cellulose particles. The breakdown values were greatly reduced with the higher water content levels in the mineral oil as shown in Fig. 4.20 a). The reduction of breakdown field strength due to the present of metal particles was also magnified by higher water content levels and the present of large concentrations of the particles as shown in Fig. 4.20 b) [122].

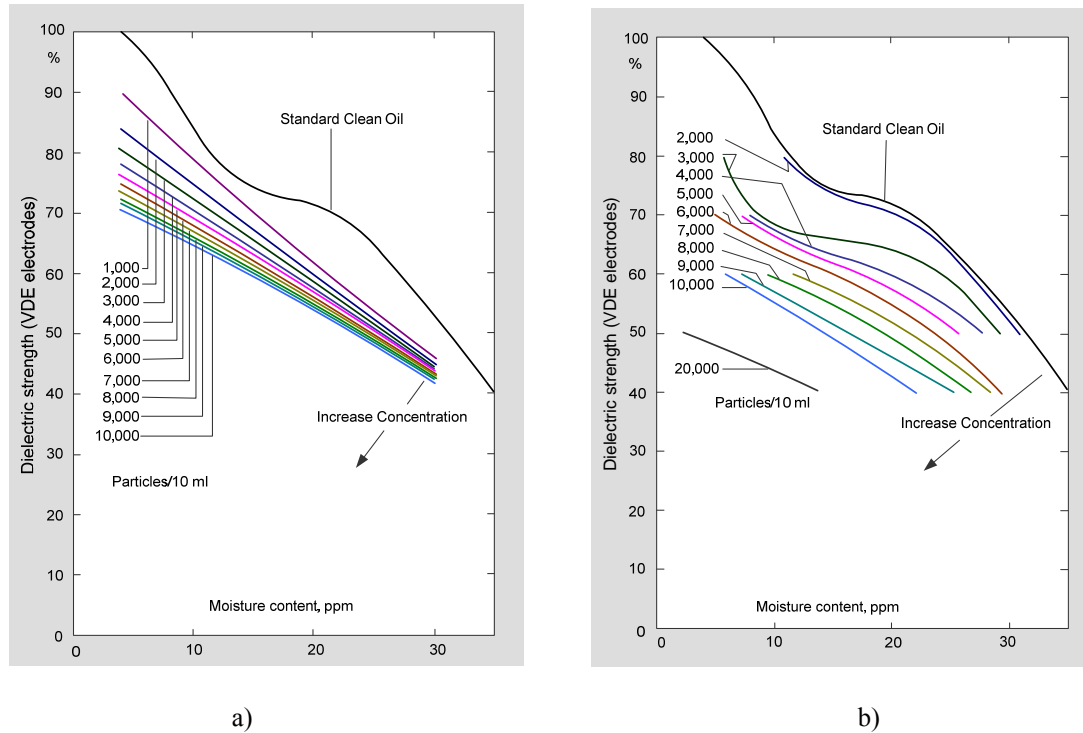


Figure 4.20: Moisture effect on breakdown strength of the mineral oil at room temperature with different concentrations

a) cellulose particles, 45 μm in size b) iron particles, 45 μm in size [adapted from [122]]

4.1.5 Mineral oil testing

Mineral oil testing is very importance to assure whether the mineral oil is met the requirement or not. A large number of tests can be applied to mineral oils. Standard tests or routine test should be used for verifying the basic characteristics of the mineral oil. Additional tests should be performed for special purposes such as the new qualification of new types of oil, the failure investigation, the research and development and the mineral oil monitoring. Table 4.8 - Table 4.10 represent the mineral oil testing standards mentioned in 4.1.2 including their information and the ways of testing application.

Table 4.8: Physical characteristic testing of mineral oils

Property	Test standard	Information	Test application
1. Color and appearance	ISO 2049	Dark color may indicate that the mineral oils start deteriorate [84]. For mineral oils in service, an increasing of the color number is an indication of contamination, oxidative or thermal deterioration, or both [19].	1)
2. Density	ASTM D 4052, ISO 3675	Density value is importance for the mineral oils used in cold climate areas, whether they are suitable or not e.g. ice crystals formed from separated water may float on the mineral oil with high density and lead to flashover on the subsequent melting [20].	3)b)
3. Viscosity	ASTM D 445, ISO 3104, IEC 61868	Ageing and oxidation of the mineral oils tend to increase viscosity. The lower viscosity, the better cooling and lower dielectric losses [20, 69].	3)b)
4. Flash point	ASTM D 93, ISO 2719	A low flash point may indicate the presence of volatile combustible product in the mineral oils [19-20].	3)b)
5. Fire point	ASTM D 92-12b	Higher fire point and flash point of the mineral oils provide low chance of fire hazard in transformers.	3)b)
6. Pour point	ISO 3016	A low pour point is important, particularly in cold climate, to ensure that oil can circulate and serve its purpose as insulating and cooling mediums [19].	3)b)
7. Interfacial tension	ASTM D 917-99a	A high interfacial tension indicates the absence of undesirable polar contaminants. A rapid decrease of interfacial tension may indicate the compatibility problems between the mineral oil and some transformer materials [20]. An increase in the level of contamination by oxidation lowers the interfacial tension of the mineral oils [19].	2)a)

Table 4.9: Chemical characteristic testing of mineral oils

Property	Test standard	Information	Test application
1. Water content	IEC 60814	High water content causes the lower breakdown voltage of the mineral oils and the sharply ageing of solid and liquid insulation [20]. Low water content is necessary to accomplish the integrity of the mineral oil, low dielectric losses and long term operation [76].	1)
2. Acidity or neutralization number	IEC 62021-1	The higher the neutralization number, the more acid existing in the mineral oils, indicates the degradation of the mineral oils, of the cellulose materials, and points out the corrosion of metal parts [20,85]. The increasing rate of acidity of the mineral oils in service relates directly to the ageing rate.	1)
3. Corrosive sulphur	IEC 62535 DIN 51353	The formation of copper sulphide is believed that it caused numerous failures in transformers and reactors.	3)a)
4. Sediment and sludge	IEC 60422 Annex C	The present of sediment and sludge may lower the heat transfer ability of the mineral oils [20].	2)
5. Particle count	IEC 60970	The existence of particles may indicate the localized overheating and/or breakdown events inside transformers.	2)
6. Oxidation stability	IEC 61125	Oxidation stability illustrates the remaining life time or life expectancy of the mineral oils under service conditions [20]. High oxidation stability is to expect longer service life time [88].	3)
7. Polychlorinated biphenyls (PCBs)	IEC 61619	PCBs in oil causes environment impact [20]. PCBs are regulated in most countries and should not be present in detectable quantities in new mineral oils [19].	3)
8. Compatibility	IEC 61125	It represents the feasibility if mixing unused oils of different origins with oil in service [20].	3)b)

Table 4.10: Electrical characteristic testing of mineral oils

property	Test standard	Information	Test application
1. Relative permittivity	IEC 60247 ASTM D 924	Relative permittivity relates to dielectric losses of the mineral oils.	2)
2. Dielectric dissipation factor (DDF)	IEC 60247, IEC 61620	DDF is very sensitive to the existence of soluble polar contaminants, ageing products or colloids in the mineral oils [20]. Degree of cleanliness and electrical conductivity of the mineral oils are represented by DDF [85].	1)
3. Power factor	ASTM D 924	A higher power factor indicates degradation of the mineral oils which may have contaminant by-products such as water, carbonization, other conducting particles or oxidation products [76].	1)
4. Resistivity	ASTM D 257, IEC 60247	Resistivity may indicate the oxidation acids, contaminants and so on. High resistivity reflects the low content of free ions and ion - forming particles, as well as a low concentration of conductive contaminants [19].	1)
5. Breakdown voltage	ASTM D1816, IEC 60156	A low AC breakdown voltage can indicate the present of contamination such as water or particles in mineral oils [20].	1)
6. Impulse breakdown voltage	ASTM D 3300, IEC 60897	Impulse breakdown voltage strongly depends upon the mineral oil chemical composition especially for the negative polarity mode and rests on the electrode polarity also [1,19].	2)

Note: 1) means a routine test, 2) means a complementary test, 3) means a special investigation test, a) means only needed under special circumstances, b) means not essential, but can be used to establish type identification, [adapted from [20]].

4.2 Partial discharge in mineral oils

4.2.1 PD definition

Partial discharge (PD) is a localized electrical discharge that only partially bridges the insulation between conductors and which may not occur next to the conductor. Generally, PD is a consequence of local stress concentrations in the insulation or on the insulation surface. PD pulses, in general, occur quite irregularly which have a duration of less than 1 μs [54]. PD can be classified as an external discharge and an internal discharge. The external discharge is referred to PD which occurs in ambient air while the internal discharge is due to the imperfections in insulating liquids, in compressed gas and in solid dielectrics. In liquid insulations, PD may take place in gas-bubbles due to thermal and electrical phenomena and in water – vapour which may be created in high field regions [123]. PD initiates the deterioration of the liquid insulation and may develop to the failure of high voltage apparatus. Up to now, the simple PD model comprising a capacitive network is accepted even though this model is not realistic in describing a physical point of view of PD [7,124-125]. This equivalent circuit is also not covered the space charge phenomena [125]. Other PD models such as the dipole model have been proposed by A. Pedersen et al [126]. More details for such dipole model was analyzed by E. Lemke [127].

4.2.2 PD in mineral oils

PD in liquids occurs in the presence of high electric fields. Electrons are accelerated by the electric field and gain energies. These electrons are able to transfer energy to other collided molecules in the vicinity especially single molecules. Then, an ionization or a degradation of the collided molecules may take place. The enhanced dissociation of the electrolyte in the electric field leads to create ions in the bulk of the liquid. A consequence of PD process may be bond scission of the liquid molecules which degrades and splits molecules into a shorter length. Then, a gaseous phase in the liquid dielectric can be formed and a gas-filled void can be generated in the area that PD occurs. The gas pressure in these voids initially is very high due to the phase transition of a certain amount of insulating liquids into the gas phase. The high pressure will expand and reduce until the pressure inside equals the pressure outside the liquid. The metal-liquid interface phenomenon is also one of the main causes for increasing of the conductivity in the insulating liquids. The metal-liquid interface is considered as an accumulation region. Ions may leave this region by escaping over an image force potential barrier. The injection current into the bulk of liquid depends on the applied voltage [128-129].

Charge injection from electrodes: in an equilibrium condition (zero applied voltage), charge layers will be created at the electrode liquid interfaces to ensure that the net electric current is zero. At sufficiently high electric field strength, the transfer of electrons at the electrodes becomes dominating mechanism for electrical conductivity in nonpolar liquid dielectrics. The formation of a double layer with the existence of a weak electrolyte may enhance the injection process into the bulk of the insulating liquid. The electric double layer models have been proposed by some researchers, for example; Helmholtz who proposed the

double layer as a capacitor with opposite charges fixed at a certain distance as shown in Fig. 4.21 a). This model was developed by Gouy and Chapman by considering the diffusive motion phenomena of the counter ions in the liquid. The ions in the liquid are attracted toward the fixed counter ions at the electrode, concurrently thermal motion makes them move into the region of liquid as demonstrated in Fig. 4.21 b). Stern have improved the double layer model composed of no exist ion area next to the metal electrode, then a fixed Helmholtz layer connects with a diffuse layer (Guoy - Chapman) as depicted in Fig. 4.21 c) [95,129-130].

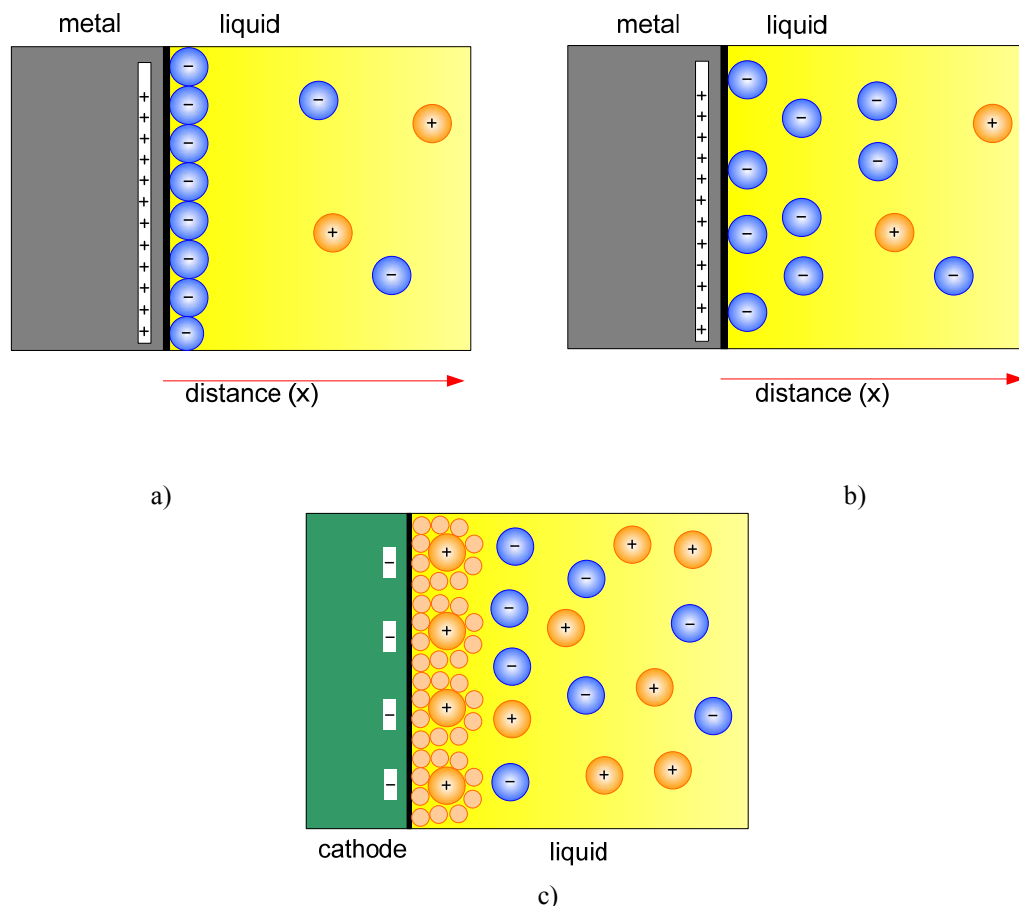


Figure 4.21: Electric double layers

a) a fixed Helmholtz layer b) a diffuse layer c) a refined double layer model [adapted from [95]]

Field emission and field ionization: the generation of charge carriers at the metal-liquid interface under externally high electric field strength of the needle - plane electrode can be explained as following; when the negative polarity at the tip, a barrier is set up between the Fermi level of the electrons in the metal and the bottom of the conduction band, the electron can leave the metal by tunneling through the barrier. In case of positive polarity at the tip, the barrier is set up between the valence electrons of the atoms or molecules of the liquid and the Fermi level in the metal. Electrons can leave from the the atoms or molecules of the liquid once the barrier small enough. In nonpolar liquids, the field strength allowing this process occurring is of the order of 15 to 20 MV/cm. Fig. 4.22 portrays the field emission and the ionization process. The field emission mechanism requires very high threshold electric filed at the electrode tip about 20 MV/cm occurring at very sharp point (tip radius $\leq 0.1 \mu\text{m}$).

The very high electric field causes the local heating in the liquid which has enough energy to generate a bubble nearby the point. For the larger point radii, (tip radius $\sim 1 - 10 \mu\text{m}$), the pre breakdown mechanism is more complex [95,129-130].

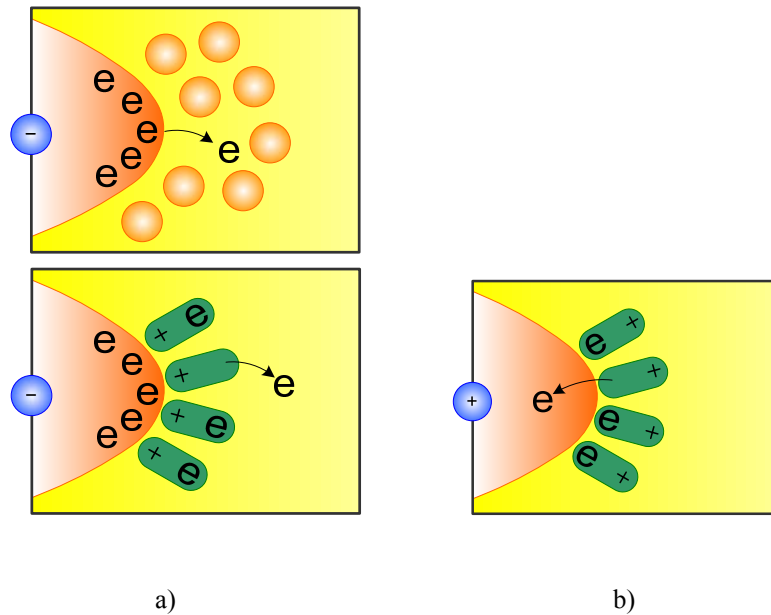


Figure 4.22: Charge generations

a) field emission b) ionization process [adapted from [95]]

When the electric field is high enough, a current pulse is associated with a strong light emission can be observed. After a delay of some ns, a shock wave is detected which is followed by the formation of a single bubble which rebounds several times before it disappears as shown in Fig 4.23. The dynamic of the bubble is governed by the viscosity of the liquid and the injected energy. It is reasonable to assume that the streamer in the liquid grows initially from single bubbles, then electron avalanches [129].

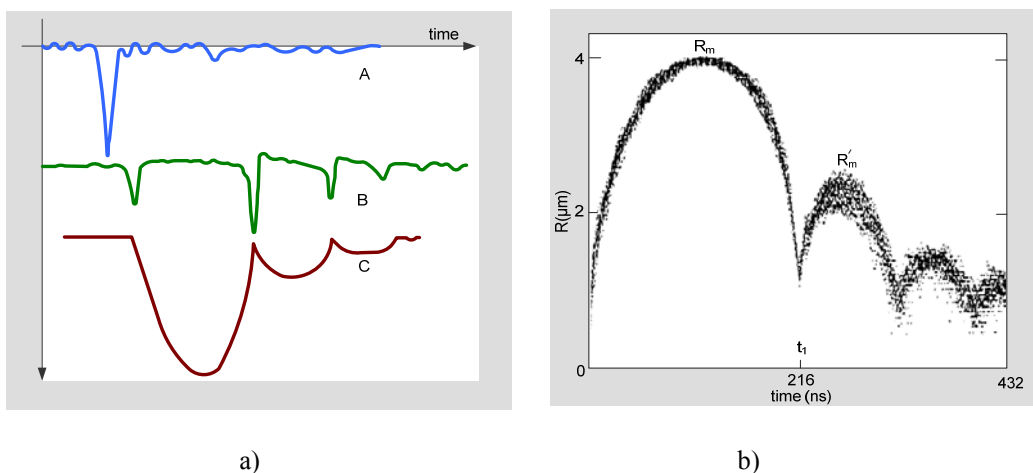


Figure 4.23: Sequence of events when discharge occurs in the liquid dielectric

a) current, emitted light and bubble relation; by which A is the current pulse (= light emission pulse), B is the initial shock wave produced by the current pulse and pressure waves due to successive bubble collapses, and C is bubble dynamics [adapted from [129]] b) Bubble radius against time in cyclohexane for a series of 30 events [adapted from [131]]

PD can appear either in a single pulse typically in the liquid phase, or in the form of a finite series of pulse bursts over a finite time interval, or in permanent discharges. The PD pulse signals can change their shapes due to changes in void sizes, charge injection, the over voltage condition and the physical and chemical degradation of the liquids. Naturally, PDs are dynamic process; every PD is an independent process. However, there is a correlation between consecutive events; every discharge more or less has an influence on the ignition of the next discharge [128,132].

4.2.3 PD sources in mineral oils

PD activity in the mineral oils can be generated by various causes for example micro discharges between conducting surfaces separated by a thin layer of oil, small fixed conducting particles at floating potential that subjected to a localized PD, free moving particles within the insulating oil which can discharge to the conductors, bouncing or rolling conducting particles on a conductive surface, fixed sharp metallic protrusions on high voltage conductors, floating electrodes and so on [133]. H.Borsi and U. Schröder focused on the influence of the water content on the PD behavior of the mineral oil. They reported that the water molecules were assumed to migrate in the direction of the needle electrode due to the higher permittivity of water compared to that of the mineral oil. The voids could initiate PD by distorting the electric field and by acting as impurities. Therefore, the PD numbers should increase with the increasing of the water content in the mineral oil. The average apparent charge decreased with increasing of water content. This was due to the decrease of PD pulse duration and the PD amplitude remained independent of the water content. The PD number decreased with the increasing of temperature which could be explained by assuming that the formation of the space charge at the needle tip was much more difficult due to a higher convection of the oil and also the relative moisture [134].

4.2.4 Predischage or streamer mechanism in mineral oils

A streamer is defined as the pre discharge channel observed in liquid dielectrics. The streamer particularly in the large air gap is considered to have a low conductivity and have a weak luminous emittance [135]. The electrical streamer which is the low density conductive structures can be formed in the region of oils which subjected to the electric field stress in the order of 1×10^8 V/m. After the streamer forming, it tends to elongate, growing form the initial point towards a grounding point. At streamer events, the optical refractive index is different from that of the surrounding liquid. The streamer produces typical shapes of transient currents and emits light signals as well. The streamer is accompanied also by shock waves. The streamer stops when its electric field becomes too small and produces a string of micro bubbles which are dissolved in the liquid. Streamer characteristics of the insulating liquids depend on the rise time and polarity of the applied voltage, the pressure and temperature and the molecular structure of the insulating liquids [135-138]. The streamer can be divided into a positive streamer and a negative streamer depending on the streamer initiated electrode. The positive streamer is initiated from the positive electrode (anode) while the negative streamer is emanated from the negative electrode (cathode).

Positive streamer: the streamer will appear in an umbrella like structure. Generally, the positive streamer in dielectric liquids is about ten times faster than the negative streamer. However, both positive and negative streamer velocity of the transformer oil are relatively in the same range [137]. Furthermore, O. Lesaint and R. Tobazeon demonstrated the observation of fast filamentary streamers and slow bush like positive streamers. The fast filamentary streamers were observed in all experimental configuration studied while the bush like positive streamers, similar to the negative streamers, occurred only in very divergent fields [61]. The positive streamer propagation was determined by the field at the tip of the steamer which was evident by the shadow graph. The positive streamer filaments detected by W.G. Chadband had a typical diameter of 5 to 10 μm . The streamer branches could only take place if there were sufficient tip charges. The greater pulse voltage provided the greater number of initial branches which propagated from the point anode. For the process of the streamer propagation, the negative charges left behind the net positive charges which constituted the new streamer tip of the filament. Behind the tip in the filament, there was the equal mixture of positive and negative charges which caused reducing of the liquid density. Therefore, these mixed charges were highly mobile compared with such charges in normal liquids. The electric field along the filament length caused the moving electrons toward the point anode and positive charges toward the streamer tip [139].

Negative streamer: at low field, the negative streamer structure is similar to the shape of a leafless tree top. The diameter of streamer branches is about 30 to 70 μm . At high field, the streamer appears as a compact bushy structure with many branches [137]. The generation of microscopic gas bubbles ($\sim 10\mu\text{m}$ in diameter) immediately precedes the streamer development. The vaporization of the liquid constitutes the main process of the streamer growth [61]. Negative discharge velocities may be an order of magnitude smaller than positive discharge [119]. D. Linhjell et al. found that the negative streamers in the pure hydrocarbons were less filamentary, more bush like without fine channel, and propagated slower than in the mineral oils or hydrocarbons with electron-attaching additives [140].

Streamer propagation mode: streamers can be categorized in different modes depending on their velocity and the polarity of the applied voltage. The characteristics of streamers such as structure, velocity, current and so on rest upon many factors such as the chemical compositions and physical properties of the liquids, pressure and temperature, the contaminant in the liquids, the applied voltage characteristics such as types of voltage, magnitude, polarity, and the electrode geometry. The positive streamer comprises of three consecutive modes: primary, secondary and tertiary streamer whereas the negative streamer appears into two consecutive stages, primary and secondary streamer [137]. Significant lower breakdown voltage and a greater ability to propagate of the positive streamer cause the most pre breakdown studies focus on the positive streamers [61,135]. However under uniform field of DC or AC, the negative streamer is found that it is responsible for the breakdown event [61]. The streamer mode propagation in the mineral oils can be concluded in Table 4.11 [66]. The streamer propagation process of positive and negative streamers in the mineral oil from starting until breakdown occurs is represented in Fig.4.24. Fig. 4.25 compares the positive streamer and negative streamer propagation of the mineral oil tested by the needle - plane electrode.

Table 4.11: Streamer propagation modes of the mineral oils [66]

Model	Streamer mode			
by Top, Massala and Lesaint	The first mode: very slow streamers	The second mode: supersonic streamers	The third mode: very fast streamers	The fourth mode: extremely fast streamers
by Badent		Primary streamer	Secondary streamer	Tertiary streamer
by Torshin		The first step: "micro crown"	gradual discharge propagation	
For very strong inhomogeneous field	0.1 to 1 mm / μs only for very sharp points ($r < 1 \mu\text{m}$) and at very low voltages	2 to 3 mm / μs normally with self-control by space charges	$\sim 10 \text{ mm} / \mu\text{s}$ starting mode at the tip and also near the counter electrode	$> 100 \text{ mm} / \mu\text{s}$ developed from the third mode, strongly accelerated streamers and it is self-luminous
For quasi homogeneous field	only for negative streamers		only at very high field strength over 50 kV/cm	

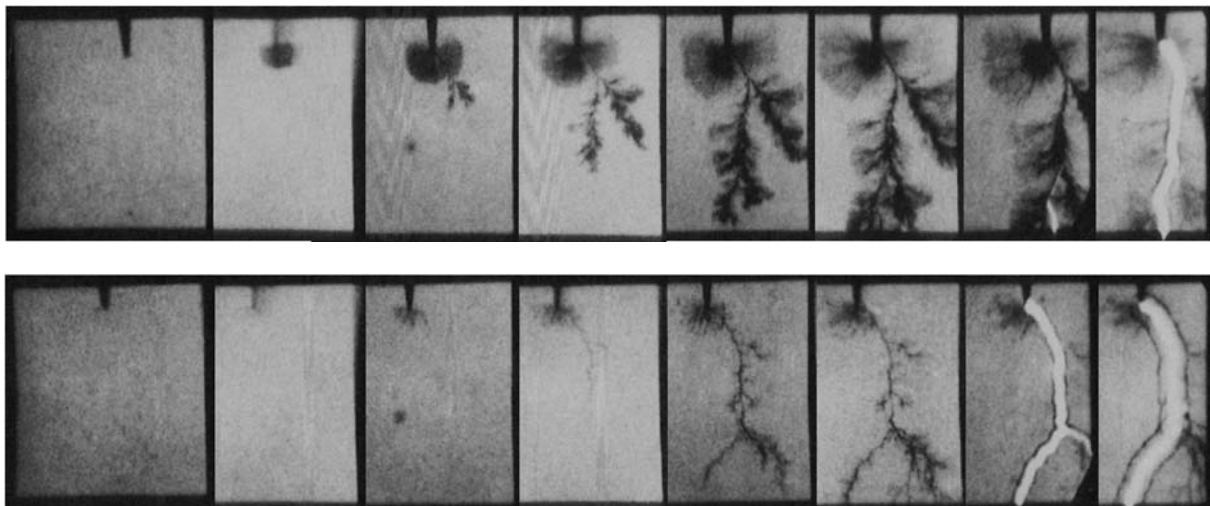


Figure 4.24: Positive and negative streamers of the mineral oils (top and bottom) experimented with the needle-plane electrode system, the streamer modes from left to right [adapted from [66]]

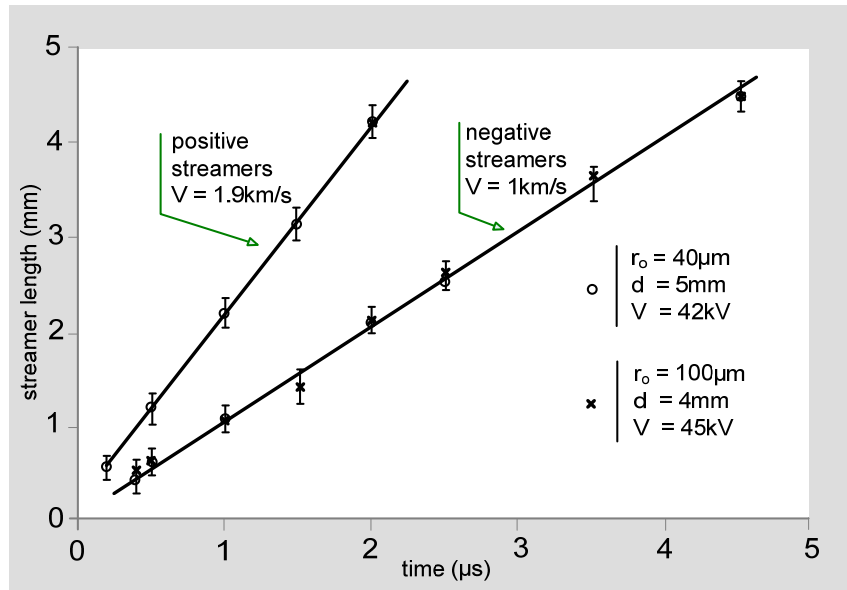


Figure 4.25: Positive streamer and negative streamer propagation of the tested electrode [adapted from [61]]

Streamers under AC stress: For AC voltage, the positive and negative streamers are formed alternatively when the streamer inception voltage is exceeded. The propagation of the streamers depends on the grow rate of the electric field. In case of the needle – plane electrode experiment, the positive streamer starts and propagates toward the counter electrode; the streamer will stop when the applied voltage falls below the extinction voltage. The streamer propagation rests on the streamer tip field strength associated with the tip voltage and its coupling with the plane electrode. Then, as soon as the voltage crosses zero, a negative structure is formed at the tip of the former positive streamer, which simultaneously changes into a negative streamer. The streamer pattern alters during the propagation due to the alternate polarity of the consecutive half wave; the straight branches of the umbrella like positive streamer disappear and several main branches are generated, then the umbrella like structures occur at the tips of bush like negative primary streamers. The fast succession of discharges is presumed that they strengthen the propagation ability of the streamers. The current and emitted light waveforms of both positive and negative streamers of the gap distance of 5-100 cm, long gap distance, are similar to those observed under impulse and step voltage [136-137,141]. The influence of various parameters such as liquid structure, electrode geometry, pressure and temperature, additive are reported in [137,141]. In transformer oils, four positive streamer propagation modes have been categorized which is 1st, 2nd, 3rd and 4th streamer propagation mode. The 1st mode is initiated at the lowest voltage magnitude. The 1st streamer mode is often ignored because it has a low probability of leading to breakdown. The 2nd streamer mode is initiated at the voltage higher than the 1st mode. The 2nd streamer mode initiates at the 50% probability of breakdown. Whereas, the dramatically rising of the streamer velocity is initiated at the 3rd streamer mode at the acceleration voltage. The transitional 3rd mode streamer is dangerous because it can quickly lead to the extremely fast 4th mode streamer with only a small increasing in applied voltage before breakdown happens. The 4th mode is initiated at the highest voltage [66,136-137]. J. George Hwang et al. delineated that the field ionization of the low number density and low ionization energy impurity molecules was the key mechanism for the 2nd mode positive streamer developed in the transformer oils. The motion of free charge carriers, especially the mobile electrons, results in joule heating which raises the temperature of the oil as the wave propagation.

Ionizing of the higher number density molecules creating more space charges leading to a larger electric field enhancement at the streamer tip is the key mechanism for the 3rd streamer [66,136]. A larger electric field causes a more efficient field ionization and also faster streamer propagation [135]. In divergent AC field, streamers always appear at the peak of sine wave, they distribute randomly in time and the inception probability grows exponentially with the applied voltage. Fig. 4.26 illustrates the streamer discharge numbers tested by various needle tip radii and applied voltages. It is found that a discharge increases exponentially with the applied voltage. At low applied voltages, only negative streamers are detected. Above a certain threshold voltage, positive streamers start to appear [61]. Streamers may reach the counter electrode without causing breakdown, although the voltage is still applied. This is because of the low conductivity of such streamer channels [141-142].

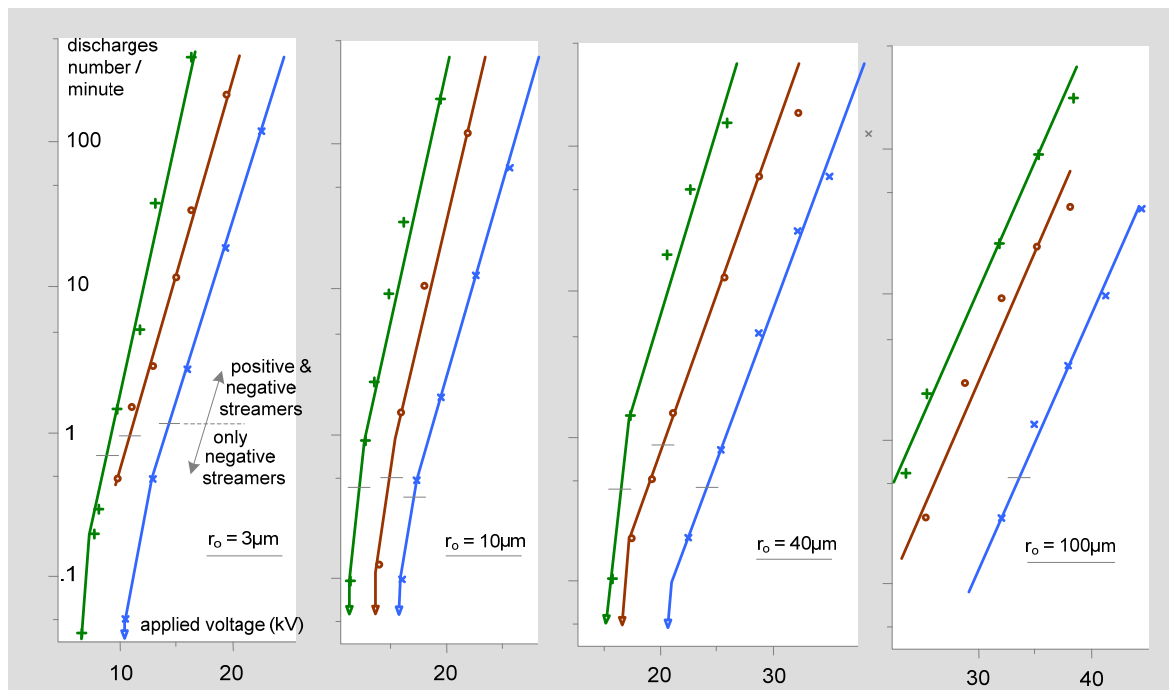


Figure 4.26: Streamer appearance frequency against applied voltage +: $d=5$ mm, o: $d=8$ mm, x: $d=13$ mm; d is the gap distance and r_o is the needle tip radius [adapted from [61]]

With uniform and moderately AC divergent field, all streamers can propagate. The breakdown is controlled by the streamer generation. Most breakdowns are due to the negative streamers because they are first generated. In very AC divergent field, the breakdown is controlled by the propagation of streamers. Therefore, the positive streamer is the mainly cause because it is easily to propagate. In general, the transformer oil is breakdown due to the positive streamers if the test is subjected to a ramp 1 kV/sec. This is because the rate of rise of the ramp voltage is fast enough that the positive streamers can appear and reach the counter electrode whereas the negative streamers occur at low voltage but very low repetition rate < 1 per minute. The streamer phenomena in the transformer oil are very comparable to the streamer phenomena under impulse but happen at the lower applied voltage [61].

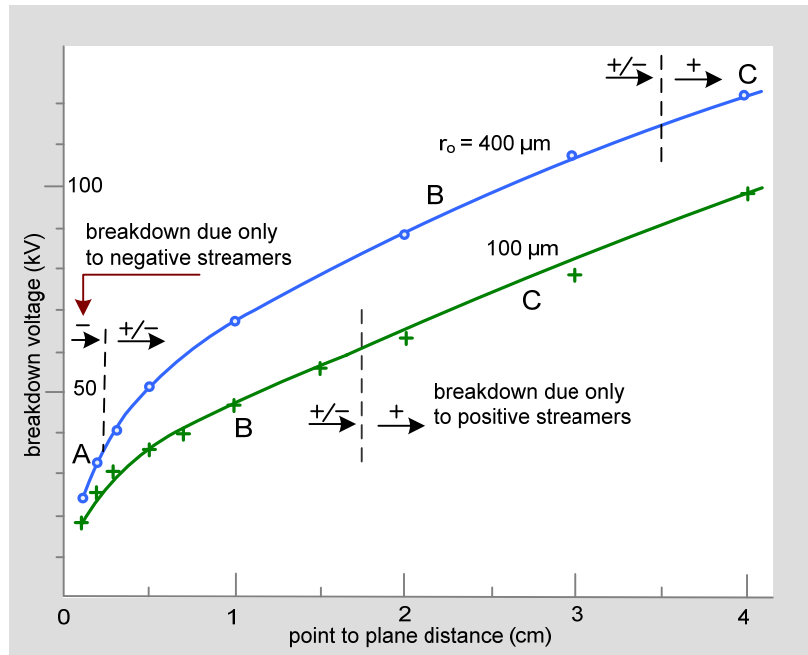


Figure 4.27: AC breakdown voltage of the transformer oil in divergent fields against gap distance (average of 10 measurements) [adapted from [61]]

4.2.5 PD measurement techniques

PD phenomena in the insulating liquids can be examined with various techniques for example one can detect a PD pulse current by measuring the voltage across a low inductance resistor using a fast digitizing oscilloscope. PD charge can be measured according to a PD conventional test circuit. The electromagnetic wave generated by PD can be detected by an antenna. Additionally, the electromagnetic field distribution can be detected by using electric field induced birefringence of the kerr effect. Besides, the pressure wave emitted from the PD phenomena can be detected by an acoustic sensor. Moreover, the emitted light can be detected by a streak camera. Besides, the schlieren optical system can record the discharge phenomena. Furthermore, high speed shadow graph technique can be applied for propagating channel detection [129,137]. Normally, most high voltage laboratories perform the PD measurement according to IEC standard because it can be used for research in laboratory scale and also can service the industrial section.

Basic PD test circuit: electrical signal generated from the PD phenomena of a high voltage apparatus or a test object, C_a , can be measured using the basic PD test circuit as shown in Fig. 4.28.

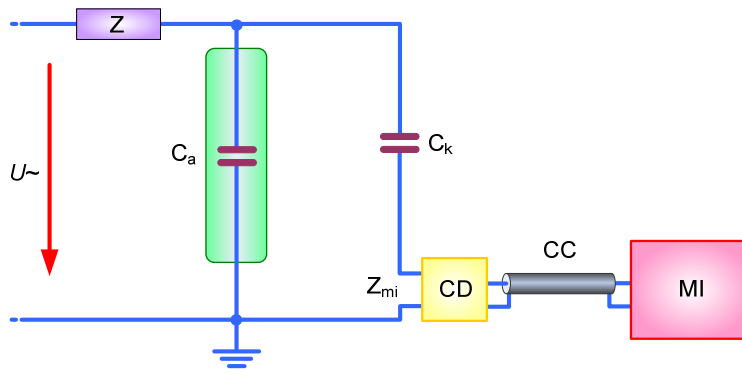


Figure 4.28: Basic PD test circuit [adapted from [54]]

Where: U_{\sim} : high-voltage supply, Z : filter, C_a : test object, C_k : coupling capacitor, Z_{mi} : input impedance of measuring system, CC : connecting cable, CD : coupling device, and MI : measuring instrument

When PD occurs, C_k releases a charge, an apparent charge of a PD pulse, q , to C_a . q is measured as the most fundamental quantity of all PD measurements. The word “apparent” was introduced because this charge is not equal to the amount of charge locally involved at the site of the discharge [7]. Normally, the coupling device can be directly connected with the low voltage arm of the coupling capacitor or can be connected between the high voltage filter and the high voltage arm of the coupling capacitor as depicted in Fig. 4.29. It can be also directly connected with the test object to improve the sensitivity of PD measurement as shown in Fig. 4.30. Using this circuit to measure PD, the coupling device and the measuring system may be destroyed, if the test object breakdowns.

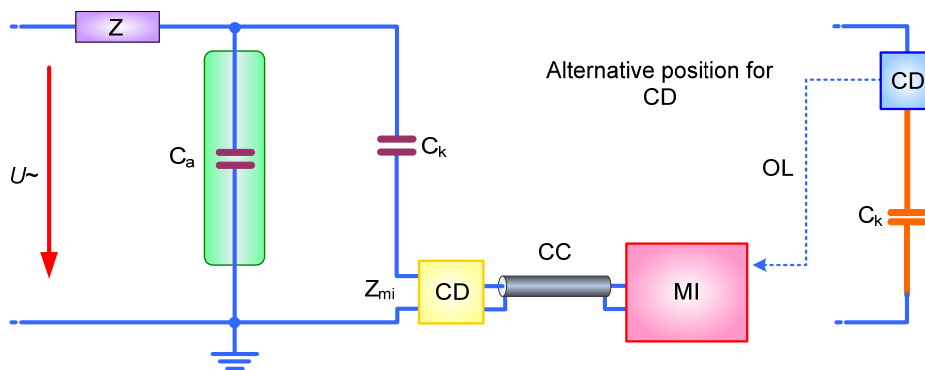


Figure 4.29: Coupling device in series with the coupling capacitor [adapted from [54]]

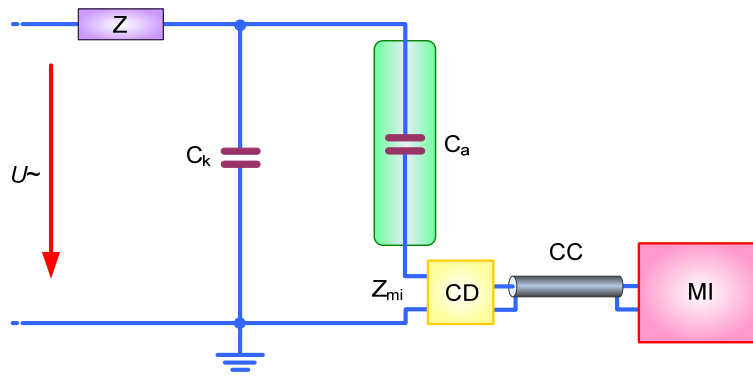


Figure 4.30: Coupling device in series with the test object [adapted from [54]]

Other PD measurement test circuits such as a balance test circuit or a polarity discrimination test circuit are also introduced by IEC to reduce the disturbance which may exist during the PD measurement is performed.

Calibration for PD measurement: the calibration of a measuring system in the complete test circuit is made to determine the scale factor k for measurement of the apparent charge. Because the capacitance C_a of the test object affects the test circuit characteristics, calibration shall be made with each new test object, except the PD experiment is made on a series of similar test objects with capacitance values within $\pm 10\%$ of the mean values. The calibration of the measuring system in the complete test circuit is carried out by injecting short-duration current pulses of known charge magnitude q_0 , into the terminals of the test object. Then, the PD measuring system will be adjusted the measured PD value as the same as the known injected PD value. Two calibration test circuits suggested by IEC are presented in Fig. 4.31.

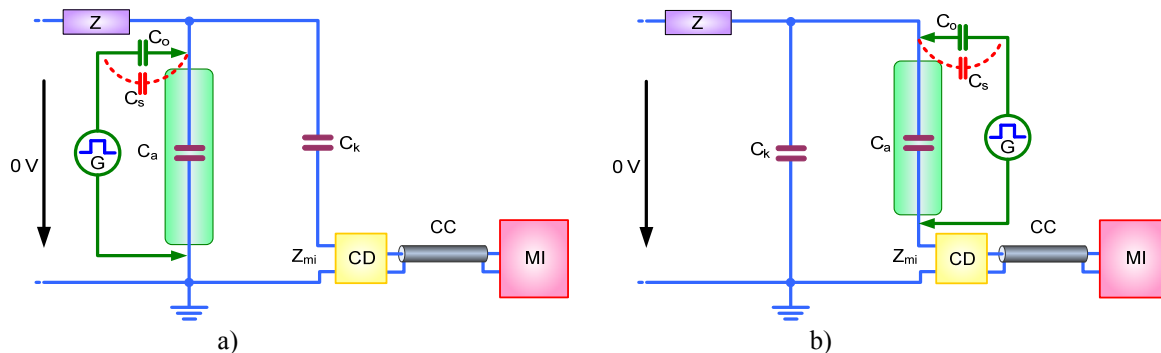


Figure 4.31: Calibration circuits

a) coupling device CD in series with the coupling capacitor b) coupling device CD in series with the test object [adapted from [54]]

Where: $U\sim$: high-voltage supply, G : step voltage generator, C_0 : calibration capacitor, Z_{mi} : input impedance of measuring system, CC : connecting cable, C_a : test object, C_k : coupling capacitor, CD : coupling device, C_s : stray capacitance, MI : measuring instrument, and Z : filter

4.2.6 PD pulse current measurement

A PD pulse current contains useful information associated with the PD mechanism and the degree of insulating dielectric degradation for example; the rise time relates to the period of electron avalanche and the streamer propagation in the process of PD extension. The di/dt may closely relate with the velocity of PD extension. Besides, a time duration of each PD pulse may be used to estimate the probability whether such PD can propagate to the counter electrode or not. Furthermore, a PD current amplitude indicates of the amount of energy which is dissipated in the liquid insulations. Consequently, the PD amplitude and the time duration including the pulse rate are related to some degree of dielectric degradation [143-144]. In liquid dielectrics, the PD pulse burst measured by wide band detector can elucidate the PD phenomena in the cavity. This phenomena is very important to describe the the partial discharge inception process of the liquids. To analyze PD pulse currents, H. Okubo et al. suggested parameters for PD pulse currents as represented in Fig. 4.32 a) where t_r is the rise time, t_f is the fall time. As one can see form the Fig. 4.32 a) that the time scale is in the range of ns because this PD pulse current pattern is firstly proposed for analysis the PD pulse waveform of SF₆ gas. These parameters can be also applied for analysis the PD pulse currents in the mineral oils as portrayed in Fig. 4.32 b) [145].

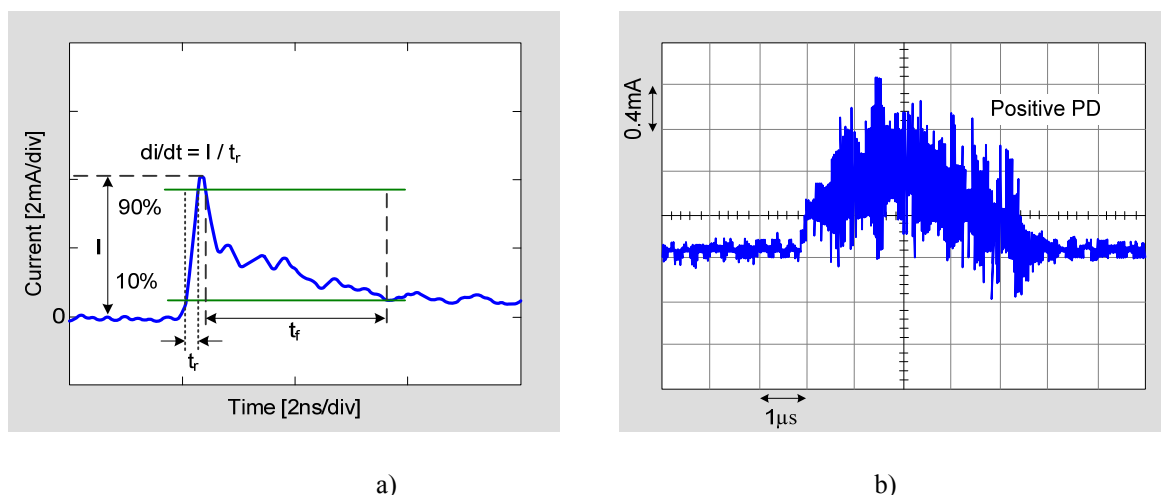


Figure 4.32: PD pulse current

a) PD pulse parameters b) example of PD pulse current in the transformer oil tested by the needle with tip radius of 10 μm , gap distance 30 mm at the applied voltage 30 kV [adapted from [145]]

H.Borsi and U. Schröder have investigated the relationship of PD pulse parameters and the applied voltages of the mineral oil experimented by a needle-plane electrode configuration with the 5 μm tip radius needle. The gap distance under the experiment was varied form 30 mm to 90 mm. The PD pulse current parameters concentrated for their work were slightly different from the aforementioned parameters as shown in Fig. 4.33 a). Four PD pulse current parameters comprised of the PD magnitude (A), the oscillating amplitude (Ass), the pulse length (Ti), and the rise time (T_i) were analyzed. They have investigated also the relationship between the apparent charge (q) and the applied voltage. It was found that the PD magnitude, the oscillating amplitude and the pulse length increased with the increasing of the applied voltage. Besides, the apparent charge depended strongly on the applied voltage. This research

group suggested that a composition of each PD pulse from some single discharges was random and was limited by the size and the number of available voids. Additionally, space charge effects caused the maximum field located in the oil volume which was not at the needle tip. The investigation results are shown in Fig. 4.33 b) - d) [146].

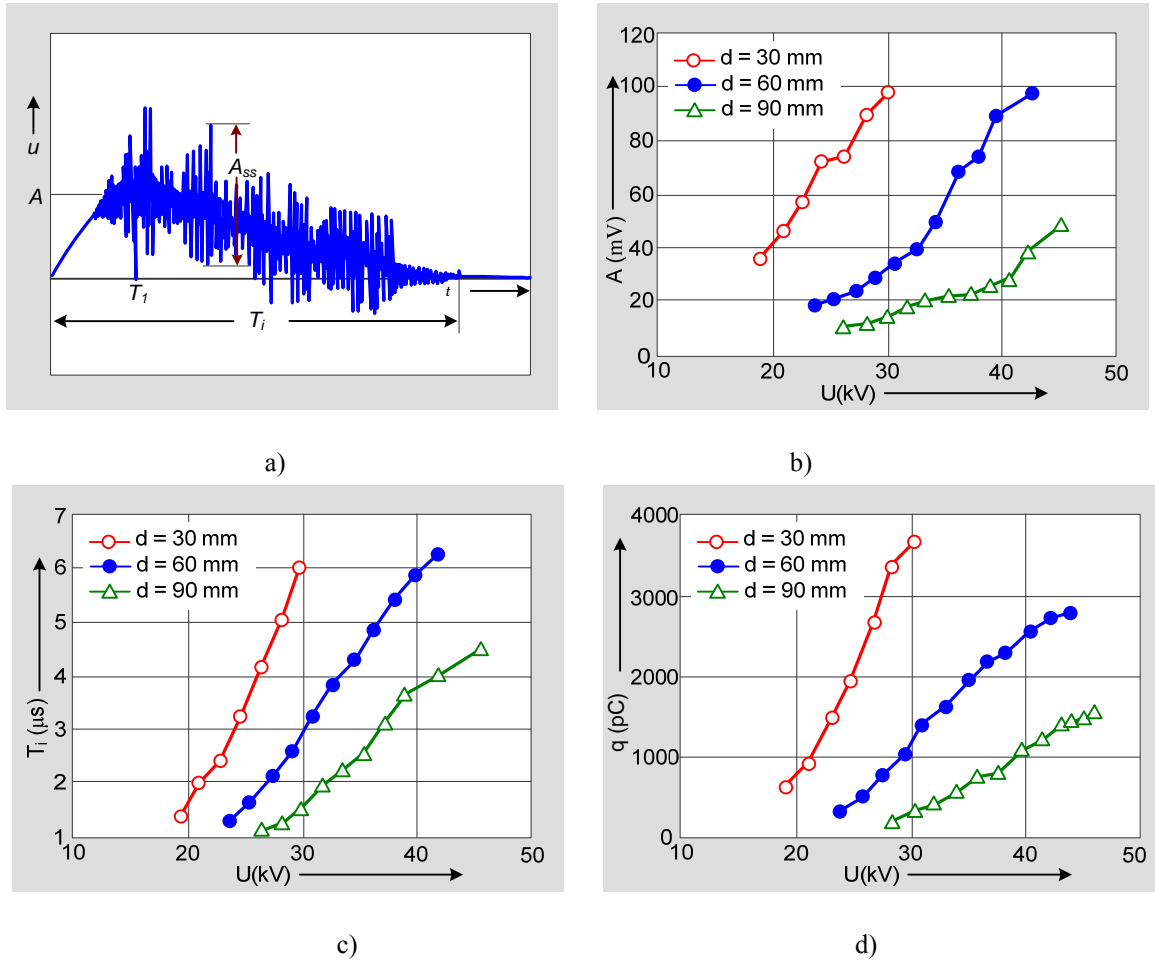


Figure 4.33: PD pulse current and apparent charge characteristic

a) investigated PD pulse parameters b) pulse magnitude (A) versus the test voltage c) PD pulse duration (T_i) versus the test voltage d) apparent charge(q) versus the test voltage [adapted form [146]]

PD pulse characteristics of the mineral oil have been an interesting topic because it can be measured by using a normal measuring apparatus in the laboratory. To analyze the PD pulse current measurement technique, M. Pompili et al. compared three types of the measuring system composed of an inductive or current probe (Tektronix type CT -1), an active probe (the field effect transistor, FET), and a resistive probe. They found that the resistive probe provided a slightly better pulse shape compared with other current measurement techniques [147]. Furthermore, in 2011, H. Moulai et al. delineated the positive current waveforms obtained from the mineral oils at different applied test voltages. Moreover, this research group compared the current pulse waveforms acquired from the mineral oil and other liquid dielectrics tested by a $10 \mu m$ tip radius needle- 40 mm diameter circular disc electrode as exhibited in Fig. 4.34. The typical PD pulse waveforms of each kind of liquid dielectrics seem to be relatively similar [144].

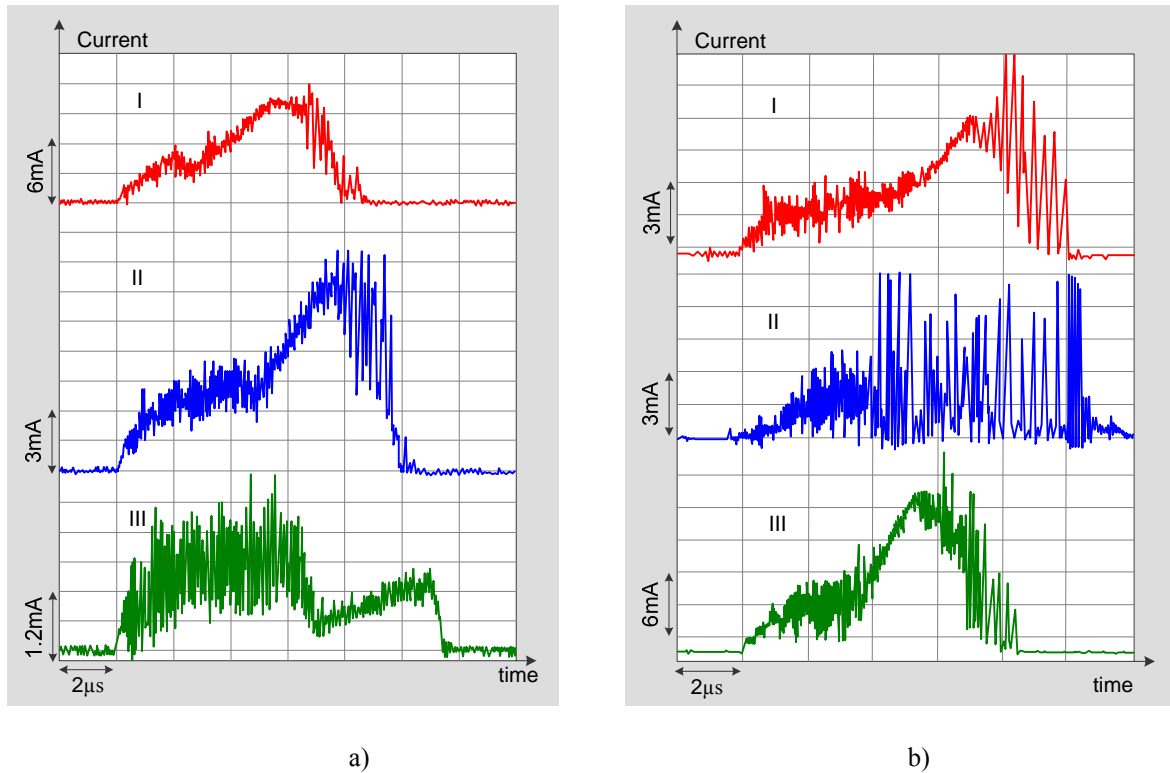


Figure 4.34: Typical positive pulse currents

a) in mineral oil: I) gap distance 7 mm, test voltage 26 kV, II) gap distance 10 mm, test voltage 28 kV, III) gap distance 18.5 mm, test voltage 28 kV, b) in different liquids at gap distance 10 mm, test voltage 25 kV: I) mineral oil II) Toluene III) Tetra-ester [adapted from [144]]

4.3 Partial discharge inception voltage

Partial discharge inception voltage (PDIV) is an important parameter which is utilized to describe the behavior and the ability of the insulating liquids to prevent or suppress partial discharges when the liquids are submitted to high electrical stress. PDIV value can be applied for the purpose of quality assurance, specification, product development and condition monitoring of the insulating liquids. Based on the momentary knowledge, PDIV in liquids is considered to be mostly related to their chemistry and relatively little affected by the liquid conditions. Generally, PDIV testing provides some advantages compared to traditional electrical characteristic testings of liquid dielectrics, for example; the PDIV test is virtually nondestructive test so the PDIV test can be performed with a large number of testing on a single sample of the liquid. Moreover, the PDIV test is easier to perform than breakdown voltage test [55].

4.3.1 PDIV definition

According to IEC 60270, PDIV is defined as the applied voltage at which repetitive PDs are first observed in the test object, when the applied test voltage is gradually increased from the lower value at which no PD is observed [54]. In practice, the partial discharge quantity must be obviously determined. At the early period of PDIV standardization, PDIV was defined as the lowest voltage at which the discharge magnitude greater than 500 pC occurred; simultaneously, the average discharge numbers per minute of 10 to 20 took place. The needle-plane electrode was first proposed for the PDIV testing [148]. Nevertheless, M. Pompili et al. argued that the specified charge value may not be suitable because under AC applied voltage which produced such high amplitude charge, a hundreds of smaller PD amplitude should be detected before [58]. Moreover, the specified charge value as the PDIV criterion was relatively high. In 1993, IEC TR 61294 was published to describe a test procedure to measure PDIV of the insulating liquids. IEC TR 61294 has specified the PDIV as the lowest voltage at which PD occurs of an apparent charge equal to or exceeding 100 pC, when the sample is tested under the specified condition [55]. However, the validity and sensitivity of this standard PDIV measurement technique is questioned [6]. Considering the signals emitted from the PD sources, there are many kinds of detected signals such as an electrical signal, electromagnetic wave, pressure wave, audible signal and emitted light. Therefore, PDIV definition can be established in many aspects depending on the PD signal detection techniques. Other than the PDIV definition according to IEC TR 61294, PDIV definition can be defined with a particular criterion. Examples of common definitions of PDIV are as following:

1. The applied voltage at which the number of specified pulse bursts per unit of time is detected. For example, the PDIV can be defined as the applied voltage at which one PD pulse burst is detected over an interval of 10 minutes.

2. The applied voltage at which the PD burst pulses recur at the rate of one or more over a specified period of the applied voltage is detected. According to this concept, the PDIV may be determined as the applied voltage at which one or more PD pulse bursts is detected over one cycle of the applied voltage.

3. The applied voltage at which a specified apparent charge recurs at the rate of one or more over a limited cycle of the applied voltage is detected. Conforming this idea, one may be defined the PDIV as the applied voltage at which a specified apparent charge ≥ 50 pC recurs regularly at least one or more PD over 10 consecutive cycles of the applied voltage is detected.

4. The voltage at which the first optical evidence of a streamer appears. This definition is widely used for the streamer formation and mechanism researches. This phenomenon will be detected by optical techniques by which the simple, transparent liquid such as n-hexane, toluene, methyl siloxane and the mineral oil are utilized for the experiments. While the most technical fluids used in high voltage apparatus are used for PD phenomena research of liquids or in solid-liquid interface including the liquid degradation characteristics and PD monitoring techniques [149-150].

To defined the PDIV definition, it must be realized that the specified PD value or PD pulse rate must not too high by which they can cause unintentional breakdown during the PDIV test is performed.

4.3.2 Partial discharge inception mechanism

General idea of the PD mechanism from starting process, developing to be a streamer and then leading to breakdown in the mineral oil gap is described in 4.2.2- 4.2.4. In this section, the first PD pulse burst mechanism will be focused which are documented in [151-157]. PD in the liquids occurs in gaseous cavities under sufficient electric field stress of the liquids. The high electrical stress regions may occur at protrusion or asperity points of the metallic surfaces. The asperity cross sections where charge injection and subsequent cavity formation can take place have been estimated to range from 10 to 100 nm². The incipient micro streamers in the liquid phase cause the vaporization in liquids and the resulting pressure wave that causes the cavity formation. This cavity expands and the PDs occur inside the cavity. Heat generated by the discharges causes further vapor production. The cavity expands continue and collapses finally when its internal vapor pressure falls to or below the ambient hydrostatic pressure within the dielectric liquid. PD in the insulating oils appears in the form of pulse bursts which compose of a series of discrete current pulses occurring over a finite time interval of a few μ s or more. The typical PD discharge pulses in the minerals oil are illustrated in Fig. 4.35. The duration of the pulse burst is approximately 1 to 5 μ s. In dielectric liquids, the existence of PD pulses and their recurrence rate are more erratic.

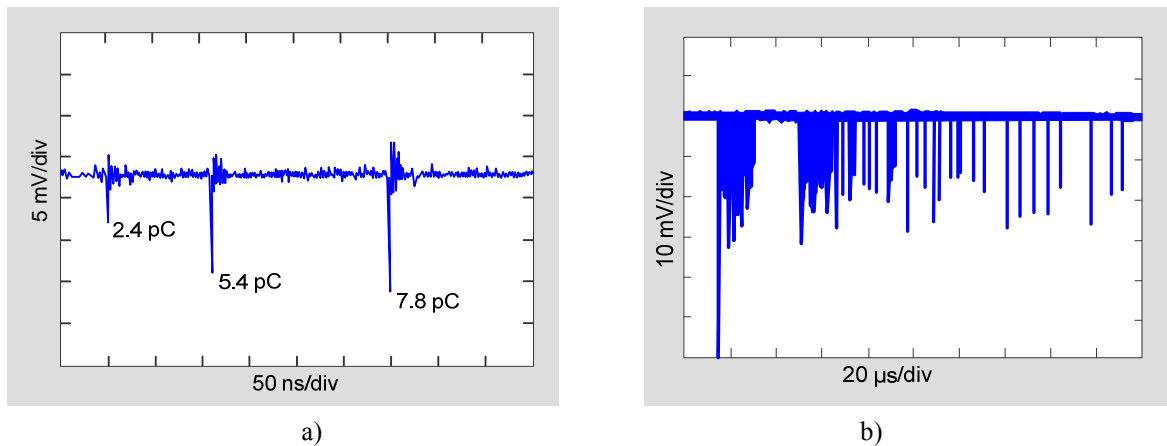


Figure 4.35: PD pulse currents in the mineral oil

a) typical PD pulse burst behavior b) irregular PD pulse burst characteristic [adapted from[149]]

As the cavity expanding in the AC field, the applied voltage which crosses the cavity is determined by the capacitive division proportion between the cavity capacitance and the dielectric capacitance. Over the period of a pulse burst, the voltage across the cavity will be changed due to the changing of capacitive cavity caused by the expanding of the cavity's size. The voltage across the cavity will be modified with the counter field or the residual voltage generated by the deposits charged form the previous PD pulse, which does not leak away entirely. The expansion cavity may not be discharged completely at the first or second time

because of the finite conductivity of the cavities' wall. When the voltage across the expanding cavity becomes equal or exceeds the breakdown voltage of the cavity, the cavity will start to breakdown. This breakdown can happen many times in the expanding cavity until the cavity abruptly collapse. Taking to account for the pressure in the expanding cavity, from theoretical calculation, the pressure in the cavity must be extremely high for example 10 MPa or can reach to 50 MPa in order to generate the sufficient charge density to support ionization process in the cavity complied with Paschen's law. The vapor pressurized cavities are estimated to range between 2 to 10 μm radius. The 10 μm cavity size is defined experimentally under AC condition in the transformer oils. The 2 μm cavity size having a cylindrical shape is estimated for the second discrete PD pulse within the PD pulse burst. If the applied voltage across the field intensified region is maintained at the PDIV level, the vapor pressurized cavities will persist in reappearing and disappearing likely without leading to breakdown streamer formation. Ideally, the discrete PD pulse sequence within a pulse burst comprises of a series of monotonically ascending magnitude PD pulses with gradually increasing separation times between the successive pulses in the pulse train. The magnitude of the discrete discharge pulses within the pulse bursts relies on the AC breakdown voltage of the cavity. In practice, some phenomena may be observed such as the magnitude of the first pulse may significant higher than that of the second pulse. The number of discrete pulses in each pulse burst and the magnitude of the pulses increase with increasing the applied voltage level. The average pulse burst duration(lifetime of the transient cavity) increases slightly with the increasing applied voltage. The magnitude of the apparent charge determines the amount of energy dissipated by the pulse burst and associates with the degree of degradation in the mineral oil due to the presence of PDs. The successive discrete discharge pulses do not always have the magnitude greater than the preceding ones at each of different test voltage levels. Because the cavity is not necessarily expanding regularity in size or the discharge is not always across the largest separation of the cavity. Occasionally, the PD pulse burst may contain only a single pulse which implies that the vapor cavity formed have abruptly collapsed. However, the magnitude of the last pulse is frequently somewhat smaller than that of the preceding pulse. This is due to after the cavity reaches its maximum expansion diameter, the cavity has began to collapse and the PD extinction commences. The most observation reveals that the most frequency appearance of a single pulse within the pulse burst is positive discharge pulses. This observed phenomena is anomalous behavior. The sum of the individual discrete apparent charges of each PD pulse burst tends toward the value of apparent charge measured by means of a narrow band detector. Furthermore, it has been reported that under AC condition, the apparent charge associated with the discharge pulses in dielectric liquids were in a range of 10 -200 pC and most discharge pulses occurred at or close to the applied voltage peaks. Up to now, There is no definite relation between amplitude growth and increasing applied voltage. Sometimes a PD of large amplitude can observed with a low applied voltage. This is possible as a result of a random movement or other particles in contact or near the electrode surface [151-157]. PD pulse bursts at PDIV and above PDIV level are depicted in Fig. 4.36 and Paschen's law diagram is presented in Fig. 4.37.

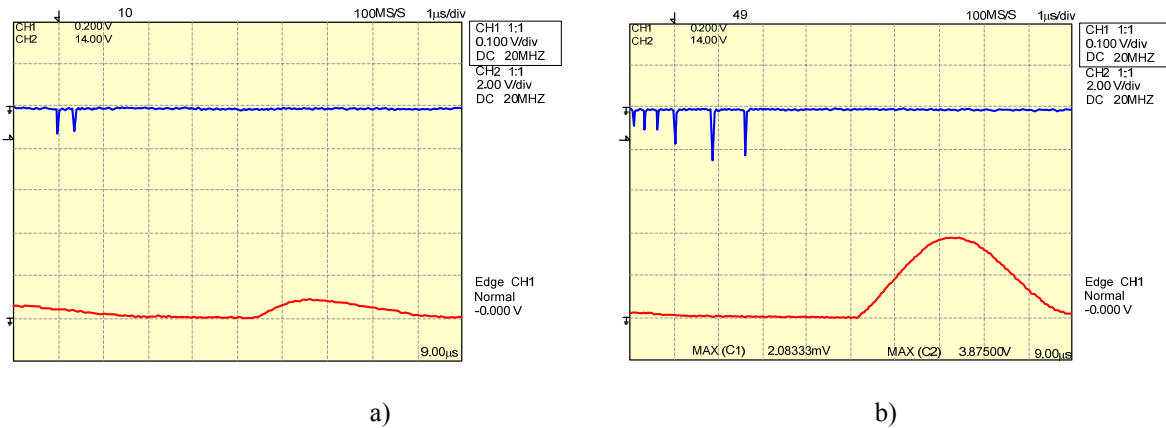


Figure 4.36. PD pulse bursts at PDIV and above PDIV level

a) at PDIV (30 kVrms) lower trace: narrow band system integration pulse 6.4 pC, upper trace: discrete PD charge (left to right) 3.2 and 3.2 pC b) at 3 kVrms above the PDIV, lower trace: narrow band system integration pulse 30.4 pC, upper trace: discrete PD pulse charge (left to right) 2.8, 2.8, 3.5, 5.5, 8.3 and 7.6 pC [adapted from [151]]

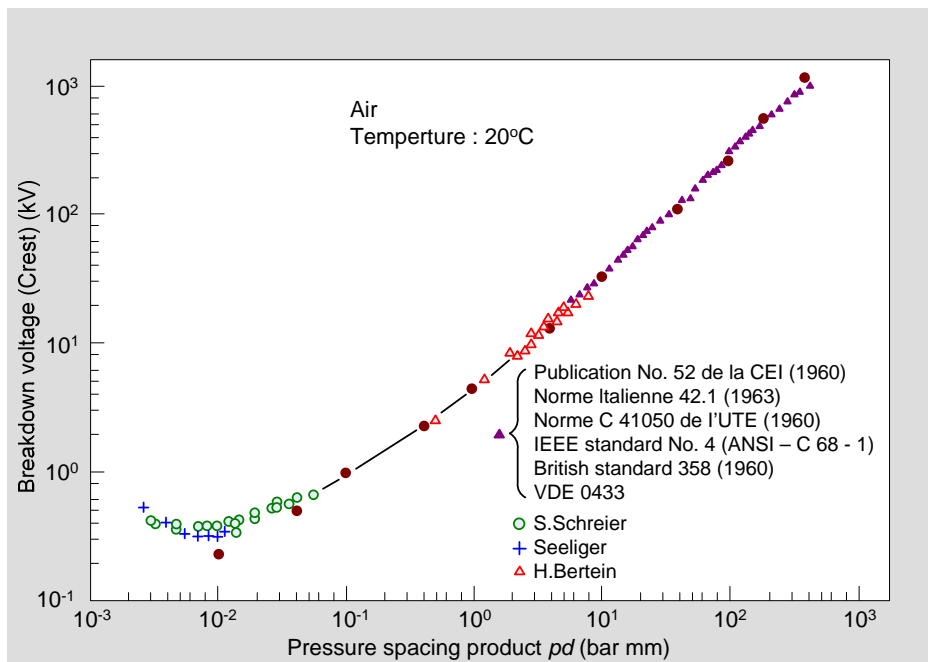


Figure 4.37: Paschen's law diagram [adapted from [7]]

4.3.3 Electrode configuration for PDIV measurement

Two types of electrode configurations have been widely used for PDIV research which comprises of a needle-plane electrode and a needle-sphere electrode system. A needle-plane electrode configuration has been introduced for PDIV testing at the beginning period of PDIV testing standard development as shown in Fig. 4.38 a). The PDIV test cell comprises of a needle and a plane electrode with gap distance of 70 mm. This gap distance provided virtually no risk of obtaining a breakdown. A metal point of radius 3 or 50 μm and a 90 mm diameter ground plane electrode with rounded edge had been introduced [148]. However, the needle -

sphere with the needle tip radius of 3 μm and sphere diameter in the range of 12.5 -13.0 mm has been selected to be the standard test electrode for PDIV measurement of the insulating liquids as portrayed in Fig. 4.38 b). The point - sphere electrode has been proposed for PDIV testing because it is relatively independent of such contaminants such as moisture and particles. This is because the critical high field condition is present within only a very small volume of the liquid under test [55]. However, the point-plane electrode is reinterested by IEC TC 10 due to its ability to provide the higher electric field stress at the needle tip [59].

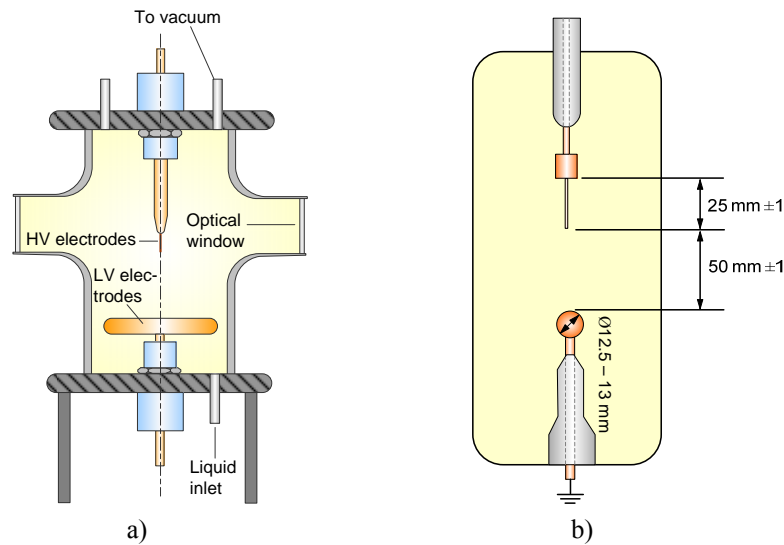


Figure 4.38: Electrode configurations for PDIV measurement

a) a needle-plane electrode system [adapted from [148]] b) a needle-sphere electrode system [adapted from [55]]

A needle - plane electrode configuration: this electrode configuration is widely used to investigate the physical phenomena of discharges. It gives high local electric field stress to simulate a local PD site. The electrode system should have high sensitivity to a small bubble discharge. Furthermore, the electrode system must withstand high mechanical and thermal stress which may occur during PDIV or PD testing. Examples of using the needle-plane electrode systems for PDIV and PD measurement have been reported in [67,158-161].

Electric field characteristic of a needle - plane electrode configuration: when the voltage is applied to the electrode system, the electric field strength occurring at the tip of the needle can be simply calculated by using a well-known equation derived by assuming that the needle tip is as the hyperboloid shape.

Electric field at tip of the needle can be computed by using the equation (4.22) [162].

$$E_{\max} = \frac{V}{r \ln \{2(a/r)^{1/2}\}} \quad (4.22)$$

Where: E is the electric field at the tip of the needle,

V is the applied voltage,

r is the radius of curvature at the apex,

a is the distance of $g + r/2$, g represents a gap distance of the electrode system.

In practice, electric field stress calculated from equation (4.22) is higher than the electric field at the tip of the experimented needle because the needle used for high voltage experiment needs to be supported by a high voltage supporting rod which reduces the electric field at the tip of the experimented needle as explained by W. Pfeiffer et al[163]. Furthermore, the field calculation carried out under AC without taking space charges into account is clearly overestimated [164]. Electric field to generate PDIV depends on the needle tip radius as reported by H. Yamashita et al.[165]. From Fig. 4.39, the smaller needle tip radius needs higher inception field to generate PDIV.

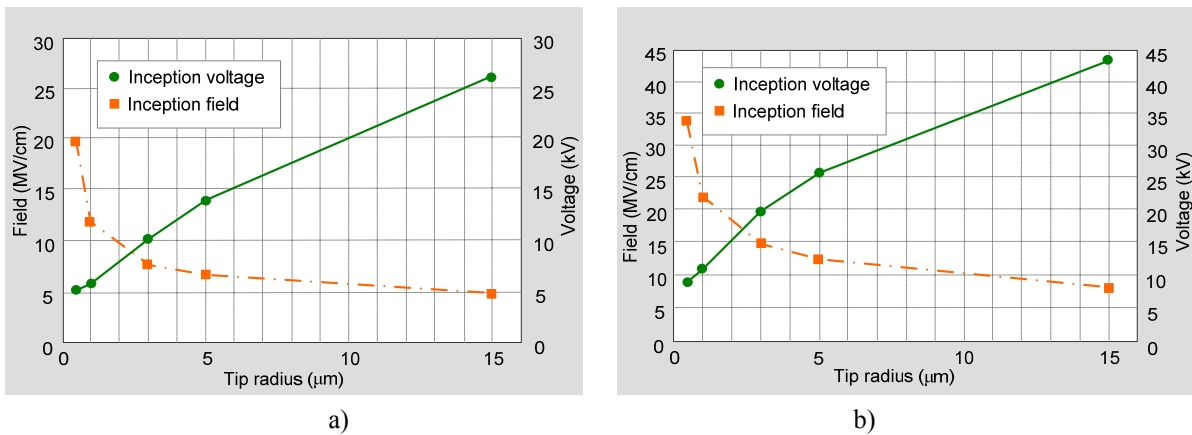


Figure 4.39: Streamer inception field strength and voltage versus tip radius in cyclohexane for a) a negative point-plane b) a positive point-plane electrodes [adapted from [165]]

To compute the electric field pattern including the maximum electric field strength at the needle tip is sophisticated and laborious work, therefore, Finite Element Method (FEM) software is a very useful tool to analyse such electric field phenomena.

Streamer characteristic against needle tip radius: In liquids, the streamer type (configuration and speed) depends on the applied voltage and the tip radius as illustrated in the schematic diagram in Fig. 4.40. In zone one, slow streamers with the velocity below 1 km/s are observed. Such streamers normally do not propagate far which are rarely to induce breakdown. In zone two, the filamentary streamers with a high velocity of over 1 km/s can be detected. These streamers can propagate longer distance and can lead to breakdown in the liquids. Above the critical point tip radius, r_c , a slow streamer cannot be observed and the voltage required to initiate a streamer is higher than a critical applied voltage, V_p .

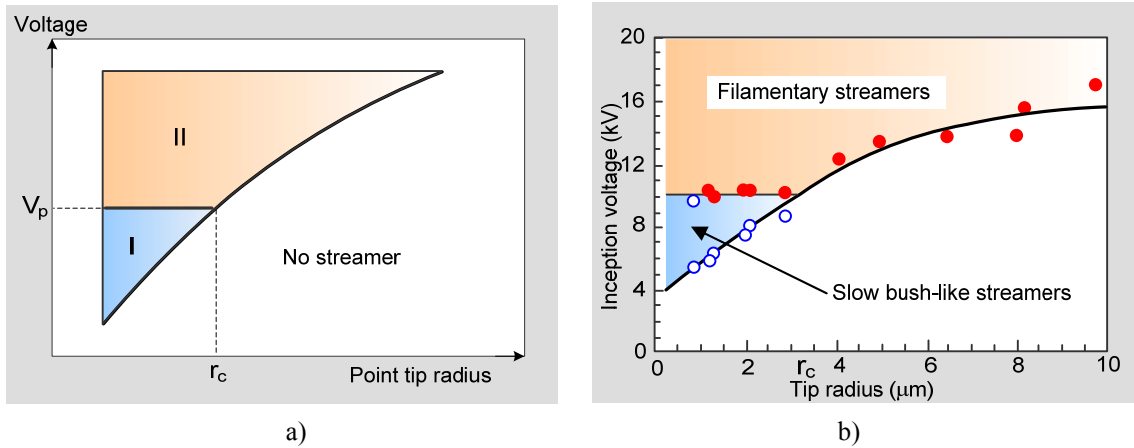


Figure 4.40: Relationship between positive streamer characteristics with the streamer inception voltage and needle tip radius

a) general idea [adapted from [166]] b) from the test experiment with the gap distance of 2.5 mm [adapted from [167]]

To compare the streamer characteristics of both positive and negative streamers, H. Yamashita et al. pointed out that for positive streamers, the streamer configuration changed from the bush like to filamentary with the increasing the tip curvature or the applied voltage. Whilst the structure of negative streamers changed from spherical to pagoda like and bush like with increasing the applied voltage or tip curvature. A slim channel connecting the streamer with the needle tip was observed for a tip radius larger than 5 μm . The experiment utilized the tungsten needles with the tip radius of 0.5-15 μm and nickel plane electrode of 35 mm with gap spacing 5 mm in cyclo-hexane [168].

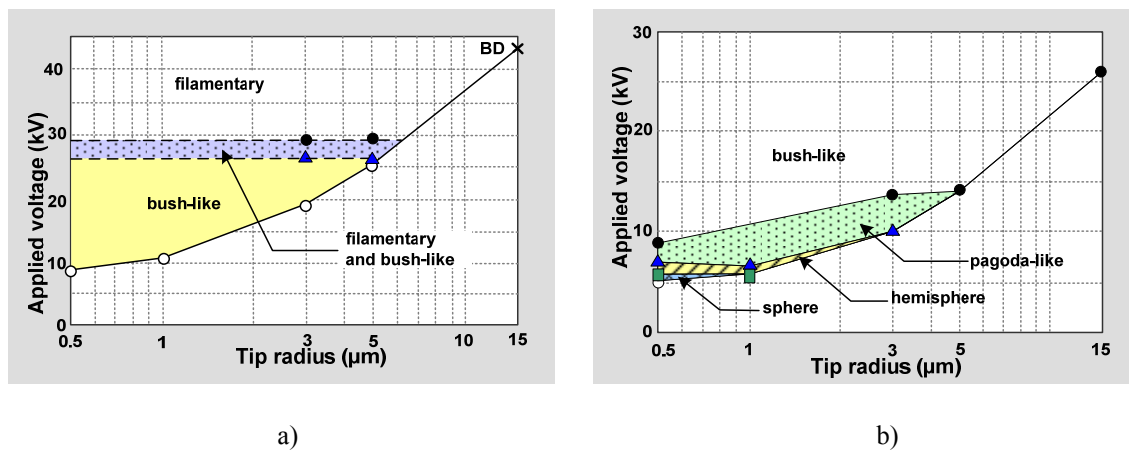


Figure 4.41: Variation of streamer structures versus tip radius

a) positive streamer b) negative streamer [adapted from [168]]

Mechanical and thermal characteristics of a needle - plane electrode configuration: Apart from high electric field stress at the tip of the needle, the needle has to withstand high mechanical and thermal stress. Erosion property of the tested electrode is a fundamental indicator to verify the mechanical property as well as the thermal property of the needle-plane electrode configuration. The erosion of the needle occurred between PDIV testing affects the

successive PDIV test values. No erosion or damage at the needle tip is required to maintain the same electric field stress pattern. A few papers have reported for such erosion problem after the needle was used for insulating liquid testing. P. Rain et al. have identified that the 3 μm tip radius stainless steel needle was gradually increased up to 5 μm after the occurrence of many streamers [169]. Furthermore, the mechanism of the needle tip erosion including the deformation at the tip of the needle was reported by R. Kattan et al. They used the needle - plane electrode configuration with the needle tip radius of 0.5-10 μm , gap distance of 0.5-3 mm which were subjected to a negative pulse voltage in the range of 5 -10 kV. The erosion was presumably a consequence of cavity erosion phenomenon attributed to the pressure pulse related with the bubble collapses [170]. Another case of the needle tip distortion was proposed by S. Patrissi et al. This needle was used for impulse testing and it was destroyed after standard lightning breakdowns [171].

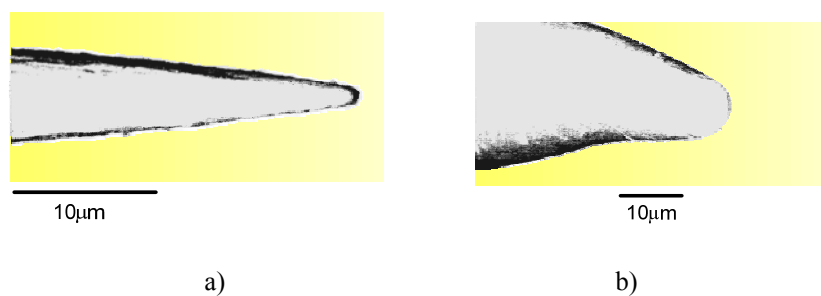


Figure 4.42: Needle profiles

a) before testing b) after an experiment [adapted from [170]]

4.3.4 PDIV measurement

PDIV test method: PDIV test procedure has a great effect on the PDIV value. According to IEC TR 61294, the test voltage is increased with a rate of 1 kV/s from zero until PDIV occurs (at the first voltage that $\text{PD} \geq 100 \text{ pC}$ is defined as PDIV). Then, the PDIV is recorded. Each needle is tested ten times. After that, the PDIV mean value of the tested liquid will be computed. Alternatively, M. Pompili et al. have proposed the applied step voltage to perform the PDIV experiment. The PDIV definition is altered to the lowest applied step voltage at which the PD pulse bursts recur at the rate of at least one PD burst over a period of 10 minutes. The applied voltage is raised in steps 2kV/step and each step is maintained for 10 minutes [151]. E. O. Forster has also employed the applied step voltage for PDIV testing. He experimented with 2kV/step applied voltage lasting 2 minutes of each step. The procedure was repeated 3 times with a rest period of 5 minutes between cycles. A minimum of 3 measuring cycles represented a compromise between the need of several determinations such as statistic requirement and the deleterious effect of each PD on the tested liquid dielectrics. However, he found that the lack of reproducibility of individual measurement was noticeable at all applied voltage of the experiment [172]. The mentioned retest number for PDIV testing by applying the step voltage conformed to the PDIV experiment carried out by M. Pompili. Furthermore, M. Pompili had varied the testing time of each applied step voltage with 2 and 5 minutes. He found that the experiment gave the similar test results [58]. Recently, X. Wang et al. modified a PDIV test method by utilizing the step voltage application with 1kV/step. This method gave the lower PDIV compared with the PDIV value obtained from the PDIV

testing standard according to IEC [6]. The applied step voltage method for PDIV measurement can be taken into account that the maintained voltage of each step represents the time required to initiate a cavity formation in the dielectric liquids. Moreover, the maintained voltage of each step for a testing period can simulate the real situation of the high voltage equipment operation subjected to a certain operating voltage level not a ramp voltage.

PDIV measurement technique: PDIV measurement technique is very closely with the PDIV definition. To perform PDIV experiment complied with IEC standard, one can set up the test circuit according to IEC 60270. Then, PD charges can be measured by a narrow band PD detector. In addition, M. Pompili et al. have proposed the dual wide/narrow band PD detection system for PD pulse current measurement. This aforementioned PD detection system consists of a wide band detector functioned to record the discrete PD pulses within the PD pulse burst in a combination with a conventional narrow band PD detector used for integrating the charge transfers of the individual pulse within the pulse burst [59]. Moreover, O. Lesaint et al. have studied the streamer inception in mineral oils by detecting the first streamer light emission using a photomultiplier. They measured the streamer inception frequency per minute as shown in Fig. 4.43. They concluded that it was impossible to define an inception voltage. Only the voltage value corresponding to an arbitrary discharge frequency such as 1 streamer/minute can be used to define PDIV.

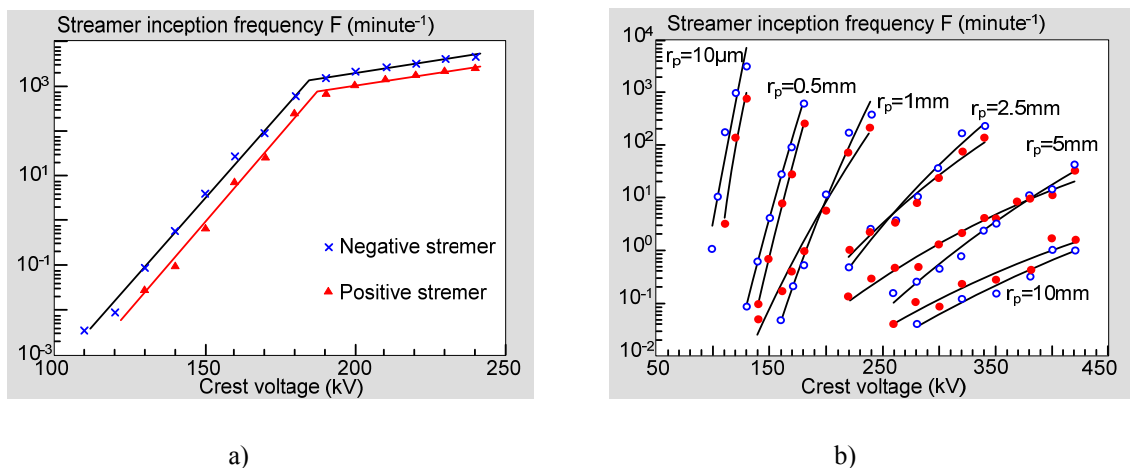


Figure 4.43: Streamer inception

a) inception frequency of positive and negative streamers in the oil without filtration, 20 ppm water content, Rod radius = 0.5 mm, gap distance = 40 cm b) streamer inception frequency versus voltage with different electrode radius r_p (40 cm gap distance, open dots: negative streamers, full dots: positive streamers) [adapted form [40]]

The streamer inception investigation by detecting the emitted light has been performed also by some researchers such as H. Yamashita et al [165].

4.3.5 Factors influencing PDIV and PD activity

There are some factors which affect PDIV and PD activity as following:

gap distance: B.Fallou et al reported that for small gap distance, PDIV and breakdown voltage merged together, and at the gap distances of 3 to 4 cm or longer, discharge was observed at the voltage lower than the breakdown voltage [148]. Furthermore, E. O. Forster

studied the effect of small gap distances on PDIV value, he addressed that the PDIV tested with the point-sphere electrode configuration with the needle tip radius of 30 μm and the 12.5 mm diameter sphere and gap distance of 10-25 mm was relatively the same. This finding led to summarize that the PDIV depended on not only the local field at the needle tip but the space charges in the bulk of liquid also [172].

Test voltage, voltage polarity, rate of increase voltage, test duration and the rest time between measurement: a large of research works has been done for studying the PD and the streamer mechanism with different of voltage types and polarities as described in 4.2.4. For PDIV under AC voltage, the recurrent rate of the PD pulse bursts was found increasing with the applied voltage. This increase was accompanied by both an increase in number of discrete PD pulses and their amplitudes within the pulse burst itself [153]. In addition, B. Fallou et al. concluded that the 1kV/sec of rising voltage and 1 minute pause can be used without a significant effect on the PDIV average value [148]. Furthermore, X. Wang et al. suggested that the PDIV values depended on the ramp speed; the higher speed applied voltage gave the higher PDIV [6]. The test duration affected also the PDIV as reported by H.Borsi and U. Schröder, they pointed out that the PD numbers decreased with the test duration when water content in the mineral oil was 5-20 ppm while the PD number was quite constant when the mineral oil contained water content of 44 ppm at 20°C [173].

The diameter of needle tip: different tip radius needles are used for PDIV, PD and streamer research; however, it seems only the streamer research by which the tip dimension effect has been studied. For AC stress, B.Fallou et al demonstrated that a small needle with tip radius of 3 μm gave a sensible reduction in PDIV compared with that obtained from the 50 μm tip radius needle. It is noted that M. Pompili et al who have long term investigated for PDIV in the mineral oil mostly use a 20 μm tip radius needle-plane electrode system with 30 mm gap distance as the test electrode.

Particles: some research works have devoted for the effect of particles on PD such as a research done by T. Van Top et al. They investigated the effect of cellulose particles on streamer initiation in the mineral oil under divergent AC field. The experiment test results are illustrated in Fig. 4.44 a). It is evidently that the steamer number is proportional to the particles [174]. Additionally, untreated oil and treated oil with different time left after treating finish were examined for PDIV and PD measurement as the results depicted in Fig. 4.44 b). The discharge pulse number is obviously oil treatment condition dependence.

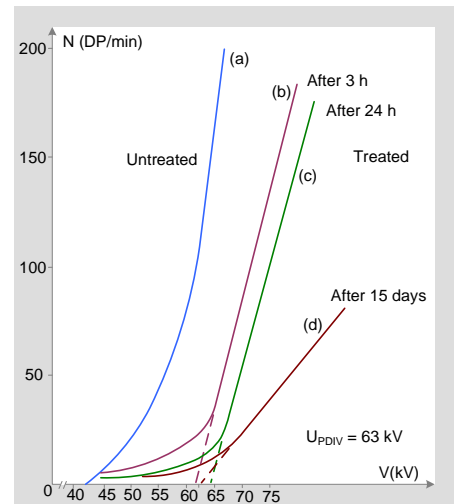
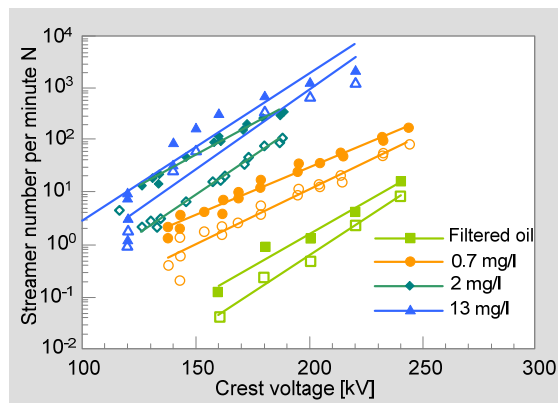


Figure 4.44: Oil condition effect on PDIV

a) influence of cellulose (needle tip radius = 0.5 mm, gap distance = 40 cm, water content: 17 ppm), positive streamers: dark symbols, negative streamers: open symbols [adapted from [174]] **b)** discharge number versus voltage of different oil treatment and time left effect after oil treatment [adapted from [148]]

Water content: The voids can initiate PD by distorting the electric field and by acting as impurities. Therefore, the PD numbers should increase with the increasing of moisture content in the mineral oil. H. Borsi et al. reported that the average apparent charges decreased with increasing of water content. Additionally, the PD amplitude remained independent of the water content [173].

Temperature and pressure: not only the breakdown voltage is affected from the liquid temperature and pressure, the PD activity also is directly affected from such parameters. According to the research work of H. Borsi et al., the decreasing of PD number with the increasing of temperature could be explained by assuming that the formation of the space charges at the needle tip was much more difficult due to a higher convection of the oil and also the relative moisture. Besides, the PDIV increased with increasing pressure complying with Parschen's law. Because of the incompressibility characteristic of the liquid, the increase pressure influences only the dissolved and undissolved gas in the liquid dielectric. This causes an increase of PDIV as well as breakdown voltage of a single gas void and decreases the PD numbers [173].

Oil conditions: H. Borsi and U. Schröder have also revealed interesting test results that PDIV and the apparent charge did obviously not rely on the oil age. Their experiment was conducted with oil samples with new oil and aged oils with 2- 28 year service condition. However, the PD number per hour decreased significantly from of 3000 PD/hour of the new oil to 900 PD/hour of the 28 year aged oil [173].

4.4 Arcing

4.4.1 Arcing definition

The electric arc, or so called as, arc discharge, arcing or arc, is a self-sustained electrical discharge that exhibits a large current with a low voltage drop. Arc characteristic is similar to a non-linear resistor. Arc discharge is the post breakdown phenomena of gas or liquid insulation. It exists with high temperature in the range of 1000°C to several thousand degree Celsius. With high currents and high temperature, arc becomes very luminous and noisy. Arc discharge produces a large number of gases and vapor spreading in its medium [175-176]. Arc discharge can be defined in terms of its luminosity, current density, and cathode fall voltage. Arc discharge is also characterized by high currents and current densities. Low intensity arcs rarely have total currents less than 1A. The current densities of arcs range from several amperes per square centimeter to more than a thousand ampere per square centimeter which are opposed to a glow discharge, in which current densities are seldom more than 50 mA/cm² [177].

4.4.2 Breakdown in mineral oils

Because arcing is the post process of the liquid insulation breakdown, it is important to understand breakdown mechanism of liquid dielectrics prior to analyze arcing phenomena in the mineral oils. The theory of liquid insulation breakdown may be divided into two conceptions. The former conception, the liquid breakdown may be explained as the gas breakdown by which the electronic breakdown for liquid insulating has been developed. The electronic breakdown mechanism seems suitable to describe the breakdown phenomena of the very high pure insulating liquids. The latter idea, the breakdown in liquid is established from the presence of the contaminant. Two types of contaminant usually found in commercial liquids which greatly influence breakdown phenomena are suspended solid particles and bubbles or cavities.

Electronic breakdown

Electrons are assumed to be ejected from the cathode into the liquid by either a field emission or by the field enhance thermionic effect. Once the electron is injected into the liquid, it gains energy from the applied field. Some electrons are accelerated until they gain sufficient energy to ionize molecules by collision and initiate avalanche. As a liquid dielectric conduction study, at low fields the conduction is largely ionic due to dissociation of impurities and increases linearly with the field strength and then, saturates at the intermediated field. At high fields approaching to breakdown, the conduction increases rapidly and tends to be unstable; an increased current is assumed that it is from the electron emission and possibly by field aided dissociation of molecules in the liquids [7,178].

Suspended solid particle mechanism

In commercial liquid dielectrics, solid impurities such as fibres or dispersed solid particles may be present. Assuming a spherical particle with radius r_p and permittivity ϵ_p is suspended in the dielectric liquids of permittivity ϵ_{liq} . Electric field causes this particle becomes polarized and experiences a force given by

$$F_e = \epsilon_{liq} r_p^3 \frac{\epsilon_p - \epsilon_{liq}}{\epsilon_p + 2\epsilon_{liq}} E \text{ grad } E \quad (4.23)$$

If $\epsilon_p > \epsilon_{liq}$, the force is directed toward a maximum field stress area, but if $\epsilon_p < \epsilon_{liq}$ the force has opposite direction. This force increases as increasing of the suspension particle permittivity. For a conducting particle for which ϵ_p is an approaching infinite value the force becomes

$$F_e = F_\infty = r_p^3 E \text{ grad } E \quad (4.24)$$

The movement of the particles by the electric force is opposed by diffusion and viscous drag of the liquid. This phenomenon clarifies a dependence of dielectric breakdown on time, concentration of particles, particle size, and the liquid viscosity. The movement of particles to the strongest region of the field leads to the bridge formation across the gap, eventually breakdown happens [7,178]. Fig 4.45 represents the breakdown phenomena mechanism in liquid dielectrics caused by the fibre bridge formation.

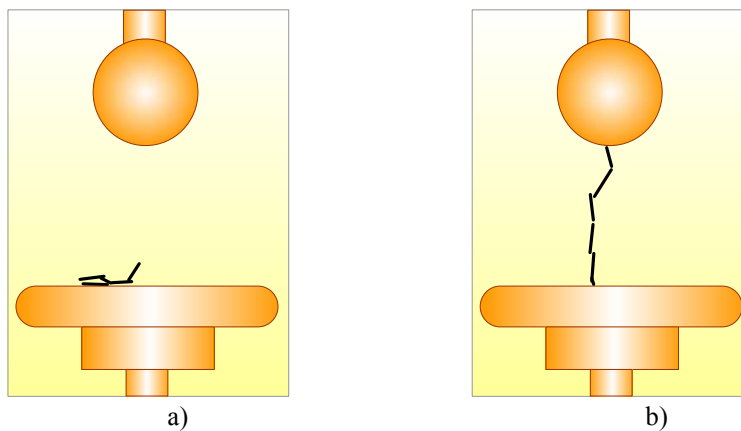


Figure 4.45: Experiment for fiber-bridge formation in the insulating liquid

a) fibers before applying the voltage b) fiber bridge, 1 minute after applying the voltage[adapted from[179]]

Cavity breakdown

Insulating liquids especially commercial liquids may contain gaseous inclusion in the form of bubbles which may be generated from the gas pocket in the electrode surface, from the changes in temperature and pressure in liquids, from dissociation of products by electron collision, or from liquid vaporization by corona discharges. The electric field in a spherical gas bubble immersed in a liquid of permittivity ϵ_{liq} is determined by

$$E_b = \frac{3E_0}{\epsilon_{liq} + 2} \quad (4.25)$$

Where E_0 is the field in the liquid with absence of the bubble. When the electric field inside the cavity becomes equal to the gaseous ionization field, discharge will take place inside the bubbles which causes the decomposition of the liquid and may lead to breakdown in liquids [7,178]. Furthermore, Z. Krasucki have proved that the breakdown in ununiform fields resulted from the formation and the growth of the vapour bubbles in the liquid. Moreover, breakdown strength depended on the time of voltage application. When the time of voltage application was too short for the vapor bubble to grow to it critical size then the breakdown strength obtained from lightning impulse was higher than that obtained under DC voltage [180]. In addition, C.G.Gaton and Z.Krasucki revealed that the bubble of gases or liquids subjected to an electric field would elongate in the direction of the field whenever ϵ_{bubble} was not equal to ϵ_{medium} . A shape of the unstable bubble would be distorted to a prolate spheroid. A non-conducting bubble for which $\epsilon_{bubble} / \epsilon_{medium} < 20$, had a stable shape at all values of the field. For a conducting bubble and a non conducting bubble for which $\epsilon_{bubble} / \epsilon_{medium} \geq 20$, they had a critical stable shape corresponding to a ratio of the major to the minor semi axis. As the field strength increasing, these bubbles would elongate until a critical shape was reached when the bubble becomes unstable [181]. A. H. Sharbaugh et al. suggested that prior to breakdown, the bubble of vapor formed in the liquid moved toward the anode [178]. Fig. 4.46 and Fig. 4.47 illustrate the water globule behavior immersing in the silicone fluid under electric field from the beginning until breakdown.

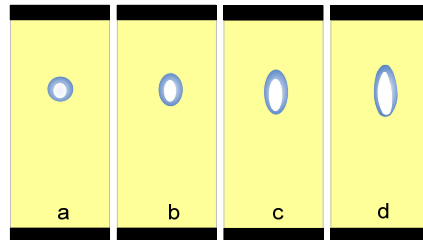


Figure 4.46: Elongation under an AC field of a water globule in the silicone fluid

a) $E = 0$ b) $E = 6.48 \text{ kV/cm}$ c) $E = 9.09 \text{ kV/cm}$ d) $E = 9.4 \text{ kV/cm}$ [adapted from [181]]

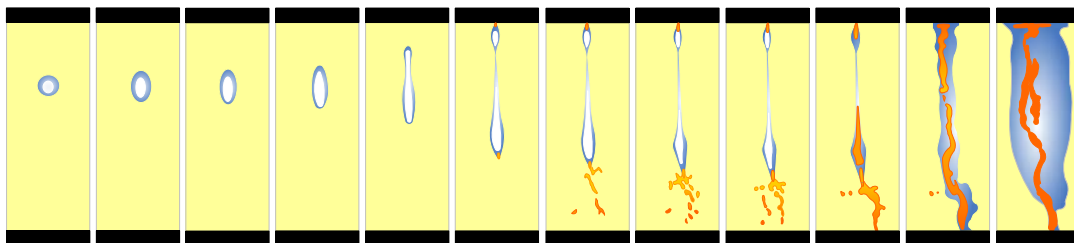


Figure 4.47: Breakdown of a liquid dielectric (silicone fluid) due to instability of a water globule above the critical field [adapted from [181]]

Examples of other liquid breakdown models such as microsecond breakdown model, sub-microsecond breakdown model, breakdown models for the liquid noble gases can be seen in [182].

Factors influencing the breakdown voltage of mineral oils: there are a large number of factors affecting the breakdown voltage of the mineral oils such as oil volume, electrode surface and configuration, mineral oil contaminant, mineral oil conditions such as temperature and pressure. W. R. Wilson described that for the small volumes of oil such as test cups, statistical variations were large and unit dielectric strength was high. For the large volume, the statistical reliability and reproducibility were greatly improved; the lower unit dielectric strength must be recognized [183]. Additionally, a reduction of breakdown strength with increasing of the electrode has been notified by W. F. Schmidt [184]. The parameters influencing the breakdown phenomena in insulating liquids such as molecular structure, time effect, electrode effect, and pressure and temperature effect have been elaborately investigated and well documented by [104,178,185-186].

4.4.3 Breakdown testing of mineral oils

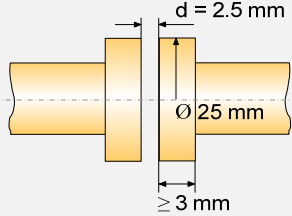
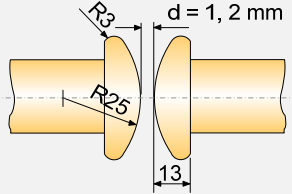
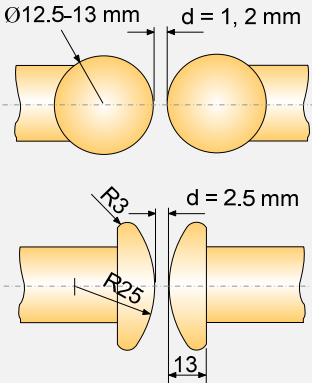
Oil breakdown testing standard: there are three oil breakdown testing standards which are widely employed in the industrial sector. Two standard methods are ASTM D 877 [187] and ASTM D 1816[188] and another is IEC 60156 [189]. All three test methods, the electrodes are mounted in a test cell which is filled with the insulating liquid being tested. The electrodes are completely covered by the insulating liquid. An appropriate AC voltage is applied to the test cell from zero until breakdown occurs which is signified by the operation of automatic circuit interruption equipment equipped in the dielectric voltage breakdown testing apparatus. According to IEC, breakdown is a disruptive discharge or spark over from one electrode to another. Table 4.12 shows various configurations of the electrodes using in the mention standards. There are some aspects to be considered before selecting the standard for oil testing as following:

Oil breakdown testing according to ASTM D 877: this method is sensitive to high moisture level and certain types of contamination particularly conductive particles. However, it is not very sensitive to the presence of moisture. If the water concentration in the oil sample at room temperature is less than 60% of saturation, the sensitivity of this method to the present of water is reduced. Besides it is not sensitive to the aging and oxidation in oil. It is not recommended for testing the filtered oil, the degassed oil, and the dehydrated oil for power system apparatus rated above 230 kV [187,190].

Oil breakdown testing according to ASTM D 1816: this method is more sensitive to moisture and oxidation in insulating oils as well as aged oil as well. Effect of particles, particularly fibers and dissolved gas content in the insulating oil sample can be observed clearly [188,190].

Oil breakdown testing according to IEC 60156: this standard test is sensitive to moisture, oxidation, conductive contaminations, suspended particles and dissolved gas content of the oil. The factors effecting on the tested oil by performing the test experiment according to IEC 60156 are analogous to the factors affecting the oil testing in accordance with ASTM D 1816 [190].

Table 4.12: Electrode configurations of ASTM and IEC standards for oil breakdown testing

Electrode configuration	Test standard
	<p><u>ASTM: D877-87 (Reapproved 1995)</u></p> <p>Standard test method for dielectric breakdown voltage of insulating liquids using disk electrodes</p> <p>:sensitive to high moisture content level and conductive particles</p>
	<p><u>ASTM: D 1816-97</u></p> <p>Standard test method for dielectric breakdown voltage of insulation oils of petroleum origin using VDE electrodes</p> <p>:sensitive to moisture, oxidation in insulating oils and oil aging</p>
	<p><u>IEC 156: 1995</u></p> <p>Insulating liquids - determination of the breakdown voltage at power frequency - test method</p> <p>:sensitive to moisture content, conductive contaminations, suspended particles and dissolved gas content of the oils.</p>

As mentioned before, there are many importance parameters effecting on oil breakdown characteristics. Therefore, the breakdown test results showed the big standard deviation which can reach up to 30% or higher as demonstrated in Fig. 4.48 a) [191]. To compare the test parameter effects from different test standards, C. Vincent et al. performed the breakdown experiments according to IEC 156 and ASTM D 1816 standards which have different test electrode configurations and test procedures such as different ramp speed applied voltage. This research group experimented also with a modified test procedure for IEC and ASTM standards by utilizing a 1 minute step by step voltage application. Besides, two different coaxial electrodes were used for breakdown test experiment as well. The test results as

depicted in Fig. 4.48 b) reveal that the breakdown voltage strongly depended on the electrode configuration and the test procedure; the 1 minute step by step voltage application provided clearly a lower breakdown probability compared to that experimented by the ramp voltage[192].

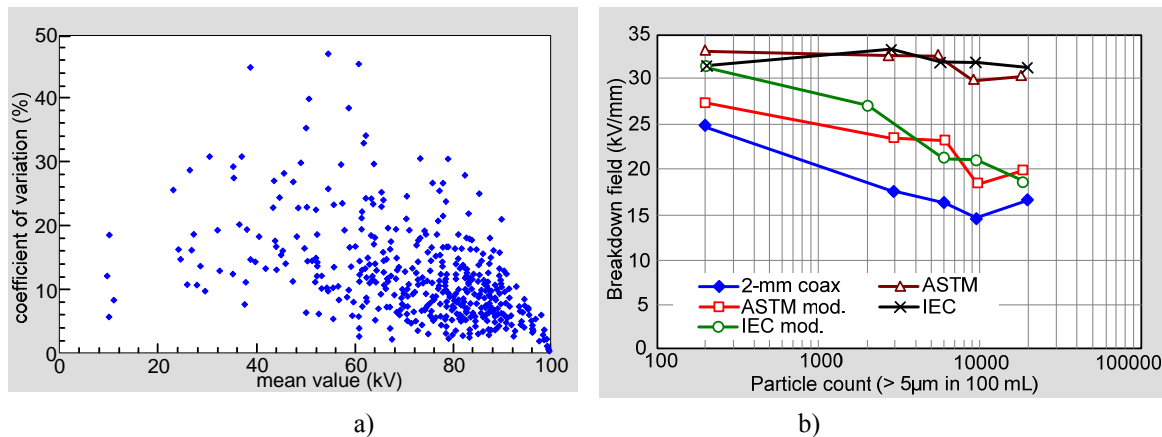


Figure 4.48: Mineral oil breakdown test results

a) coefficient of variation versus mean value for 459 single breakdown tests according IEC 60156 [adapted from [191]] b) Influence of electrode configurations and test procedures on the breakdown characteristics of in service contaminated mineral oil [adapted from [192]]

4.4.4 Arcing in mineral oils

Arcing mechanism: in general, arcing investigation has been performed for gas insulation especially under DC field as shown in Fig. 4.49 a). From Fig.4.49 a) the glow-to-arc transition between points H and I is triggered by the electron emission from the cathode caused by high heat load occurring in the high current density regions of the abnormal glow discharge. When the discharge settles down to the point I determined by the internal impedance of the power supply, the arc will be in the non-thermal and low intensity zone which is characterized by total currents between approximately 1 and 50 A. However, non-thermal, low intensity arcs may operate in rare cases outside the limits of this range. This zone depicts a negative resistance characteristic of arcing. Beyond point J up to point K, at approximately 20 to 50 A, the arc operates with a nearly flat or slowly rising voltage-current characteristic, which is called the thermal or high intensity arc [177]. King has proposed a famous voltage-current characteristic of free burning arc obtained from the experiment as shown in Fig. 4.49 b). He investigated the relationship between the voltage and arcing current in the wide range by varying the electrode gaps. From Fig. 4.49 b) the arcing current is divided into 3 zones; zone A represents the spark breakdown or the flash over with an unstable leader turning into the arc column as the breakdown with lightning impulse voltage. Zone B is in the current magnitude of 0.1 ampere to nearly 100 amperes. At this zone, the normal negative characteristic of arc begins. The cross section area of arc column increases with increasing current, resulting in an increase in its temperature. The elevated temperature causes thermal ionization, producing more charge particles, electrons and ions leading to high electrical conductivity of gas. Therefore, the voltage is reduced to a certain lower potential level. One part of this dissertation performed the feasibility study of arcing phenomena in this current zone with the reason of limited current of the power supply not more than 900 mA. In

zone c with the current above 100 A, the plasma jet is observed. The plasma jet becomes prominent which causes self-generated gas blasts [97].

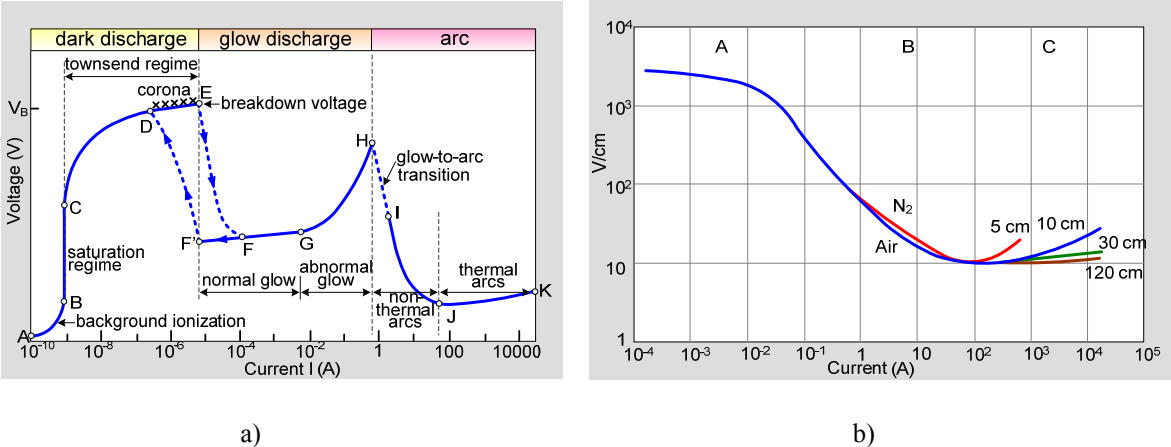


Figure 4.49: Voltage-current characteristic of the DC electrical discharge

a) overview [adapted from[177]] b) voltage-current experiment for arcing [adapted from[97]]

The visual characteristics and the voltage distribution along the axis of an arc discharge are illustrated in Fig.4.50. Basically, a linear arc will be considered for the fundamental investigation of arc. The linear arc, usually axis symmetric, is operated in a symmetry linear configuration between two electrodes. The fundamentally linear arc is the free-burning arc either horizontal or vertical configuration as shown in Fig.4.51. In case of horizontal electrodes, the buoyancy of the hot gases causes a horizontal linear arc to blow upward. For the free-burning vertical arc, the cathode is usually operated at the top, in order to better balance the heat loads on the two electrodes. Under the force of gravity, the buoyant hot gases rise and deposit an enhanced heat load on the cathode; to counter this, the cathode is put at the top, so that the heat load due to the cathode jet on the anode will not increase the heat deposition on the upper electrode further [177].

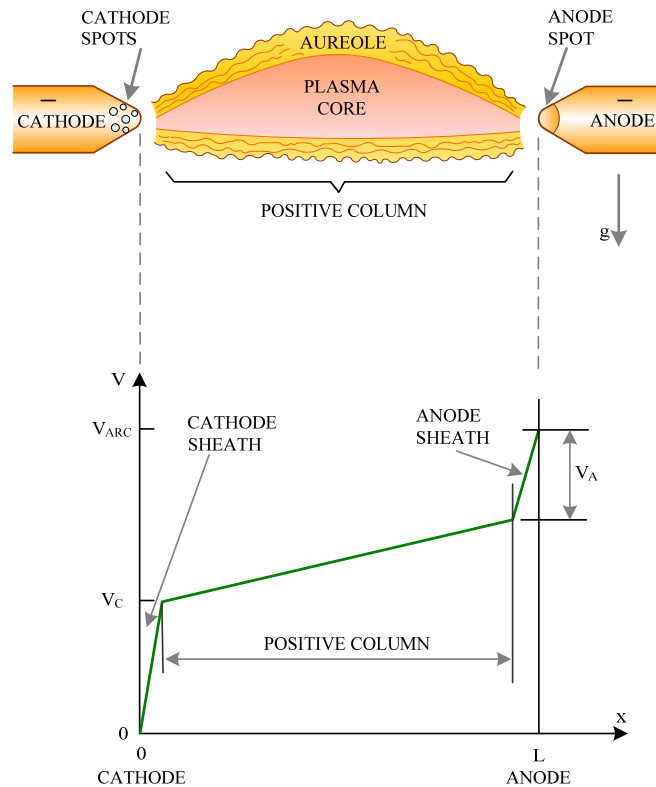


Figure 4.50: A schematic drawing of the visual characteristics and voltage distribution along the axis of an arc discharge [adapted from [177]]

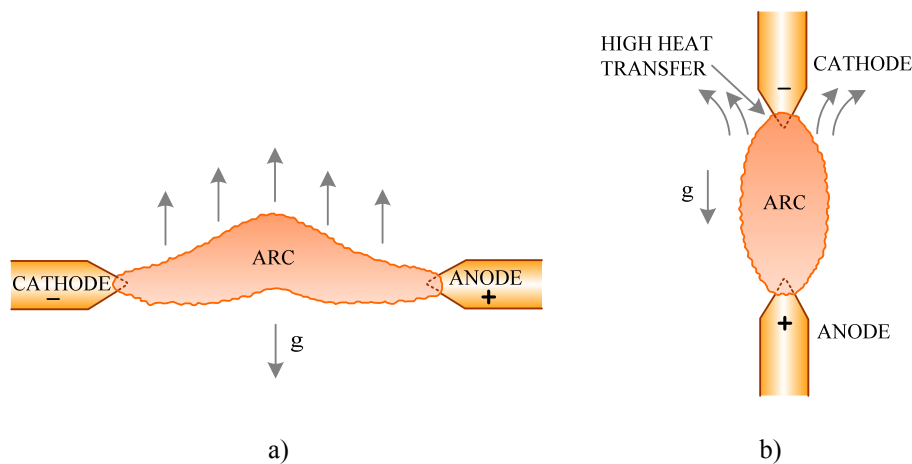


Figure 4.51: Two configurations of the free-burning arc

a) horizontal electrode alignment b) vertical electrode alignment [adapted from [177]]

AC arcing: After arcing is initiated, arcing current will increase with the decreasing of arc resistance. Simultaneously, the arcing voltage reduces to a certain value which is relatively low to maintain itself. After approaching the peak value, the current decreases down to nearly zero, at the same time the arc resistance will increase. A higher arcing voltage is needed to maintain the arc. If the voltage across the arc is not high enough, arc will be unstable and will become extinguished even before reaching the zero value. The arc shortly collapses before the current reaches its normal zero value at the end of each half cycle. The arc will reignite again when the current flows in the opposite direction in the following half cycle if the

required reignition voltage is sufficient which is higher than the voltage needed for sustaining the arc. If the arc is reestablished, the current will increase again in the reversal polarity and the voltage will fall reaching its minimum value which is practically constant during most of the half cycle in the region of maximum current. Fig. 4.52 represents the relationship between current, voltage, and temperature of 10 ampere AC 50 Hz arcing.

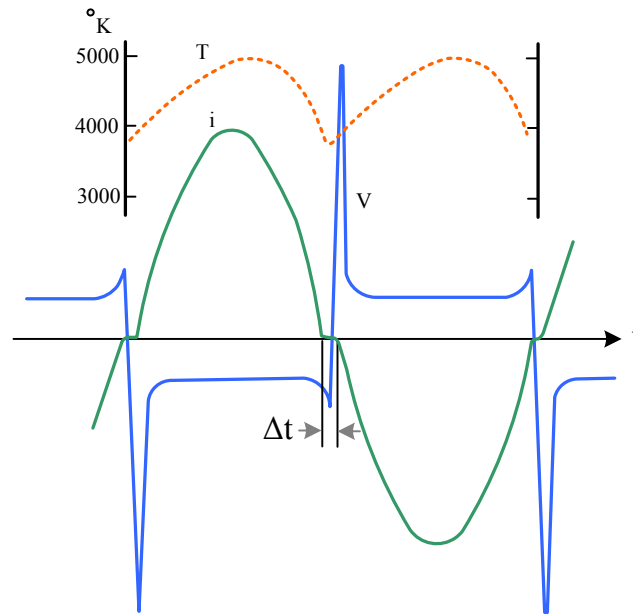


Figure 4.52: Time variations of current, voltage, and temperature for a 50 Hz, 10 A arc, 3 mm long, in air between copper electrodes[adapted form [193]]

Arcing in mineral oil phenomena: when arcing is generated in the mineral oils especially in the oil circuit breakers, gas bubbles and arcing by-products are produced. The high temperature of arc as possible in the range of 5,000 to 15,000 Kelvin causes the rapidly vaporized of the oil surrounding the arcing electrode. Then, the vaporized gas generates gas bubbles, which totally surround the arc. The composition of these bubbles is approximately composed of 20% of acetylene, 60 to 80% of hydrogen and the remainder consists of smaller proportions of methane and other gases. As can be seen in Fig. 4.53, within the gas bubble, three zones can be distinguished. In the innermost zone containing the dissociated gases, this zone is direct contact with the arc and its temperature drops to between 500 and 800 Kelvin. This gaseous zone is surrounded by a vapor zone where the vapor is superheated in its inside layers and is saturated at the outside layers. The outmost zone is one of boiling liquid where at the outside boundary the liquid temperature is practically equal to the relative ambient temperature [175]. Kazou Bekki et al. presented that the dielectric constant of liquid affected the arc discharge phenomena. They explained that the showering arc was observed for arcing of the high dielectric constant liquids such as methanol and water [194]. A showering arc is characterized by large, rapid voltage fluctuation appearing. This arc occurs normally when the electric contact breaks an inductive circuit [195]. For the low dielectric constant liquid such as n - hexane with dielectric constant 1.89, the steady arc like arcing in air was observed. To study breaking arc or switching arc phenomena in dielectric liquids, three range of current are classified as following; very large load current (more than 10 amperes), low load current (0.1 to several amperes) and very small load current which does not induce arc (lower than 0.2 mA) [194].

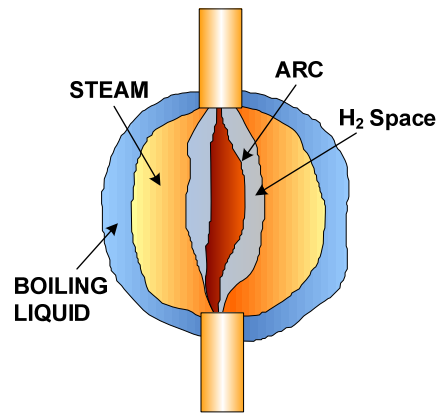


Figure 4.53: Gas bubbles produced by an arc surrounded by mineral oil [adapted form [175]]

The restoration property of dielectric liquids has been studied. J.H. Tortai et al. addressed that the liquid dielectrics with the smallest ratio of carbon versus hydrogen in their molecular formula present the best restoration property after a DC negative pulse arc [196].

Arcing by- products: mineral degradation after arcing depends on the energy dissipated in the tested oil. G. St-Jean et al. conducted the arcing experiment which dissipated total energy about 60 kJ in the liquid dielectrics. They found that several properties were not sensitive to arcing phenomena in the liquids such as the inhibitor content, the neutralization number, the water content and the viscosity of the oils. The moderate deterioration in $\tan\delta$ and the interfacial tension were observed. Whereas the dielectric breakdown strength was considerable reduction tested according to ASTM D 877 and ASTM D 1816. Large increases in dissolved combustible gases and suspended carbon particles with mostly in the range of 25 -50 μm diameter were found. The generated gases were divided into two parts; the former was free, mixed with air in the head space of the test equipment, and the latter gases remained dissolved in the liquids [197].

4.4.5 Arcing test

It is very difficult task to perform arcing test or breakdown testing with high voltage and high current specification. A high power source needed to accomplish the aforementioned task is not suitable to apply for liquid testing especially in commercial aspect. Therefore, to perform arcing investigation, a researcher may apply the short circuit criteria for breakdown test as a minimum requirement for arcing current. Table 4.13 shows the required currents for breakdown testing of insulating liquids according to international standards which the short circuit current is limited in the range of mA up to few hundreds mA.

Table 4.13: Short circuit current of power supply and circuit interrupting time of oil testing international standards [adapted form [198-199]]

Test standard	Short circuit current of transformer(mA)[199]	Circuit interrupting within(ms)[198]
IEC 156/1995	10..25 if $U_{test} > 15$ kV	≤ 20
VDE 0370	10..25 if $U_{test} > 15$ kV	≤ 20
ASTM D 877	No numerical value is given	≤ 50 if $I_{max} \geq 0.2$ A and ≤ 83 if $I_{max} < 0.2$ A
ASTM D 1816	1..10/kV	≤ 50 if $I_{max} \geq 0.2$ A and ≤ 83 if $I_{max} < 0.2$ A

4.5 Erosion analysis

4.5.1 Erosion of the electrode used for electrical testing of mineral oils

The erosion of the electrodes may occur after the electrodes are used for insulation tests for a certain time. The erosion process is accelerated by the persistent discharges or arcing of the electrode system. Erosion happens due to the melting and evaporation of the electrode material. The vaporization of the material is the main mechanism of erosion during occurring of the high current interval. The arc energy heats the material until liquefaction and then vaporizes the material during the further energy supply. Fig. 4.54 shows the energy flows of a short arc causing the erosion of electrodes [193,200]. The high temperature of the arc causes melting, vaporization and ablation of the metal. Material from the electrodes can transfer between anode and cathode. This material will migrate and become adhesion on the counter electrode surfaces. Material transfer may cause by heat input asymmetry of electrodes, asymmetry of force from arcing, asymmetry of electrode thermal properties, electrode mechanical properties, and asymmetry of cooling conditions [201]. After migration, the melting materials may be re-deposited back onto the electrode surfaces or be loss to the surrounding media [202].

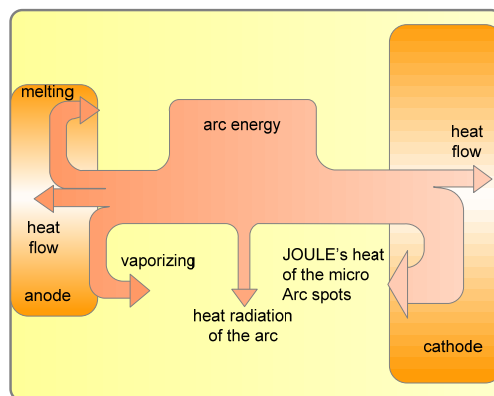


Figure 4.54: Diagram of erosion process of arcing tested electrode [adapted from [200]]

Examples of the needle tip erosion form the streamer testing of the mineral oil as shown in Fig. 4.42. Besides, S. Patrissi et al. depicted the erosion of needles used for three standard lightning impulse breakdown testings, 80kV negative polarity and 120 kV positive polarity, of perfluoro polyether(PFPE) and transformer oil(AGIP ITE 360) in [171]. The shapes of the needles were dramatically distorted compared to the original one after the impulse breakdown test as shown in Fig. 4.55 a). Generally, electrode materials, arc voltage, arc current, arc temperature, and the insulating medium characteristics are the main factors of the electrodes' erosion. The appearance of electrode spots relates to the electrode erosion behavior, higher temperature and smaller spot size leading to more erosion. Unfortunately, the erosion quantification is a difficult task. The amount of erosion may be defined as a loss of electrode material that will be determined by means of weighing experiment. However, weight loss is not a good measure of erosion because mass transport and redeposition in regions away from the arc attachment obscure the effect of the arc's operation [203]. An example of arc erosion rates of different material tested by 12,000 ampere, 60 Hz, half cycle arc is illustrated in Fig. 4.55 b) [204]. Table 4.14 represents the material characteristics used for high current application such as a contact material of circuit breakers.

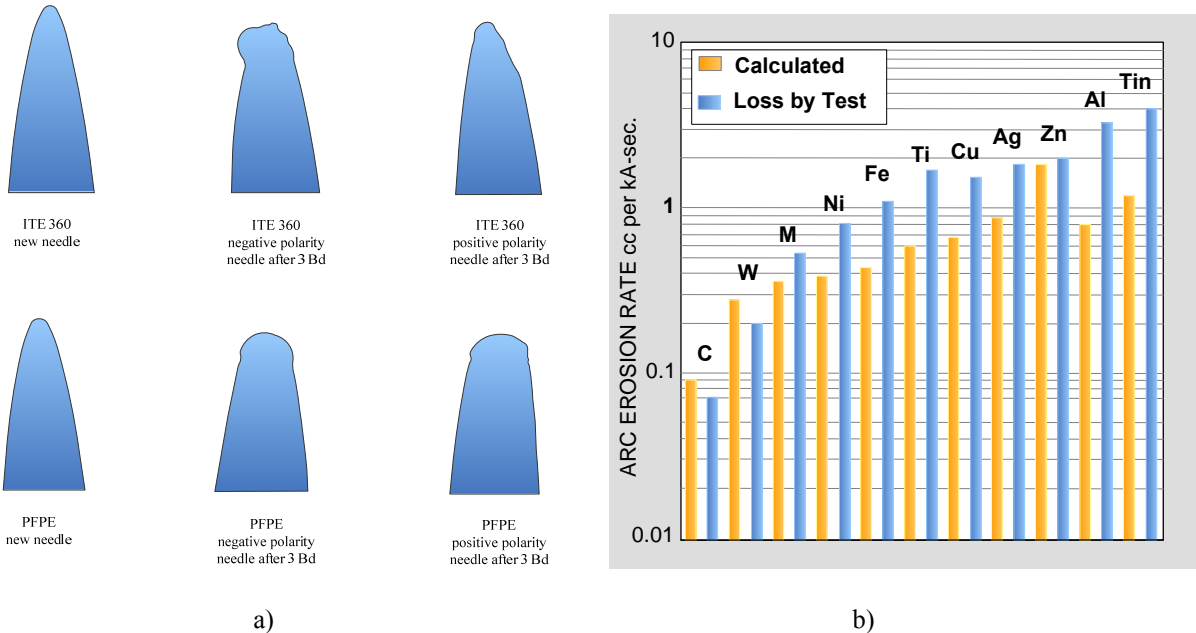


Figure 4.55: Needle erosion

a) needle tips before and after three standard lightning breakdown tests of transformer oil (ITE 360) and PFPE for both polarities [adapted from [171]] b) comparison of measured arc erosion rates and calculated vaporization rates of different elements, based on half cycle arc of about 12,000 ampere, 60 Hz [adapted from [204]]

Table 4.14: Softening and melting temperatures for contact materials [175]

Material	Resistivity: ρ $\Omega \text{ cm } 10^{-6}$	Hardness: H $\text{Kg/cm}^2 10^3$	Softening Temp (Kelvin)	Melting Temp (Kelvin)
Au	2.2	2-7	373	1336
Ag	1.63	3-7	423	1233
Al	2.9	1.8-4	423	931
Zn	6.16	3-4	443	692
Cu	1.8	4-7	463	1356
Ni	9.0	7-20	793	1728
Pt	11.0	4-8	813	2046
Mo	4.8	18	1172	2883
W	5.5	12-40	1273	3653

4.5.2 Scanning electron microscope and energy dispersive X – ray for erosion analysis

To study electrode erosion, scanning electron microscope (SEM) is a very powerful instrument. With SEM, it permits the observation and characterization of materials on a nanometer to micrometer scale [205]. The topography of electrodes is acquired by reading the secondary electrons (SE images). Moreover, the image of the surface morphology of a specimen as well as the information of the surface compositions can be identified by reading the backscattered electrons (BSE images) and the energy dispersive X-ray (EDX) respectively. SEMs are almost exclusively equipped with EDX or energy-dispersive spectroscopy (EDS). The general structure of SEM and EDX equipment are depicted in Fig. 4.56 a) and b) respectively.

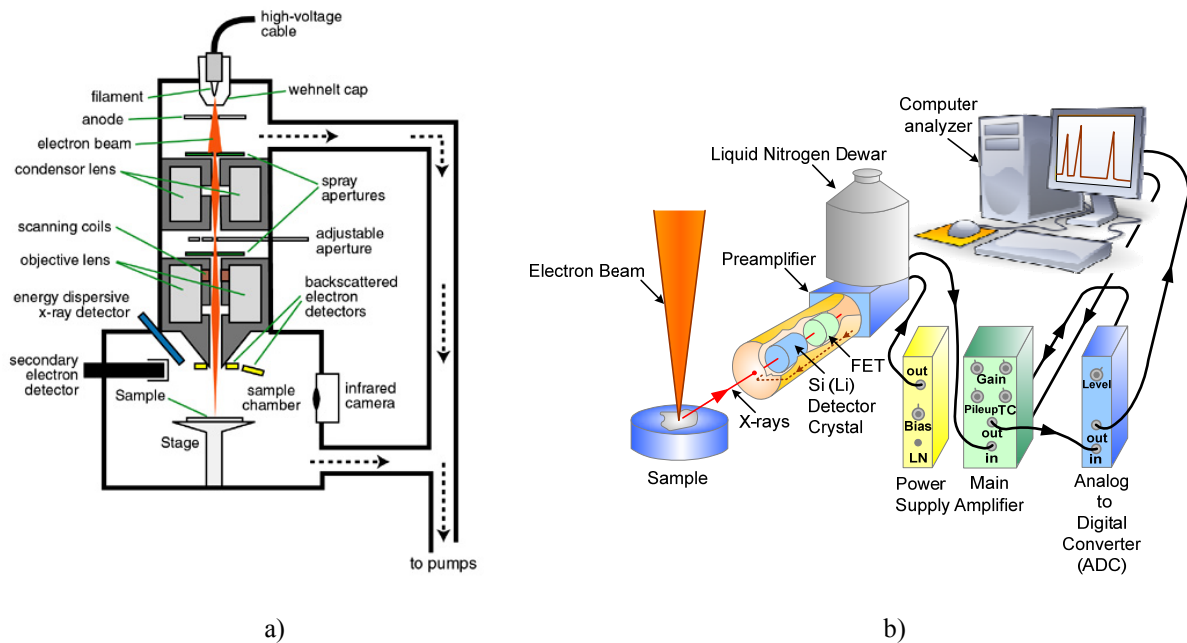


Figure 4.56: Structure details of SEM and EDX

a) SEM [adapted from [206]] b) EDX equipment [adapted from [205]]

SEM and EDX principles: with SEM technique, the electron beam generated from the electron gun is accelerated and controlled by a series of lens down to the specimen. Multi signals composed of backscattered electrons, secondary electrons, X-Rays, Auger electrons, cathodoluminescence are generated from the test specimen as shown in Fig. 4.57. These signals will be detected by the detector and processed to produce an image or spectrum on the monitor display. The results from SEM technique are useful for analysis the topography and morphology of the test specimen. With EDX or EDS technique, it is used for identifying the elemental composition of a sample or small area of interest on the sample. An EDX system operates by counting X-ray emissions, X-ray photons entering the X-ray detector, from the test sample according to their energy content. EDX analysis can be performed on the SEMs which is equipped with an EDX system [207-209].

SEM and EDX signals: when the electron beam interacts with the specimen, two types of interaction can take place, which are inelastic events and elastic events. In the inelastic event, the energy transfer from the electron beam which is less than 50 eV excites the incident electron leaves the atom of the test specimen. The ionized electron is termed as a secondary electron. The production of secondary electron is very related to the specimen topography due to the transfer energy is very small. As a consequence, the secondary electrons can exit are very near the surface (< 10 nm) of the specimen. The leaving of a lower electron which is emitted from the atom during the secondary electron processing causes an inner shell has a vacancy. If a higher energy electron falls into the lower energy shell to fill the vacancy, an **X-Ray characteristics** of that energy transition will be produced. The beam specimen interaction is illustrated in Fig. 4.57- Fig. 4.58. For the elastic event, after the beam electron interacts with the electric field of the nucleus of an atom of the specimen. The beam electron direction alters without a significant change in the energy of the beam electron (less than 1 eV). The elastically scattered beam electron deflected back out of the specimen is named a **backscattered electron**. Backscatter electrons have a greater energy and can escape from deeper areas within the specimen. They are more readily produced by high atomic weight

elements. The backscattered electrons have energy in the range of 50 eV to nearly the incident beam energy. However, most backscattered electrons retain at least 50% of the incident beam energy. The product of a backscattered electron represents the surface morphology of the electrode such as the layers on the specimen surface. It can be used to visualize differences in elemental composition. The higher the average atomic number of the area being analyzed, the greater the probability is that a backscattered electron will be generated [207-210].

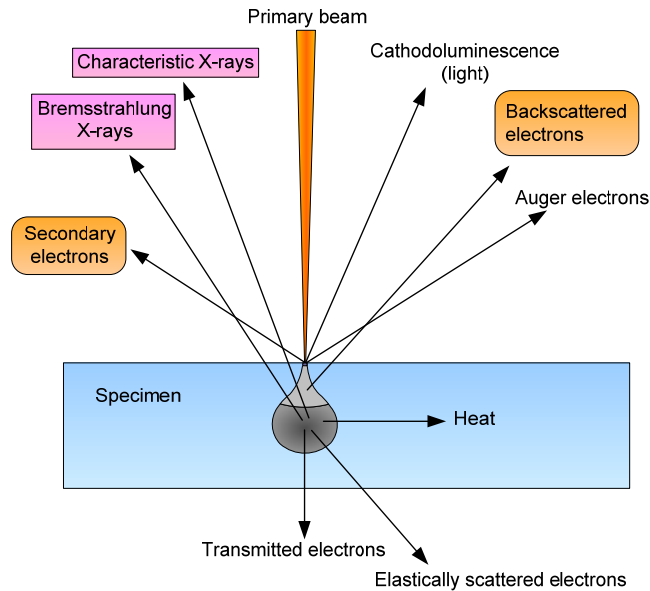


Figure 4.57: Beam specimen interaction signals caused by the electron beam (primary beam)[adapted from [208]]

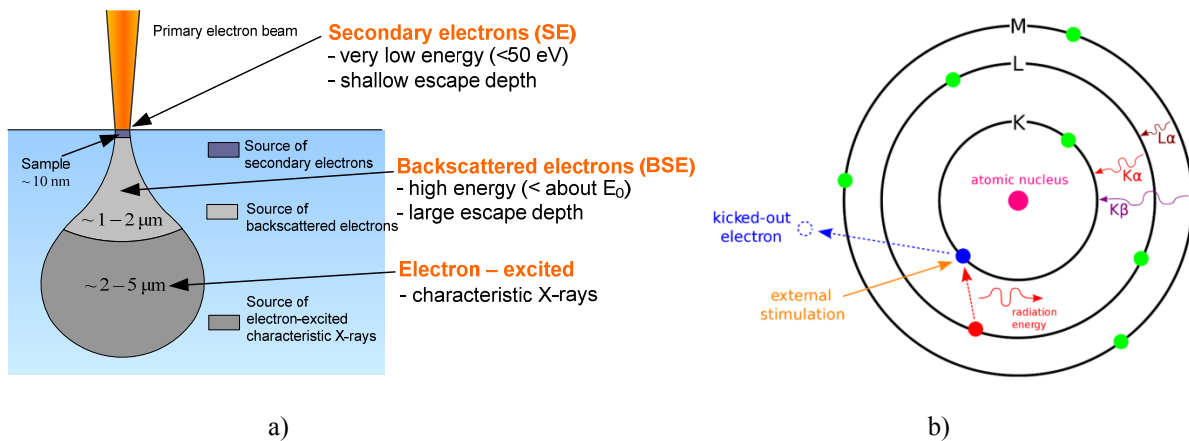


Figure 4.58: Beam specimen interactions

a) effect of electron beam on the test specimen [adapted from [208] and [211]] b) X-ray process [adapted from [212]]

X-rays or light emitted from atoms will have a characteristic energy which is unique to the element from which it originated. Two basic types of X-rays are produced on inelastic interaction of the electron beam with the specimen atoms [213]:

• **Characteristic X-rays** result when the beam electrons eject inner shell electrons of the specimen atoms.

• **Continuum (Bremsstrahlung) X-rays** result when the beam electrons interact with the nucleus of the specimen atoms.

Characteristic X-rays reveal themselves as peaks imposed upon a background of continuum X-rays as shown in Fig. 4.59. The X-ray counts are plotted in histogram format (with the energy levels on the x-axis), forming an EDX spectrum. The EDX spectrum formed contains peaks that correspond to the elements present in the sample. X-ray spectroscopy is a valuable tool for qualitative and quantitative element analysis. Each element has characteristic peak positions corresponding to the possible transitions in its electron shell. The presence of copper, for example, is indicated by two K peaks at about 8.0 and 8.9 keV and a L peak at 0.85 eV as shown in Fig. 4.59. In heavy elements like tungsten, a lot of different transitions are possible and many peaks are therefore present as shown in Fig. 4.60 [205].

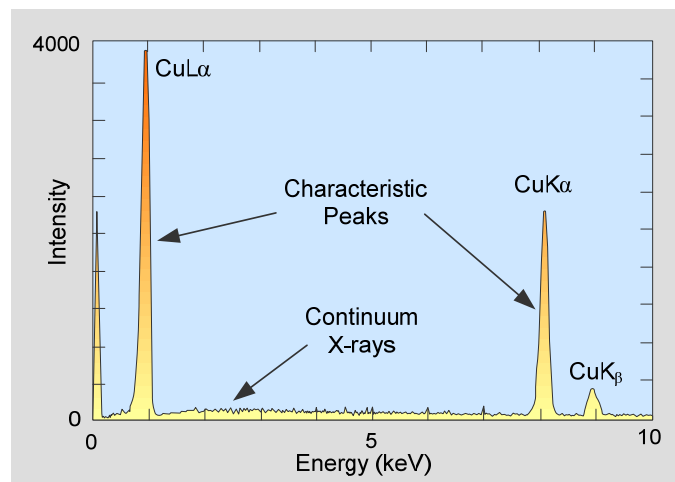


Figure 4.59: X-ray spectrum of copper showing K-series and L-series X-ray peaks and the continuous X-ray spectrum (bremsstrahlung or continuum) obtained from a Si(Li) EDS detector with an ultrathin (diamond) X-ray window [adapted from [205]]

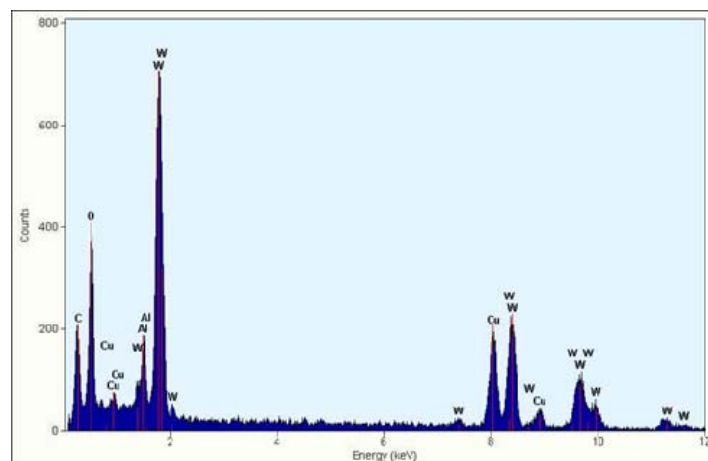


Figure 4.60: X-ray spectrum of an aluminum tungsten oxide on a carbon foil supported on a copper grid [adapted from [214]]

4.6 Statistic for test result analysis

After the experiment was done, statistic techniques were selected to analyse the test results. The mean and standard deviation were selected to describe the test data. Then, the distribution of the test data will be modeled to select the suitable distribution to explain the test result. Normally, normal distribution and weibull distribution are widely utilized to describe the PD and breakdown of dielectric materials.

Sample mean (\bar{x}): \bar{x} is the average or mean of the test data. If a test data set consists of the n data observations x_1, x_2, \dots, x_n , the sample mean \bar{x} can be calculated from

$$\bar{x} = \frac{\sum_{i=1}^n x_i}{n} \quad (4.26)$$

and
$$\sum_{i=1}^n x_i = x_1 + x_2 + \dots + x_n \quad (4.27)$$

Sample variance: to measure the spread of the test data, the variance s^2 is computed from

$$s^2 = \frac{\sum_{i=1}^n (x_i - \bar{x})^2}{n-1} \quad (4.28)$$

The standard deviation s of the test data can be calculated from the square root of the variance

$$s = \sqrt{\frac{\sum_{i=1}^n (x_i - \bar{x})^2}{n-1}} \quad (4.29)$$

To analysis the distribution pattern of the test data, normal distribution and weibull distribution analysis were selected to treat the test data. The normal probability density function (PDF) can be calculated from the given formula (4.30). The normal probability density function is a bell-curve which is symmetric at about μ .

$$f(x) = \frac{1}{\sigma\sqrt{2\pi}} e^{-(x-\mu)^2/(2\sigma^2)}, \quad -\infty \leq x \leq \infty \quad (4.30)$$

Where $f(x)$ is probability density function of parameter x

σ is the population variance of the distribution

μ is the population mean value of the distribution

In practice, all of the population measurements are not available. Therefore, the sample mean and sample variance are utilized. The normal cumulative distribution function (CDF) is

calculated from the sum (integral) of the frequencies from the lowest value up to the considered point x .

The weibull distribution is a very common tool in reliability analysis. The weibull distribution is flexible and adaptable for various kinds of data analysis [215]. The two-parameter weibull distribution is the most widely used for the failure or destructive test data. Weibull distribution is suitable for data that have a variant rate of failure in function of voltage with progressive stress test, or of a function of time with constant voltage test [216]. The weibull cumulative distribution function is shown in equation (4.31) and the weibull probability density function can be calculated from (4.32).

$$H(x; \alpha, \beta) = 1 - e^{-\left(\frac{x}{\alpha}\right)^\beta} \quad (4.31)$$

$$h(x) = \beta \frac{x^{\beta-1}}{\alpha^\beta} e^{-\left(\frac{x}{\alpha}\right)^\beta} \quad (4.32)$$

Where x is the measured variable representing the failure event such as PDIV or breakdown voltage

$H(x)$ is the probability of failure at a voltage less than or equal to x .

$h(x)$ is probability density function of parameter x

α is the scale parameter and is positive.

β is the shape parameter and is positive.

Considering the two parameter weibull distribution, α represents the PDIV or breakdown voltage at the cumulative failure probability of 63.2%. It is analogous to the mean of the normal distribution. The shape parameter β is a measure of the range of the failure voltages. The larger β illustrates the smaller range of breakdown voltages. The β is analogous to the inverse of the standard deviation of the normal distribution. Therefore, the observation data dispersion can be evaluated from β . Moreover, when the shape parameter is less than 1, the failure rate decreases with the increasing test voltage. Conversely, the failure rate increases with increasing of the test voltage when the shape parameter is greater than 1. The higher the β value, the greater is the rate of increase. When the β value increases above 2, the shape of the weibull PDF will approach the symmetrical normal distribution and at $\beta = 3.4$ the weibull PDF is relatively the same as the normal PDF [216-218].

The weibull parameters can be estimated from the maximum likelihood, the least square regression method or the graphical method performed with a weibull probability paper [215-217]. BS EN 61649 [215] and IEEE 930 [217] provide a guidance to perform an analysis of weibull distribution for a failure data. To analyze the test data statistic distribution, Minitab program version 14 is utilized. The distribution that is suitable for describing the data and the distribution parameters are analyzed. The probability plot will be implemented to identify the right or suitable distribution of the test data. Anderson-Darling statistic (AD) is one of the goodness-of-fit statistics which is provided in Minitab program. AD is used to compare the fit of the competing distributions of the test data [219]. The AD is a measure of how far the plot

points fall from the fitted line in a probability plot. A smaller AD indicates that the distribution fits the data better [219]. This work uses the AD to verify the right distribution. Moreover, a p-value obtained from the goodness of fit test is also taken into account that there is enough evidence in the data to reject the null hypothesis, H_0 , or not. The null hypothesis is assumed that the test data or the population follows a selected distribution model [220]. The p - value is used to measure the plausibility of a null hypothesis. The smaller of the p - value, the less plausible is the null hypothesis [221-222]. In mintab program, if the p - value is greater than 0.05 (the type I error is normally specified 0.05 (5%) or there is a 5% chance that the wrong decision is made), the assumption that the selected distribution is well defined the tested data is accepted. Generally, if the p- value less than 0.05, it suggests that the data do not follow the selected distribution. In statistic point of view, if the p-value smaller than 0.01, it is normally taken to indicate that the null hypothesis is not a plausible statement. Then the null hypothesis can be rejected that means the selected distribution is not correct. If the p-value in the range of 0.01- 0.1, it is taken to indicate that the data analysis is inconclusive. There is some evidence that the null hypothesis is not plausible, but the evidence is not overwhelming. If the p-value larger than 0.1, it is revealed that the null hypothesis is a plausible statement and should be accepted [221]. From the probability plot, the selected (given) distribution is a good fit if [223]:

- The data points roughly follow a straight line (or the smaller AD)
- The p-value is greater than 0.05

Futhermore, the parameters obtained from the distribution are also calculated by Minitab. The application of weibull distribution for dielectric breakdown was described in [224-227]. The weibull distribution is not only employed for breakdown or time to breakdown analysis but also for PD characteristic analysis. The examples of weibull and mixed weibull application for PD analysis can be found in [228-230].

5 Experiment test set up

5.1 Electrode systems and test specimen for PDIV experiment

5.1.1 Electrode systems for PDIV experiment

The PDIV investigation took place in the test vessel equipped with a needle-plane electrode arrangement. The gap distance of the electrode system was set up at 25 mm and 50 mm. Tungsten needle electrodes with the tip radius of 10 μ m, 20 μ m and 40 μ m, respectively, were used as the high voltage electrode while the brass plane electrode with 75 mm diameter was used as the grounded electrode for preliminary PDIV investigation. Moreover, the plane electrode with diameter of 50 mm and the sphere electrodes with the diameter of 12.7 mm, 25.4 mm, 50.8 mm and 76.2 mm respectively were used as the grounded electrode for PDIV experiment with different grounded electrodes. Tungsten needles give high melting temperature about 3,653 Kelvin and high hardness capacity about 12-40 x 10³ kg/cm² [175]. Tungsten needles were provided from two companies from Austria and Japan. Table 5.1 summarizes the electrode system using for PDIV experiment and Table 5.2 depicts the tip profiles of tungsten needles used in this experiment.

Table 5.1: Electrode systems utilized for PDIV experiment

Electrode	Test experiment
<p>Group 1</p> <p>1. Tungsten needles with tip radius of 10μm, 20μm, and 40μm and with needle length of 60 mm, 60 needles from BAUR company, Austria</p> <p>2. Brass plane electrodes with diameter of 75 mm, 15 electrodes from HV workshop TUG</p>	<p>Group 1</p> <p>1. Preliminary PDIV experiment: Test 7.2.1</p> <p>2. Effect of PDIV test methods on PDIV characteristics: Test 7.2.2</p> <p>3. PD pulse train characteristics from preliminary PDIV test: Test 7.4.1</p> <p>4. SEM and EDX analysis for PDIV electrode systems: Test 7.6.1</p>
<p>Group 2</p> <p>1. Tungsten needles with tip radius of 10μm, 20μm, and 40μm and with needle length of 60 mm, 200 needles from Ogura company, Japan. 12 needles with tip radius of 10μm with needle length of 40 mm (adapted from the original needles form Ogura)</p> <p>2. Brass plane electrodes with diameter of 50 and 75 mm, 15 electrodes, from HV workshop TUG</p> <p>3. Steel sphere electrodes with diameter of 12.7 mm, 25.4 mm, 50.8 mm and 76.2 mm, 10 sphere electrodes for the smallest size, 2 spheres for other sizes from Kugel Pompel company, Austria</p>	<p>Group 2</p> <p>1. Effect of grounded electrodes on PDIV and PD characteristics: Test 7.2.3</p> <p>2. Effect of needle length on PDIV and PD characteristics: Test 7.2.4</p> <p>3. Effect of water content and oil temperature of mineral oil on PDIV and PD characteristics: Test 7.2.5</p> <p>4. Effect of PDIV test circuits on PDIV and PD characteristics: Test 7.2.6</p> <p>5. Breakdown voltage characteristic of the mineral oil: Test 7.3</p> <p>6. PD pulse characteristics: Test 7.4.2</p>

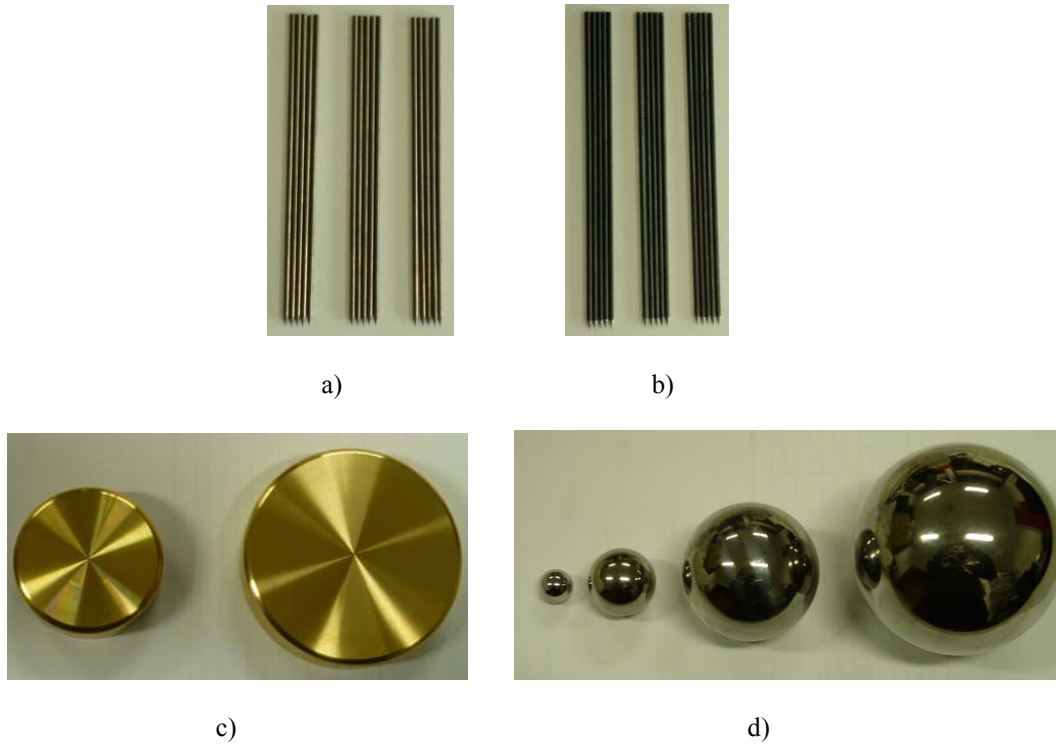
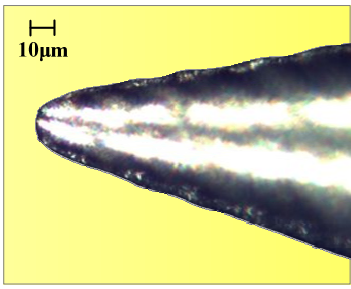
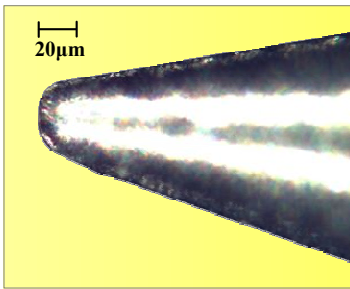
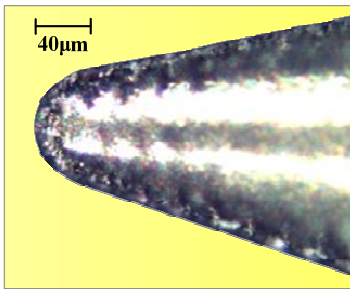
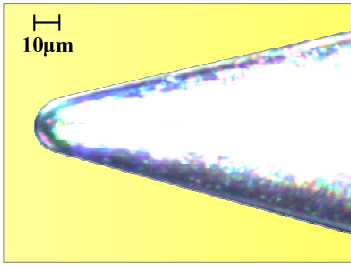
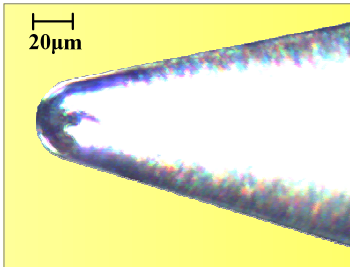
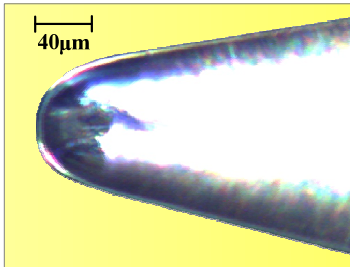


Figure 5.1: Electrodes for PDIV experiment

a) needles with tip radius of $10\mu\text{m}$, $20\mu\text{m}$, and $40\mu\text{m}$ from BAUR company b) needles with tip radius of $10\mu\text{m}$, $20\mu\text{m}$, and $40\mu\text{m}$ from Ogura, c) brass plane electrodes with diameters of 50 and 75 mm, d) sphere electrodes with the diameter of 12.7 mm, 25.4 mm, 50.8 mm and 76.2 mm from left to right

Table 5.2: Zoom of the tip profiles of the example needles

Needle	$10\mu\text{m}$ tip radius	$20\mu\text{m}$ tip radius	$40\mu\text{m}$ tip radius
BAUR			
Ogura			

Note: the tip of the $10\mu\text{m}$ tip radius needles from BAUR company was not good as the tip profile of other needle sizes because of the difficulty of production.

5.1.2 Test cells for PDIV experiment

Three test cell configurations were prepared for different PDIV experiments. The needle-plane electrode test cell was set up for the preliminary PDIV experiment and for the most PDIV experiment as illustrated in Fig. 5.2. The needle-sphere electrode system was prepared for investigating of the effect of grounded electrode configurations on PDIV value in part of grounded sphere electrodes as delineated in Fig. 5.3. Then, the temperature sensor, heating blanket and the heater were equipped with the needle - plane electrode test cell to support the study of water content and temperature effect on PDIV as demonstrated in Fig. 5.4. The capacitance of the electrode system was about 10.1-10.2 pF for the needle-plane configuration. The capacitance was measured by using the electronic bridge, LDIC TD SMART.

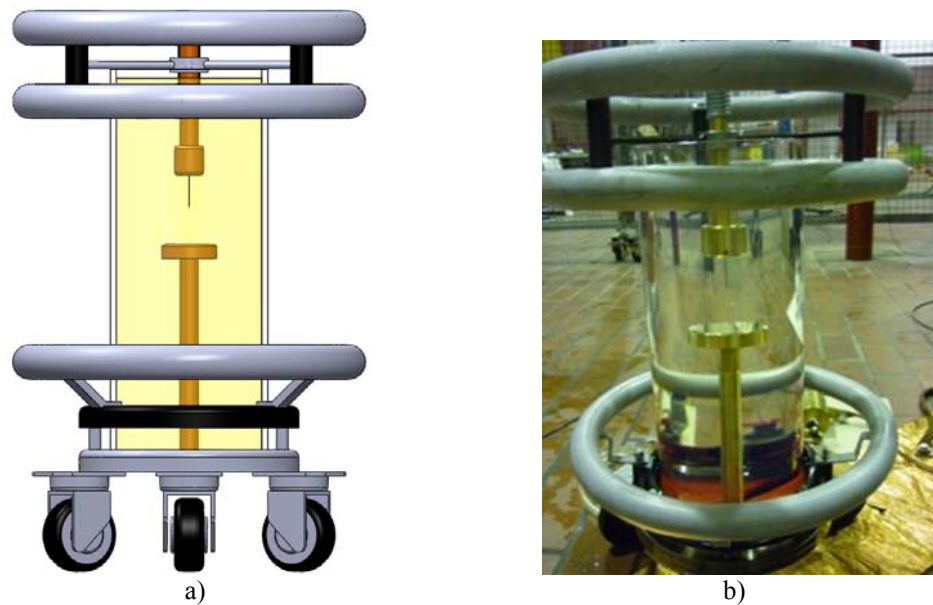


Figure 5.2: Needle - plane electrode test cell

a) diagram b) test cell configuration

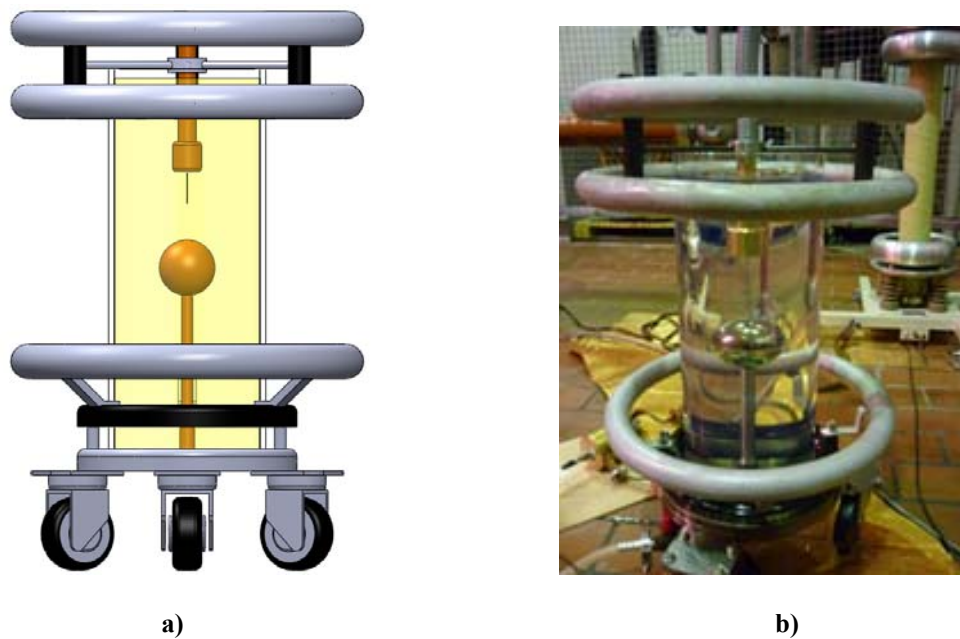


Figure 5.3: Needle - sphere electrode test cell

a) diagram b) test cell configuration

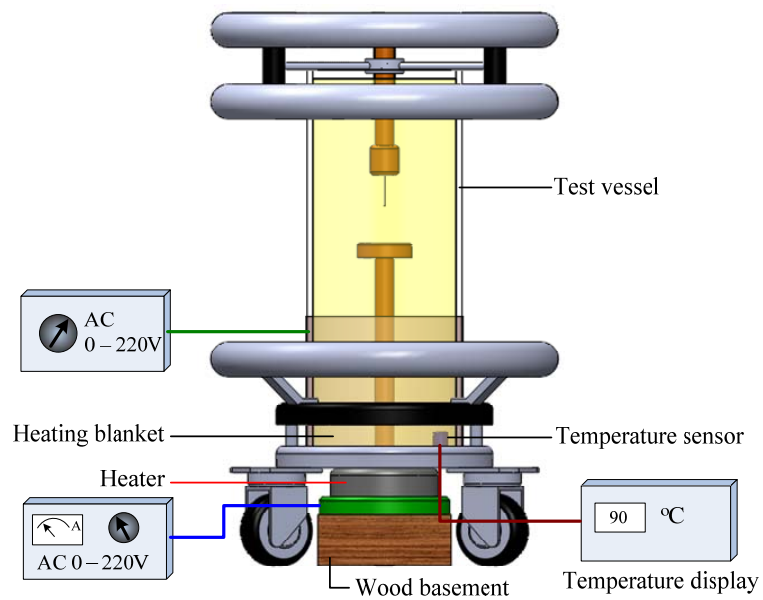


Figure 5.4: Diagram of the needle - plane electrode test cell for water content and temperature effect on PDIV value experiment

5.1.3 Mineral oil preparation for PDIV experiment

The mineral oil prepared for PDIV experiment was pre-treated by an industrial oil retreat machine which can filter the particles in the mineral oil with the particle size of 2.5 μm . During the mineral oil treatment process, such mineral oil was exposed to a temperature of 50°C in a vacuum about 10^{-2} mbar. The oil treatment process had spent about 3 hours. The water content of the treated mineral oil was approximatedly 3 - 4 ppm for new oil used for group 2 PDIV experiment and about 5-9 ppm utilized for group 1 PDIV experiment and arcing test. The water content of the mineral oil was measured by Karl-fisher titration technique (coulometric). The water content of the treated mineral oil was measured at least 2 times. The third measurement would be performed if the first and the second water content were different larger than 0.5 ppm. Then, the average of water content value was calculated. Next, the average AC breakdown voltage of the treated mineral oil was tested in accordance with IEC 60156 by using DTA 100 E [189]. The average AC breakdown voltage was about 75 - 95 kV. Furthermore, relative permittivity and dielectric loss of the mineral oil sample were measured.



a)



b)

Figure 5.5: Mineral oil for PDIV experiment

a) Nynas Nytro 4000 x b) the oil treatment machine



a)



b)

Figure 5.6: Water content measurement

a) Karl-fisher Metrohm 832 coulometer b) laboratory scale



a)



b)

Figure 5.7: Basic mineral oil characteristic measurement

a) BAUR DTA -100E for breakdown voltage test b) BAUR DTL for relative permittivity and dielectric loss measurement

Then, the mineral oil was filled in the test cell. The experiment was started after filling process about 20 minutes. The mineral oil preparation was similarly for the most experiments which utilizing the mineral with water content less than 10 ppm. Besides, for the high water content mineral oil which had to be prepared for studying the effect of water contents on PDIV value needed an additional preparation as described in annex C. The mineral oil used for the group 1 PDIV experiment was a little bit different with the mineral oil used for the group 2 PDIV experiment.

5.2 PDIV test set up

5.2.1 Test circuit for PDIV measurement

The investigation of PDIV characteristics of the mineral oil was performed under atmospheric condition in high voltage laboratory. The test circuit diagram and experiment test set up are depicted in Fig. 5.8 and Fig. 5.9 respectively.

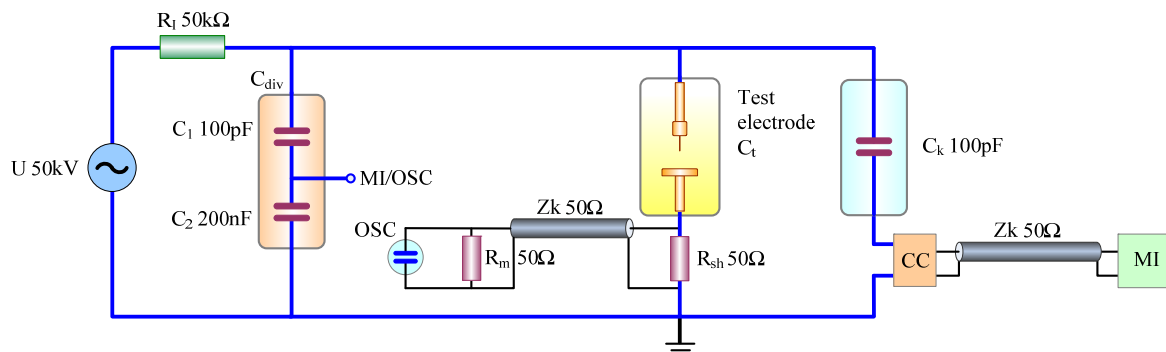


Figure 5.8: Test circuit diagram for PDIV experiment

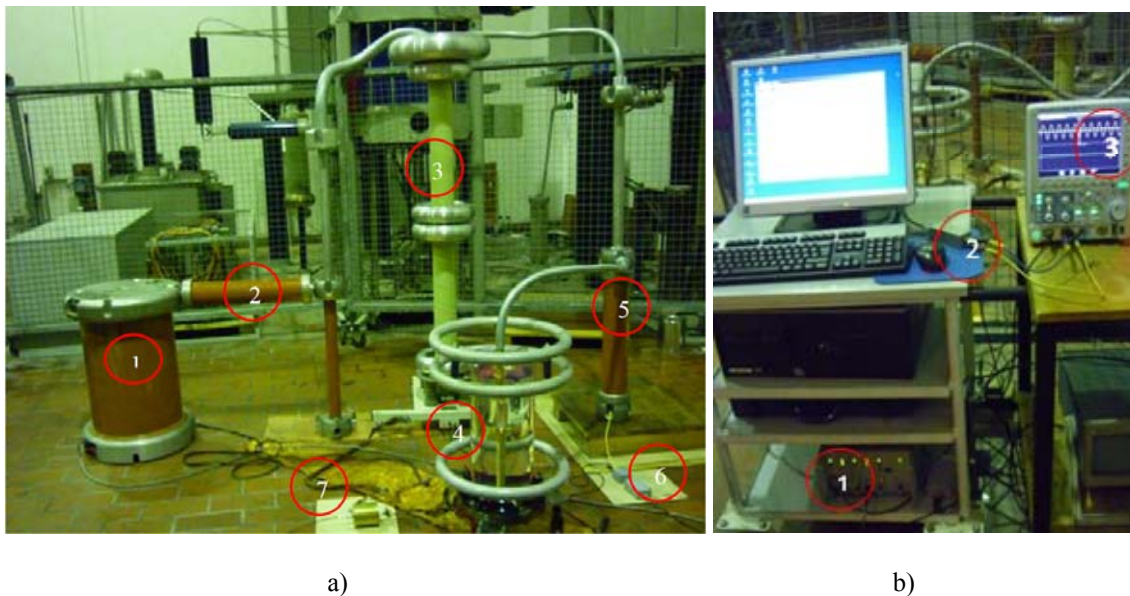


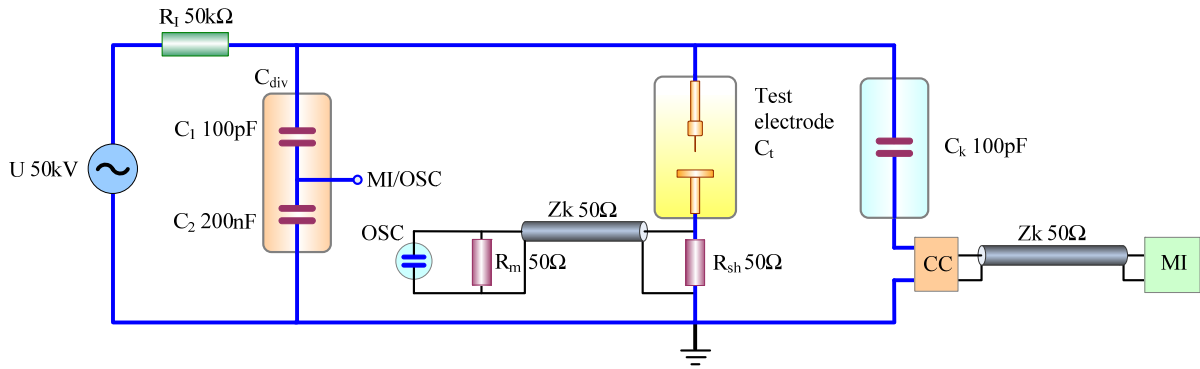
Figure 5.9: Test circuit setup

a) test circuit set up b) measuring system

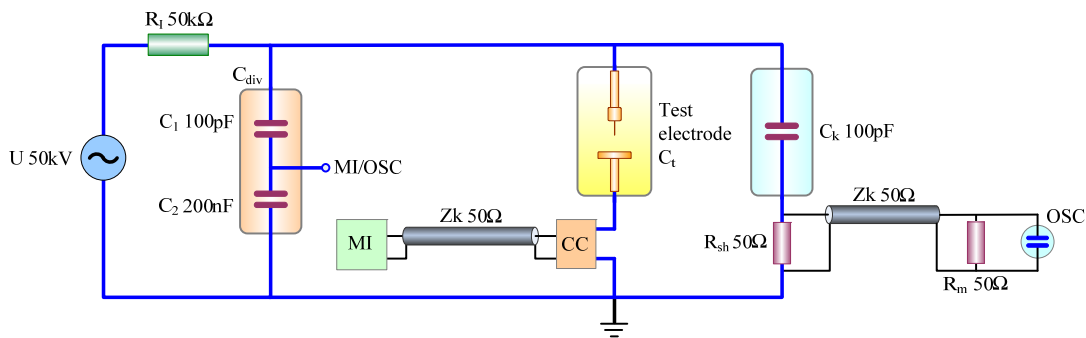
Where a) 1. High-Voltage supply 50 kV, 2. Current limiting resistor, R_1 : 50 k Ω , 3. Capacitive voltage divider, C_{div} :200kV, ratio 2,000:1, 4. Test vessel, C_t , 5. Coupling capacitor, C_k :100 kV, 100 pF, 6. Coupling device, CC, 7. Shunt resistor, R_{sh} : 50 Ω , b) 1. Measuring instrument ICM, 2. Matching impedance, R_m : 50 Ω , 3. Oscilloscope, Yokogawa DLM 2054, 2.2GS/s, 500 MHz

5.2.2 Test circuit for PDIV experiment with different PDIV test circuits

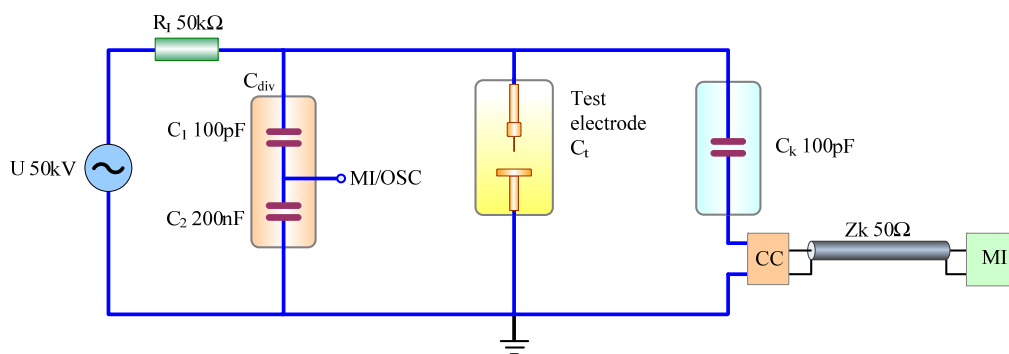
To study the effect of PDIV test circuits on PDIV value, 4 test circuits were set up as circuit diagrams shown in Fig 5.10. The test circuit 1 was used as the main test circuit for all of PDIV experiment.



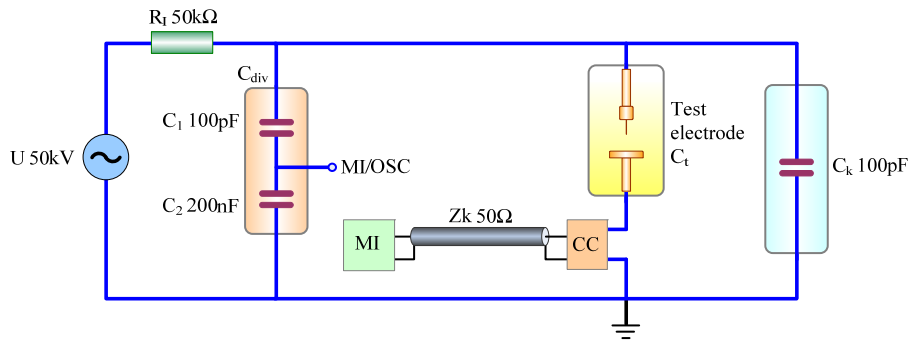
a)



b)



c)



d)

Figure 5.10: Test circuit diagrams for PDIV experiments

a) Test circuit 1 as a general PDIV test circuit b) Test circuit 2 c) Test circuit 3 d) Test circuit 4

5.3 Electrode systems and test specimen for arcing experiment

5.3.1 Electrode systems for arcing experiment

The tungsten rod electrodes with the diameter of 1 mm and 2 mm with the curvature of 0.2 mm as portrayed in Fig. 5.11 a) were used for arcing investigation. Arcing experiments were conducted in the test vessel with the rod-plane electrode arrangement as represented in Fig. 5.11 b). Fig. 5.11 c) exhibits the zoom in at the tip of the arcing rods. Besides, Table 5.3 summarizes the arcing electrodes used for arcing investigation.

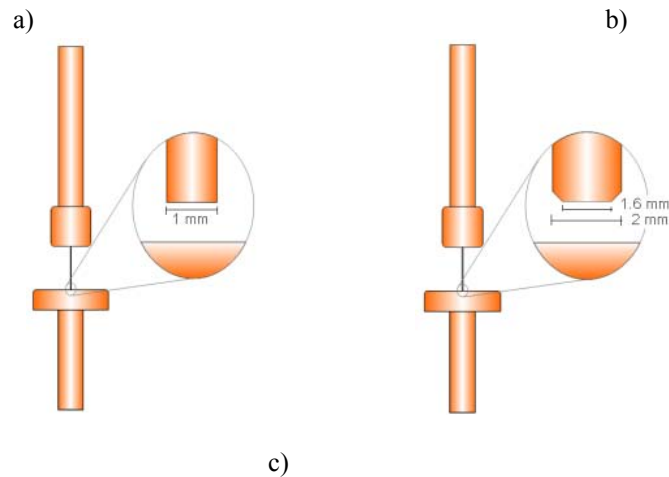
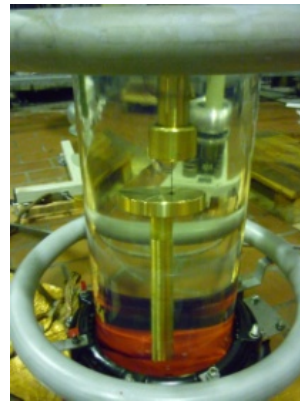
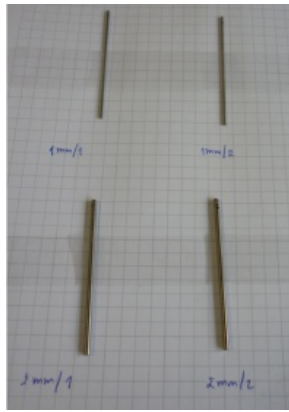


Figure 5.11: Arcing electrodes

a) arcing rods b) arcing rod in a test cell c) arcing rod diagram

Table 5.3: Electrode systems for arcing experiment

Electrode	Test experiment
1. Tungsten rods with the diameter of 1 mm and 2 mm with the curvature of 0.2 mm and with the length of 60 mm, 20 rods from China tungsten, China 2. Brass plane electrodes with diameter of 75 mm, 15 electrodes, from HV workshop TUG	1. Preliminary arcing test experiment: Test 7.5 2. SEM and EDX analysis for arcing electrode systems :Test 7.6.2

5.3.2 Mineral oil preparation for arcing experiment

The mineral oil for arcing test was prepared as the same as the low water content mineral employed for PDIV experiment.

5.4 Arcing test circuit set up

The investigation of arcing experiment was performed under atmospheric condition in high voltage laboratory. The test circuit diagram and experiment test set up are shown in Fig. 5.12 and Fig. 5.13 respectively.

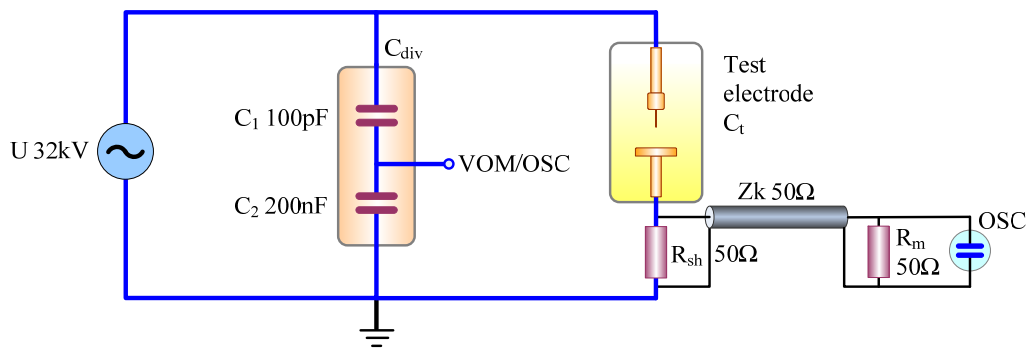
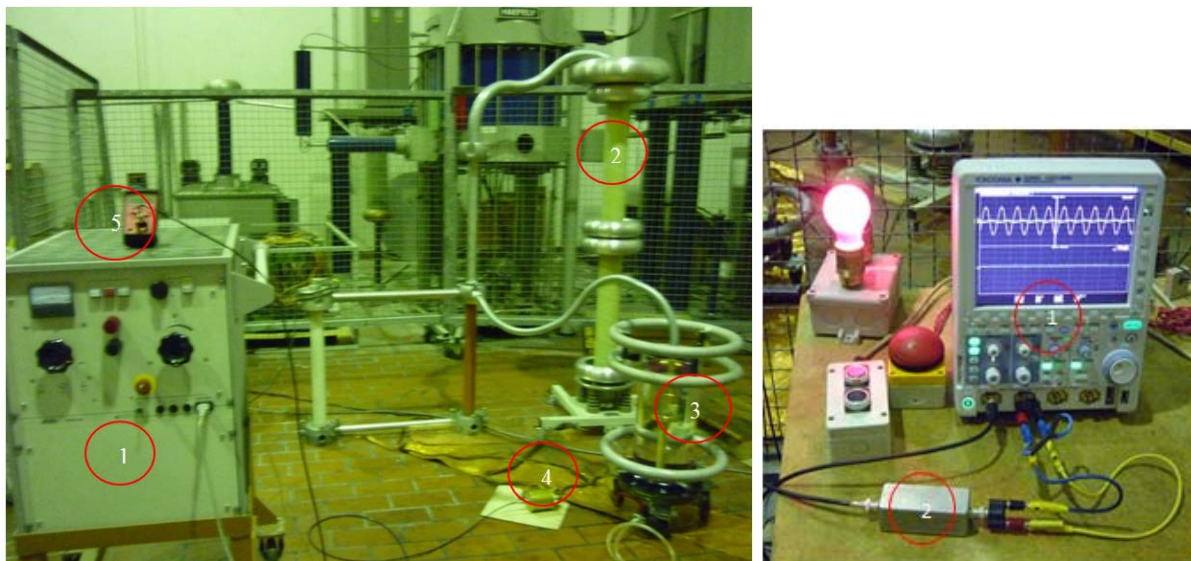


Figure 5.12: Test circuit diagram for arcing test



a)

b)

Figure 5.13: Test set up for arcing test

where: a) 1. High-voltage supply 8/16/32 kV, 5.5 kVA, 2. Capacitive voltage divider, C_{div} : 200 kV, ratio 2,000:1, 3. Test vessel rod – plane electrode arrangement, C_t , 4. Shunt resistor, R_{sh} ; 50 Ω , 5. Multimeter, b) 1. Oscilloscope, Yokogawa DLM 2054, 2.2GS/s, 500 MHz, 2. Matching impedance, R_m : 50 Ω

5.5 SEM and EDX analysis

Six needles and six plane electrodes randomly selected from the original and PDIV tested electrodes including six rods and six plane electrodes from the original and from the maximum arcing current test electrodes were prepared to be investigated by SEM and EDX test techniques. These experiments were performed by FELMI-ZFE: The Austrian Centre for Electron Microscopy and Nano Analysis. SE images, BSE images and EDX spectrum of the electrodes were created and analyzed.

5.6 Electric field simulation

The patterns of electric field distributions of electrode systems were simulated in order to compare with the results from the laboratory experiment. First of all, the simulation program :COMSOL Multiphysics, were used to simulate the needle - plane electrode system (the needle without the needle supporting electrode). Then, the simulation results were compared with the exact calculated results obtained from the formula 4.22. The comparison was done to make a certain that the further calculation of various dimensions of the real tested electrodes will give the corrected electric field value and correct pattern. The voltage level of the electrode systems for all simulation calculation was specified as 100 volts. The mesh generation of finite element program plays a predominant role on the correction of the filed simulation. Fig. 5.14 illustrates the examples of mesh generation for electric field simulation.

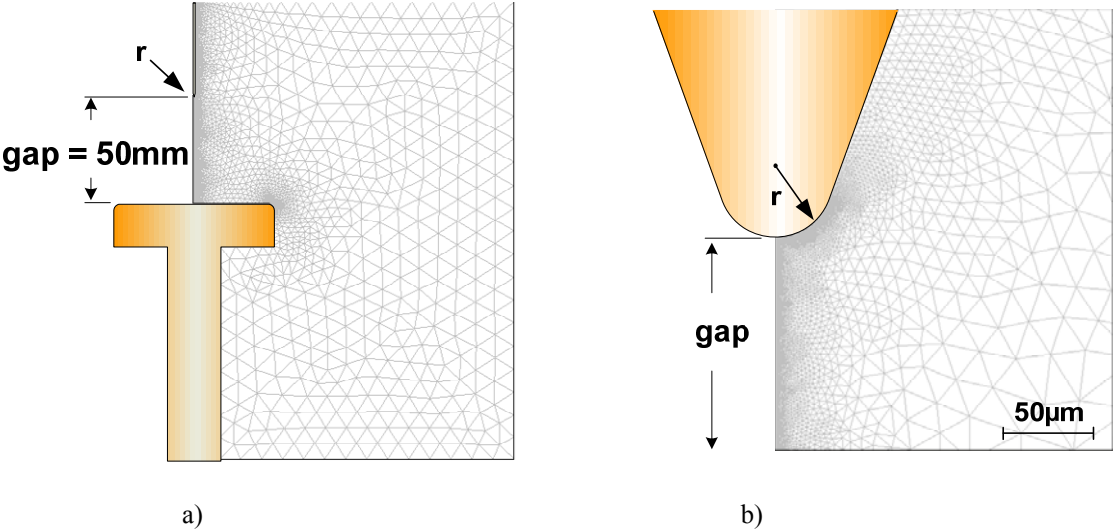


Figure 5.14: Mesh generation for electric field simulation

a) generating meshes b) zoom in of the generating meshes at the needle tip

The basic equation which is solved by the computer program can be expressed by Laplace 's equation as

$$\nabla^2 V = 0 \quad (5.1)$$

which can be rewritten as a two – dimensional Laplace 's equation as following

$$\frac{\partial^2 V}{\partial x^2} + \frac{\partial^2 V}{\partial y^2} = 0 \quad (5.2)$$

Where V is electric potential (volt)

For the boundary setting: the test voltage at the high voltage electrode was set as 100 volts and the grounded boundary voltage was set to zero and other boundary was set to be zero charge.

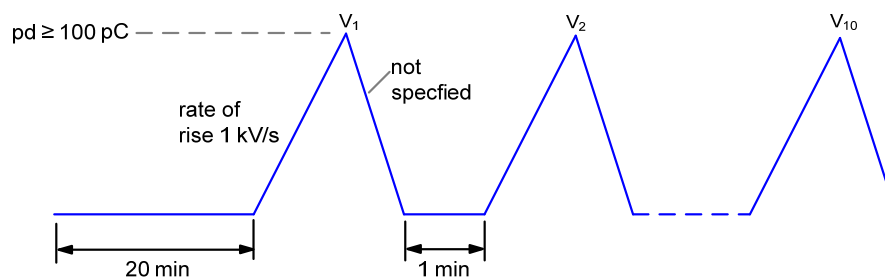
6 Experiment test procedure

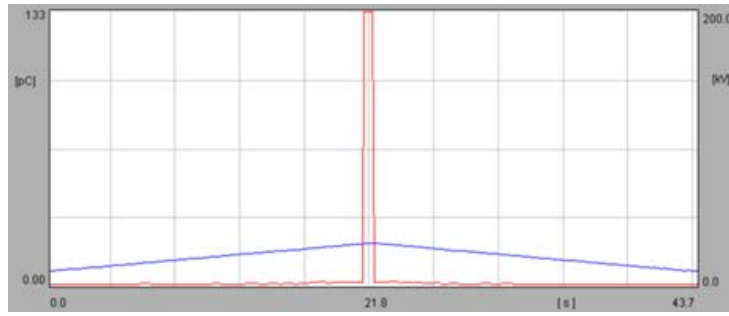
6.1 PDIV test procedure

Generally, PDIV value strongly depends on the PDIV definition associated with PDIV test methods. The most PDIV experiments in this dissertation, the PDIV test procedure was performed in accordance with IEC standard (M1) and also the combine PDIV test method with 100 pC charge detection (M2). Other 4 PDIV test methods were performed in order to study the effect of PDIV test methods on the PDIV characteristics. Details of each PDIV test procedure are described below.

6.1.1 PDIV standard test method (M1): IEC test method

The test procedure was performed in accordance with IEC TR 61294[55]. The test voltage was increased with a rate of 1 kV/s from zero until PDIV occurred (according to IEC TR 61294, at the first voltage that $PD \geq 100$ pC is defined as PDIV). Then, PDIV was recorded. Each needle – plane electrode was tested ten times in succession. For the preliminary PDIV test, 9 needles of each needle tip radius were investigated. For other PDIV experiments, only three needles of each needle tip radius were experimented. After that, the mean value PDIV (U_{PDIV}) of each electrode configuration was computed.





b)

Figure 6.1: PDIV standard test procedure (IEC)

a) test diagram b) experimental testing; the blue line is the tested voltage raise and the red line is PD activity

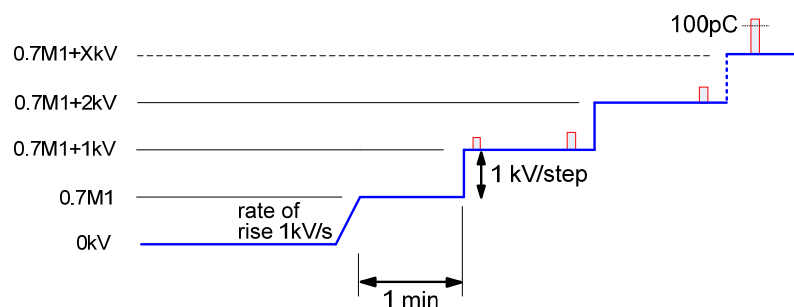
6.1.2 Combine PDIV test method with 100 pC charge detection (M2 and M3)

1) Combine PDIV test method 2 (M 2): 1 min /kV/step, 100 pC charge detection

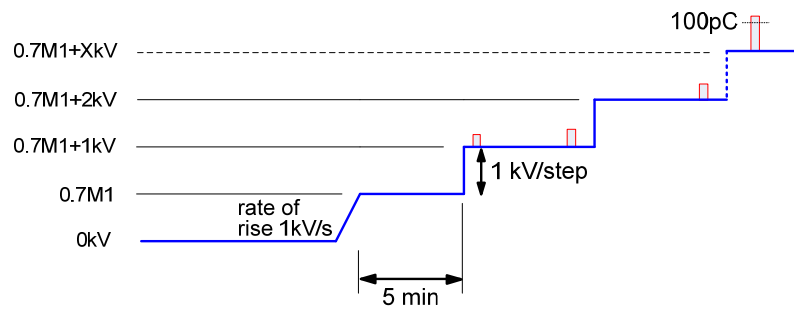
The test voltage was applied to the electrode arrangement with a rate of 1 kV/s from 0 to 70% of the PDIV value obtained from the first method (M 1). Then, the test voltage was increased in steps with 1 kV per step with a step duration of 1 minute until PDIV, the first voltage that $PD \geq 100$ pC, was detected. After that, the test voltage is step down to zero. The electrode system is de-energized for 3 minutes. Each needle-plane electrode was tested five times in succession. After that, the mean value PDIV (U_{PDIV}) from 5 PDIV testings was computed. Three needles with identical tip radius were investigated. Finally, the mean value PDIV of each electrode configuration from three identical needle-plane electrodes was computed.

2) Combine PDIV test method 3 (M3): 5min/kV/step, 100 pC charge detection

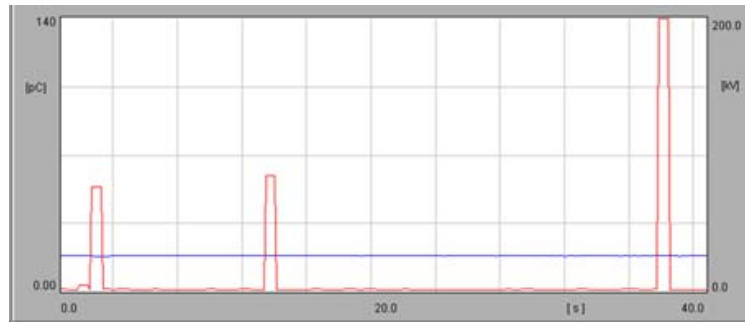
Details of the M3 test procedure were relatively similar to the M2 test procedure except the step duration was adjusted to 5 minutes.



a)



b)



c)

Figure 6.2: Combine PDIV test method with 100 pC charge detection

a) M2 test diagram b) M3 test diagram c) experimental testing: the blue line is the tested voltage raise and the red line is PD activity

6.1.3 Combine PDIV test method with the first PD pulse current detection (M4 and M5)

1) Combine PDIV test method 4 (M 4): 1 min /kV/ step, the first PD pulse current detection

For this experiment, the test voltage was applied to the electrode arrangement with a rate of 1 kV/s from 0 to 60% of the PDIV value obtained from the first method (M 1). Then, the test voltage was increased in steps with 1 kV per step with a step duration of 1 minute until the first observed PD pulse which had the PD pulse amplitude equal or higher than 2 times of background noise was detected; at this voltage level, the test voltage was recorded as the PDIV. After that, the test voltage is step down to zero. The electrode system is de-energized for 3 minutes. Each needle-plane electrode was tested five times in succession. After that, the mean value PDIV (U_{PDIV}) from 5 PDIV testings was computed. Three needles with identical tip radius were investigated. Finally, the mean value PDIV of each electrode configuration from three identical needle-plane electrodes was computed.

2) Combine PDIV test method 5 (M 5): 5 min /kV/ step, the first PD pulse current detection.

Details of the M5 test procedure were relatively similar to the M4 procedure except the step duration was adjusted to 5 minutes.

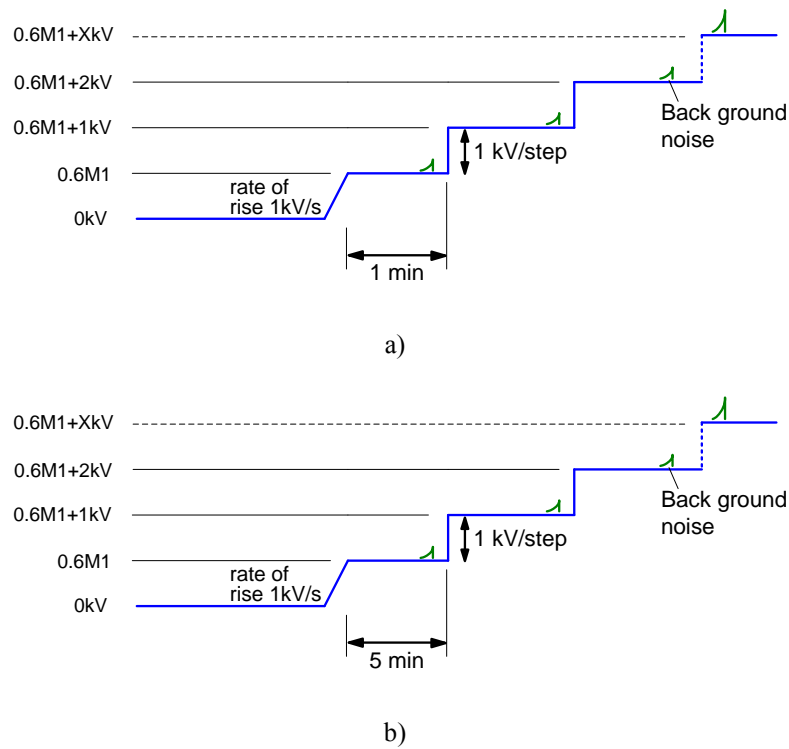


Figure 6.3: Combine PDIV test method with the first PD detection

a) M4 test diagram, b) M5 test diagram,

6.1.4 Up and down PDIV test method with 100 pC charge detection (M 6)

The test voltage was applied to the electrode arrangement with a rate of 1 kV/s from 0 to 70% of the PDIV value obtained from the first method (M 1). Then, the test voltage was increased in steps with 1 kV per step with a step duration of 1 minute until PDIV; the first voltage that $PD \geq 100$ pC, was detected. Then, the applied voltage was reduced by 1 kV. At this applied voltage level, if $PD < 100$ pC, the applied voltage was again raised by 1 kV otherwise the applied voltage was reduced another 1 kV if $PD \geq 100$ pC was detected. The process was repeated until a predetermined number n of the voltage value, V_1, V_2, \dots, V_{100} was obtained. After that, the mean value PDIV (U_{PDIV}) of each electrode configuration was computed.

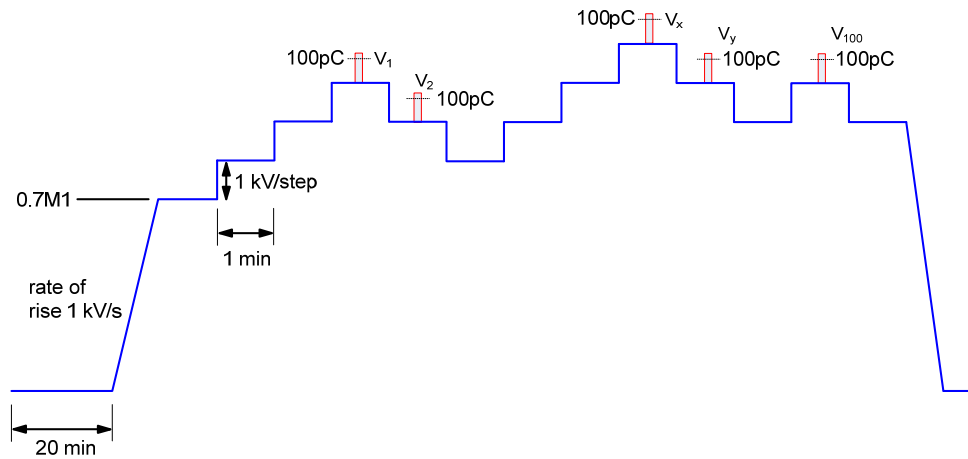


Figure 6.4: Up and down PDIV test method with 100 pC charge detection

6.2 PD activity measurement

After PDIV measurement was done, PD activities were examined at the PDIV level. The phase-resolved PD patterns and PD charge quantities (Q_{IEC}) of the mineral oil were measured and recorded with the conventional PD measurement, ICM.

6.3 PD pulse current measurement

PD pulse currents were detected by the shunt resistor of 50Ω . Then, the current signals were sent to the digital oscilloscope, Yokogawa DLM 2054, 2.2 GS/s, 500 MHz for displaying and recording.

6.4 Arcing test procedure

Arcing voltages and arcing currents were investigated with two gap distances, 0.3 and 0.8 mm respectively. The test experiment was modified from IEC 60156 [189]. After installing the rod-plane electrode, the rod diameter of 1 mm with gap spacing of 0.8 mm, the mineral oil was filled in to the test cell before performing the experiment about 20 minutes. Then, the AC test voltage was applied to the electrode system from zero until a complete arcing occurred, the completed arcing was determined as the first minimum arcing current was equal or higher than 100 mA. The test voltage was kept at that arcing voltage level for 10 seconds. The arcing current and arcing voltage were recorded. In addition, PD pulse currents before the arc occurred as well as the arcing current signals were detected by using the 50 ohm shunt resistor which were displayed and recorded by oscilloscope. The oil sample was tested for one arcing rod with the same procedure for 6 times in succession with 3 minutes pause of each arcing test. The test was also conducted with other four rods of 1 mm diameter with gap distance of 0.8 mm. The mean value of arcing currents (I_{ARC}) and arcing voltages (U_{ARC}) were calculated. After that, the test was carried on with the other rods with diameter of 1 mm, with

gap distance of 0.3 mm and the rods with diameter of 2 mm (with the curvature of 0.2 mm) with gap distance of 0.8 and 0.3 respectively. Furthermore, one brass plane electrode was prepared for the arcing test with three rods under the same condition.

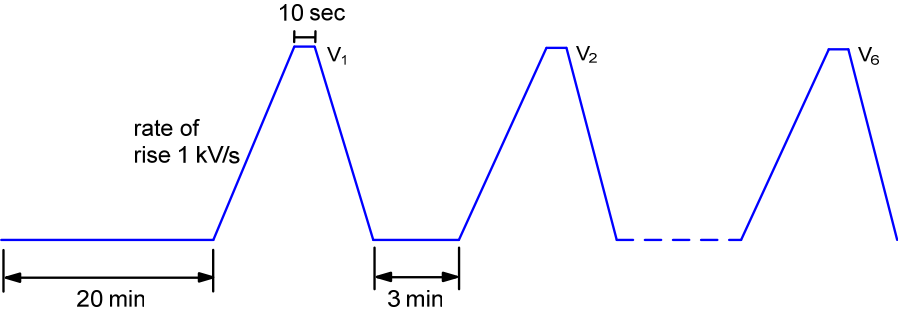


Figure 6.5: Arcing test diagram

7 Test results

7.1 Electric field simulation

The electric field simulation test results of the needle (without high voltage supporting rod) - plane electrode configuration obtained from FEM program and from the exact calculation using formula 4.22 were nearly the same. Then, the electric field distributions of electrode systems for PDIV and arcing experiments were simulated as presented in 7.1.1- 7.1.4.

7.1.1 Electric field patterns of the electrode systems with different tip radius needles for preliminary PDIV test

The electric field distributions pattern of the electrode systems affects substantially the PD, PDIV and breakdown characteristic of the insulation system. Fig. 7.1 shows the electric field magnitude line distributions of the needle- plane electrode systems and the electric field at the tip of the needles respectively. Table 7.1 summarizes the maximum electric field of the needle- plane electrodes used for preliminary PDIV experiment.

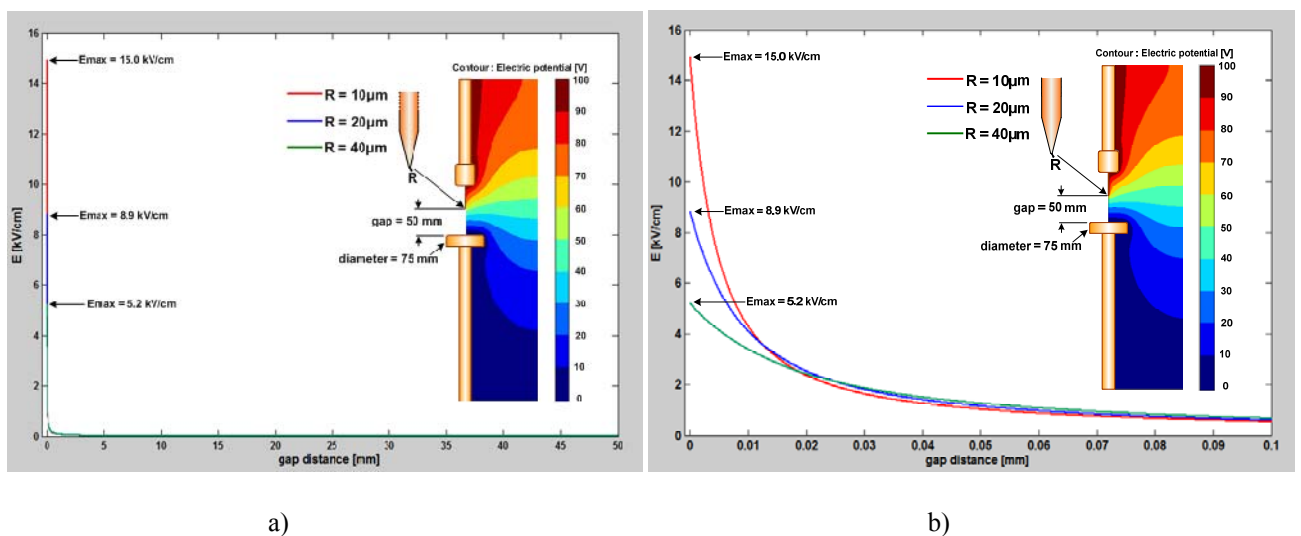



Figure 7.1: Electric field magnitude line distributions of the needle- plane electrode systems

a) electric field distribution of the tested electrode systems b) electric field at the needle tips

Table 7.1: Maximum electric field magnitude of the electrode systems for preliminary PDIV test as a function of needle tip radii

Electrode configuration	Gap distance (mm)	Maximum electric field strength (kV/cm)		
		tip radius 10 μm	tip radius 20 μm	tip radius 40 μm
 Needle-plane electrode (75 mm dia.)	50	15.0	8.9	5.2

7.1.2 Electric field patterns of the electrode systems with different tip radius needles and different grounded electrode types and dimensions

The electric field distribution patterns of the electrode systems with different needle tip radii, different grounded electrode types and dimensions as well as different gap distances are relatively the same. Fig. 7.2 represents the electric field magnitude line distributions near the tips of the needles of the needle-plane electrode systems with the needle tip radius of 10 μm , 20 μm and 40 μm , plane diameter of 50 mm and 75 mm, and gap distance of 25 mm and 50 mm respectively. Fig. 7.3 illustrates the electric field magnitude line distributions in the vicinity of the tips of the needles of the needle-sphere electrode systems with the needle tip radius of 10 μm , 20 μm and 40 μm , the sphere electrodes with diameter of 12.7, 25.4, 50.8 and 76.2 mm, and gap distance of 25 mm and 50 mm respectively. The maximum electric field magnitudes of different electrode configurations both the needle-plane and the needle-sphere electrode systems are depicted in Table 7.2.

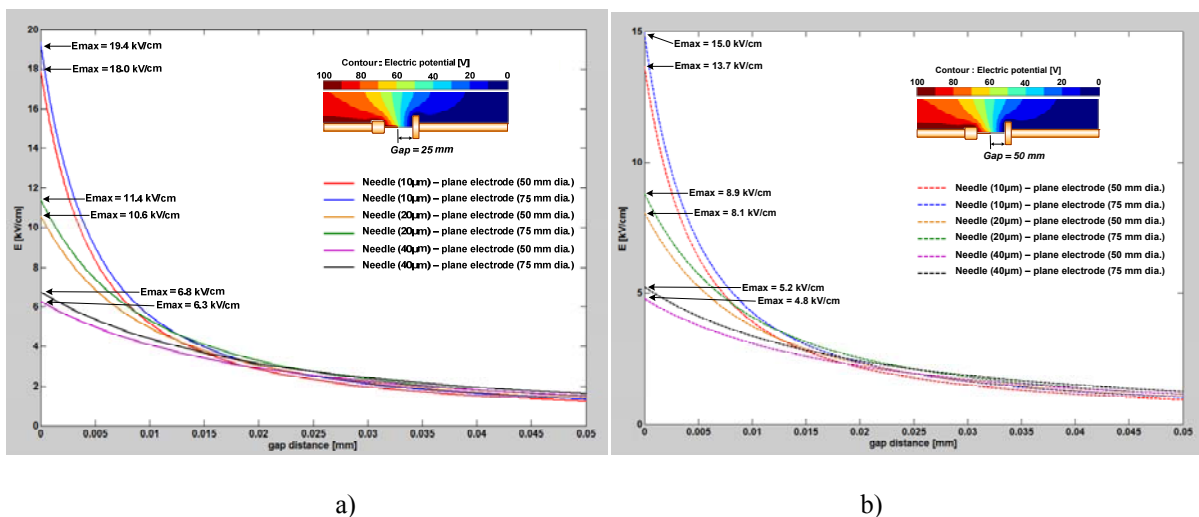
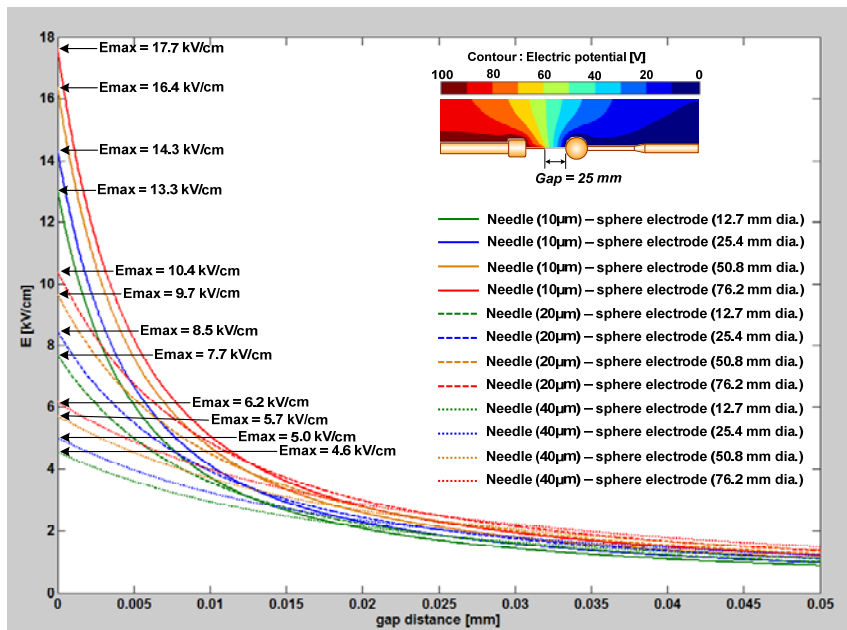
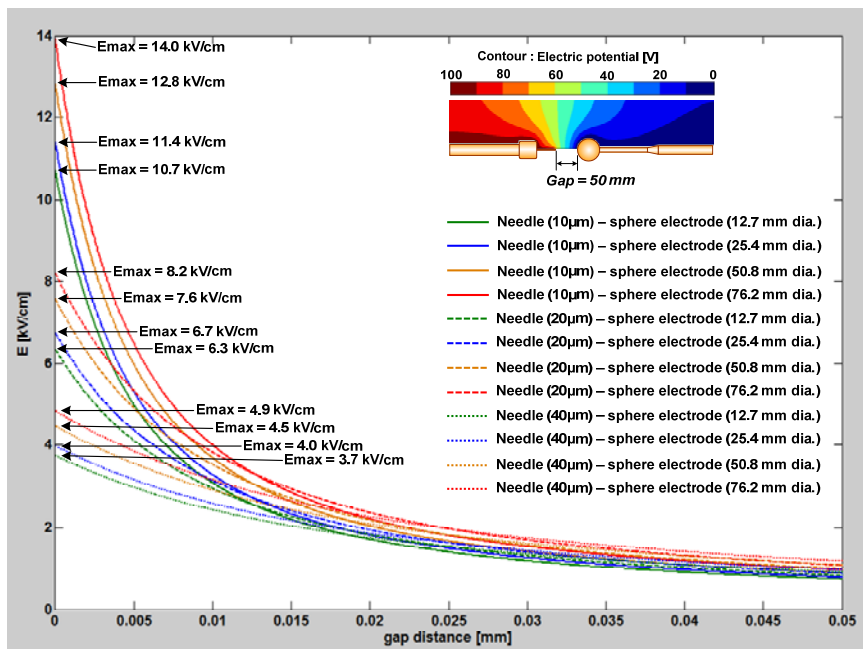


Figure 7.2: Electric field magnitude line distributions near the needle tips of the needle-plane electrode systems with different gap distances

a) electric field distribution of the tested electrodes with gap distance of 25 mm b) with gap distance of 50 mm



a)



b)

Figure 7.3: Electric field magnitude line distributions near the needle tips of the needle-sphere electrode systems with different gap distances

a) electric field distribution of the tested electrodes with gap distance of 25 mm b) with gap distance of 50 mm

Table 7.2: Maximum electric field magnitude of the electrode systems with different needle tip radii, different electrode shapes and gap distances







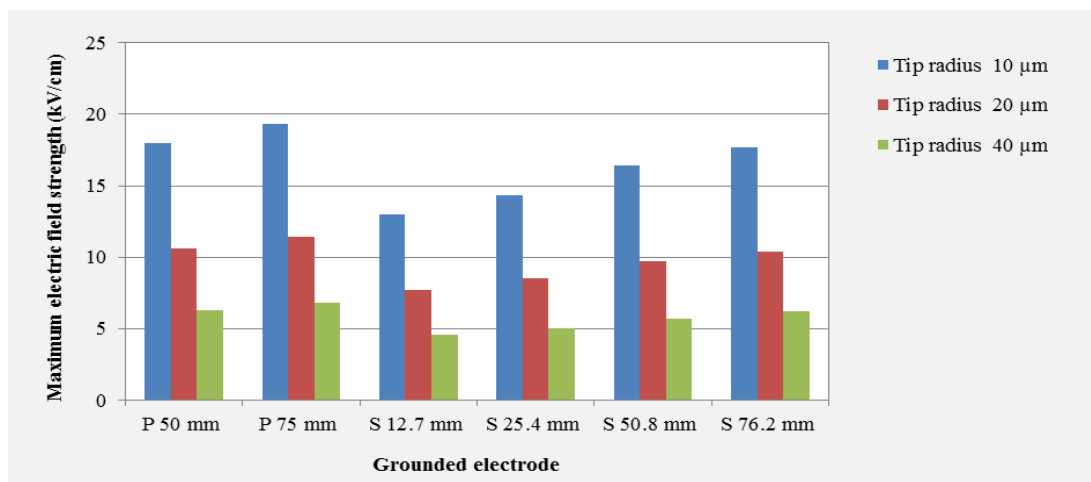
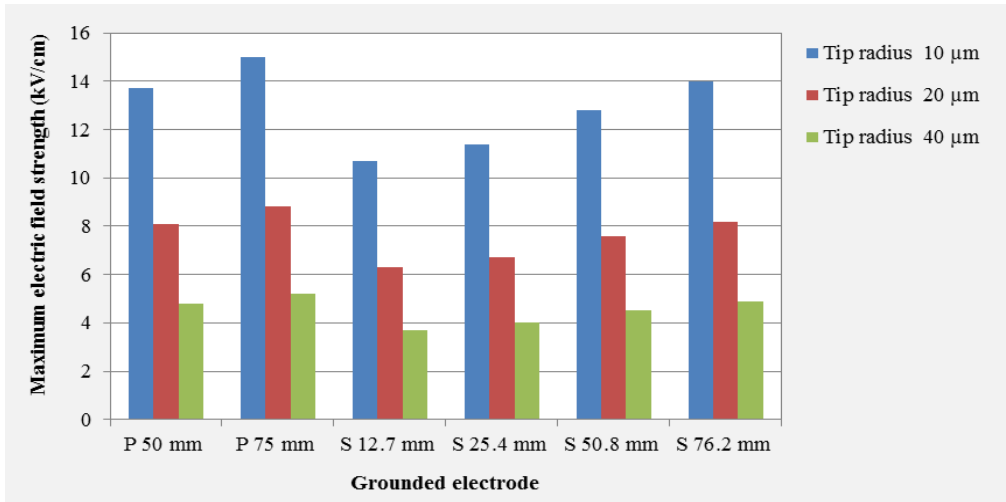
Electrode configuration	Gap distance (mm)	Maximum electric field strength (kV/cm)		
		tip radius 10 μm	tip radius 20 μm	tip radius 40 μm
 Needle - plane electrode (50 mm dia.)	25	18.0	10.6	6.3
	50	13.7	8.1	4.8
 Needle - plane electrode (75 mm dia.)	25	19.4	11.4	6.8
	50	15.0	8.9	5.2
 Needle - sphere electrode (12.7 mm dia.)	25	13.3	7.7	4.6
	50	10.7	6.3	3.7
 Needle - sphere electrode (25.4 mm dia.)	25	14.3	8.5	5.0
	50	11.4	6.7	4.0
 Needle - sphere electrode (50.8 mm dia.)	25	16.4	9.7	5.7
	50	12.8	7.6	4.5
 Needle - sphere electrode (76.2 mm dia.)	25	17.7	10.4	6.2
	50	14.0	8.2	4.9

Fig. 7.4 below shows that the needle tip radii have a strong influence on the maximum electric field strength. However, the grounded electrodes have not much an effect on the electric field strength.



a)



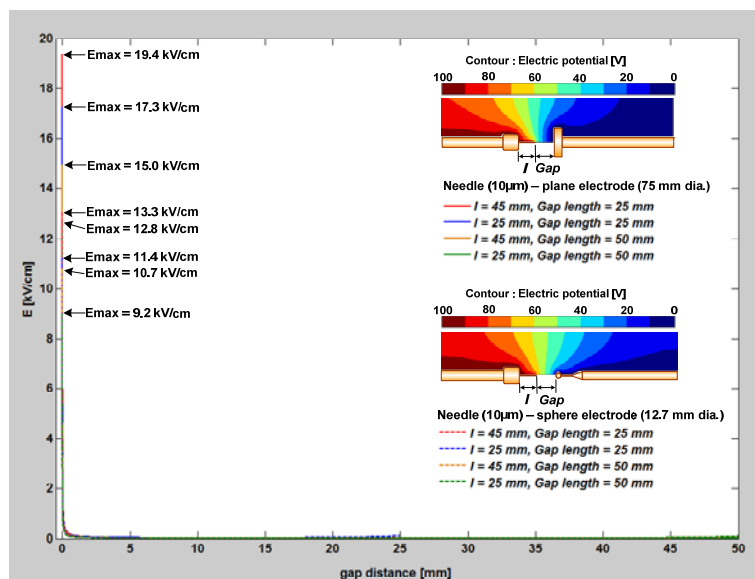
b)

Figure 7.4: Maximum electric field magnitude of the electrode systems with different needle tip radii, different electrode shapes and gap distances: p represents a plane electrode and s represents a sphere electrode

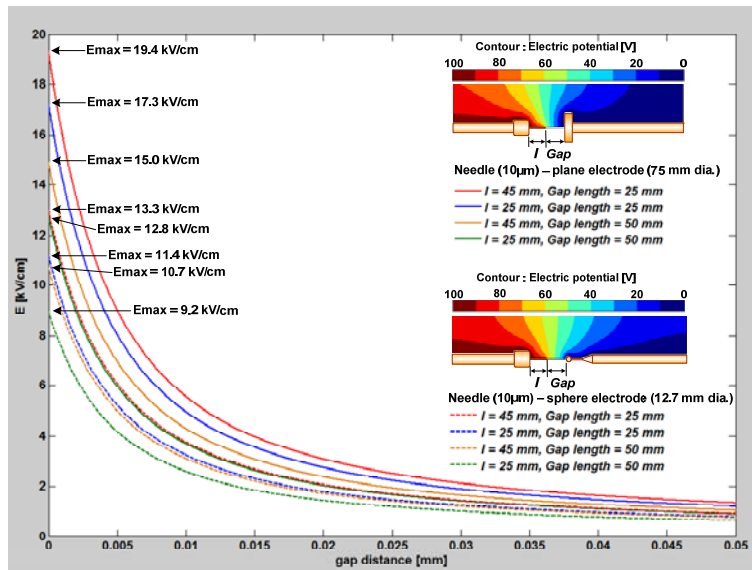
a) gap distance of 25 mm b) gap distance of 50 mm

7.1.3 Electric field patterns of the electrode systems for needle electrodes with different needle lengths

Electric field distribution of the 10 μm tip radius needle-75 mm diameter plane electrode and of the 10 μm tip radius needle - 12.7 mm diameter sphere electrode configuration with needle length of 25 mm and 45 mm were simulated. The electric field magnitude line distributions of these electrode systems are illustrated in Fig.7.5. The maximum electric field magnitude of these electrode systems are depicted in Table 7.3.



a)





b)

Figure 7.5: Electric field magnitude line distributions of the needle-plane and of the needle-sphere electrode systems with different needle lengths

a) electric field distributions of the tested electrode systems b) at the needle tips

Table 7.3: Maximum electric field magnitude of the electrode systems with different needle lengths

Electrode configuration	Gap length (g: mm)	Maximum electric field strength (kV/cm)	
		$l = 25$ mm	$l = 45$ mm
 Needle – plane electrode (75 mm dia.)	25	17.3	19.4
	50	12.8	15.0
 Needle – sphere electrode (12.7 mm dia.)	25	11.4	13.3
	50	9.2	10.7

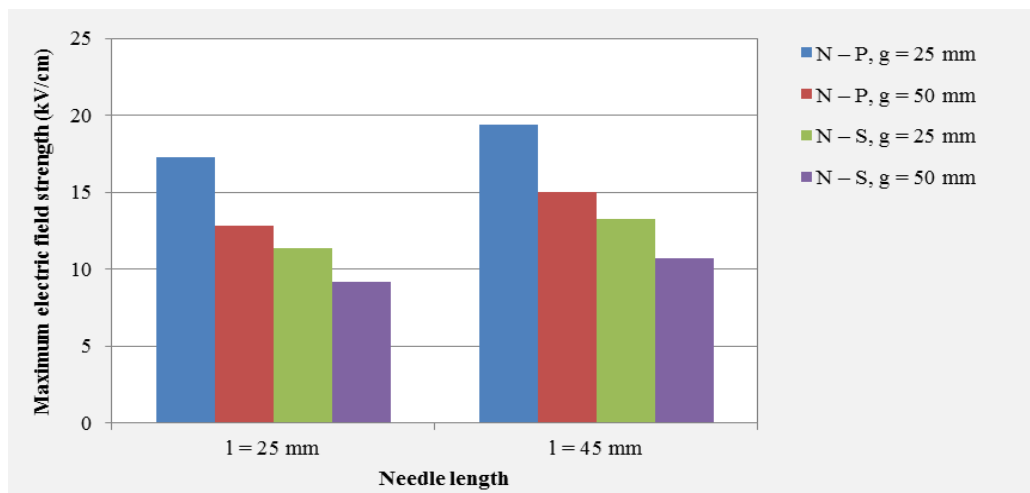
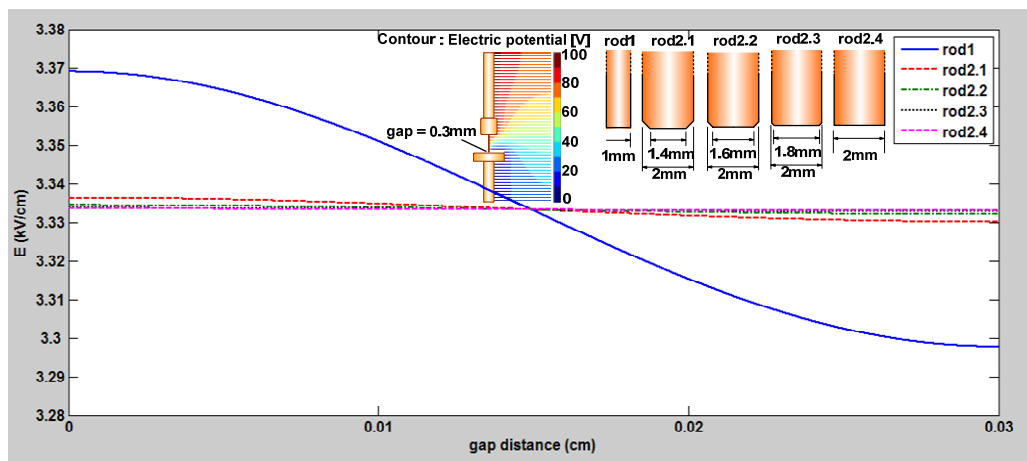


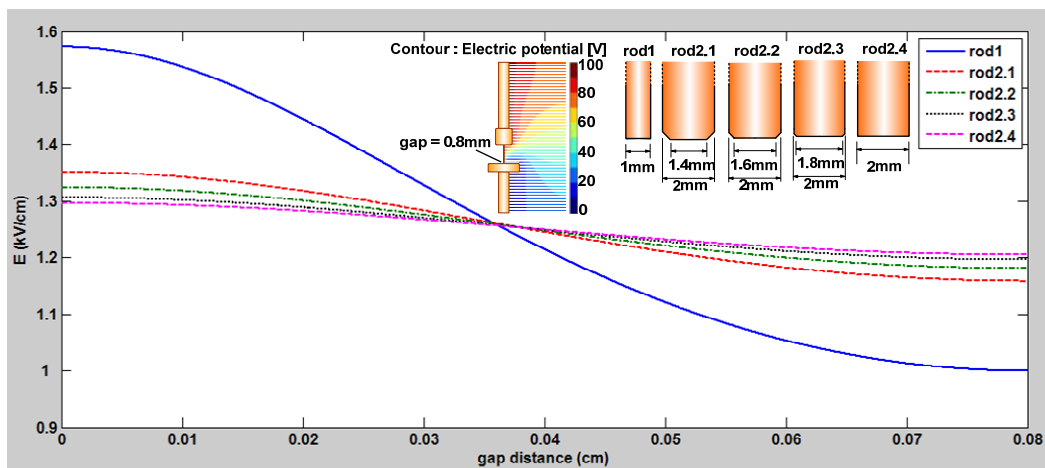
Figure 7.6: Comparison of maximum electric field magnitude of the electrode systems with different needle lengths

7.1.4 Electric field patterns of the electrode systems with different diameter rods and different gap distances

The electric field magnitude line distributions of the electrode systems for arcing test with gap distances of 0.3 mm and 0.8 mm are shown in Fig.7.7. According to Fig. 7.7 the electric field of the 2 mm diameter rod-plane electrode with the rod curvature of 0.1 mm, 0.2 mm and 0.3 mm are analogous. The 2 mm diameter rods with the curvature of 0.2 mm was selected for arcing experiment compared with arcing test with the 1 mm diameter rods. The 2 mm diameter rod with the curvature of 0.2 mm was selected to perform arcing test because it was not difficult to prepare and the curvature configuration at the rod tip which might affect the arcing current and erosion could be investigated. Fig. 7.8 represents the electric field magnitude line distributions of the experimented rod- plane systems. The summary of maximum electric field magnitudes of the arcing rod- plane electrodes employed in the arcing experiment is listed in Table 7.4.



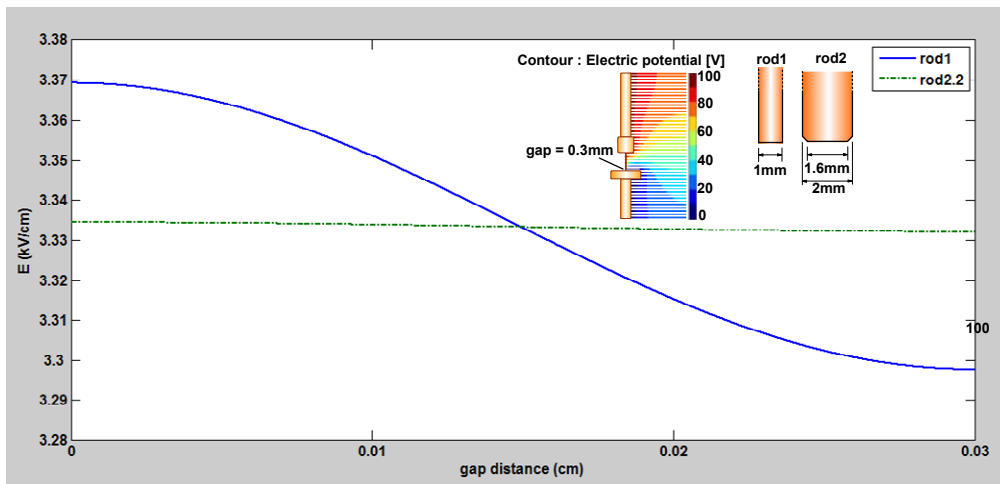
a)



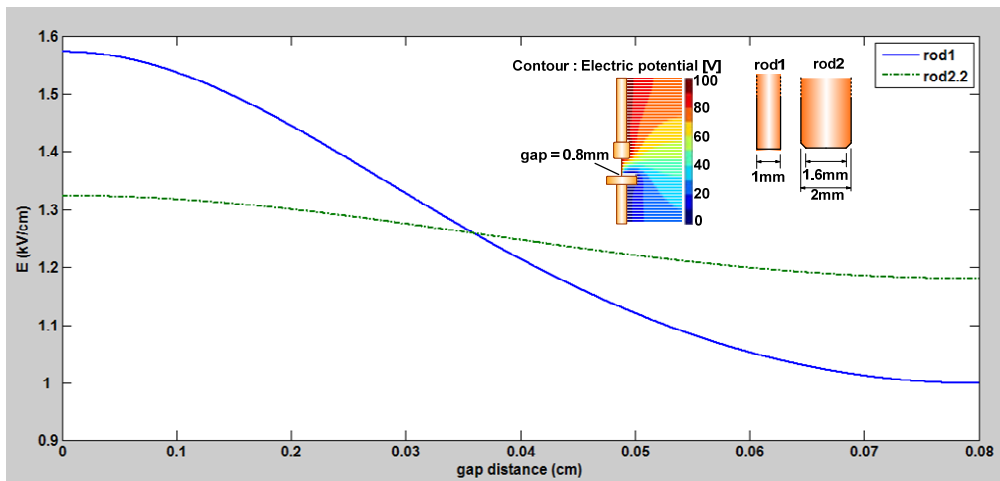
b)

Figure 7.7: Electric field magnitude line distributions of the rod-plane electrode systems with

a) gap distance of 0.3 mm b) gap distance of 0.8 mm



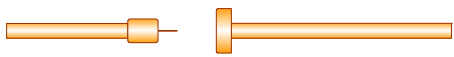
a)



b)

**Figure 7.8: Electric field magnitude line distributions of the arcing rod- plane electrode systems with
a) gap distance of 0.3 mm b) gap distance of 0.8 mm**

Table 7.4: Maximum electric field magnitude of the experimented rod-plane electrode systems

Electrode configuration	Gap length (mm)	Maximum electric field strength (kV/cm)	
		Rod dia of 1 mm	Rod dia of 2 mm with the curvature of 0.2 mm
 Rod – plane electrode (75 mm dia.)	0.3	3.37	3.33
	0.8	1.58	1.33

7.2 PDIV characteristics of the mineral oil

7.2.1 Preliminary PDIV experiment

The preliminary PDIV test was performed to investigate the basic parameters which affected the PDIV value. The basic investigation parameters comprised of the needle tip radius, the test sequence in case of three different tip radius needles 10 μ m, 20 μ m, 40 μ m were used to perform the PDIV experiment with the same mineral oil, and the possibility PDIV testing numbers for one oil test sample. This preliminary test employed the needles from BAUR company. The PDIV test circuit was set up according to IEC 60270 and the PDIV test procedure was experimented according to IEC 61294. The test experiment was divided into two parts as the PDIV experiment A and the PDIV experiment B.

The PDIV experiment A was carried out with 9 oil samples. 3 different tip radius needles with 10 μ m, 20 μ m, 40 μ m were used for PDIV testing of each oil test sample. For the first oil sample, the PDIV experiment tested by the 10 μ m tip radius needle was carried out, the PDIV and PD activity were recorded. Then, the experiment was carried out with 20 μ m, and 40 μ m tip radius needle respectively. For the second oil test sample, the PDIV experiment was achieved with the 20 μ m tip radius needle. After that, further PDIV experiments were done by using the 40 μ m and 10 μ m tip radius needle respectively. For the third oil test sample, the PDIV experiment was performed with the 40 μ m tip radius needle. Next, the PDIV experiments were implemented by using the 10 μ m and 20 μ m tip radius needle respectively. The fourth and seventh oil test samples were carried out similarly as the first oil test sample, while the fifth and the eighth oil test samples were experimented analogously as the second oil sample. The sixth and the ninth oil test samples were tested equivalent to the third oil test sample.

The PDIV experiment B was done with 3 oil samples. One oil sample was tested with 5 needles with the same needle tip radius.

The PDIV test results from both experiments are listed in Table 7.5 and Table 7.6 and summarized in Table 7.7 and Fig. 7.9 respectively.

Table 7.5: Mean value PDIV from 10 time testings of each needle-plane arrangement as a function of needle tip radius with σ_u as standard deviation in kV obtained from the preliminary PDIV experiment A

Needle tip radius	Needle number										
	N1	N2	N3	N4	N5	N6	N7	N8	N9	U_{PDIV}	σ_U
10 μ m	31.9	28.8	32	28.7	29.6	34.4	31.8	32.9	30.7	31.2	1.9
20 μ m	34.3	35.2	34.2	35.7	35.9	40.1	38.0	35.3	33.8	35.8	2.0
40 μ m	47.0	44.0	48.0	41.3	40.9	41.6	42.7	41.3	42.4	43.2	2.6

Table 7.6: Mean value PDIV from 10 time testings of each needle- plane arrangement as a function of needle tip radius with σ_u as standard deviation in kV obtained from the preliminary PDIV experiment B

Needle tip radius	Needle number						
	N10	N11	N12	N13	N14	U_{PDIV}	σ_U
10 μm	30.9	29.3	30.4	30.4	31.9	30.6	1.0
20 μm	35.5	35.1	37.7	34.9	31.7	35.0	2.1
40 μm	41.9	41.3	40.2	41.3	43.1	41.6	1.1

Table 7.7: Comparison of the mean value PDIV from preliminary PDIV experiment A and B

Test experiment	Needle tip radius					
	10 μm		20 μm		40 μm	
	U_{PDIV}	σ_U	U_{PDIV}	σ_U	U_{PDIV}	σ_U
experiment A	31.2	1.9	35.8	2.0	43.2	2.6
experiment B	30.6	0.9	35.0	2.1	41.6	1.1

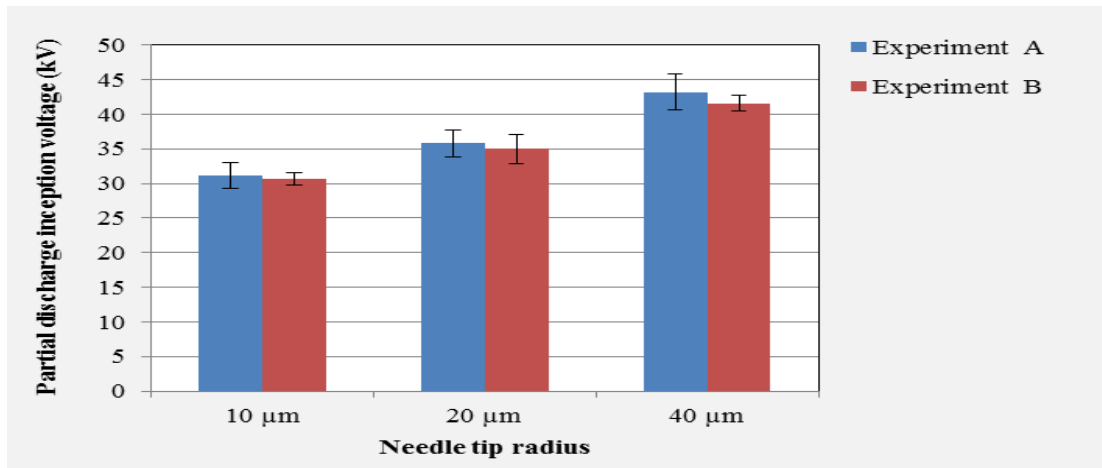


Figure 7.9: Comparison of the mean value PDIV as a function of needle tip radius with σ_U as standard deviation in kV obtained from test experiment A and B

From the test results, the mean value PDIV depended clearly on the needle tip radius. The PDIV obtained from the needle-plane electrode with the needle tip radius of 10 μm , 20 μm , and 40 μm was about 31 kV, 35 kV and 42 kV respectively. The standard deviation was about 6 percent. The PDIV acquired from experiment A and experiment B was relatively the same. Therefore, one oil sample can be tested with three different tip radius needles of 10 μm , 20 μm , 40 μm or can be experimented with the identical needle tip radius at least 5 needles. To analyze the distribution of the test data, firstly, the distribution of each raw test data obtained from each needle-plane electrode system had to be analyzed. Then, the distribution of PDIV value of each experiment will be investigated.

Distribution statistic for PDIV test of each needle-plane electrode: the PDIV raw data obtained from the needle (needle 1)- plane electrode configuration depicted in Table 7.8 was selected to analyze the distribution. The 10 raw data PDIV values were modelled using normal, weibull, lognormal, and exponential distribution. The probability plot as shown in Fig.7.10 illustrates the goodness of fit test of each distribution whether it was fit with the PDIV raw data or not.

Table 7.8: PDIV raw data obtained from the needle (number 1)-plane electrode configuration

Needle Tip Radius	Testing number										U_{PDIV}	σ_U
	1	2	3	4	5	6	7	8	9	10		
10 μm	30.2	30.8	29.5	28.8	31.8	36.6	29.7	36.0	32.8	32.8	31.9	2.7
20 μm	32.6	33.7	35.1	32.7	31.4	32.1	34.8	37.7	37.4	35.3	34.3	2.2
40 μm	45.9	48	50	42.7	47.5	47.2	50	50	43.8	45.2	47.0	2.6

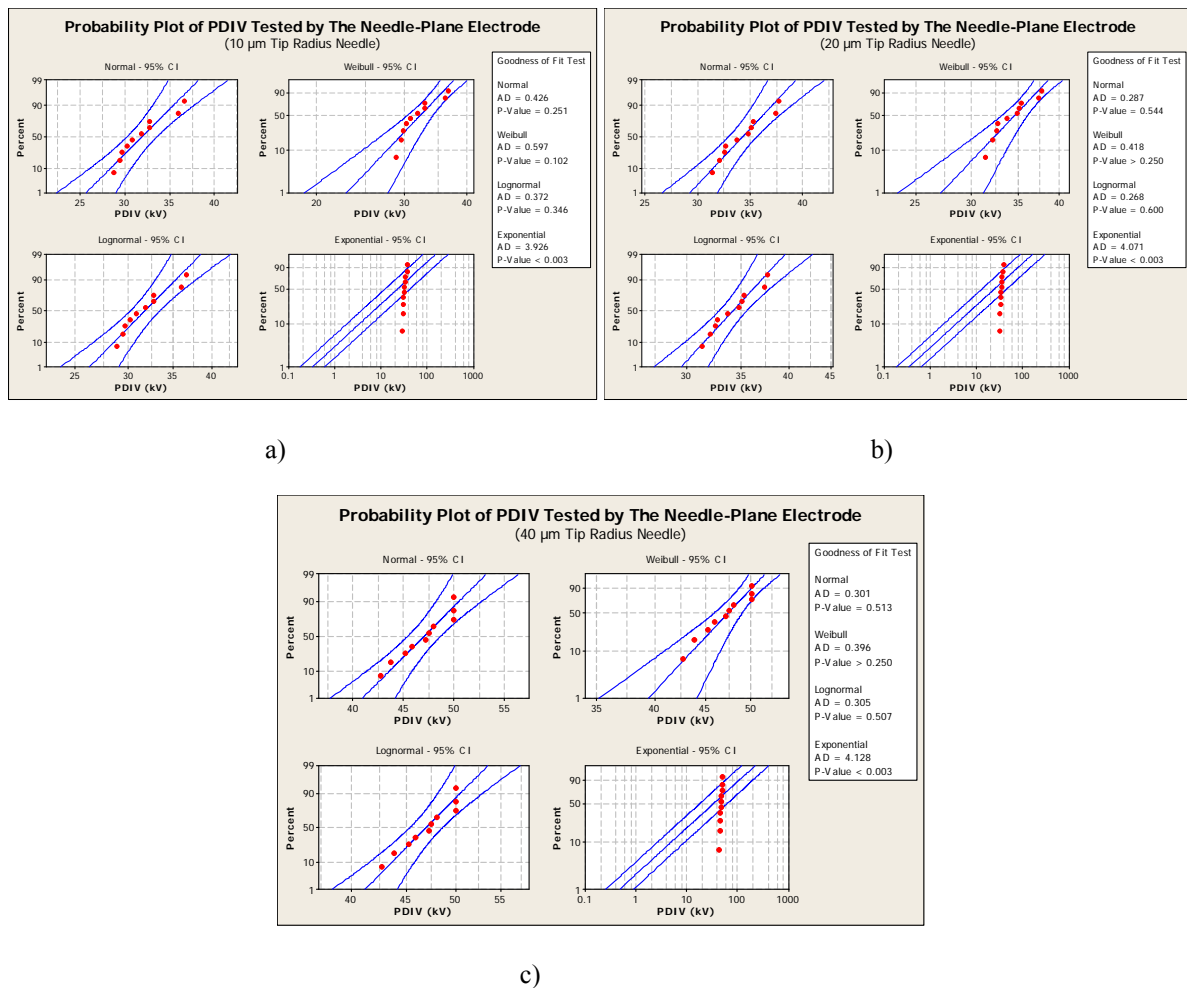


Figure 7.10: Probability plot of PDIV raw data obtained from the needle (needle 1) - plane electrode configuration

The probability plot shows that the normal distribution was a little bit fitter than weibull and log normal distribution for the PDIV experiment tested by 10µm, 20µm and 40 µm tip radius needles as one can compare with the Anderson - darling goodness-of-fit values. However, the weibull and log normal distribution provided also a well description for PDIV test data. In this case, the exponential distribution was very poor model for the PDIV raw data. In addition, the p value which was higher than 0.05 indicated that there was not enough evidence in the raw data to reject the null hypothesis for normal, weibull and log normal distribution that meant these three distributions were good fit for the PDIV raw data. The next step analysis, the probability plot of normal and weibull distibuiton will be examined to compare the PDIV test results obtained from different needle tip radii-plane electrode systems. The histogram and the probability plot of normal distribution and weibull distribution for PDIV test data comparing between needle tip radii are shown in Fig. 7.11.

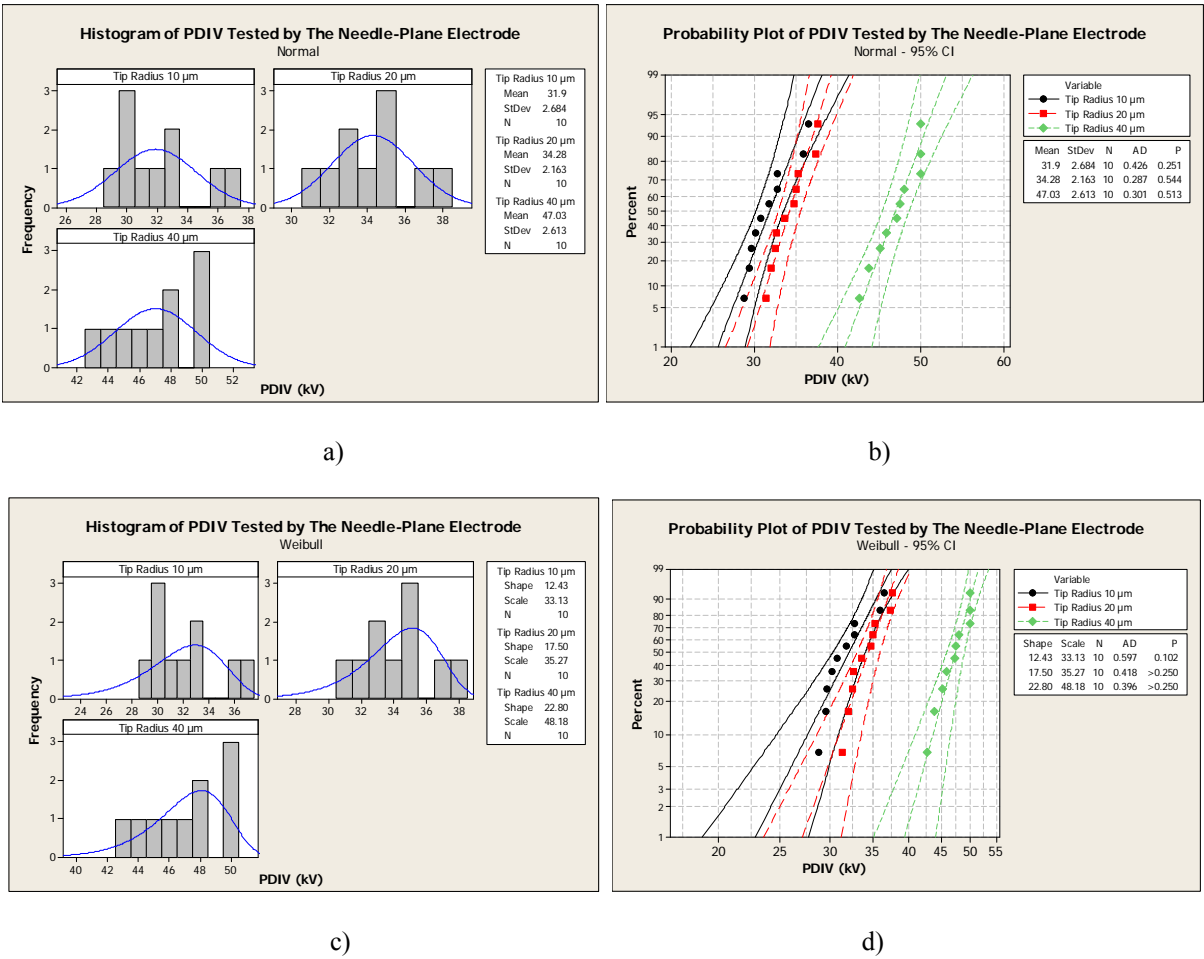


Figure 7.11: Histogram and the probability plot for PDIV raw data

a) histogram with normal distribution plot b) probability plot of normal distribution c) histogram with weibull distribution plot d) probability plot of weibull distribution

From the test result of PDIV raw data, it was founded that both normal and weibull distributions could be used to explain the distribution of the the test data. The normal distribution was a little bit fitter than weibull distribution.

Distribution statistic of PDIV experiment A and B: the distribuion of the test results form the PDIV experiment A and B were modelled as shown in Fig. 7.12- Fig. 7.13. The distributions revealed that the test results from experiment B was a little bit fitter with the normal and weibull distribution than the test results from experiment A. The scale parameters form weibull distribution were more or less a little bit higher than the mean values obtained from the normal distribution for all test experiments.

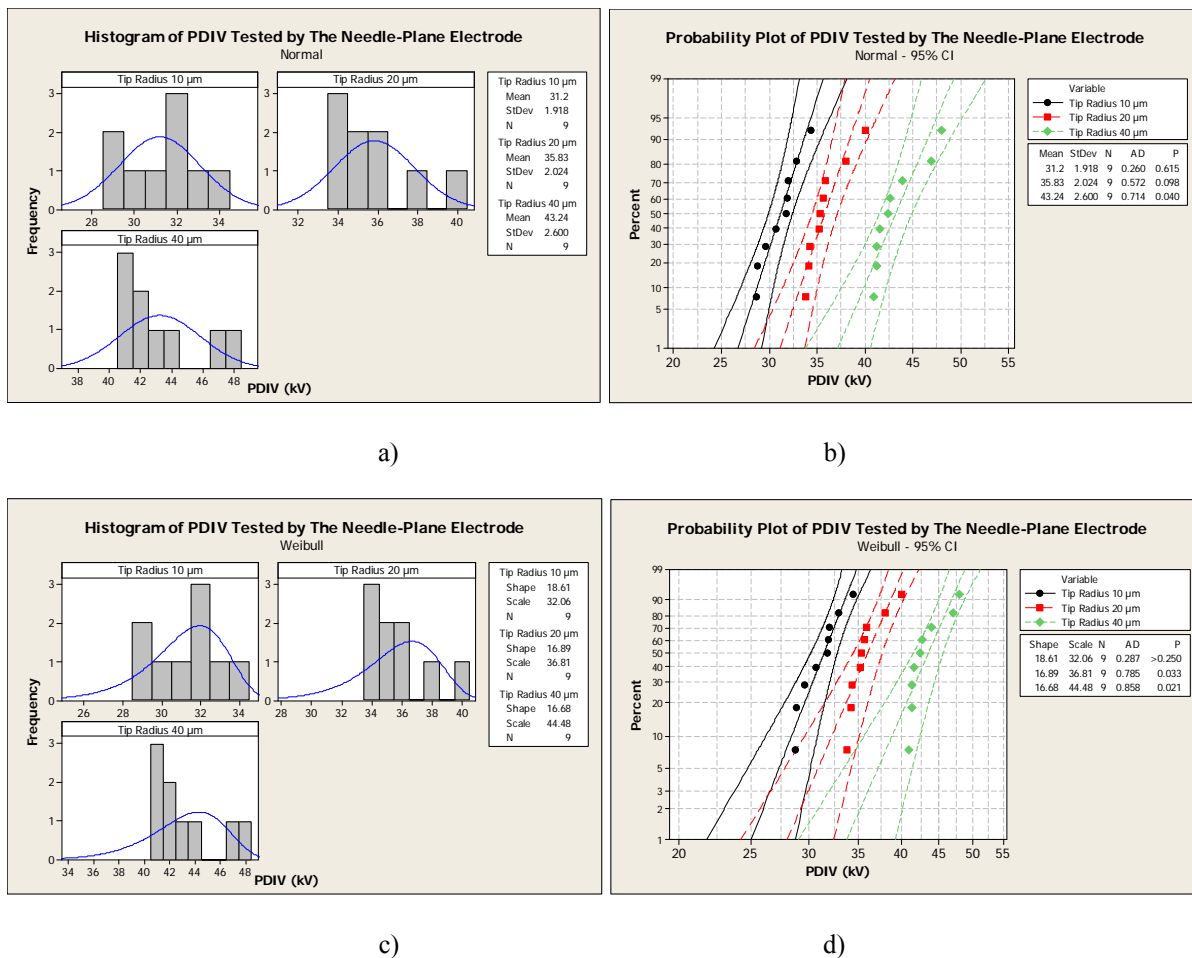


Figure 7.12: Histogram and the probability plot for PDIV experiment A

a) histogram with normal distribution plot b) probability plot of normal distribution c) histogram with weibull distribution plot d) probability plot of weibull distribution

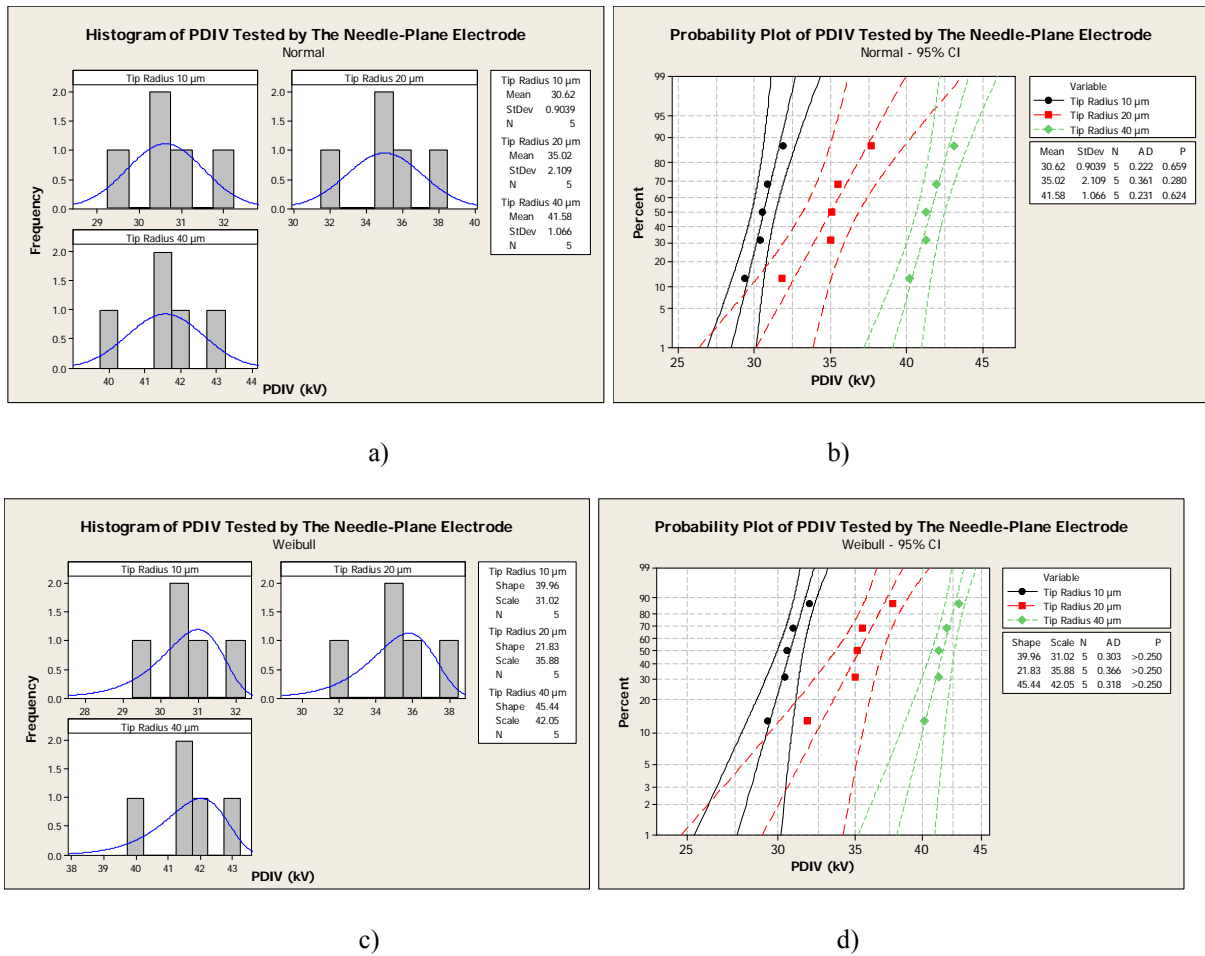


Figure 7.13: Histogram and the probability plot for PDIV experiment B

a) histogram with normal distribution plot b) probability plot of normal distribution c) histogram with weibull distribution plot d) probability plot of weibull distribution

At PDIV value, the PD charge and PD activity including PD pulse train were measured. Table 7.9 and Fig. 7.14 demonstrate the average charge quantity obtained from the test experiments. Fig. 7.15 and Fig. 7.16 represent the distribution of charge quantity in both normal and weibull distribution respectively.

Table 7.9: Average charge quantity from PDIV experiment A and B

Needle tip radius	Experiment A		Experiment B	
	U_{PDIV} (kV)	Q_{IEC} (pC)	U_{PDIV} (kV)	Q_{IEC} (pC)
10 μm	31.2	226.3	30.6	226.2
20 μm	35.8	324.2	35.0	303
40 μm	43.2	520.4	41.6	491.2

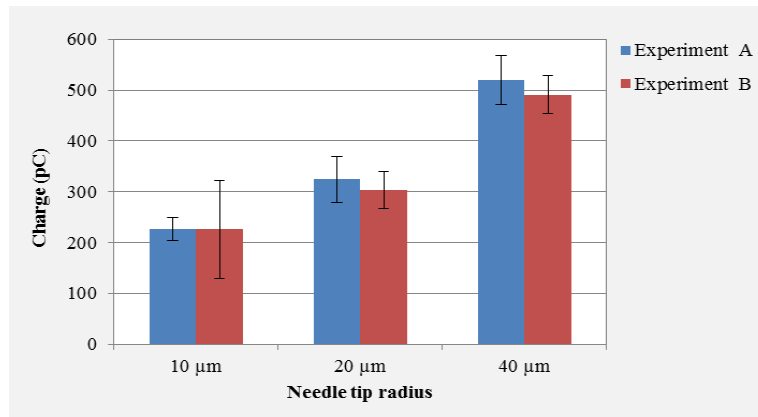


Figure 7.14: Comparison of the average charge values as a function of the needle tip radius obtained from test experiment A and B

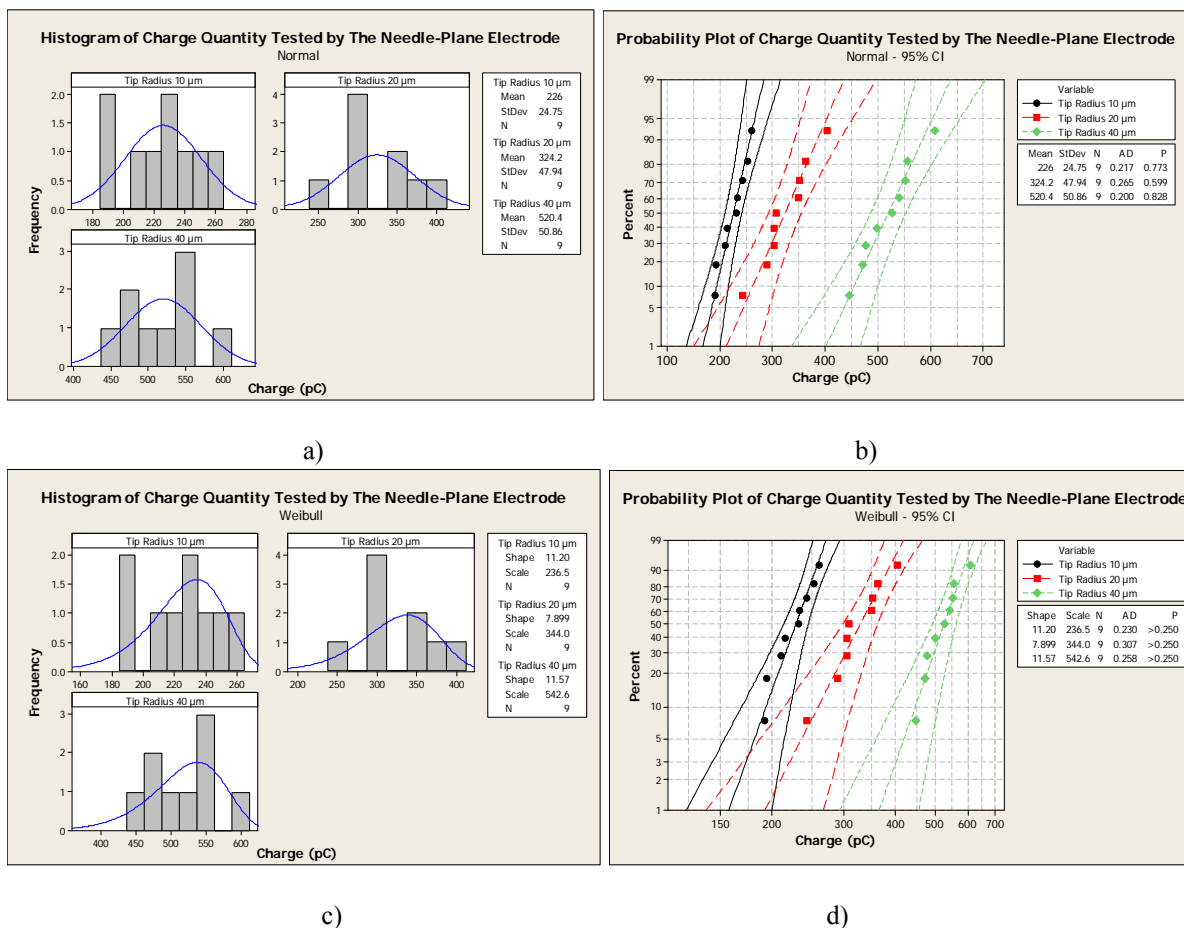
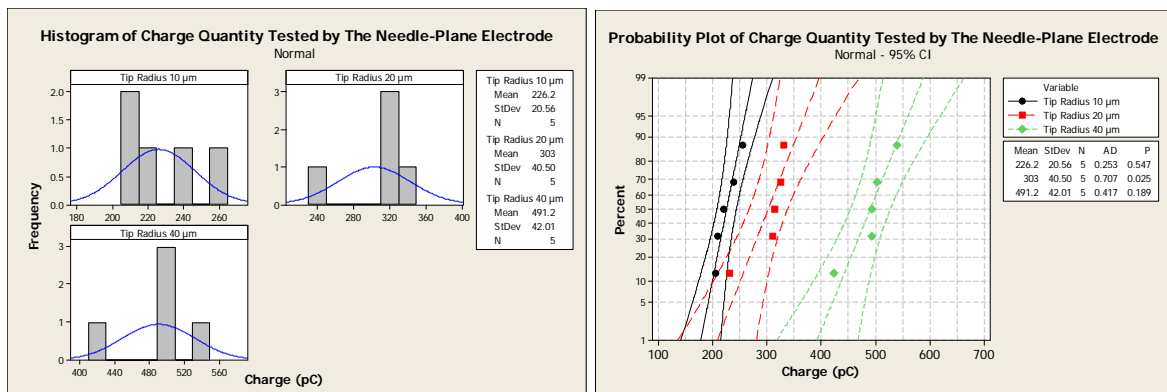


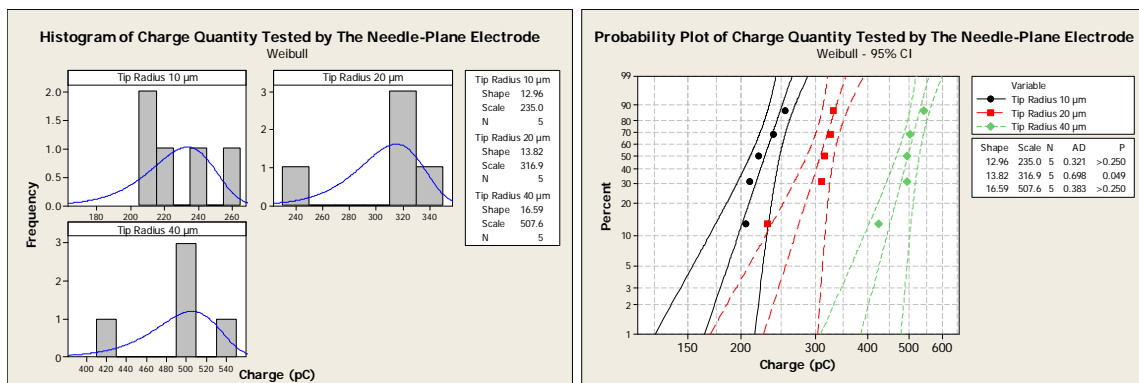
Figure 7.15: Histogram and the probability plot of the average charge values from experiment A

a) histogram with normal distribution plot b) probability plot of normal distribution c) histogram with weibull distribution plot d) probability plot of weibull distribution



a)

b)



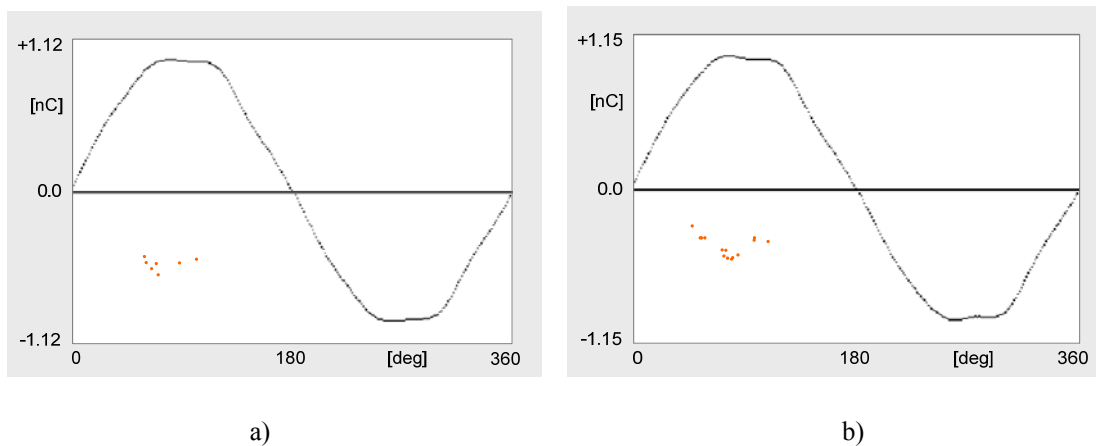
c)

d)

Figure 7.16: Histogram and the probability plot of the average charge values from experiment B

a) histogram with normal distribution plot b) probability plot of normal distribution c) histogram with weibull distribution plot d) probability plot of weibull distribution

PD activities of the mineral oil tested by needle-plane electrode arrangements with different needle tip radii were analogous. Examples of PD activities of the mineral oil tested by needle-plane electrode arrangements with the 10 μm tip radius needle-plane electrodes at the PDIV level obtained from both PDIV experiments are shown in Fig. 7.17- Fig. 7.18.

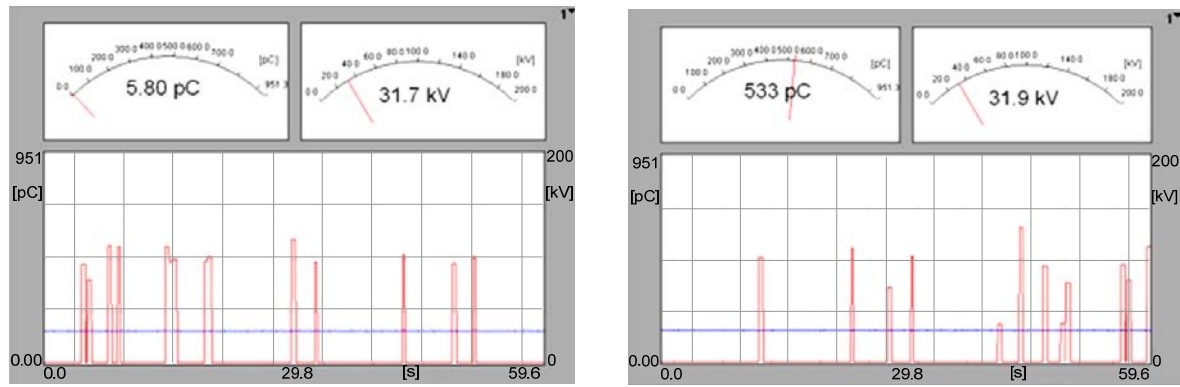


a)

b)

Figure 7.17: PD activities at the PDIV test level

a) 31.8 kV, Q_{IEC} 244 pC from the test experiment A b) 30.5 kV, Q_{IEC} 208 pC from the test experiment B



a)

b)

Figure 7.18: PD activities at the PDIV test level 31.8 kV from the experiment A; blue line is the tested voltage and the red line is PD activity

a) PD activity at the first record b) PD activity at the second record

From the PDIV preliminary test results, it was found that:

1. PDIV depended clearly on the needle tip radius. PDIV from the needle - plane electrode with the needle tip radius of 10 μ m, 20 μ m, and 40 μ m was about 31 kV, 35 kV and 42 kV respectively. The standard deviations of the PDIV test results were less than 3 kV.

2. PDIV values obtained from the test experiment A and the test experiment B were relatively similar. Therefore, one oil sample could be tested with three different tip radius needles of 10 μ m, 20 μ m and 40 μ m or could be experimented with the identical tip radius needles at least 5 needles.

3. At PDIV level, the PD charges recorded for 1 minute were more than 200 pC. The higher amplitude PD charges occurred between the angle of 55-125 degree of the phase-resolved PD diagram.

4. Normal and weibull distributions could be used to describe the mean value PDIV and the average charge test results.

Furthermore, PDIV and PD activity could be performed at 1.1 PDIV level without breakdown voltage happened. At 1.1 PDIV level, the PD charge, PD activity and PD pulse current amplitude including the PD pulse current repetition rate were higher than at PDIV level.

7.2.2 Effect of PDIV test methods on PDIV characteristics

The aim of this experiment was to investigate the effect of the PDIV test methods on PDIV of the mineral oil, Nynas 4000x, with water content less than 10 ppm. The PDIV test was experimented by using tungsten needle electrodes with the tip radius of 10 μ m, 20 μ m, and 40 μ m respectively as the high voltage electrode while the brass plane electrode with 75 mm diameter was used as the grounded electrode. The gap distance of the electrode system was fixed at 50 mm. The test circuit was set up according to IEC 60270. Six types of the PDIV test methods (M1-M6) were performed. Details of the test methods are describes in chapter 6. The PDIV test results are illustrated in Fig. 7.19- Fig.7.21. The PDIV mean value obtained from each test method is shown in Table 7.10 and Fig. 7.22.

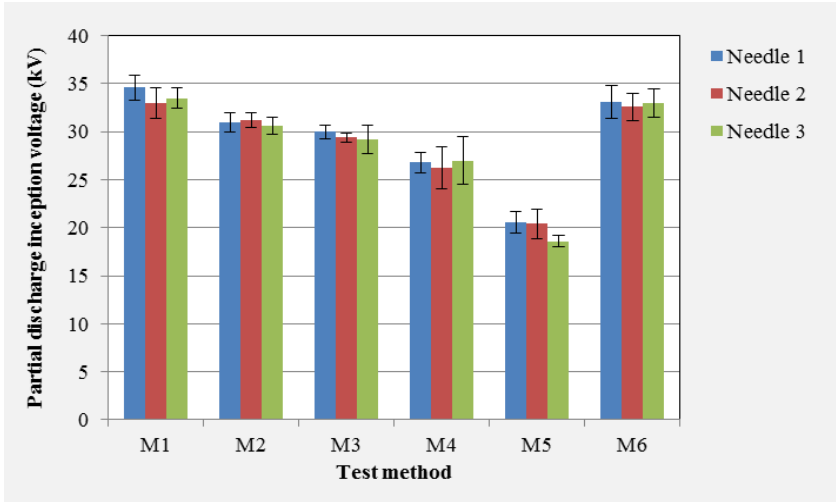


Figure 7.19: Mean value PDIV of the 10 μ m tip radius needle-plane electrode configuration as a function of the test methods

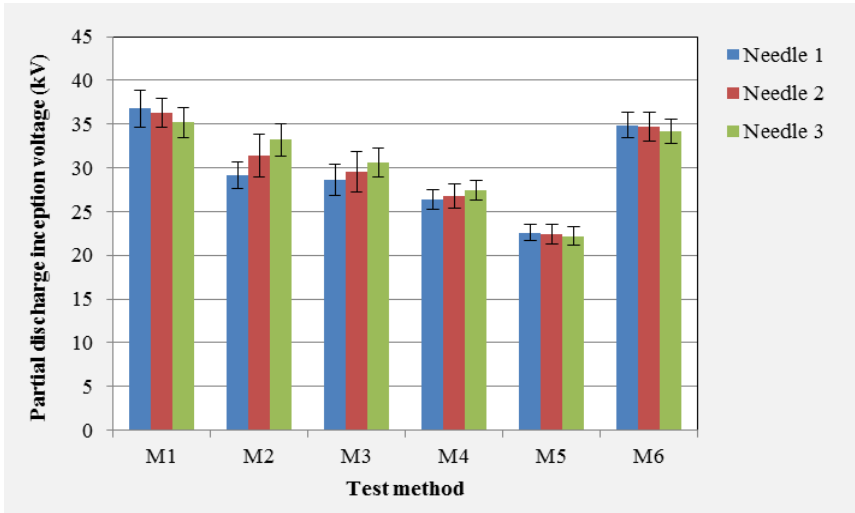


Figure 7.20: Mean value PDIV of the 20 μ m tip radius needle-plane electrode configuration as a function of the test methods

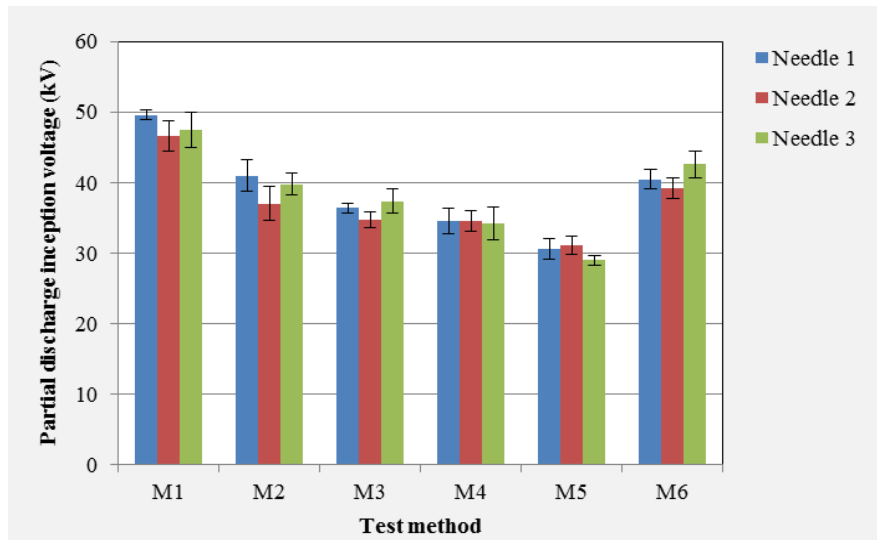


Figure 7.21: Mean value PDIV of the 40 μm tip radius needle-plane electrode configuration as a function of the test methods

Table 7.10: Mean value PDIV obtained for different PDIV test methods tested by the needle- plane electrode arrangements with 50 mm gap spacing

Test technique	Needle tip radius		
	10 μm	20 μm	40 μm
1. IEC TR 61294 ; 1kV/sec	33.7	36.1	47.9
2. Combine PDIV test method (M2):1 min/1kV/step (100 pC detection)	30.9	31.3	39.3
3. Combine PDIV test method (M3): 5 min/1kV/ step (100 pC detection)	29.5	29.5	36.2
4. Combine PDIV test method (M4):1 min/1kV/step (PD pulse detection)	26.7	26.9	34.5
5. Combine PDIV test method (M5):5 min/1kV/step (PD pulse detection)	19.9	22.4	30.3
6. Up and down PDIV test method (100 times, 100 pC detection)	33.1	34.6	40.9

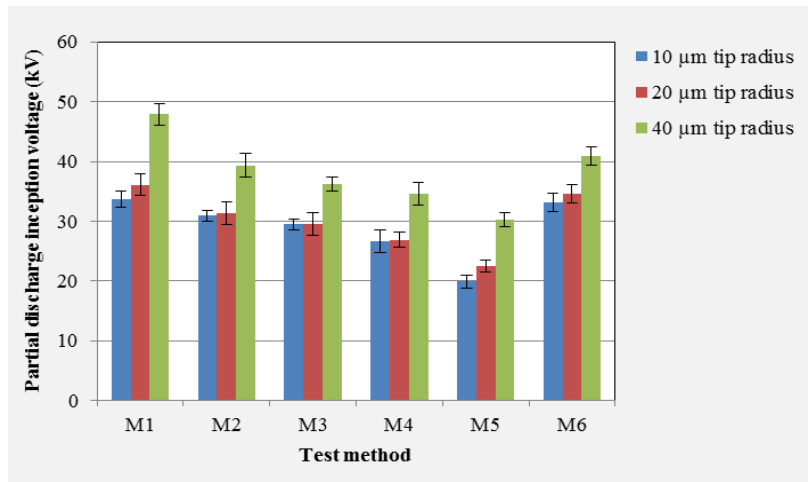


Figure 7.22: Mean value PDIV obtained from different PDIV test methods tested by the needle-plane electrode arrangement with 50 mm gap spacing

According to the experiment, the PDIV value depended strongly on the test method and the needle tip radius. The examples of the distribution of the test data obtained from the 10 μm tip radius needle (needle 1) - plane electrode configuration are shown in Fig. 7.23.

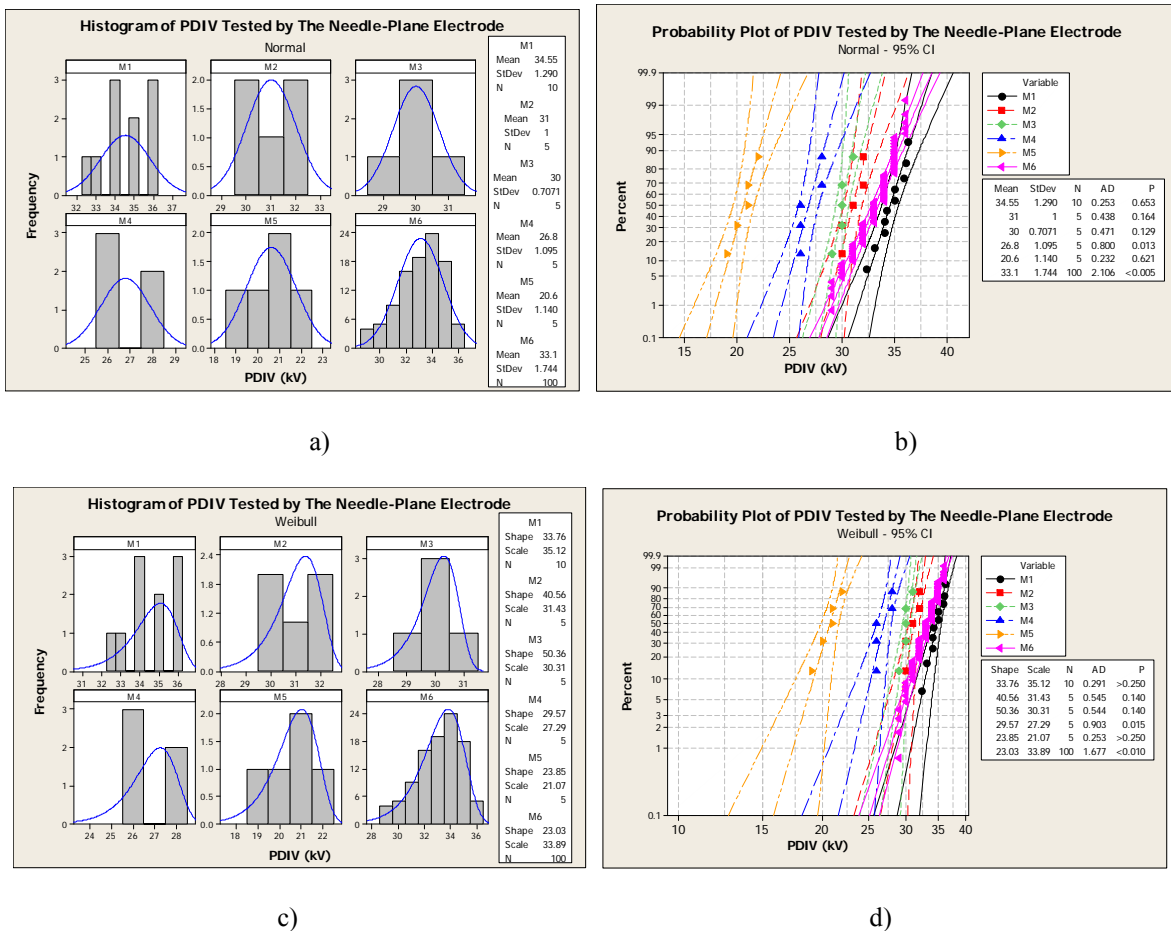


Figure 7.23: Normal and weibull distribution of the PDIV test data obtained from the 10 μm tip radius needle(needle 1) - plane electrode configuration as a function of test methods
a) histogram with normal distribution plot b) probability plot of normal distribution c) histogram with weibull distribution plot d) probability plot of weibull distribution

Most of the test data can be modelled by normal and weibull distributions except the test data obtained from M4. To measure PDIV by measuring the first PD pulse was quite difficult because of noise signals. Besides, the test result was subjective depending on the researcher who performed the experiment, he had to make decision that the detected signal was PD or noise signal.

Up and down PDIV testing: up and down PDIV test method was done 100 times of each electrode configuration. Three needles of each identical tip radius needle were investigated. The mean PDIV value obtained from each needle-plane electrode configuration was computed when the test number was 10, 20, 30, 50, 75, and 100 times as depicted in Table 7.11 and Fig. 7.24.

Table 7.11: Mean value PDIV obtained form up and down experiment

Needle tip radius		U _{PDIV} (kV)							
		Number of testing						U _{PDIV} max	U _{PDIV} min
		10	20	30	50	75	100		
10 μm	Needle I	31.7	31.9	32.8	32.9	33.3	33.1	36	29
	Needle II	32.3	32.9	32.5	32.7	32.9	33.3	37	30
	Needle III	31.7	33.0	32.7	32.6	32.8	32.9	36	29
	Average	31.9	32.6	32.7	32.8	33.0	33.1	36	29
20 μm	Needle I	34.1	34.9	34.9	34.7	35.5	34.9	38	31
	Needle II	34.1	35.0	35.2	34.7	34.4	34.7	38	31
	Needle III	32.9	32.9	33.4	33.8	34.1	34.2	37	31
	Average	33.7	34.3	34.5	34.4	34.7	34.6	38	31
40 μm	Needle I	39.1	40.2	40.2	40.5	40.2	40.5	43	37
	Needle II	37.7	38.3	38.9	39.0	38.9	39.2	42	36
	Needle III	40.7	41.3	41.8	42.7	43.1	42.6	47	39
	Average	39.2	39.9	40.3	40.7	40.7	40.9	44	37

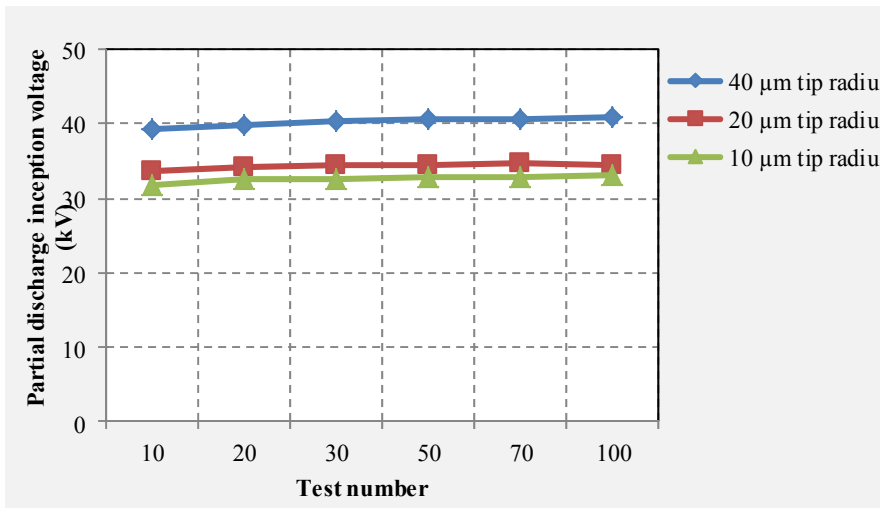


Figure 7.24: Mean value PDIV obtained from up and down PDIV test as a function of number of testing

The example of the test data distribution obtained from the 10 μm tip radius needle - plane electrode configuration is presented in Fig 7.25. Fig. 7.26 depicts the 100 time mean value PDIV from up and down PDIV testing tested by various tip radius needles- plane electrodes.

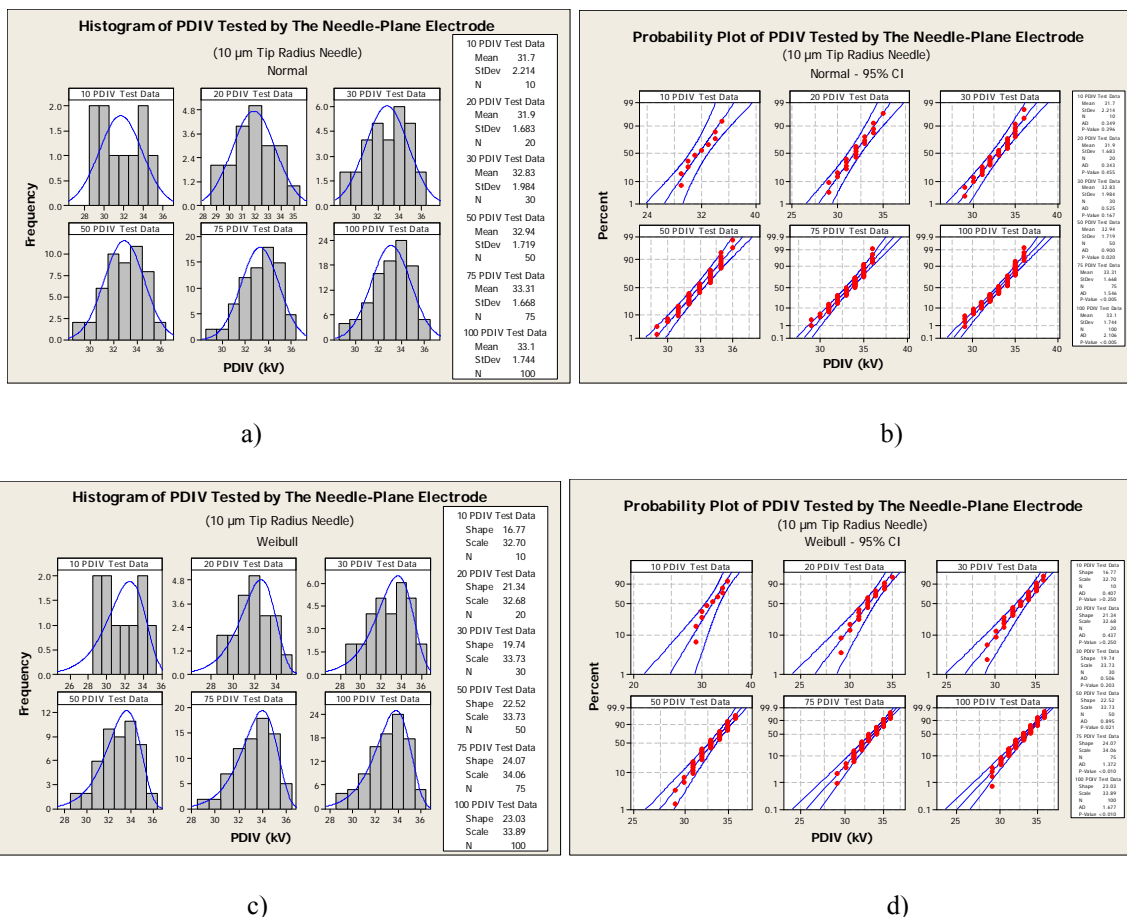
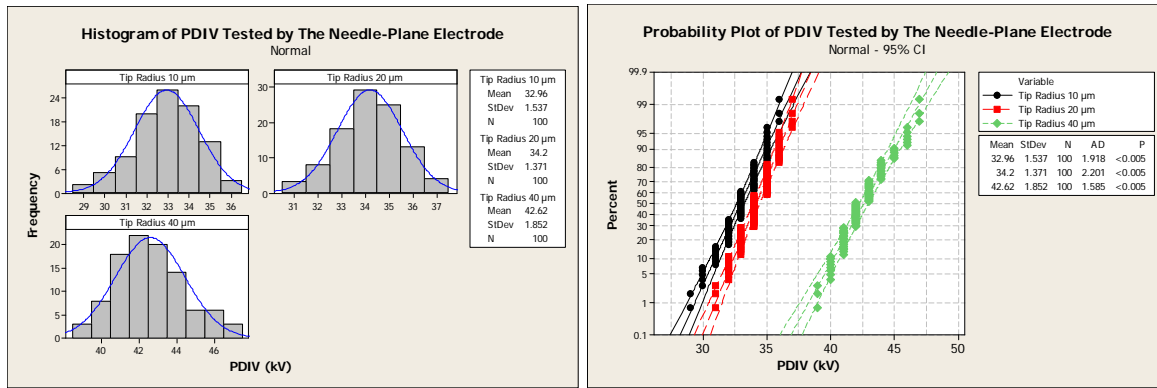


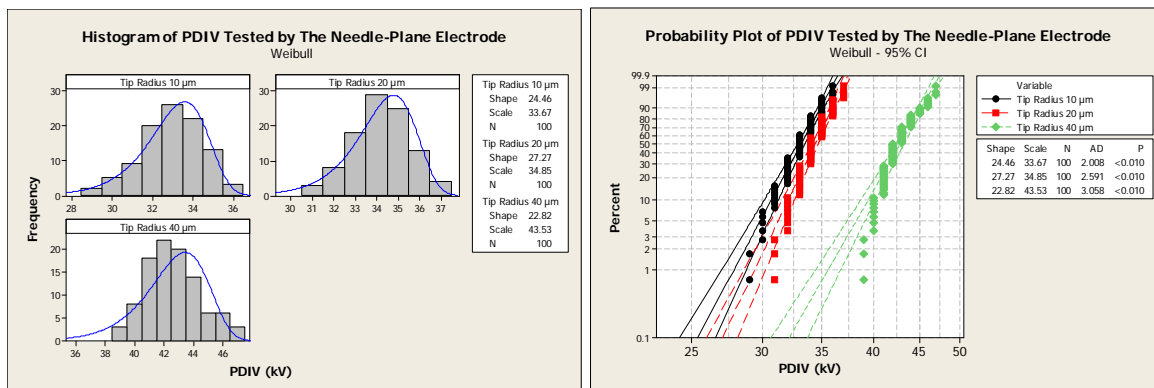
Figure 7.25: Normal and weibull distribution of up and down PDIV value obtained from the 10 μm tip radius needle (needle 1) -75 mm diameter plane electrode configurations

a) histogram with normal distribution plot b) probability plot of normal distribution c) histogram with weibull distribution plot d) probability plot of weibull distribution



a)

b)



c)

d)

Figure 7.26: Normal and weibull distribution of up and down PDIV value obtained from 100 time testings of various tip radius needles (needle 3) – plane electrode configurations

a) histogram with normal distribution plot b) probability plot of normal distribution c) histogram with weibull distribution plot d) probability plot of weibull distribution

PDIV values were vigorously dependent on the PDIV test methods. IEC test method (M1) gave the highest PDIV. The PDIV acquired from the second and third test method were nearly the same. The PDIV acquired from the fifth test procedures was the lowest PDIV value. The test results showed that a step duration for maintaining the testing voltage had more influence on the PDIV value in case of measuring the first PD pulse current, M 4 and M 5. The PDIV acquired from the sixth test method (M6) were lower a bit than the PDIV from the standard PDIV test method(M1) tested by the 10 μm and 20 μm tip radius needles with plane electrode system. The results had also suggested that the 20 μm tip radius needle- plane electrode gave a little bit PDIV higher than the 10 μm tip radius needle- plane electrode for the test procedure M2- M4 and M6. Considering the up and down PDIV test method, the test results from 10, 20, 30, 50, 75 and 100 times were not much different. To analyze the up and down PDIV test data for 10, 20, and 30 time testings, normal and weibull distribution with confident level 95% could be used to describe. With the 50 time testings or more, normal and weibull distribution with confident level 95% were not suitable to describe the test results.

7.2.3 Effect of grounded electrodes on PDIV and PD characteristics

This experiment aimed to investigate the effect of electrode configurations on PDIV and PD of the mineral oil. The test experiment was performed with a needle-plane and a needle-sphere electrode configuration, under room temperature. The PDIV test circuit was set up according to IEC 60270. The tungsten needle electrodes with the tip radius of 10 μ m, 20 μ m, and 40 μ m respectively were used as the high voltage electrode while the brass plane electrode with a diameter of 75 mm as grounded electrode. The gap distance of the electrode system was set up at 25 mm and 50 mm respectively. Two PDIV test methods, M1 (IEC test method) and M2 (combine PDIV test method: 1 min /kV/step, 100 pC detection), were performed. Details of the test procedures are described in chapter 6. The PDIV value and PD activity at PDIV level were recorded. Furthermore, the PD pulse currents were examined at the PDIV level as well. Besides, the plane electrode with diameter of 50 mm and the sphere electrodes with the diameter of 12.7 mm, 25.4 mm, 50.8 mm and 76.2 mm respectively were used as the grounded electrode.

7.2.3.1 PDIV and PD experiment

The PDIV values and PD charge quantities(Q_{IEC}) of the mineral oil tested by various electrode systems are shown in Table 7.12. As one can see from this table, the PDIV experiment (IEC test method) tested by the 20 μ m and 40 μ m tip radius needles with the gap spacing of 25 mm was limited at the specified applied voltages due to the reason of breakdown phenomena which might happen during the PDIV experiment was performed. For the gap distance of 50 mm, the PDIV experiment was also limited at 50 kV of the maximum voltage of the high voltage source. Moreover, the comparison of the PDIV value and charge quantity obtained from IEC and combine PDIV test methods tested by the 10 μ m needle tip radius and various grounded electrode systems are shown in Fig. 7.27- Fig. 7.28 respectively. The PDIV value and charge obtained from combine PDIV test method of the electrode systems are shown in Fig. 7.29- Fig. 7.30 respectively.

Table 7.12: Mean value PDIV (kV) and average PD charge quantity (pC) of the mineral oil as function of electrode configurations with the gap distance of 25 and 50 mm

Parameter	Needle tip radius (μm)	Grounded electrode											
		Gap distance 25 mm						Gap distance 50 mm					
		Plane dia. (mm)		Sphere dia. (mm)				Plane dia.(mm)		Sphere dia. (mm)			
		50.0	75.0	12.7	25.4	50.8	76.2	50.0	75.0	12.7	25.4	50.8	76.2
PDIV IEC	10	24.0	22.4	33.7	29.0	25.8	24.1	32.4	30.3	40.0	35.5	32.9	31.1
	20	> 31	> 31	> 35	> 34	> 33	> 31	40.2	39.1	> 50	47.8	45.1	43.1
	40	> 33	> 33	> 36	> 35	> 35	> 33	48.7	45.8	> 50	> 50	> 50	> 50
PDIV Combine	10	20.3	19.4	27.6	23.2	20.9	20.8	27.0	25.4	31.7	29.9	29.3	25.8
	20	23.5	22.5	32.8	29.0	25.1	24.1	32.3	30.1	38.6	36.2	34.8	30.9
	40	30.2	26.9	35.4	32.2	31.2	28.0	36.5	34.7	44.7	42.9	41.2	37.6
Q _{IEC} IEC	10	335	378	356	326	326	393	259	270	257	326	254	290
	20	NA	NA	NA	NA	NA	NA	407	486	NA	509	495	579
	40	NA	NA	NA	NA	NA	NA	654	656	NA	NA	NA	NA
Q _{IEC} Combine	10	176	216	167	149	195	156	137	133	106	104	112	144
	20	249	295	220	299	241	242	213	239	171	202	200	230
	40	482	440	296	408	417	437	277	332	290	295	303	373

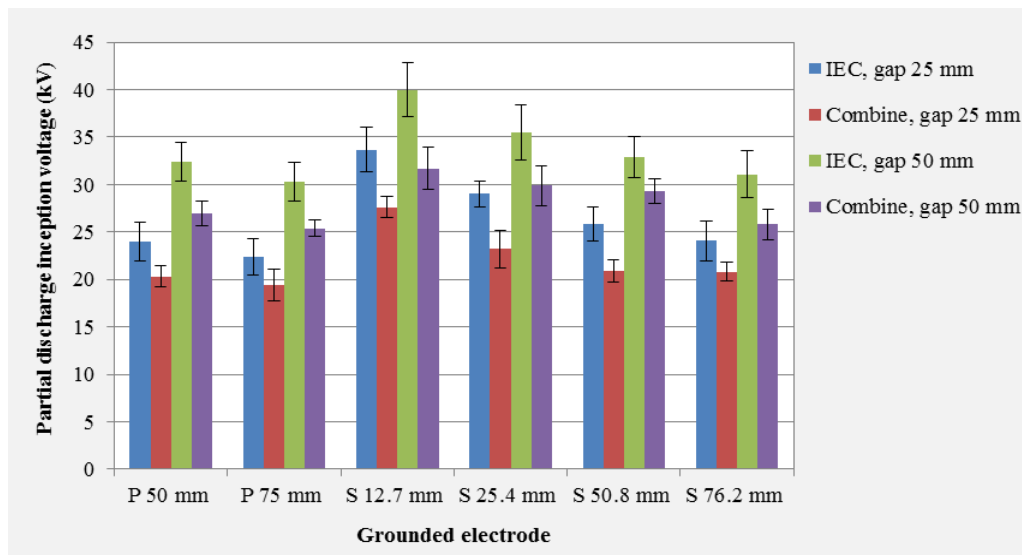


Figure 7.27: Mean value PDIV obtained from different PDIV test methods tested by the 10μm tip radius needle with various grounded electrode systems; P represents a plane electrode and S represents a sphere electrode

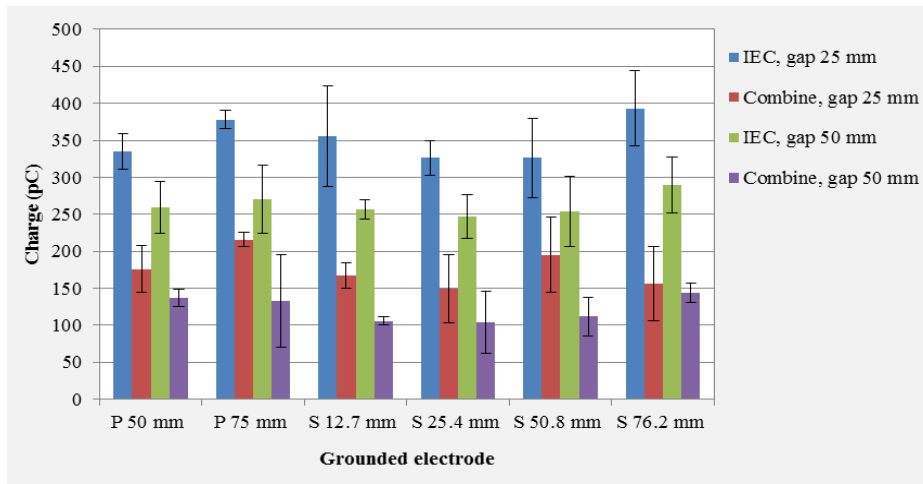
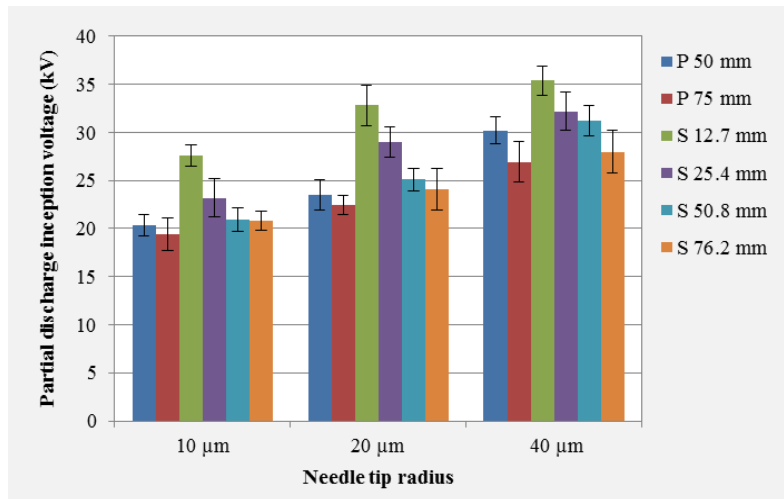
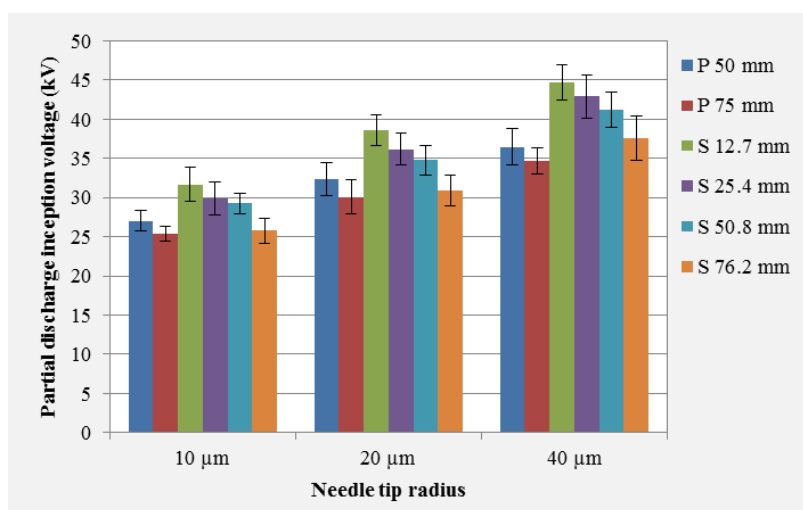


Figure 7.28: Average charge quantities obtained from different PDIV test methods tested by the 10 μ m tip radius needle with various grounded electrode systems; P is a plane electrode and S is a sphere electrode

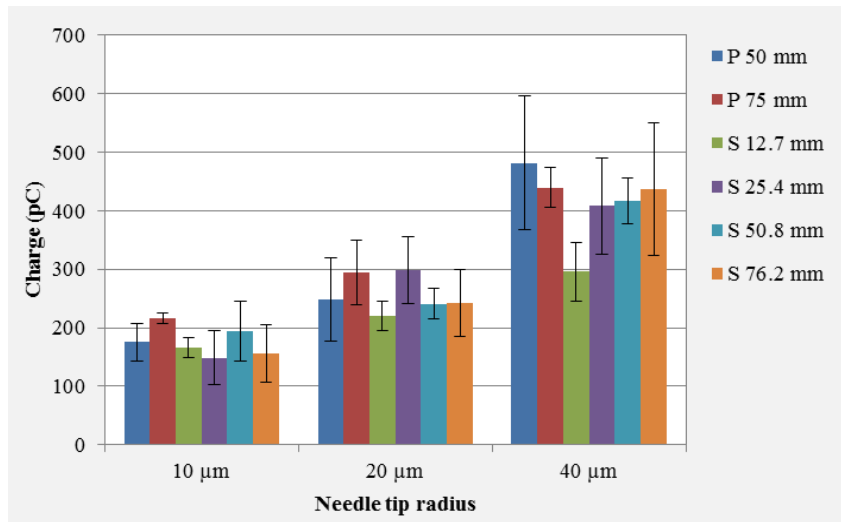


a)

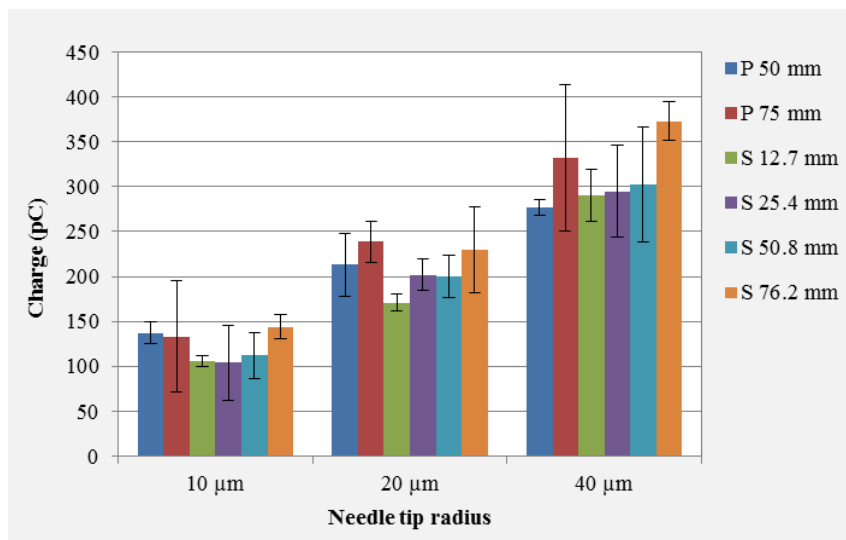


b)

Figure 7.29: Mean value PDIV obtained from the combine PDIV test method of the electrode systems a) gap distance of 25 mm b) gap distance of 50 mm; P is a plane electrode and S is a sphere electrode



a)

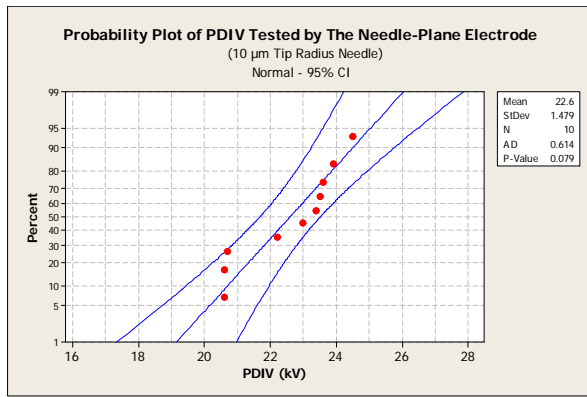


b)

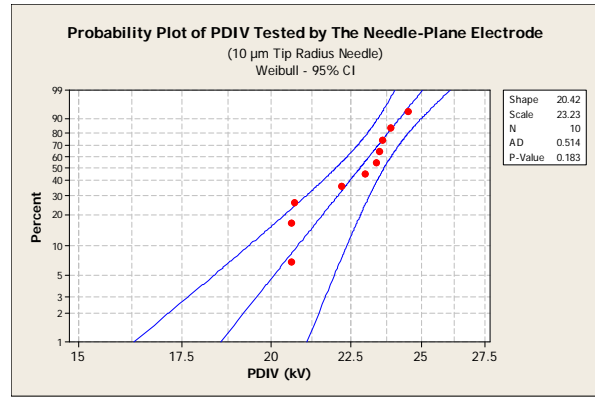
Figure 7.30: Average charge quantities obtained from the combine PDIV test method of the electrode systems

a) gap distance of 25 mm b) gap distance of 50 mm; P is a plane electrode and S is a sphere electrode

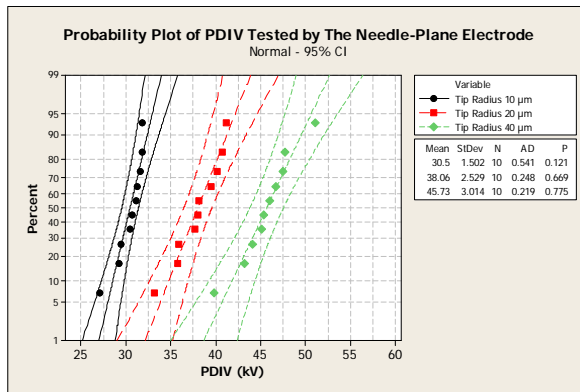
The examples of distribution obtained from the raw data of the needle (needle 1) with various grounded electrodes of each case study are plotted in normal and weibull distribution as shown in Fig.7.31- Fig. 7.34.



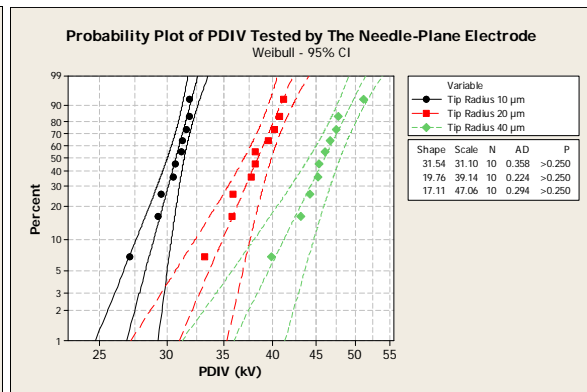
a)



b)



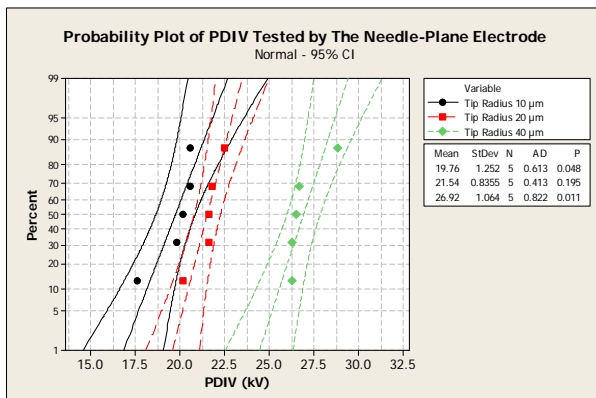
c)



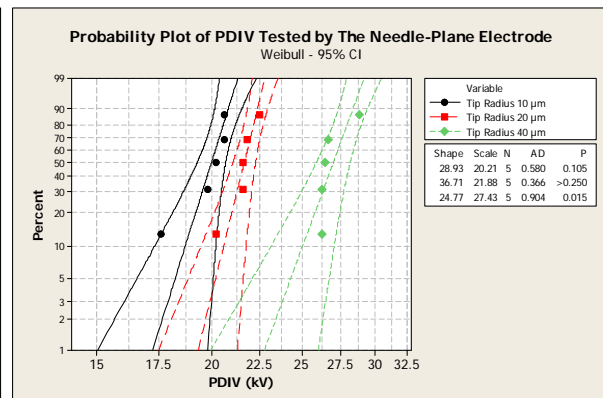
d)

Figure 7.31: Normal and weibull distribution of PDIV value obtained from the 10 μm tip radius needle-75 mm diameter plane electrode (a-b) and obtained from various tip radius needles-75 mm diameter plane electrode(c-d) tested according to IEC test method

a) normal distribution of PDIV value, gap distance 25 mm b) weibull distribution of PDIV value, gap distance 25 mm c) normal distribution of PDIV value, gap distance 50 mm d) weibull distribution of PDIV value, gap distance 50 mm



a)



b)

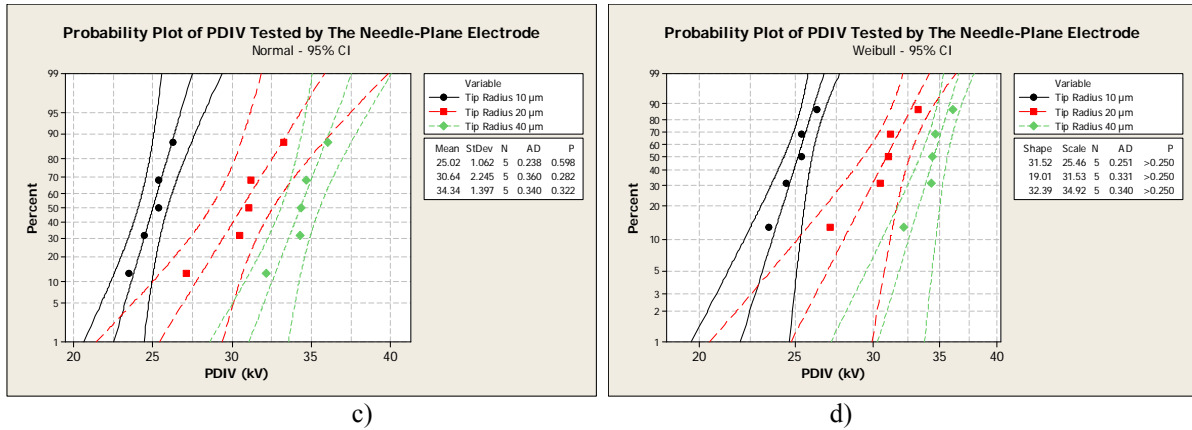


Figure 7.32: Normal and weibull distribution of PDIV value obtained from various tip radius needles - 75 mm diameter plane electrode tested according to the combine PDIV test method

a) normal distribution of PDIV value, gap distance 25 mm b) weibull distribution of PDIV value, gap distance 25 mm c) normal distribution of PDIV value, gap distance 50 mm d) weibull distribution of PDIV value, gap distance 50 mm

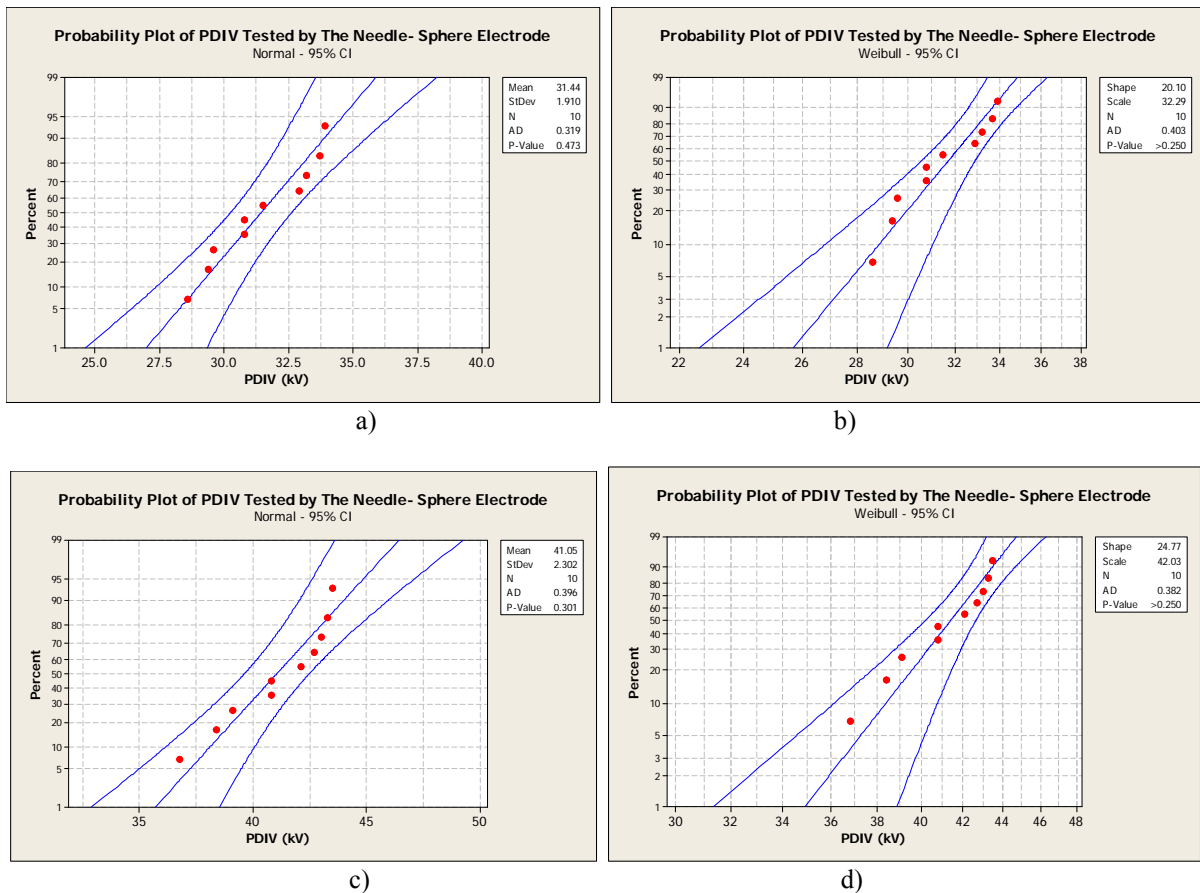


Figure 7.33: Normal and weibull distribution of PDIV value obtained from the 10 μm tip radius needle-12.7 mm diameter sphere electrode tested according to IEC test method

a) normal distribution of PDIV value, gap distance 25 mm b) weibull distribution of PDIV value, gap distance 25 mm c) normal distribution of PDIV value, gap distance 50 mm d) weibull distribution of PDIV value, gap distance 50 mm

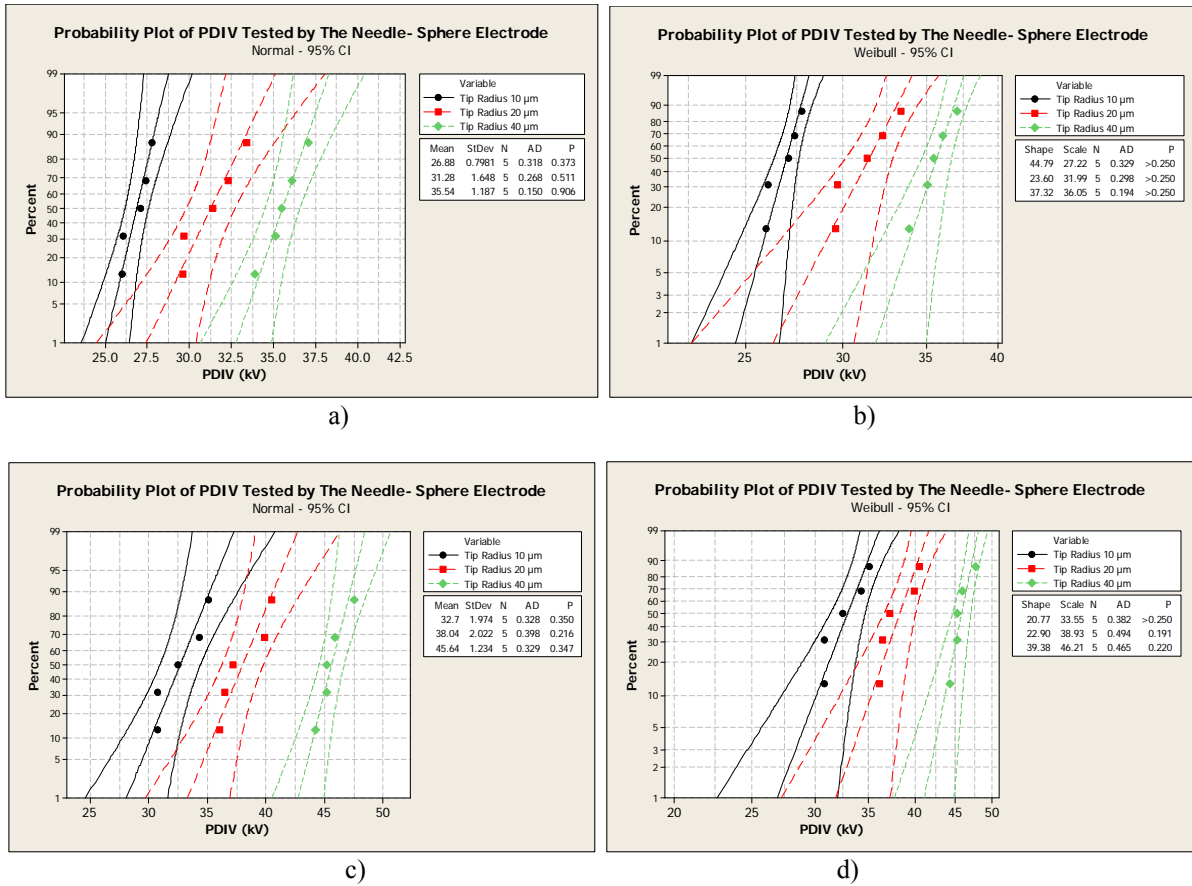


Figure 7.34: Normal and weibull distribution of PDIV value obtained from various tip radius needles - 12.7 mm diameter sphere electrode tested according to the combine PDIV test method

a) normal distribution of PDIV value, gap distance 25 mm b) weibull distribution of PDIV value, gap distance 25 mm c) normal distribution of PDIV value, gap distance 50 mm d) weibull distribution of PDIV value, gap distance 50 mm

7.2.3.2 PD activity

The phase-resolved PD and ϕ -q-n PD characteristic of the mineral oil experimented by the same test method using the needle-plane and the needle-sphere electrode systems were relatively similar patterns. However, the PDIV values obtained from both test methods (IEC and the combine PDIV test method) were different. Therefore, the PD characteristics at the PDIV level of each test method were distinct as shown in Fig. 7.35.

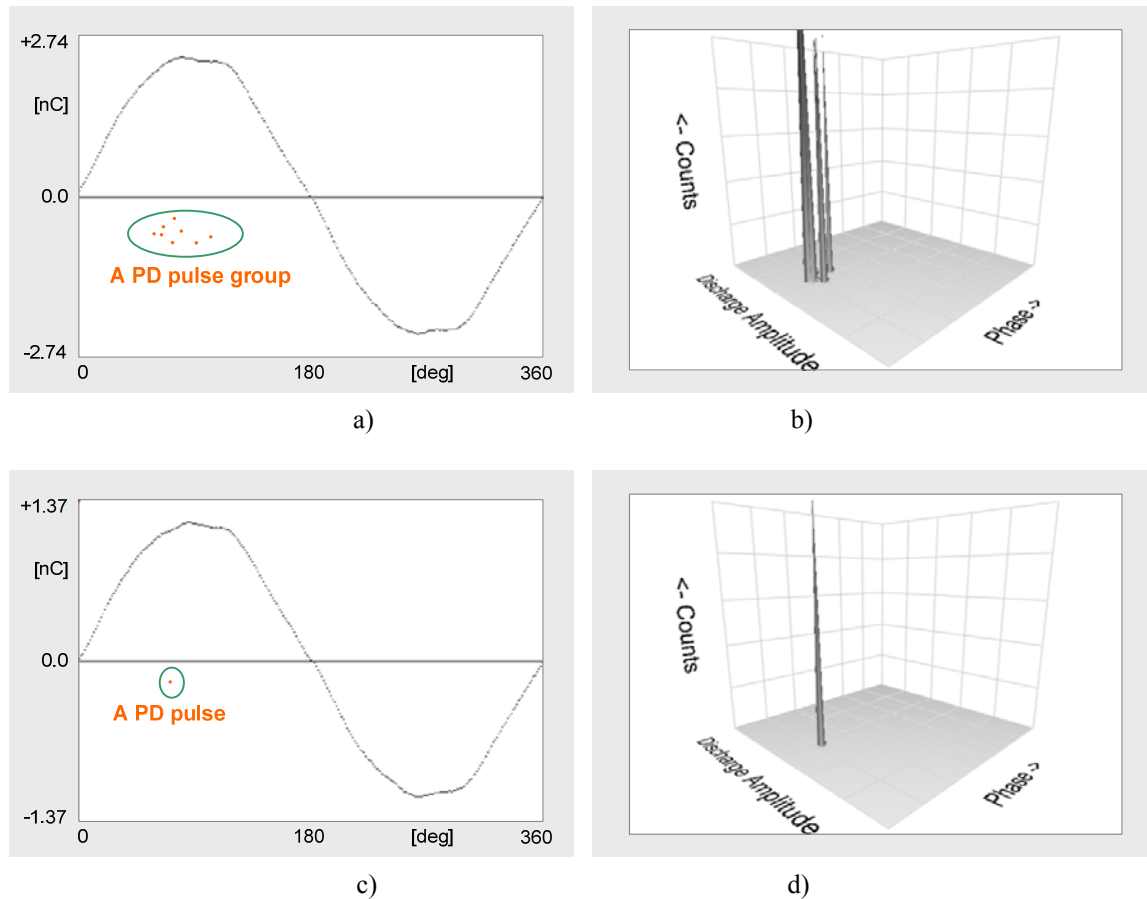


Figure 7.35: Phase-resolved PD and θ -q-n PD characteristic recorded for one minute tested by the 10 μm tip radius needle - 75 mm diameter plane electrode with gap distance of 50 mm

a) phase- resolved PD and b) θ -q- n PD characteristic from IEC test method at PDIV level of 30.5 kV, Q_{IEC} 311 pC, Q_{PEAK} 777 pC c) Phase – resolved PD d) q – θ - n PD characteristic from the combine PDIV test method at PDIV level of 24.9 kV, Q_{IEC} 73.4 pC, Q_{PEAK} 184 pC

According to the experiment, it was found that the PDIV depended on electrode configurations especially the needle tip radii and gap distances. PDIV relied also on the PDIV test methods. The test results showed that the 10 μm tip radius needle -75 mm diameter plane electrode provided the lowest PDIV compared with other electrode configurations. The combine PDIV test method produced the PDIV, charge value (Q_{IEC}) and also the charge repetition rate lower than measuring by IEC method. At PDIV level, tested by IEC method, the PD charge amplitudes recorded for 1 minute were higher than 200 pC. PDs occurred between the angles of 35-135 degree of the phase - resolved PD diagram. For the combine PDIV testing, it produced the PD charge amplitudes recorded for 1 minute in the range of 104-216 pC depending on the gap distance of electrode configurations. Only one or two PDs with lower charge amplitudes occurred nearly or at 90 degree of the phase - resolved PD diagram when the PD activities were examined at the PDIV level obtained from the combine PDIV test method.

7.2.3.3 The first PD charge at PDIV value

Some breakdown events happened when the charge was recorded for 1 minute at PDIV or 1.1 PDIV value. Therefore, the first charge value measured at PDIV level should be an interesting value. This experiment aimed to investigate the first charge value happening at the PDIV level. The test experiment was performed with a needle-plane electrode system with 10 μ m, 20 μ m, and 40 μ m tip radius needles as the high voltage electrode and 75 mm diameter brass plane electrode as grounded electrode. The gap distance was fixed at 25 and 50 mm. The experiment was done ten times for each needle-plane configuration. Three needles of each identical tip radius needle were investigated. After that, the charge average value of each electrode configuration was computed.

Table 7.13: Average value of the first PD charge at PDIV level

Needle tip radius	Gap 25 mm		Gap 50 mm	
	U_{PDIV} (kV)	Q_{IEC} (pC)	U_{PDIV} (kV)	Q_{IEC} (pC)
10 μ m	22.4	276	30.3	205
20 μ m	31 ¹⁾	597	39.1	375
40 μ m	33 ²⁾	709	45.8	643

Note: 1) the value of 31 kV was not the mean value PDIV of the 20 μ m tip radius needle- plane electrode system with 25 mm gap distance. The 31 kV applied voltage was approaching the PDIV value of this electrode system. The first PD charge was measured at this voltage value in order to avoid the breakdown occurring in the experiment. 2) the value of 33 kV was also not the mean value PDIV of the 40 μ m tip radius needle - plane electrode system with 25 mm gap distance. The experiment was done at this voltage level with the same reason of avoiding breakdown.

Fig. 7.36 represents the relationship between the first charge quantity at the PDIV level of the needle-plane electrode systems. The example of the charge behaviors obtained from 3 identical 10 mm tip radius needles-plane electrode with gap distance of 50 mm is depicted in Fig. 7. 37.

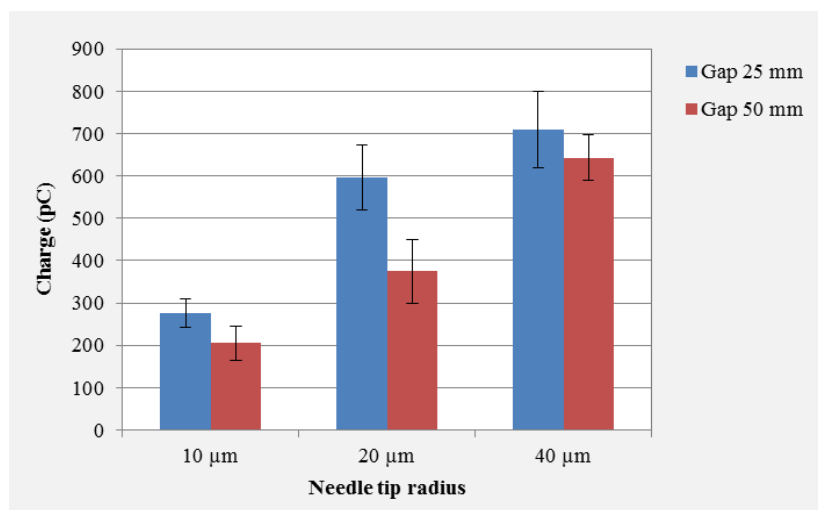
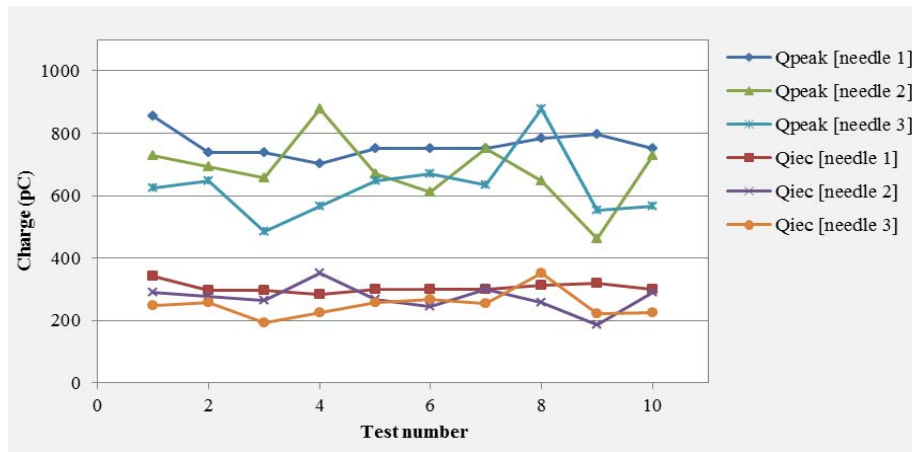
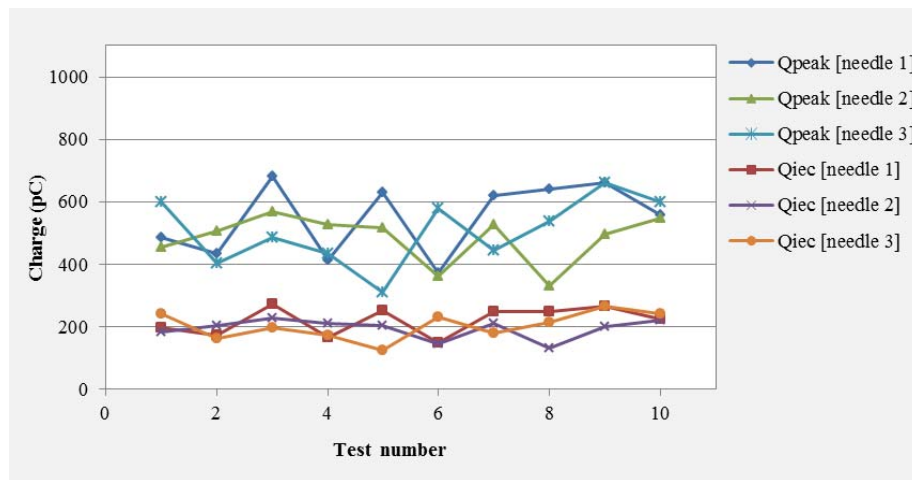


Figure 7.36: Average first charge quantity at PDIV level of the needle- plane electrode systems



a)



b)

Figure 7.37: The first charge behaviors at PDIV level obtained from the 10 μm tip radius needle – 75 mm diameter plane electrode configuration

a) gap distance 25 mm b) gap distance 50 mm

From Fig. 7.37, one can see that the Q_{IEC} is about 0.4 Q_{peak} . The distribution of the first charge was analyzed. The examples of the first charge raw data modelled by normal and weibull distributions are shown in Fig. 7.38. The first charge data could be modelled with normal and weibull distribution. For the gap distance 25 mm, the first charge values obtained from the 20 μm tip radius needle - plane electrode system were approaching to the group of first charge acquired from the 40 μm tip radius needle - plane electrode configuration. However, the first charges obtained from different tip radius needles were obviously separated when the electrode systems were tested with 50 mm gap distance.

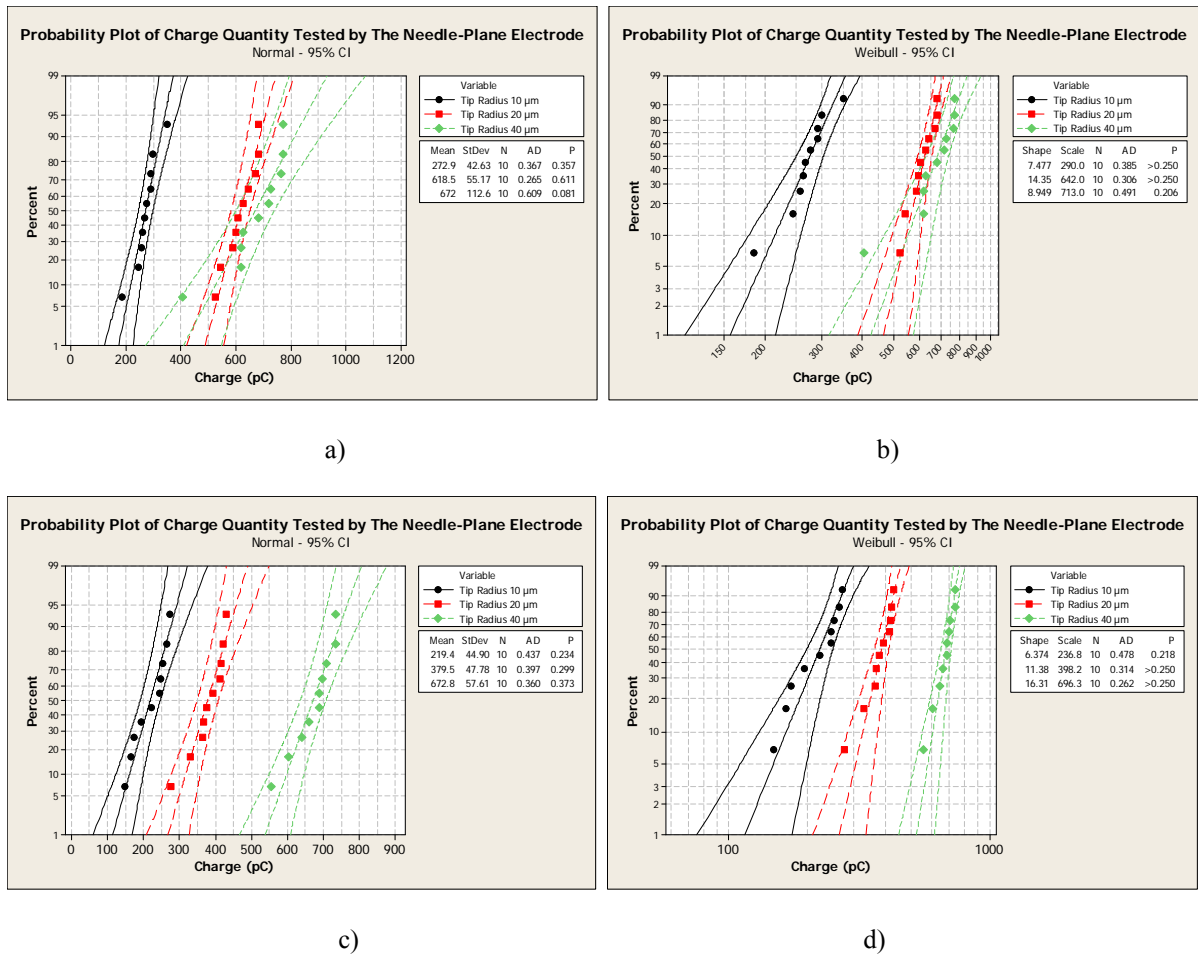


Figure 7.38: Normal and weibull distribution of the average first charge at PDIV level

a) normal distribution of the first charge, gap distance 25 mm b) weibull distribution of the first charge, gap distance 25 mm c) normal distribution of the first charge, gap distance 50 mm d) weibull distribution the first charge, gap distance 50 mm

7.2.3.4 Breakdown events during PDIV test

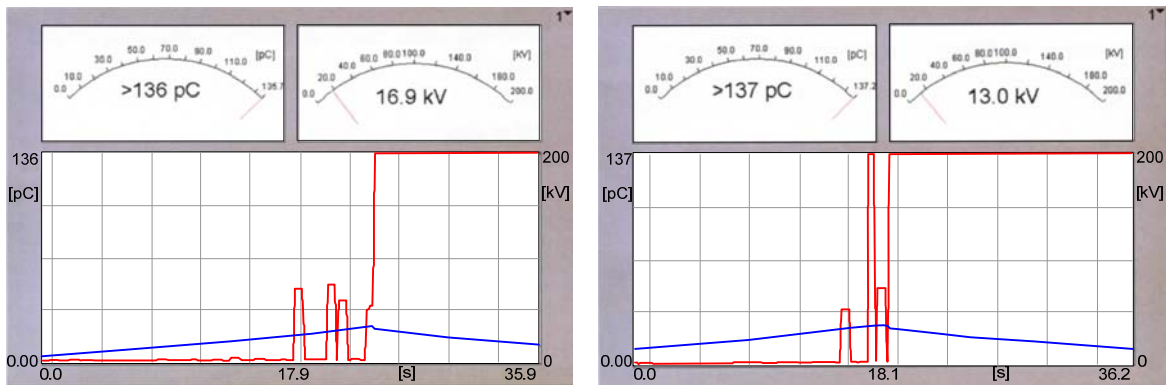
7 breakdowns occurred during performing the PDIV experiment with 20μm and 40μm tip radius needle-plane electrode configurations and 20μm tip radius needle-sphere electrode configurations with the gap spacing of 25 mm. Therefore, the applied voltage to such electrode systems for the further experiments was limited at the specified voltage values to avoid breakdown phenomena. Table 7.14 demonstrates breakdown cases occurring during the PDIV experiments were performed. The breakdown phenomena were also detected by the ICM and the oscilloscope as represented in Fig. 7.39. Breakdown events caused the damage of needle tip, therefore, such needles cannot be used any more for PDIV or PD investigation. Furthermore, breakdown may cause the destruction of the PD measuring system. Table 7.15 gives the examples of breakdown needle figures compared to the original needle figure.

Table 7.14: Breakdown cases during performing the PDIV experiments according to IEC test method

No	Tip radius (µm)	Grounded electrode	Ubd (kV)	Testing process before breakdown event occurred	PDIV(kV) before breakdown occurring	voltage limited for next PDIV test
1	20	plane with 75 mm dia.	34.8	raising the voltage up before finding the fourth PDIV	31kV averaged from 3 PDIV testings	33.0
2	20	plane with 75 mm dia.	33.0	raising the voltage up before finding the second PDIV	30kV for the first PDIV testing, the breakdown occurred while the second PDIV test was testing	31.0
3	40	plane with 75 mm dia.	36.0	stepping the voltage down after finding the fifth PDIV	32.4kV averaged from 4 PDIVtestings, the fifth PDIV was 36.4kV and breakdown happened.	35.0
4	40	plane with 75 mm dia.	35.0	Stepping the voltage down after finding the sixth PDIV	34.9kV averaged from 5 PDIV testings, the sixth PDIV was 35.9 kV and breakdown happened.	33.0
5	20	Sphere with 76.2 mm dia.	32.8	At 1.1 PDIV level for PD activity recording	29.8kV averaged from 10 PDIV testings	31.0
6	20	Sphere with 50.8 mm dia.	34.7	at PDIV level, the voltage was kept constant for 1 min for PD activity recording	34.7kV averaged form 10 PDIV testings	33.0
7	20	sphere with 50.8 mm dia.	34.0	raising the voltage up before finding the fourth PDIV	29.5kV averaged form 3 PDIVtestings, breakdown occurred at the fourth PDIV testing	33.0

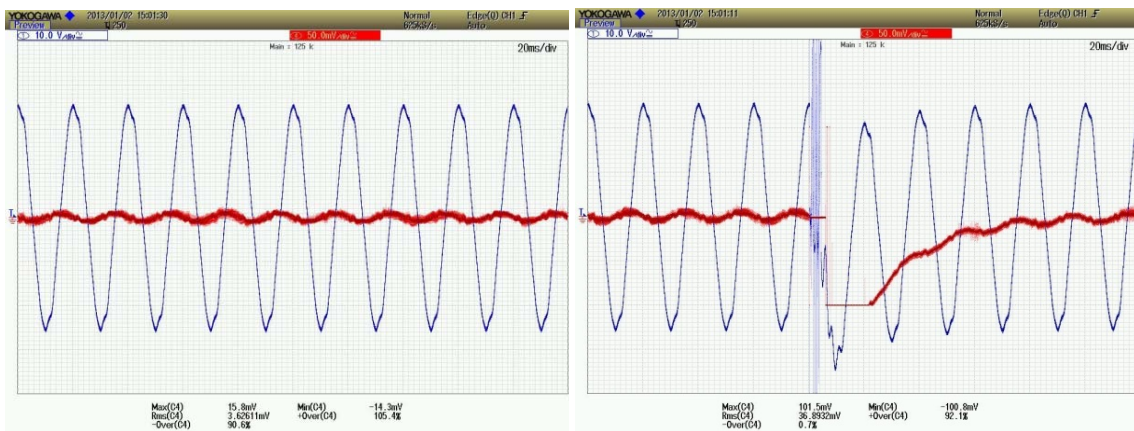
Note: 1. Ubd is the breakdown voltage

2. PDIV activity was also measured at 1.1 PDIV level for needle-plane electrode systems with the gap spacing of 50 mm without breakdown happened. However for the gap distance of 25 mm, breakdown happened at 1.1 PDIV level tested by the 20 µm tip radius needle - 76.2 mm diameter sphere electrode configuration. After that, the PDIV activity at 1.1 PDIV level was not investigated for every electrode configuration.



a)

b)



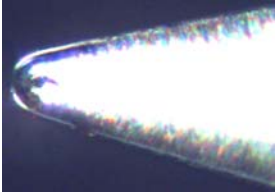
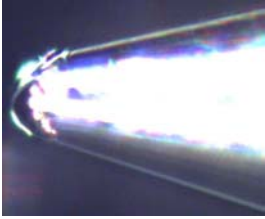
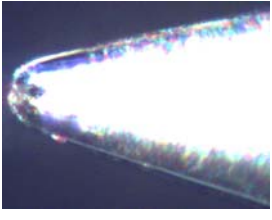
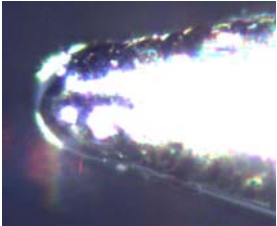
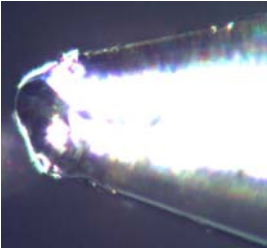
c)



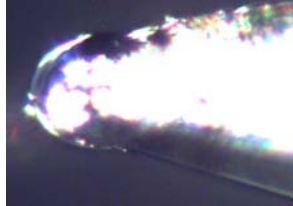
d)

Figure 7.39: Breakdown events during PDIV measurement recorded by ICM and the oscilloscope

- a) the second breakdown of the 20 μm tip radius needle-75 mm diameter plane electrode recorded by ICM
 b) breakdown event of the 40 μm tip radius needle-75 mm diameter plane electrode recorded by ICM
 c) test voltage before breakdown recorded by the oscilloscope d) breakdown of the needle- sphere electrode configuration with the needle tip radius of 20 μm and sphere diameter of 76.2 mm recorded by the oscilloscope: the blue line is the test voltage and the red line is the PD current

Table 7.15: Needle configurations before and after breakdown occurring

Needle configuration	Description
<p>original 20 μm tip radius needle</p> 	<p>The average tip radius for the original 20 μm tip radius needle was about 19.90μm -20.20 μm. For the original 10 μm tip radius needle, the average needle tip radius was about 10.20 μm - 10.50 μm. For the original 40 μm tip radius needle, the average needle tip radius was about 40.30 μm - 40.90 μm.</p>
<p>Breakdown 20 μm tip radius needle</p> 	<p>Needle number 1 after breakdown. The needle tip radius was decreased to 19.70 μm.</p>
<p>Breakdown 20 μm tip radius needle</p> 	<p>Needle number 2 after breakdown. The needle tip radius was decreased to 19.70 μm.</p>
<p>Breakdown 40 μm tip radius needle</p> 	<p>Needle number 3 after breakdown. The needle tip radius was decreased to 39.27 μm.</p>
<p>Breakdown 40 μm tip radius needle</p> 	<p>Needle number 4 after breakdown. The needle tip radius was major changed</p>

<p>Breakdown 20 μm tip radius needle</p> 	<p>Needle number 5 after breakdown. The needle tip radius was increased to 22.34 μm.</p>
<p>Breakdown 20 μm tip radius needle</p> 	<p>Needle number 6 after breakdown. The needle tip radius was increased to 36.10 μm</p>
<p>Breakdown 20 μm tip radius needle</p> 	<p>Needle number 7 after breakdown. The needle tip radius was increased to 33.51 μm</p>

7.2.4 Effect of needle lengths on PDIV and PD characteristics

Needle length is one of important parameters which may affect PDIV value. The needle length has effect on the electric field strength of the electrode system as presented in 7.1.

7.2.4.1 PDIV and PD experiment

The experiment was performed by using the needle - plane electrode with the 10 μm tip radius needle and a brass plane electrode with diameter of 75 mm compared with PDIV measuring by the 10 μm tip radius needle - a steel sphere electrode with diameter of 12.7 mm. This sphere electrode diameter is in the range of the standard sphere electrode for the PDIV test recommended by IEC 61294. The lengths of the needles were specified as 25 ± 0.5 mm and 45 ± 0.5 mm respectively. Two gap distances of 25 mm and 50 mm were fixed for investigation. The needle length of 25 mm and the gap distance of 50 mm are according to IEC 61294. The mineral oil, Nynas nytro 4000x, with water content less than 10 ppm was used for this research. The laboratory experiment was conducted with two PDIV test techniques. The first PDIV experiment was implemented consistent with IEC 61294. Three needles with the same needle length were used to investigate for each electrode configuration. The mean value PDIV of each electrode arrangement was computed. After that, PD activities were measured and recorded for 1 minute at the PDIV level. The latter PDIV test experiment is the combine PDIV test method. PDIV was detected and recorded. Then, PD activities were examined at the PDIV level and recorded for 1 minute. Both IEC and combine PDIV experiments are explained in chapter 6. The average PDIV values of the

needle-plane and needle-sphere electrode systems are depicted in Table 7.16 and Fig. 7.40-Fig. 7.41 respectively.

Table 7.16: Mean value PDIV and average charge quantity at PDIV level of the electrode arrangements as a function of needle lengths, gap distances and test methods

Electrode arrangement	Gap length (g: mm)	U_{PDIV} (kV)				Q_{IEC} (pC)			
		IEC method		Combine method		IEC method		Combine method	
		$l = 25$ mm	$l = 45$ mm	$l = 25$ mm	$l = 45$ mm	$l = 25$ mm	$l = 45$ mm	$l = 25$ mm	$l = 45$ mm
Needle-plane	25	24.0	22.4	20.4	19.4	279.3	377.7	133.7	215.3
	50	33.0	30.3	27.3	25.4	200.0	270.0	100.4	132.0
Needle - sphere	25	35.2	33.7	29.5	27.6	190.3	356.3	113.3	167.3
	50	42.1	40.0	38.4	31.7	121.3	257.3	95.0	106.4

Where: l represents the needle length.

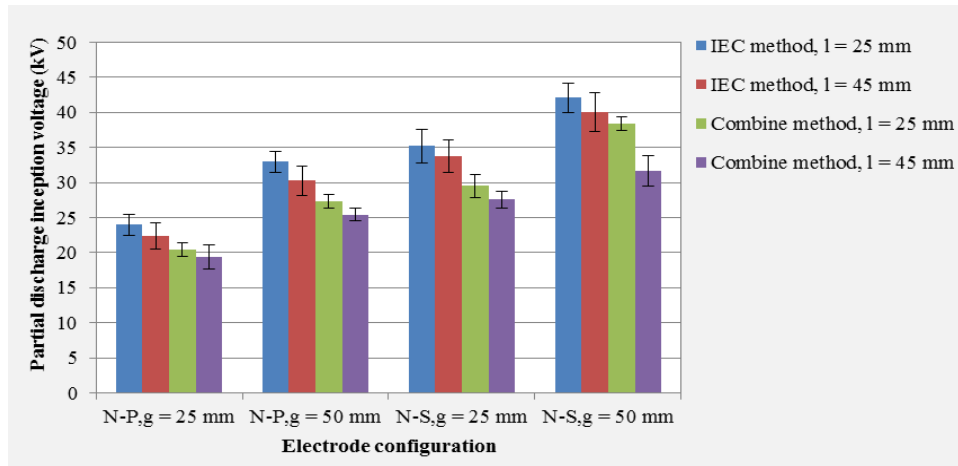


Figure 7.40: Mean value PDIV obtained from different needle lengths and PDIV test techniques

Where N-P is the needle-plane electrode, N-S is the needle-sphere electrode, g is the gap distance of the electrode and l is the needle length

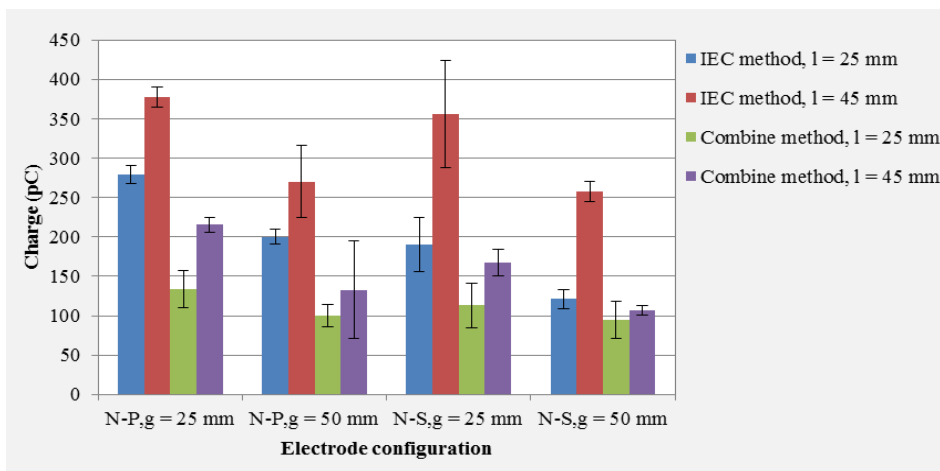


Figure 7.41: Relationship between average charge values of each electrode configuration

Where N-P is the needle-plane electrode, N-S is the needle - sphere electrode, g is the gap distance of the electrode and l is the needle length

The example of distribution of raw data (the needle number 1- plane or sphere grounded electrode system) was modelled with normal and weibull distributions as illustrated in Fig. 7.42- Fig. 7.47.

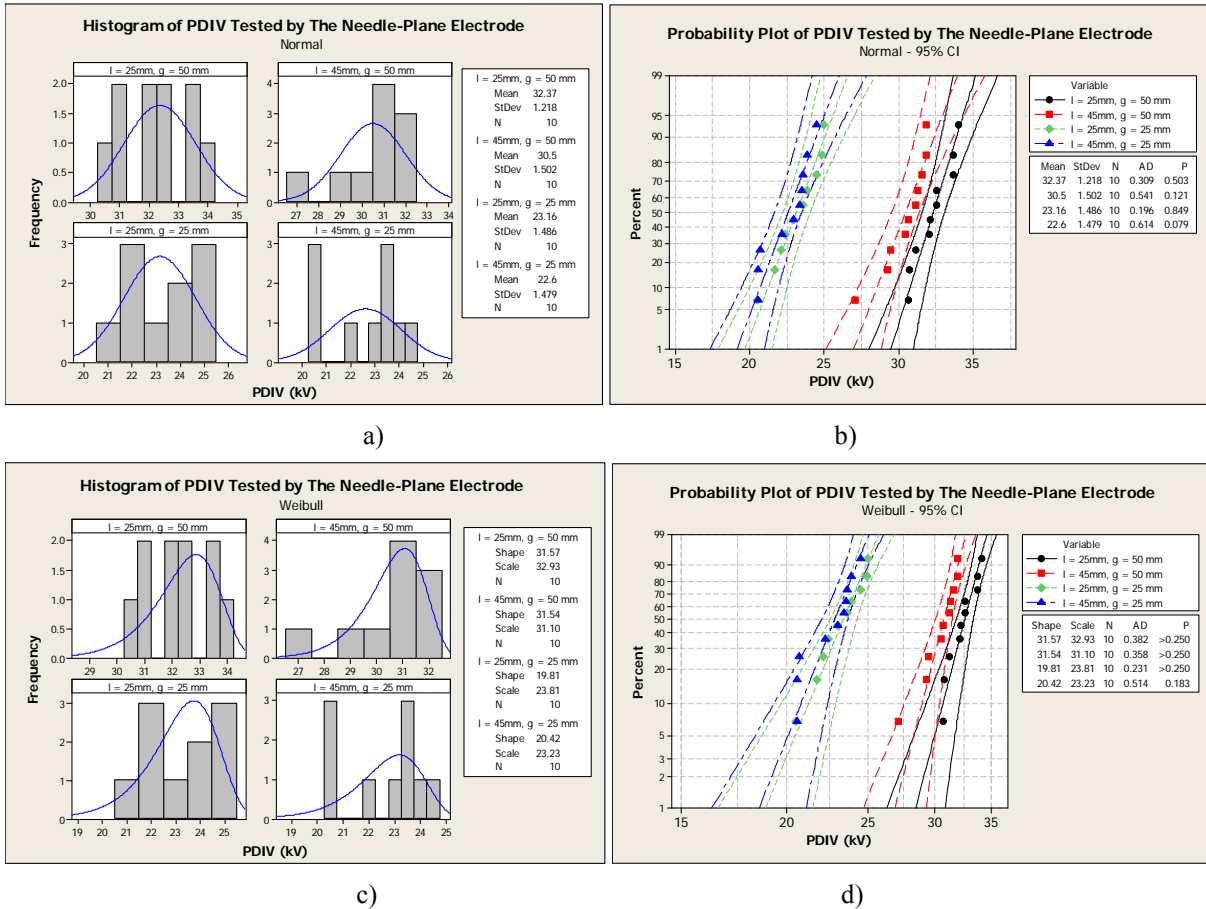
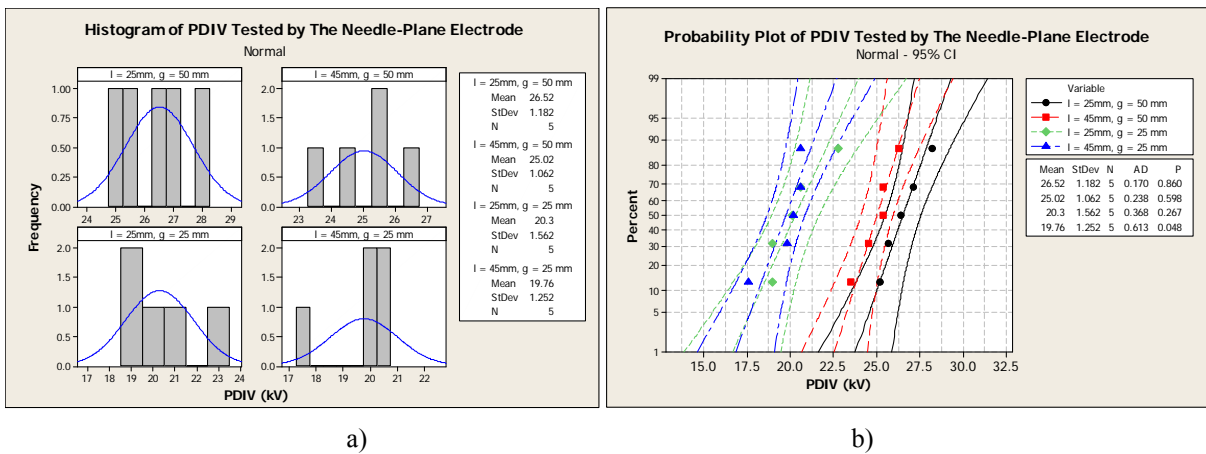
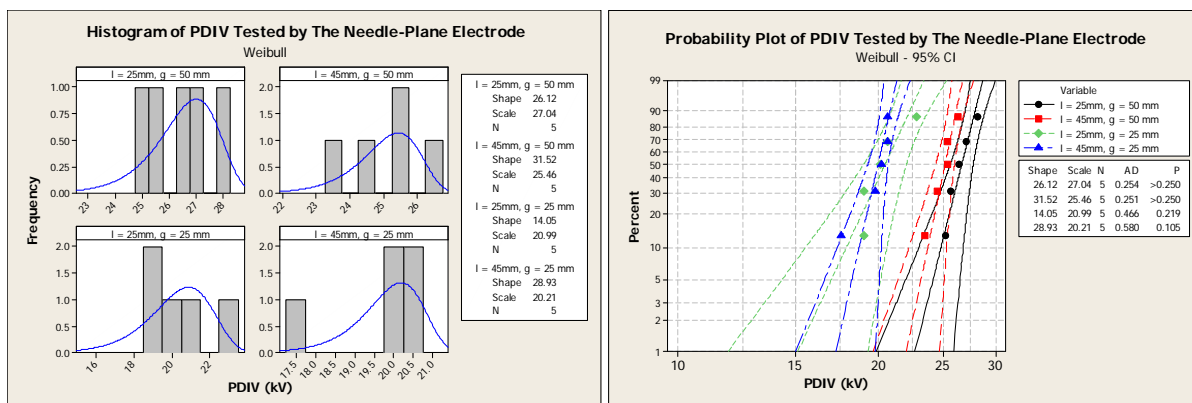


Figure 7.42: Normal and weibull distribution of PDIV value obtained from the needle-plane electrode systems tested according to IEC test method
a) histogram with normal distribution plot b) probability plot of normal distribution c) histogram with weibull distribution plot d) probability plot of weibull distribution



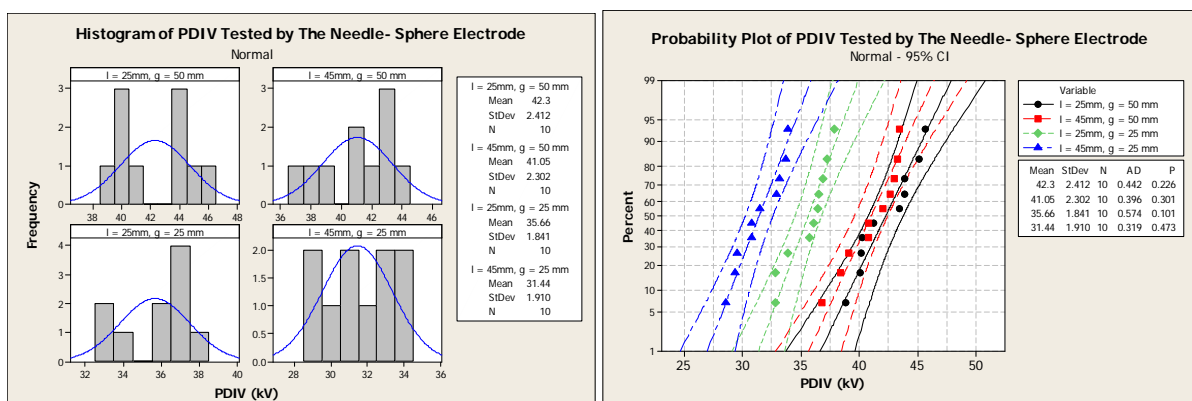


c)

d)

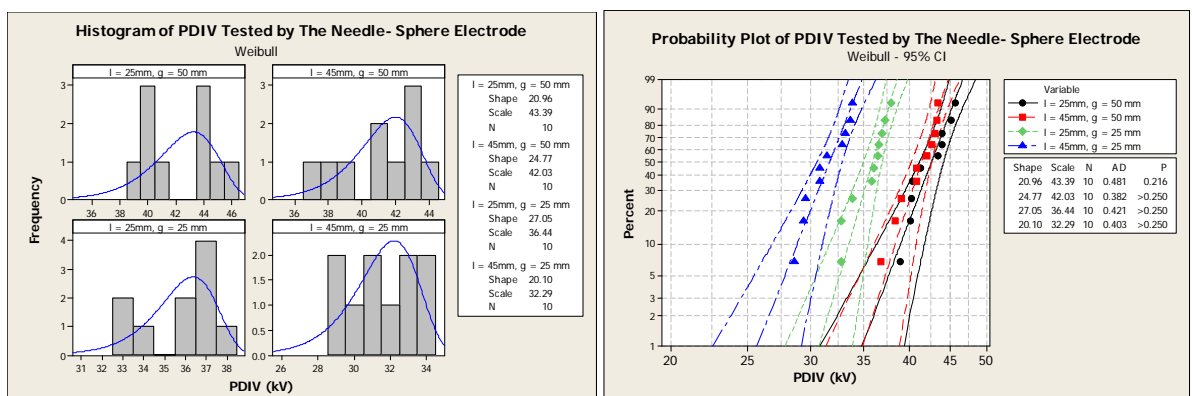
Figure 7.43: Normal and weibull distribution of PDIV value obtained from the needle-plane electrode systems tested according to the combine PDIV test method

a) histogram with normal distribution plot b) probability plot of normal distribution c) histogram with weibull distribution plot d) probability plot of weibull distribution



a)

b)



c)

d)

Figure 7.44: Normal and weibull distribution of PDIV value obtained from the needle-sphere electrode systems tested according to IEC test method

a) histogram with normal distribution plot b) probability plot of normal distribution c) histogram with weibull distribution plot d) probability plot of weibull distribution

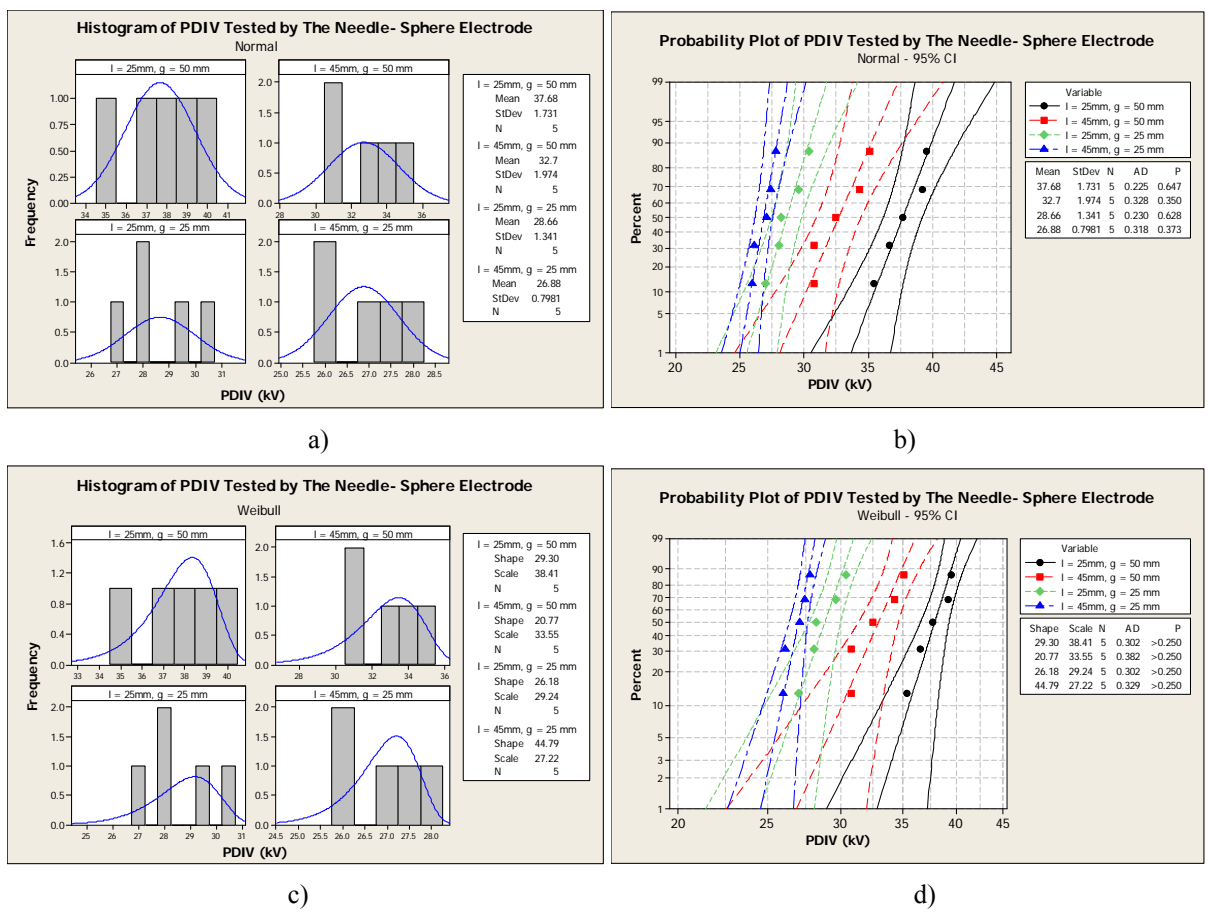
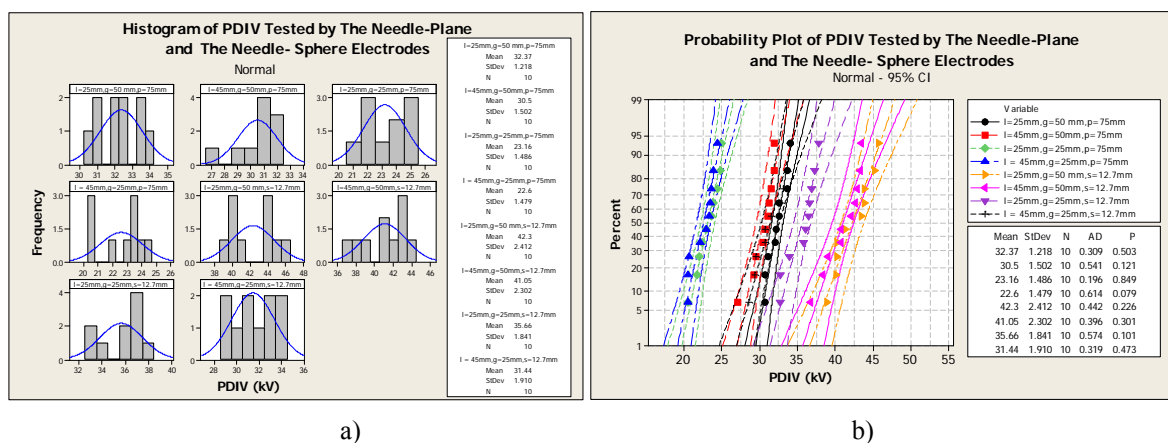
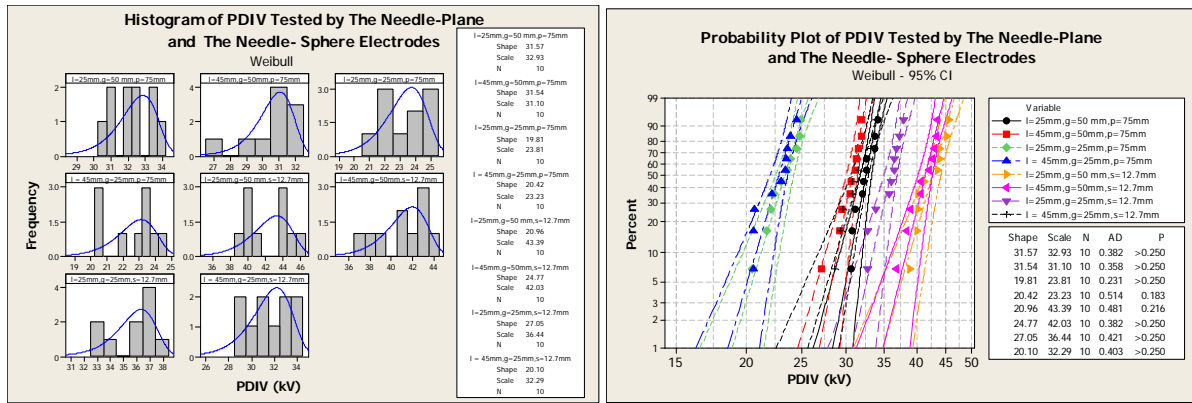


Figure 7.45: Normal and weibull distribution of PDIV value obtained from the needle-sphere electrode systems tested according to the combine PDIV test method

a) histogram with normal distribution plot b) probability plot of normal distribution c) histogram with weibull distribution plot d) probability plot of weibull distribution



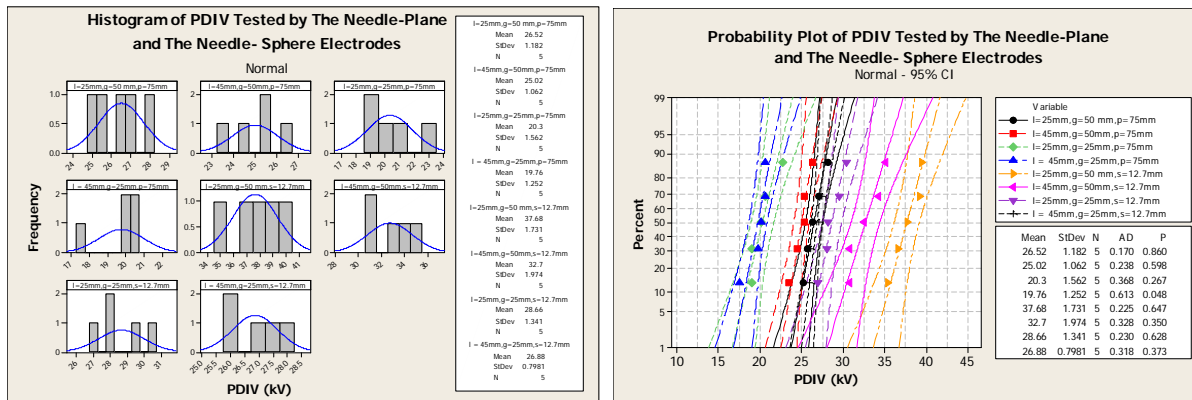


c)

d)

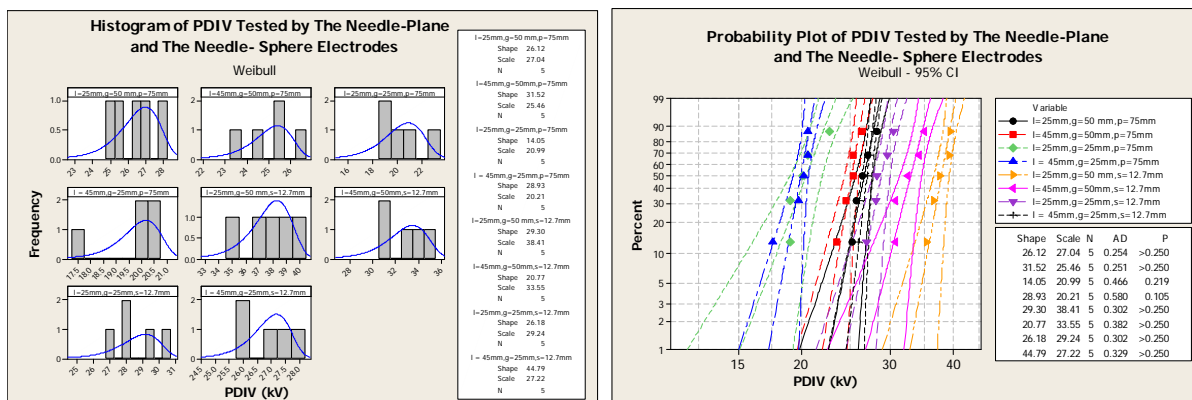
Figure 7.46: Normal and weibull distribution of PDIV value obtained from the needle-sphere electrode systems and the needle-plane electrode systems tested according to IEC test method

a) histogram with normal distribution plot b) probability plot of normal distribution c) histogram with weibull distribution plot d) probability plot of weibull distribution



a)

b)



c)

d)

Figure 7.47: Normal and weibull distribution of PDIV value obtained from the needle-sphere electrode system and the needle-plane electrode system tested according to the combine PDIV test method

a) histogram with normal distribution plot b) probability plot of normal distribution c) histogram with weibull distribution plot d) probability plot of weibull distribution

7.2.4.2 PD activity

In this experiment, the distribution of charges was not modeled as normal or weibull distribution because the charge value was recorded only 3 three times for each identical electrode configuration. Therefore, the raw data of each electrode configuration was not suitable to be modelled. Examples of phase - resolved PD patterns of the mineral oil subjected to the needle-plane electrode configuration and the needle - sphere electrode configuration tested with IEC and the combine PDIV test methods are shown in Fig. 7.48- Fig. 7.50 respectively.

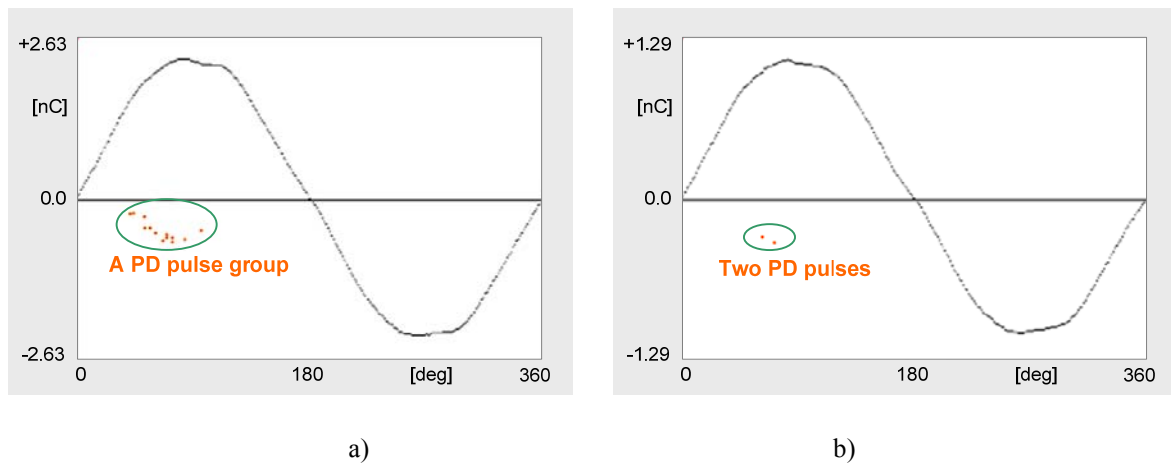


Figure 7.48: Phase- resolved PD characteristics recorded for one minute at the PDIV value tested by the needle-plane electrode system with the needle length of 25 mm and the gap distance of 25 mm

a) at PDIV level of 23.5 kV obtained from IEC standard test method, Q_{IEC} 273 pC, Q_{PEAK} 683 pC b) at PDIV level of 20.5 kV, acquired from the combine PDIV test method, Q_{IEC} 138 pC, Q_{PEAK} 345 pC

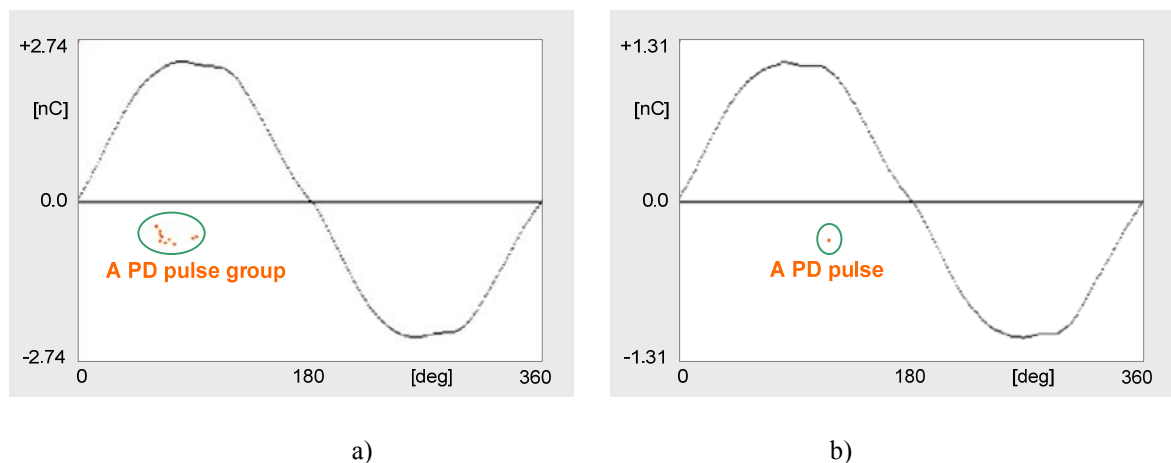


Figure 7.49: Phase-resolved PD characteristics recorded for one minute at the PDIV value tested by the needle- plane electrode with the needle length of 45 mm and the gap distance of 50 mm

a) at PDIV level of 30.5 kV obtained from IEC standard test method, Q_{IEC} 285 pC, Q_{PEAK} 712 pC , b) at PDIV level of 25.1 kV acquired from the combine PDIV test method, Q_{IEC} 128 pC, Q_{PEAK} 321 pC

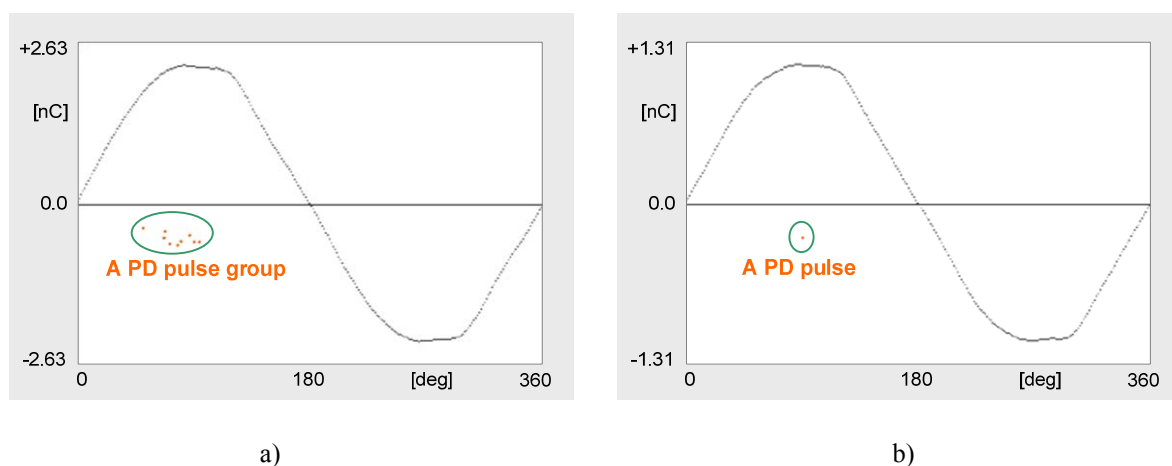


Figure 7.50: Phase-resolved PD characteristics recorded for one minute at the PDIV value tested by the needle- sphere electrode with the needle length of 45 mm and the gap distance of 50 mm

a) at PDIV level of 38.9 kV obtained from IEC standard test method, Q_{IEC} 265 pC, Q_{PEAK} 662 pC, b) at PDIV level of 32.0 kV acquired from the combine PDIV test method, Q_{IEC} 108 pC, Q_{PEAK} 269 pC

PDIV value tested by the needles with needle length of 25 mm and 45 mm were not much different. The PDIV value was related with the electric field strength of each electrode configuration. The needle-plane electrode with the needle length of 25 mm generated the PDIV value higher the PDIV from the needle-plane electrode with the needle length of 45 mm about 1-2.5 kV. In case of the needle-sphere electrode, the needle length had more effect on PDIV when the combine PDIV test measurement was performed. The test results demonstrated that the needle- plane electrodes with the plane diameter of 75 mm had higher sensitivity to detect PDIV than the needle-sphere electrode with the sphere diameter of 12.7 mm. The needle- plane electrodes with the plane diameter of 75 mm can detect PDIV at the lower voltage level with higher charge values compared with detected by the needle - sphere electrode with the sphere diameter of 12.7 mm. The test results represented also that the shorter gap distance produced the higher charge values. The higher PD repetition rate happened when the PD measurement was performed at the PDIV level obtained from IEC standard test. Whereas, only one or two PDs were found nearly 90 degree of applied voltage when the experiment was performed at the PDIV level obtained from the combine method. Furthermore, the PDIV test results can be described by normal and weibull distributions.

7.2.5 Effect of water contents and temperatures of the mineral oil on PDIV and PD characteristics

Normally, PDIV measurement of the liquid insulation is performed under atmospheric condition. However, in practice, insulating liquids in the high voltage equipment are used in wide range of operating temperatures with different water contents. Therefore, this work purposed to study the PDIV characteristics of the mineral oil under difference oil conditions tested by a needle - plane electrode system. The PDIV test experiment was set up according to IEC 60270. Tungsten needle electrodes with the tip radius of 10 μ m were used as the high voltage electrode while the brass plane electrode with a diameter of 75 mm as grounded electrode. The 10 μ m tip radius needle was selected to use for this experiment due to it provided the lowest PDIV value compared with other two needle tip radii, 20 μ m and 40 μ m. Besides, there was no breakdown event happening during PDIV experiment was performed by the 10 μ m tip radius needles. The gap distance of the electrode system was set up at 50 mm. The test procedure was carried out in accordance with IEC 61294 (M1) and also the combine PDIV test method (M2). In the testing experiment, the PDIV of the mineral oil, Nynas 4000x, with different oil conditions were investigated. The mineral oil with water content 4 \pm 2, 20 \pm 2 ppm and 40 \pm 2 ppm were prepared and examined under room temperature, 40 \pm 2 $^{\circ}$ C, 60 \pm 2 $^{\circ}$ C, 90 \pm 2 $^{\circ}$ C respectively. The PD activities and the PD pulse currents of the mineral oil with different conditions were also investigated.

7.2.5.1 Mineral oil preparation for different oil conditions

The mineral oil prepared for this experiment was pre-treated by the industrial oil retreat machine which can filter the particles in the mineral oil with the particle size of 2.5 μ m. The water content of the treated mineral oil was about 3- 4 ppm. Then, the average AC breakdown voltage of the treated mineral oil was tested in accordance with IEC 60156 by using DTA 100 E. The average AC breakdown voltage was about 87 kV. To set up the higher water content mineral oil, the steam from the boiling distilled water was mixed with the 8 liter treated mineral oil which was heating. After the mixed steam-treated mineral oil cooldown, the water content of the mixed steam-treated mineral oil was checked. This process would be repeated until the water content of the mixed steam mineral oil was in the range of specified values. Let the high water content mineral oil cooled down for further 15 hours. Then, the high water content mineral oil without the droplet water was transferred to the glass boxes. Now, the high water content mineral oil was ready to mix with the low water content mineral oil in the test cell to get the specified high water content mineral oil for PDIV experimenting. Details for high water content mineral oil preparation are in annex C.

To control mineral oil temperature, the heating blanket and the commercial heater were used. The temperature of the mineral oil was controlled by controlling the applied voltage of the heaters. The temperature was detected by the temperature sensor during the experiment.

7.2.5.2 PDIV and PD experiment

A test circuit arrangement for PDIV and PD activity investigation was set up according to IEC 60270. The PDIV test procedure was performed in accordance with IEC 61294. Three identical tip radius needles were used to investigate for each electrode configuration. After that, the PDIV mean value of each electrode configuration was computed. Then, the PD pulse currents and PD activities were investigated at the PDIV level. Moreover, PDIV experiment

was also performed with the combine PDIV test method as described in chapter 6. The PDIV value and the charge activity were measured and recorded. To maintain the mineral oil characteristics, one oil sample was tested under room temperature (17°C - 22°C) with relative humidity of 29% - 45% until 90±2°C. This process spent about 16 hours for one oil sample investigation. The PD pulse current was recorded only at the PDIV value obtained from IEC test method due to the limit of time for testing. The mean value of PDIV and charge at different oil conditions and test methods are summarized in Table 7.17- Table 7.18 respectively.

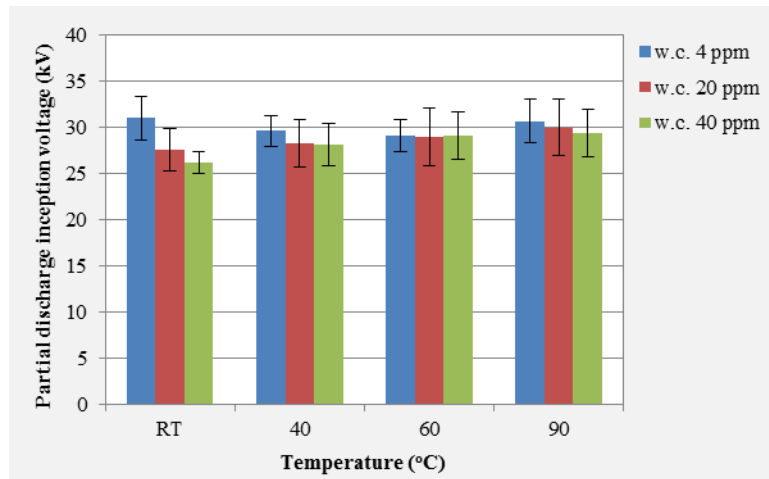
Table 7.17: Mean value PDIV of the mineral oil with different oil conditions obtained from different test methods

Test method	Temperature (°C)	U _{PDIV} (kV)		
		4 ppm	20 ppm	40 ppm
IEC	RT	31.0	27.6	26.2
	40	29.6	28.3	28.1
	60	29.1	29.0	29.1
	90	30.7	30.0	29.4
Combine	RT	25.4	23.8	21.8
	40	23.9	23.6	23.2
	60	23.6	23.4	23.3
	90	23.0	22.7	23.4

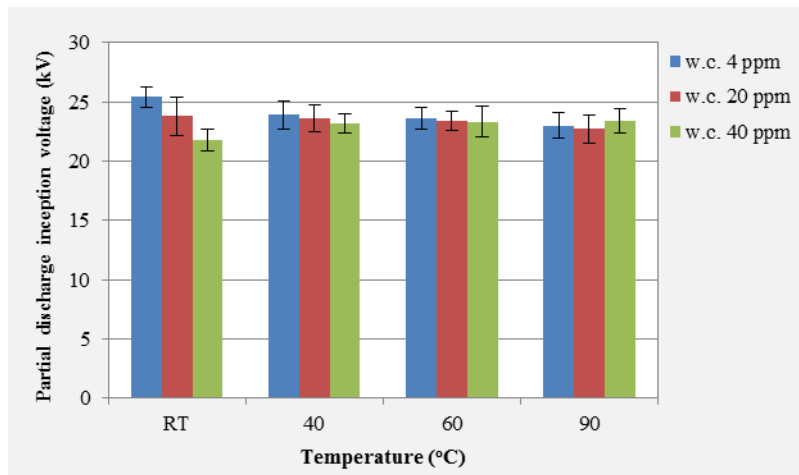
Table 7.18: Average charge quantity of the mineral oil with different oil conditions obtained from different test methods

Test method	Temperature (°C)	Charge quantity (pC)		
		4 ppm	20 ppm	40 ppm
IEC	RT	338	240	211
	40	338	235	235
	60	292	258	270
	90	366	296	283
Combine	RT	143	131	105
	40	114	114	88
	60	81	104	109
	90	98	93	77

Average PDIV values of the mineral oil with different water contents as function of oil temperatures tested by IEC method and the combine PDIV test method are shown in Fig. 7.51 -Fig.7.53. Fig. 7.54 combines the PDIV values obtained from both test methods.



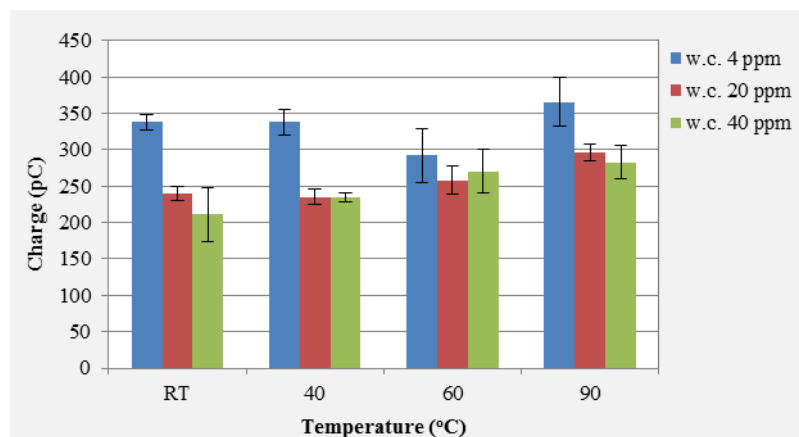
a)



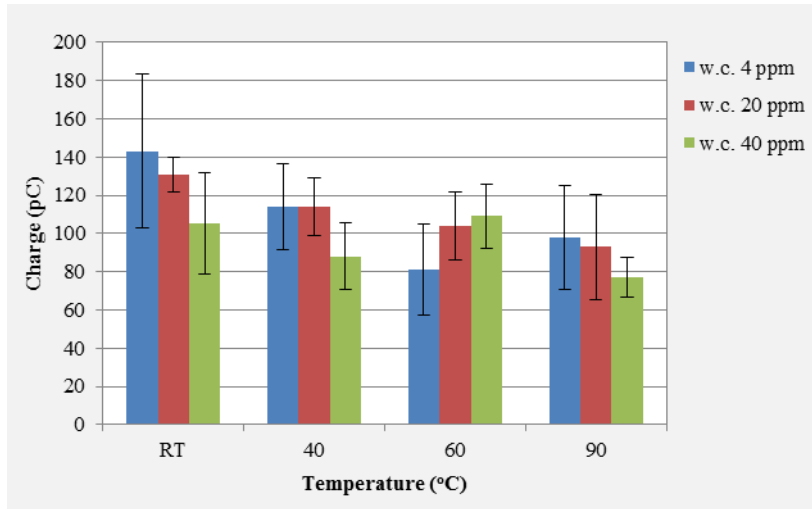
b)

Figure 7.51: Mean value PDIV of the mineral oil with different water contents as a function of oil temperatures tested by

a) IEC method b) combine PDIV test method



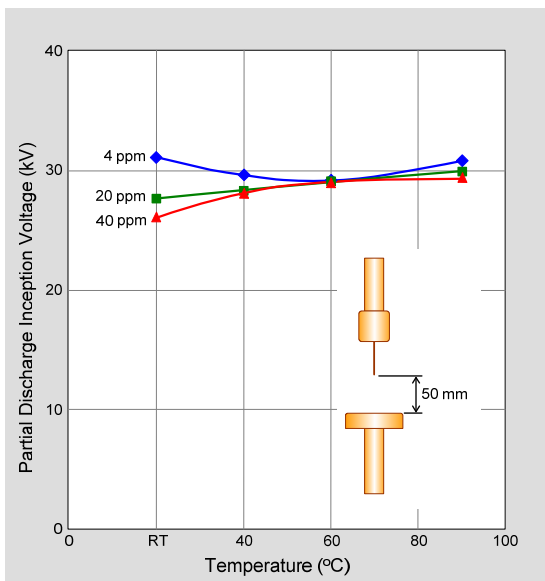
a)



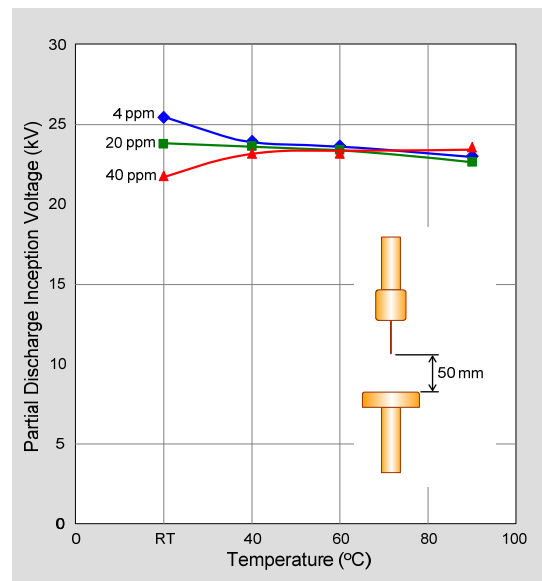
b)

Figure 7.52: Comparison average charge values of the mineral oil with different water contents as a function of oil temperatures tested by

a) IEC test method b) combine PDIV test method



a)



b)

Figure 7.53: Mean value PDIV of the mineral oil with different water contents as a function of oil temperatures tested by

a) IEC test method b) combine PDIV test method

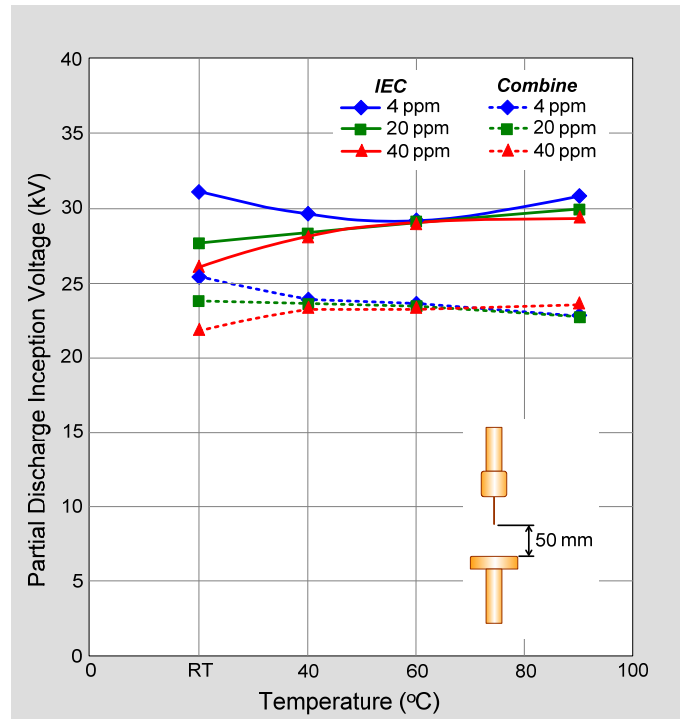
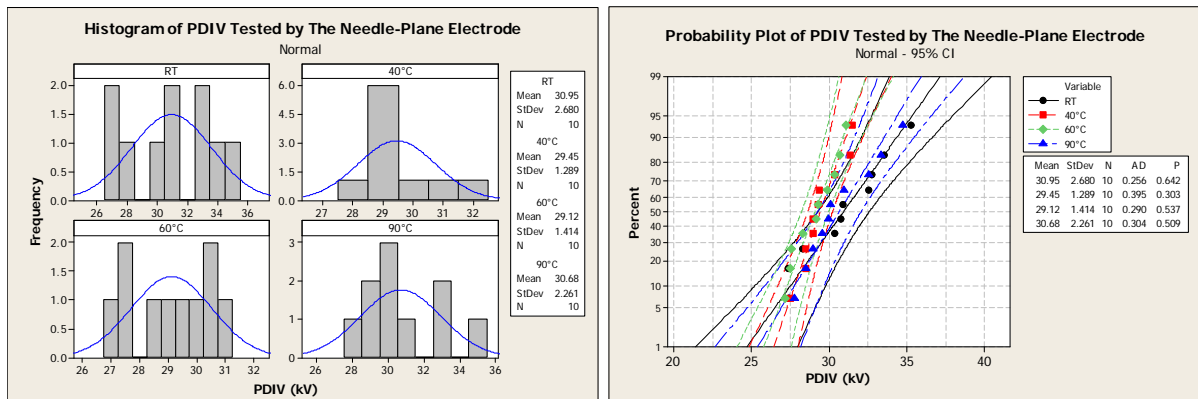


Figure 7.54: Comparison mean value PDIV of the mineral oil with different water contents as a function of oil temperatures tested by IEC test method and the combine PDIV test method

The distribution of the test data (raw data of the needle 1- plane electrode system) was analyzed as normal distribution and weibull distribution as shown in Fig. 7.55- Fig 7.57.



a)

b)

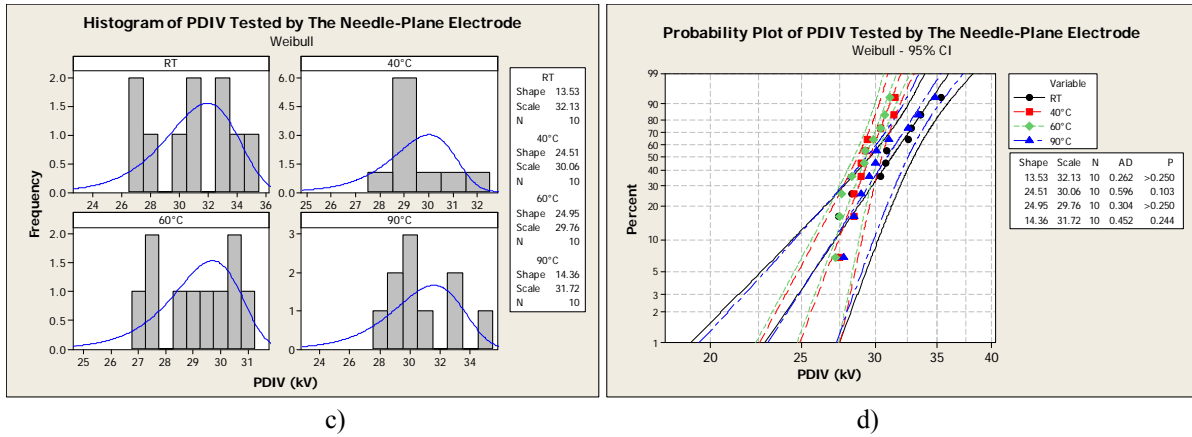


Figure 7.55: Normal and weibull distribution of PDIV value obtained from the 10 μ m tip radius needle - 75 mm diameter plane electrode of the mineral oil with water content of 4 ppm at various oil temperatures (IEC test method)

a) histogram with normal distribution plot b) probability plot of normal distribution c) histogram with weibull distribution plot d) probability plot of weibull distribution

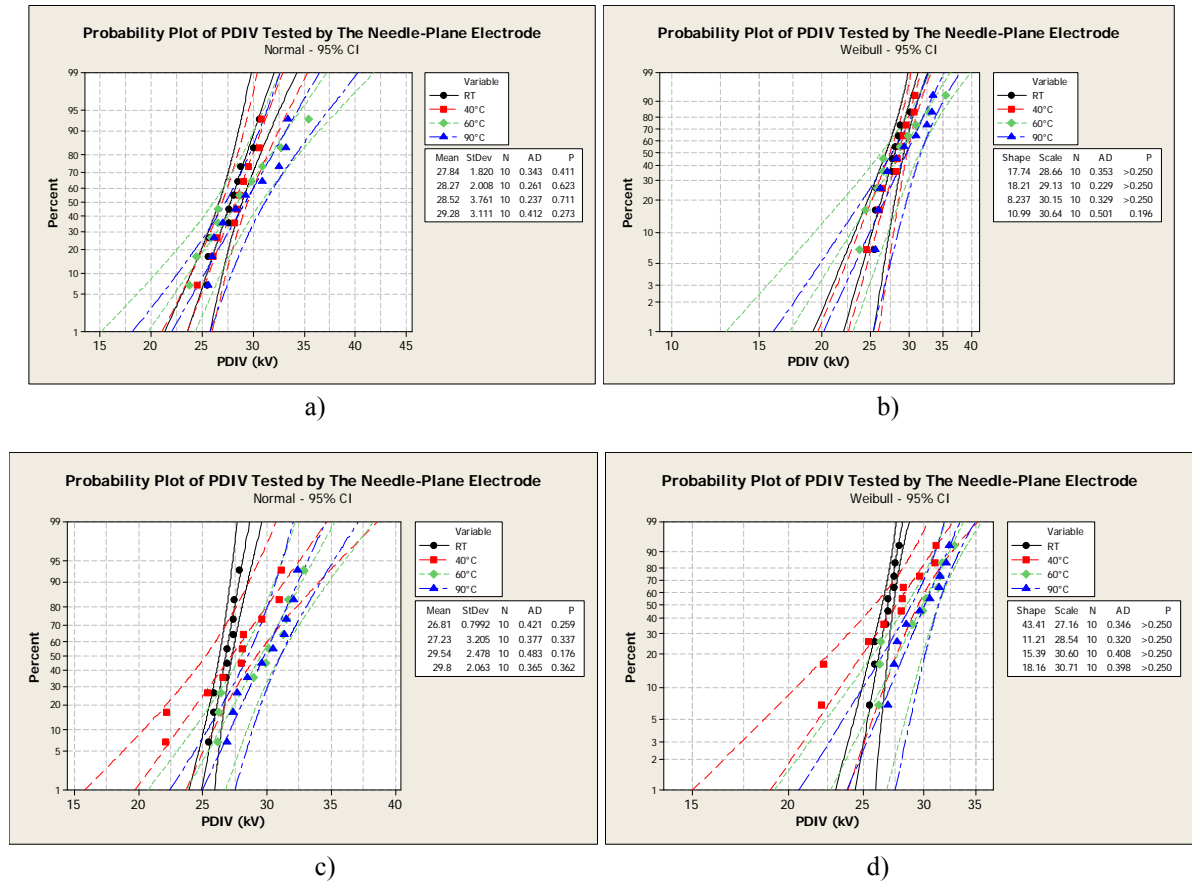
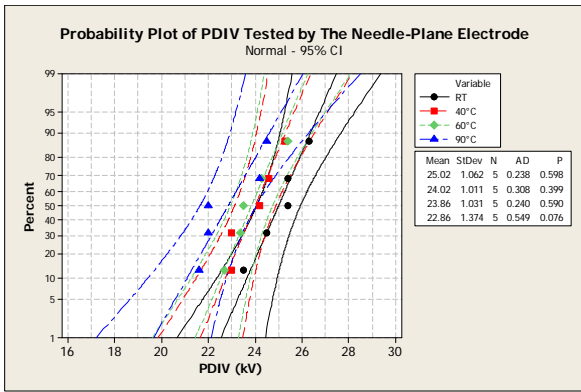
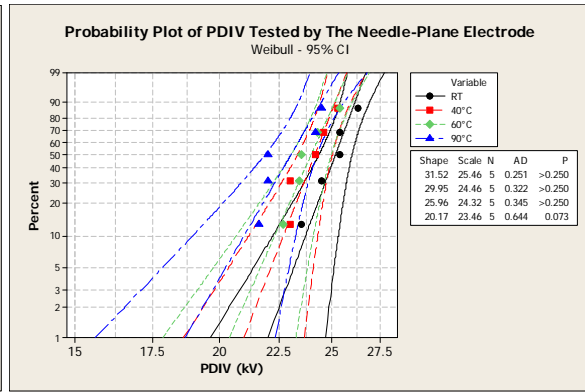


Figure 7.56: Normal and weibull distribution of PDIV values obtained from the 10 μ m tip radius needle - 75 mm diameter plane electrode of the mineral oil with various oil temperatures and water contents (IEC test method)

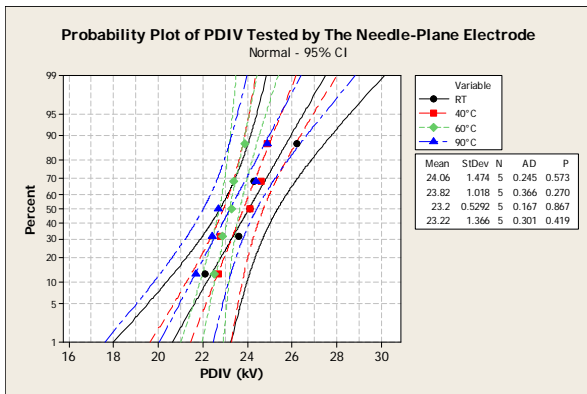
a) probability plot of normal distribution b) probability plot of weibull distribution of PDIV values of the mineral oil with water content 20 ppm c) probability plot of normal distribution d) probability plot of weibull distribution of PDIV values of the mineral oil with water content 40 ppm



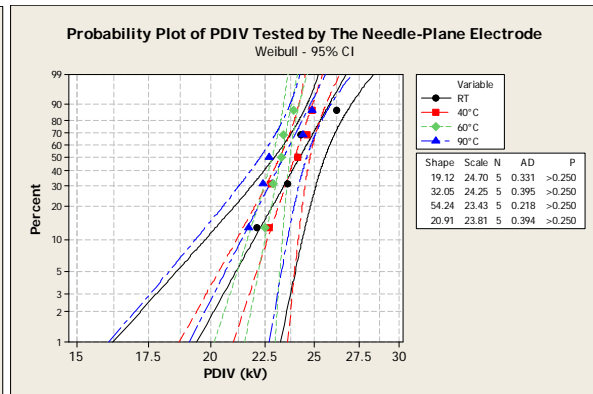
a)



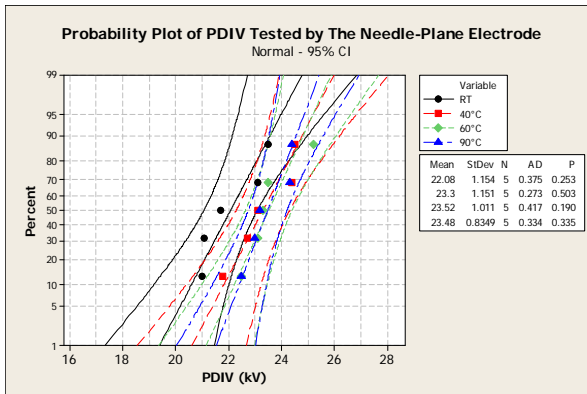
b)



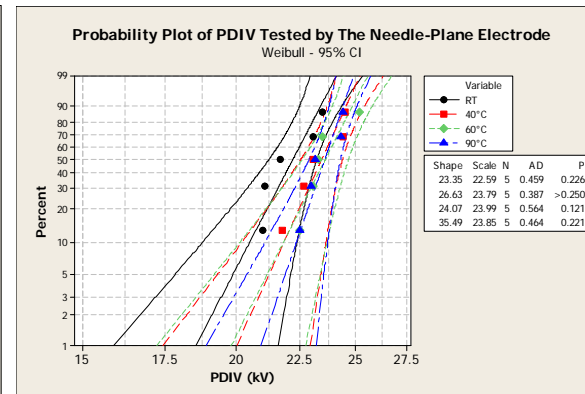
c)



d)



e)



f)

Figure 7.57: Normal and weibull distribution of PDIV value obtained from the 10 μm tip radius needle - 75 mm diameter plane electrode of the mineral oil with various oil temperatures (the combine PDIV test method)

a) probability plot of normal distribution b) probability plot of weibull distribution of PDIV values of the mineral oil with water content 4 ppm c) probability plot of normal distribution d) probability plot of weibull distribution of PDIV values of the mineral oil with water content 20 ppm e) probability plot of normal distribution f) probability plot of weibull distribution of PDIV values of the mineral oil with water content 40 ppm

At room temperature, the water content in the mineral oil influenced more or less on PDIV value. However, at the higher temperature, the PDIV values of the mineral oil with different water contents were relatively the same. At room temperature, breakdown voltage of the mineral oil with different water contents was also measured according to IEC 60156 as summarized in Table 7.19. Breakdown voltage of the mineral oil was clearly different when the mineral oil contained different water contents. The comparison between breakdown voltage and PDIV value of the mineral oil with different water contents at room temperature is shown in Fig. 7.58.

Table 7.19: Breakdown voltage value of the mineral oil with different water contents

Water content (ppm)	Breakdown voltage (kV)	Standard deviation (%)
4	86.7	9.7
20	62.5	12.5
40	34.2	13.9

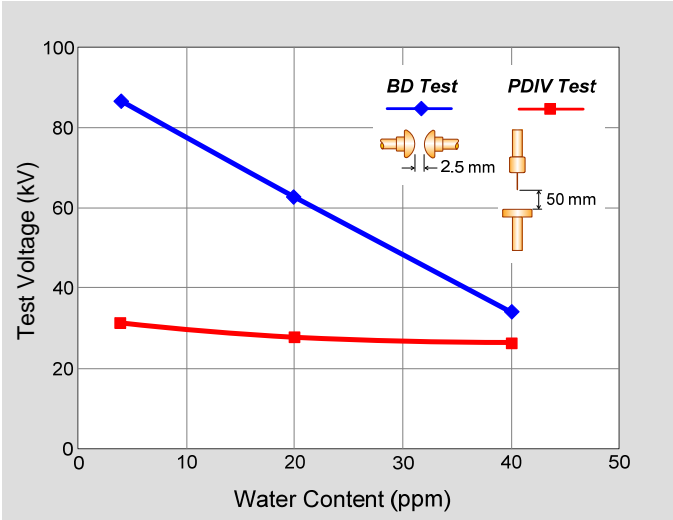


Figure 7.58: Breakdown voltage and mean value PDIV at room temperature with different water contents

7.2.5.3 PD activity

The PD charge quantity (Q_{IEC}) at PDIV level as function of water contents and temperatures is presented in Table 7.18. Examples of phase-resolved PD characteristics of the mineral oil with water content of 4 ppm at the PDIV levels as function of oil temperatures and the examples of phase-resolved PD characteristics of the mineral oil at the PDIV levels under room temperature as function of water contents are illustrated in Fig. 7.59- Fig. 7.60 respectively.

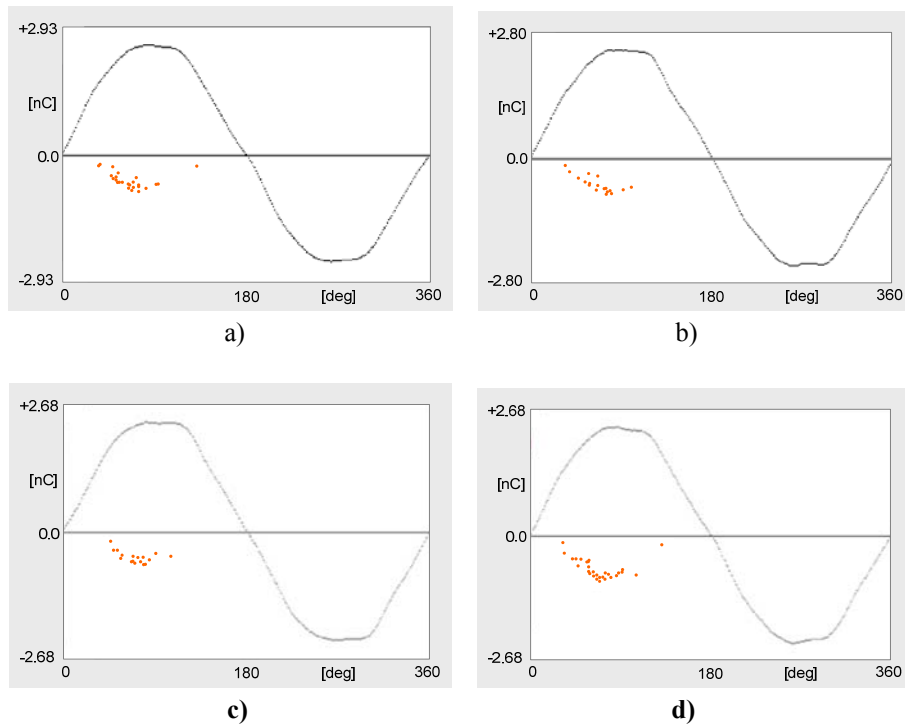


Figure 7.59: PD phase-resolved diagram of the mineral oil with water content 4 ppm at different oil temperatures recorded for 1 minute at the PDIV levels obtained from IEC test method

a) room temperature: PDIV level of 30.3 kV, Q_{IEC} 332 pC, Q_{PEAK} 831 pC b) 40°C: PDIV level of 29.0 kV, Q_{IEC} 318 pC, Q_{PEAK} 794 pC c) 60°C: PDIV level of 28.6 kV, Q_{IEC} 271 pC, Q_{PEAK} 676 pC d) 90°C: PDIV level of 30.1 kV, Q_{IEC} 389 pC, Q_{PEAK} 972 pC

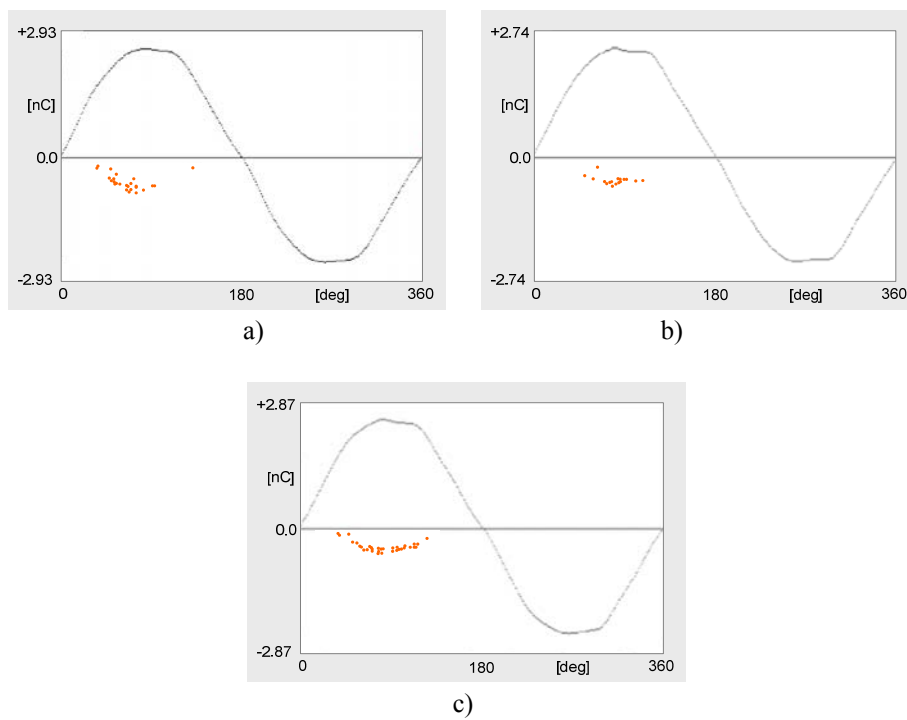


Figure 7.60: PD phase-resolve diagram of the mineral oil under room temperature with different water contents recorded for 1 minute at the PDIV levels obtained from IEC test method

a) 4 ppm: PDIV level of 30.3 kV, Q_{IEC} 332 pC, Q_{PEAK} 831 pC b) 20 ppm: PDIV level of 27.2 kV, Q_{IEC} 250 pC, Q_{PEAK} 626 pC c) 40 ppm: PDIV level of 26.8 kV, Q_{IEC} 235 pC, Q_{PEAK} 587 pC

7.2.5.4 Relative permittivity, dielectric loss and resistivity of the mineral oil with various water contents and temperatures

Temperature and water contents have also effect on other characteristics of the mineral oil such as permittivity, dielectric loss and so on. Fig. 7.61 represents the relationship between relative permittivity and oil temperature with various water contents. Fig. 7.62 depicts the relationship between the oil temperature and the loss factor of different water content mineral oils. The mineral oil characteristics at various temperatures are summarized in Table 7.20.

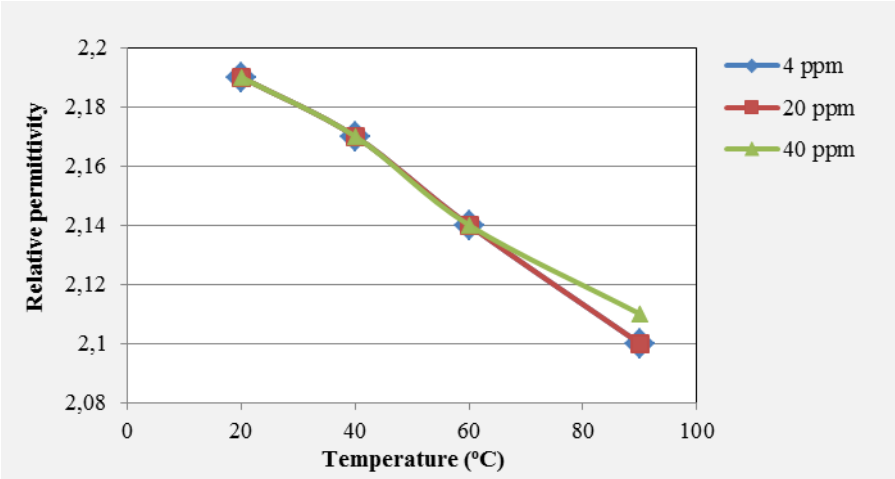


Figure 7.61: Relative permittivity of the mineral oil with different water contents and temperatures

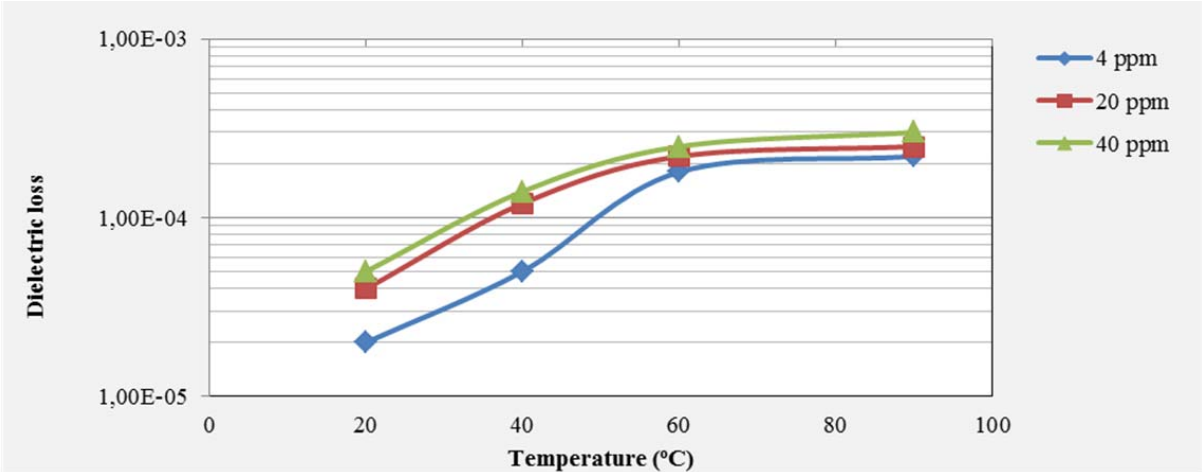


Figure 7.62: Loss factor of the mineral oil with different water contents and temperatures

Table 7.20: Mineral oil characteristics with different water contents and temperatures

Water content (ppm)	Temp (°C)	ϵ_r	$\tan \delta$	ρ^+ (Ωm)	ρ^- (Ωm)
4	20	2.19	2.00E-05	>20E+12	>20E+12
	40	2.17	5.00E-05	>20E+12	>20E+12
	60	2.14	1.80E-04	5.80E+12	1.14E+13
	90	2.10	2.20E-04	1.10E+12	2.10E+12
20	20	2.19	4.00E-05	>20E+12	>20E+12
	40	2.17	1.20E-04	1.90E+13	>20E+12
	60	2.14	2.20E-04	4.70E+12	1.00E+13
	90	2.10	2.50E-04	9.30E+11	2.10E+12
40	20	2.19	5.00E-05	>20E+12	>20E+12
	40	2.17	1.40E-04	1.85E+13	>20E+12
	60	2.14	2.50E-04	4.40E+12	1.35E+13
	90	2.11	3.00E-04	8.60E+11	1.80E+12

7.2.6 Effect of PDIV test circuits on PDIV and PD characteristics

7.2.6.1 PDIV and PD experiment

This topic intended to study the effect of test circuits on PDIV and PD characteristics. Four PDIV test circuits were set up as explained in chapter 5. The PDIV test was experimented by using tungsten needle electrodes with the tip radius of 10 μm as the high voltage electrode and the brass plane electrode with 75 mm diameter used as the grounded electrode. The gap distance of the electrode system was fixed at 50 mm. PDIV experiment was performed conforming IEC 61294. The PDIV measurement of each needle-plane electrode was measured 20 times. The mean value PDIV of the mineral oil obtained from each test circuit was computed at the first 10 PDIV and at 20 PDIV testings. The mean value PDIV of each test circuit is shown in Table 7.21 and Fig. 7.63.

Table 7.21: Mean value PDIV obtained form different PDIV test circuits

Test circuit	U_{PDIV} (kV)	
	10 PDIV measurements	20 PDIV measurements
Test circuit 1	29.9	30.4
Test circuit 2	31.8	31.4
Test circuit 3	31.5	31.6
Test circuit 4	30.0	31.0

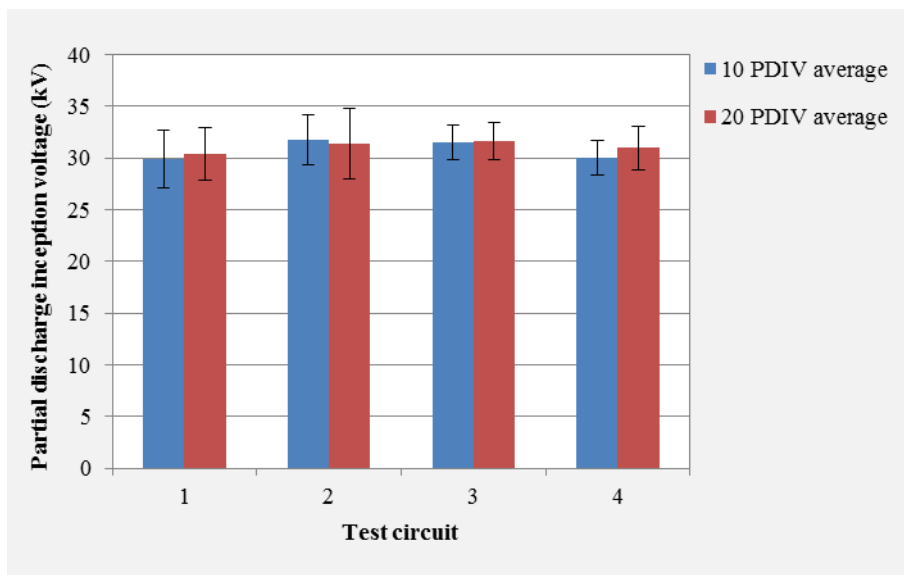
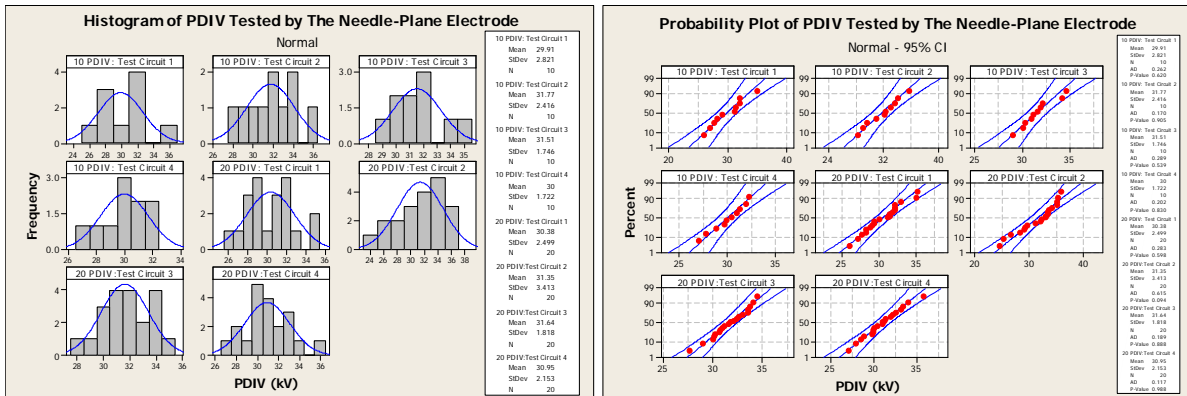


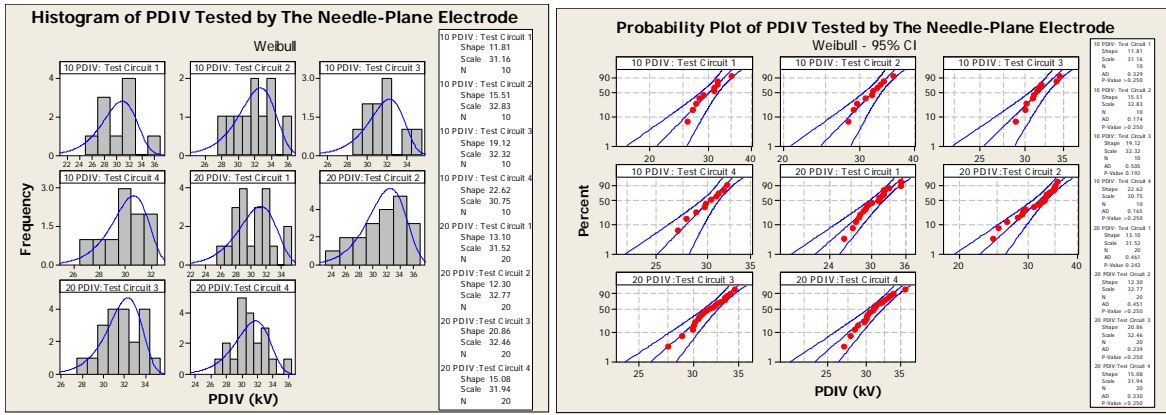
Figure 7.63: Mean value PDIV of different PDIV test circuits

The distribution of PDIV value obtained from different test circuits was modelled with normal and weibull distributions. The distributions are shown in Fig. 7.64- Fig. 7.65 respectively.



a)

b)

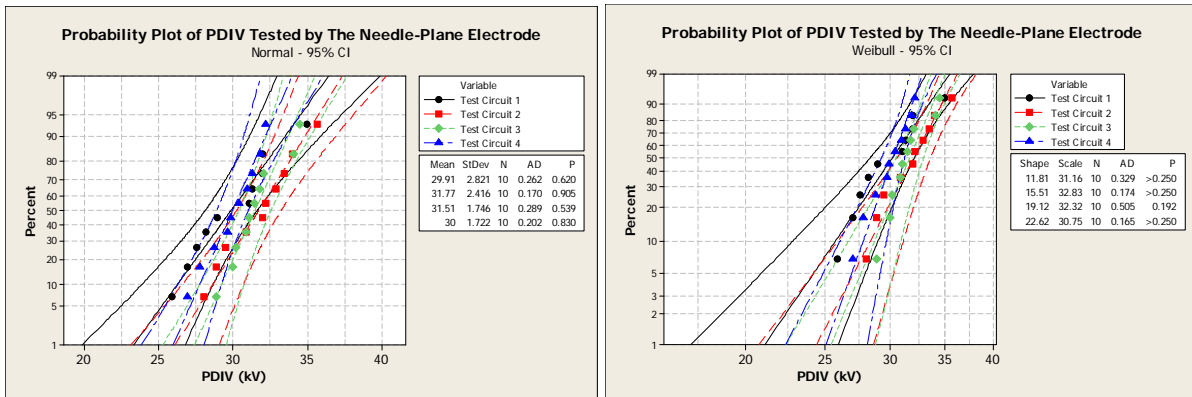


c)

d)

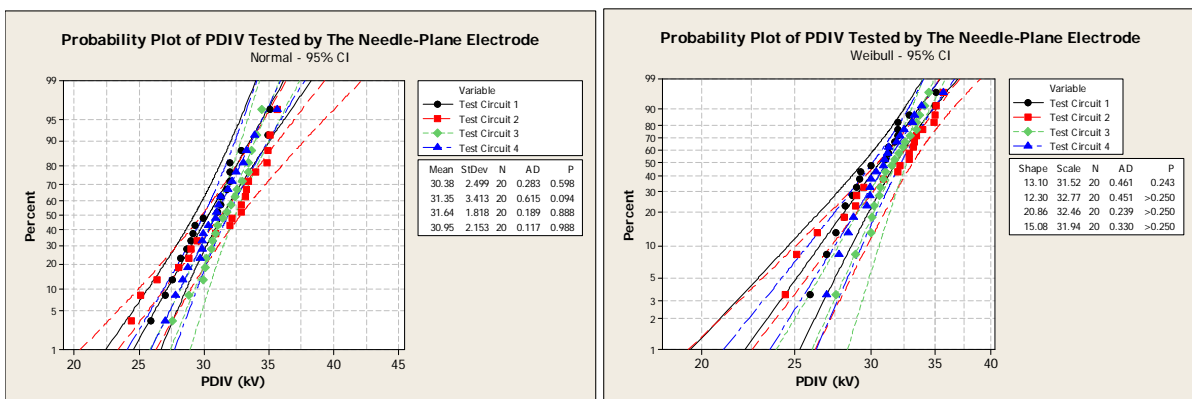
Figure 7.64: Normal and weibull distribution of PDIV value obtained from different test circuits

a) histogram with normal distribution plot b) normal distribution probability plot c) histogram with weibull distribution plot d) weibull distribution probability plot



a)

b)



c)

d)

Figure 7.65: Normal and weibull distribution of PDIV value obtained from different test circuits

a) normal distribution of PDIV value obtained from 10 time testings b) weibull distribution of PDIV value obtained from 10 time testings c) normal distribution of PDIV value obtained from 20 time testings d) weibull distribution of PDIV value obtained from 20 time testings

7.2.6.2 PD activity

The phase-resolved PD characteristics were different due to different test circuits. Examples of phase-resolved PD obtained from different PDIV test circuits are shown in Fig. 7.66.

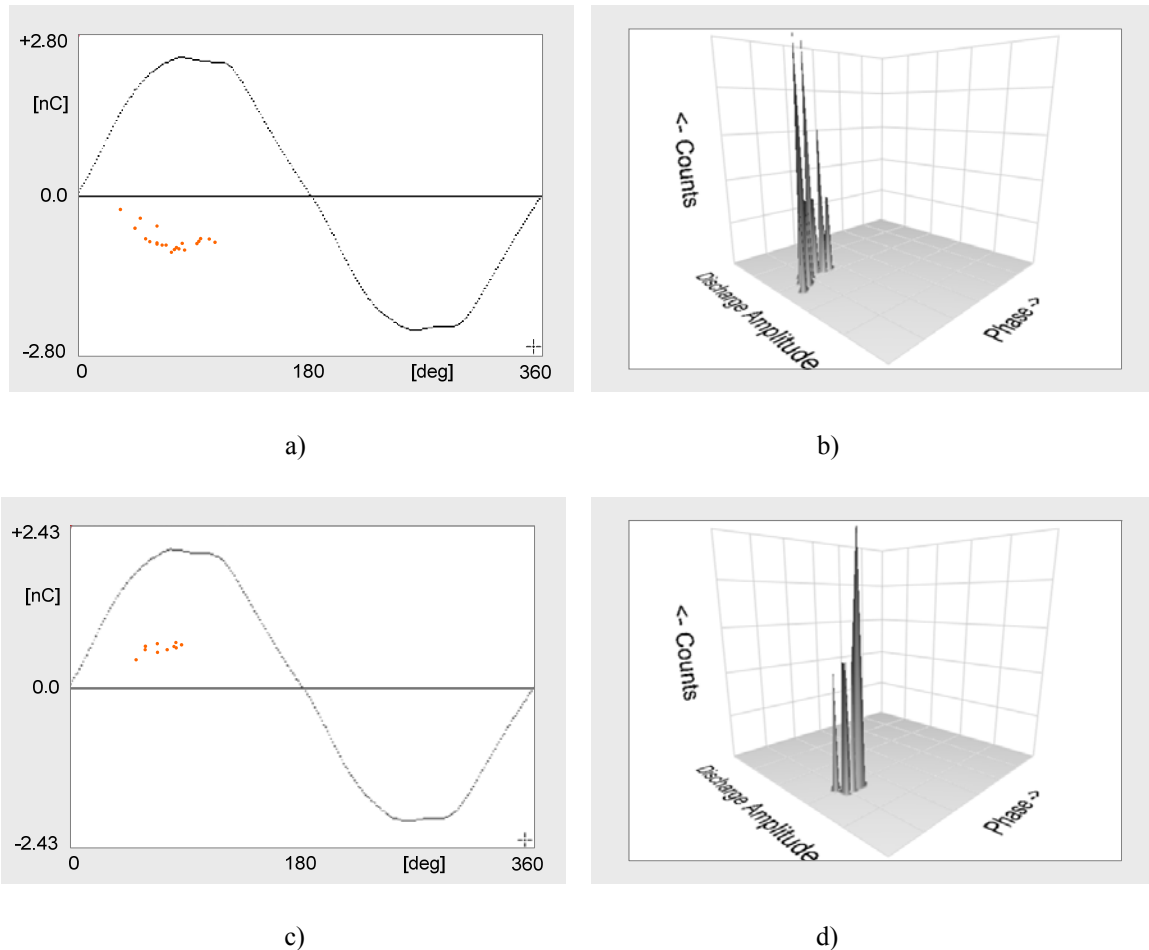


Figure 7.66: PD phase-resolved diagram recorded for 1 minute at PDIV level of different test circuits

- a) PD phase-resolved diagram from PDIV test circuit 1
- b) q-θ-n PD diagram from PDIV test circuit 1
- c) PD phase resolved diagram from PDIV test circuit 2
- d) q-θ-n PD diagram from PDIV test circuit 2

From the test results, four different test circuits provided the relatively similar PDIV values. However, the PDIV patterns were obviously different depending on the position of coupling device connected to the coupling capacitor or the test vessel. From the experiment, the PD signal detector such as the coupling device or the shunt resistor which directly connected to the test vessel provided the higher sensitivity to detect the PD signals. Comparing the PDIV value acquired from all test circuits, the PDIV value were nearly the same. Therefore, the researchers can do the experiment with the suitable PDIV test circuit for each purpose.

7.3 Breakdown voltage characteristic of the mineral oil

The occurring of breakdown events causes serious dangerous for the measuring equipment. This test topic dealt with the breakdown voltage of the needle- plane electrode system with the gap distance of 25 mm and 50 mm respectively. The tungsten needle electrodes with the tip radius of 10 μ m, 20 μ m, and 40 μ m respectively were used as the high voltage electrode while the brass plane electrode with a diameter of 75 mm as grounded electrode. The gap distance of the electrode system was set up at 25 mm and 50 mm respectively. The test voltage was applied to the electrode arrangement with a rate of 1 kV/s from zero until breakdown occurred. The test voltage was limited at 50 kV. Three needles of each identical tip radius needle were investigated. After that, the breakdown mean value of each electrode configuration was computed as shown in Table 7.22.

Table 7.22: Breakdown voltage compared with PDIV of the needle- plane electrode configurations

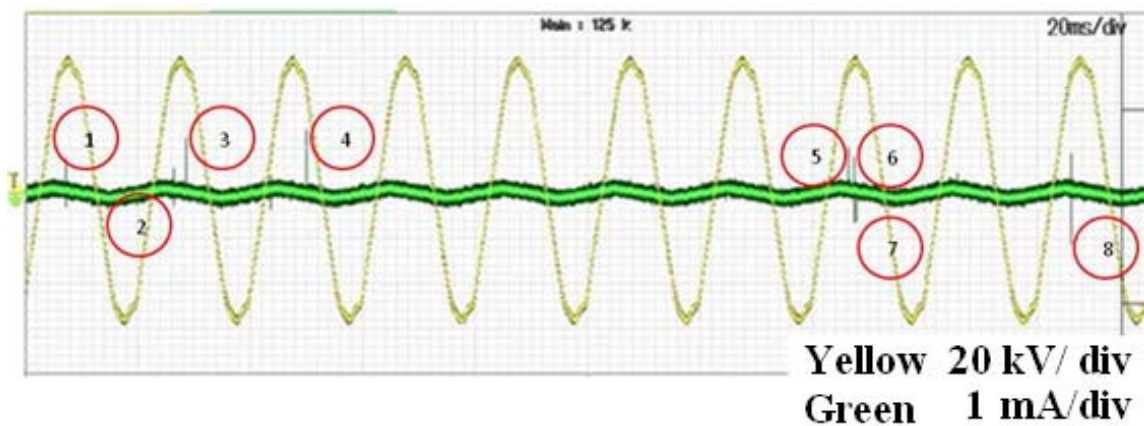
Needle tip radius	Gap 25 mm		Gap 50 mm	
	U_{PDIV} (kV)	U_{bd} (kV)	U_{PDIV} (kV)	U_{bd} (kV)
10 μ m	22.4	35.0	30.3	>50
20 μ m	>31	37.1	39.1	>50
40 μ m	>33	39.0	45.8	>50

From the test results, the breakdown voltage depended on the electrode configurations especially gap distance. With 25 mm gap distance, the PDIV zone was approaching the breakdown zone especially for the 20 μ m and 40 μ m tip radius needle-plane electrode configurations. From the PDIV values, the PD charges recorded for 1 minute and the first PD charges, the simple diagram used to explain PD and breakdown mechanism under PDIV test according to IEC 61294 was developed as described in the next chapter.

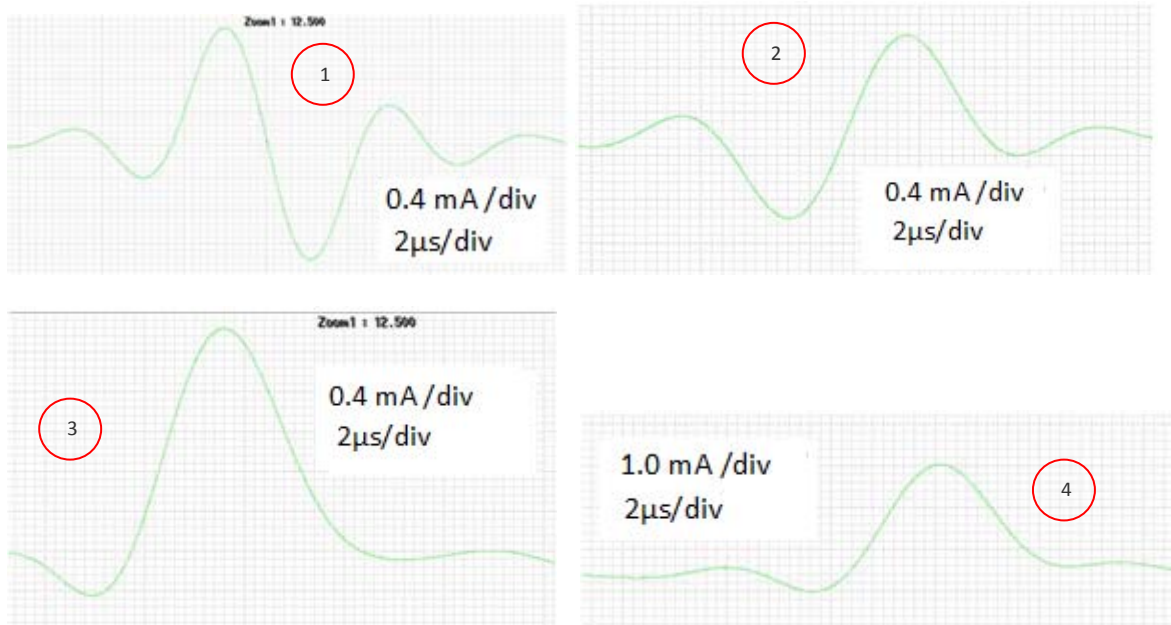
7.4 PD pulse current

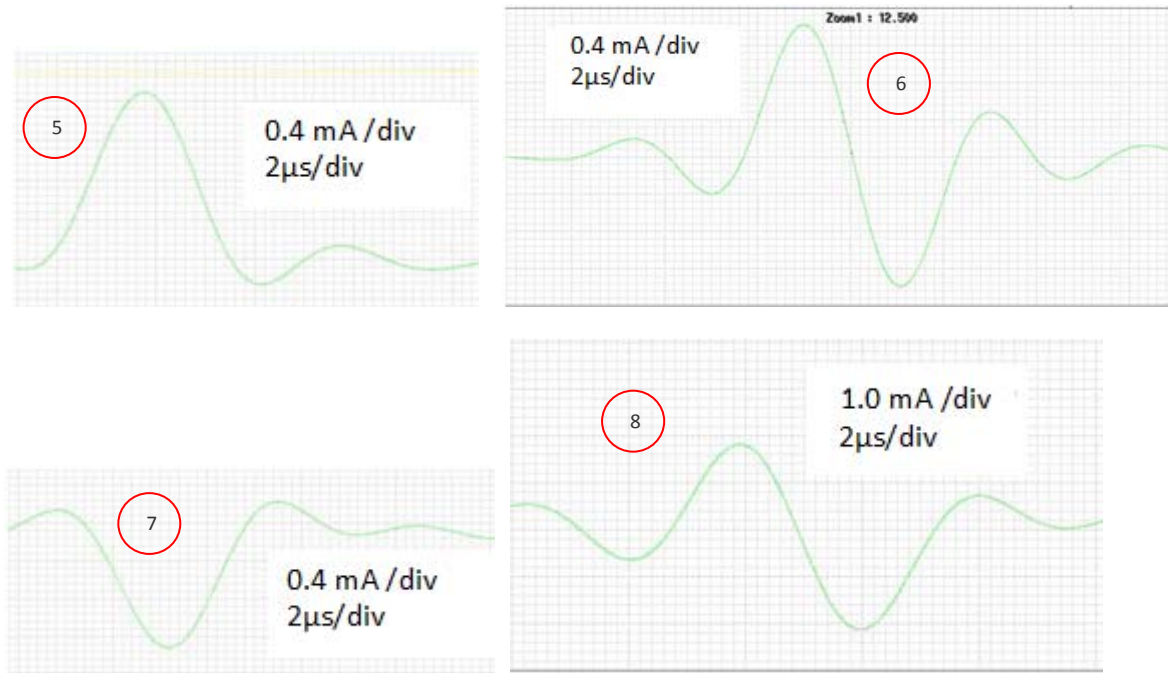
7.4.1 PD pulse train characteristics from preliminary PDIV test

PD pulse current behaviors were detected by the shunt resistor of 50 ohm at PDIV level. PD pulses normally took place near or at 90 degree of phase voltage. The patterns of PD pulse train obtained from different tip radius needle-plane electrode configurations were not different. The examples of PD pulse train and PD signals in the PD pulse train detected with the low effective bandwidth measurement for locating the PD positions at PDIV level tested by the 20 μm tip radius needle-plane arrangement are shown in Fig. 7.67.



a)





b)

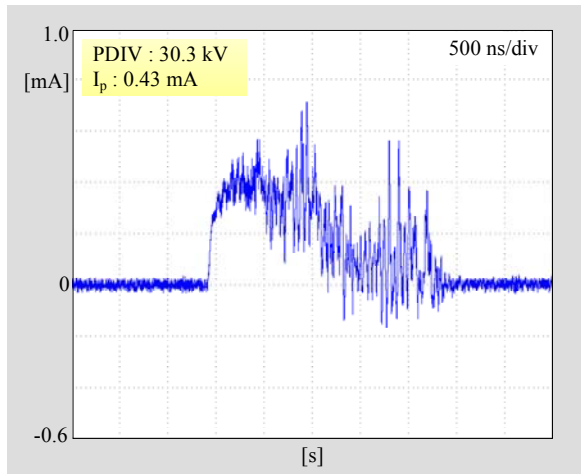
Figure 7.67: PD pulse train of the mineral oil tested by the needle-plane electrode arrangement, needle tip radius of 20 μm , N11, at PDIV of 37.9 kV in preliminary PDIV experiment

a) PD pulse train b) current pulse wave forms (low bandwidth measurement for locating PD position)

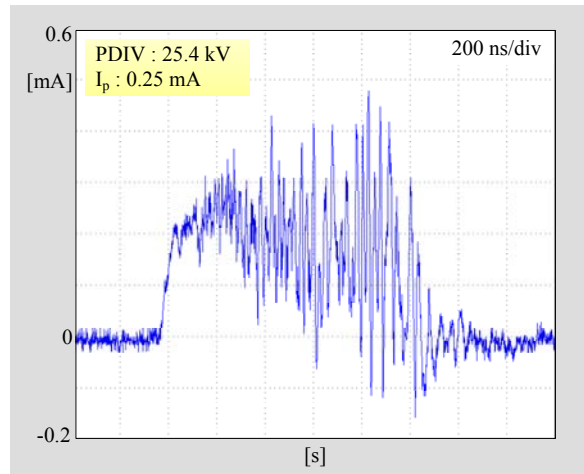
7.4.2 PD pulse characteristics

7.4.2.1 PD pulse currents from different grounded electrode experiments

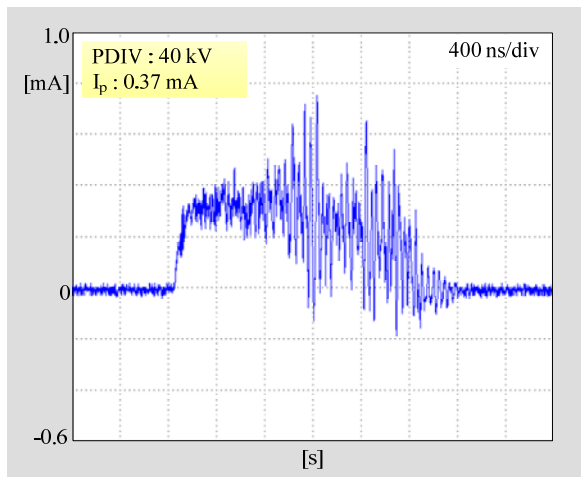
PD pulse currents of the mineral oil investigated by the needle-plane electrode and needle-sphere electrode were relatively the same patterns. The amplitude and time duration of the PD pulse current depended on the PDIV value as examples shown in Fig.7.68. Fig.7.69 represents the 10 PD pulse currents recorded continuously at the PDIV level. The PD pulse current characteristic, PD pulse amplitude, time duration and rise time tested by each electrode configuration are summarized and illustrated in Table 7.23 - 7.24 respectively.



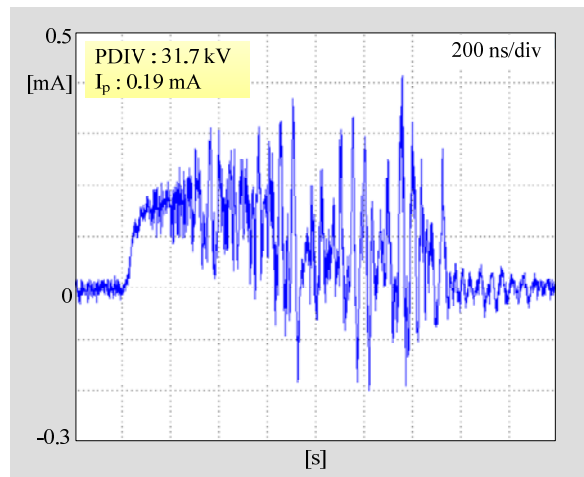
a)



b)



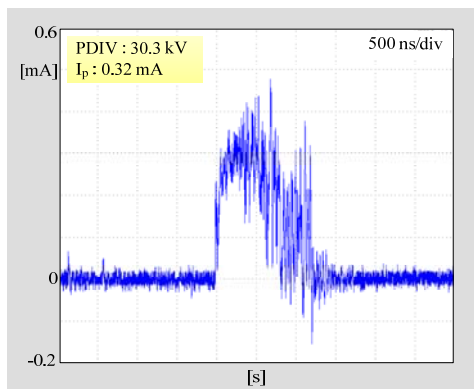
c)



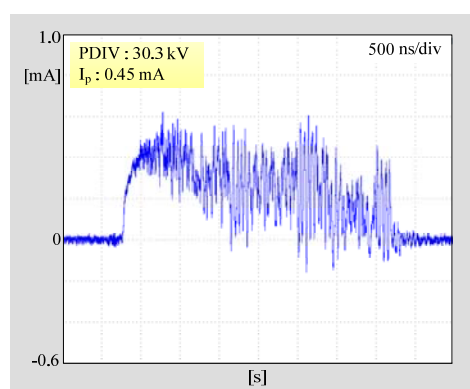
d)

Figure 7.68: PD pulse currents of the mineral oil tested by the 10 μm tip radius needle-75 mm diameter plane electrode and tested by the 10 μm tip radius needle-12.7 mm diameter sphere electrode, gap spacing of 50 mm at PDIV level obtained from

a) IEC method for the needle- plane electrode system b) combine PDIV test method for the needle-plane electrode system c) IEC method for the needle-sphere electrode system d) combine PDIV test method for the needle-sphere electrode system



a)



b)

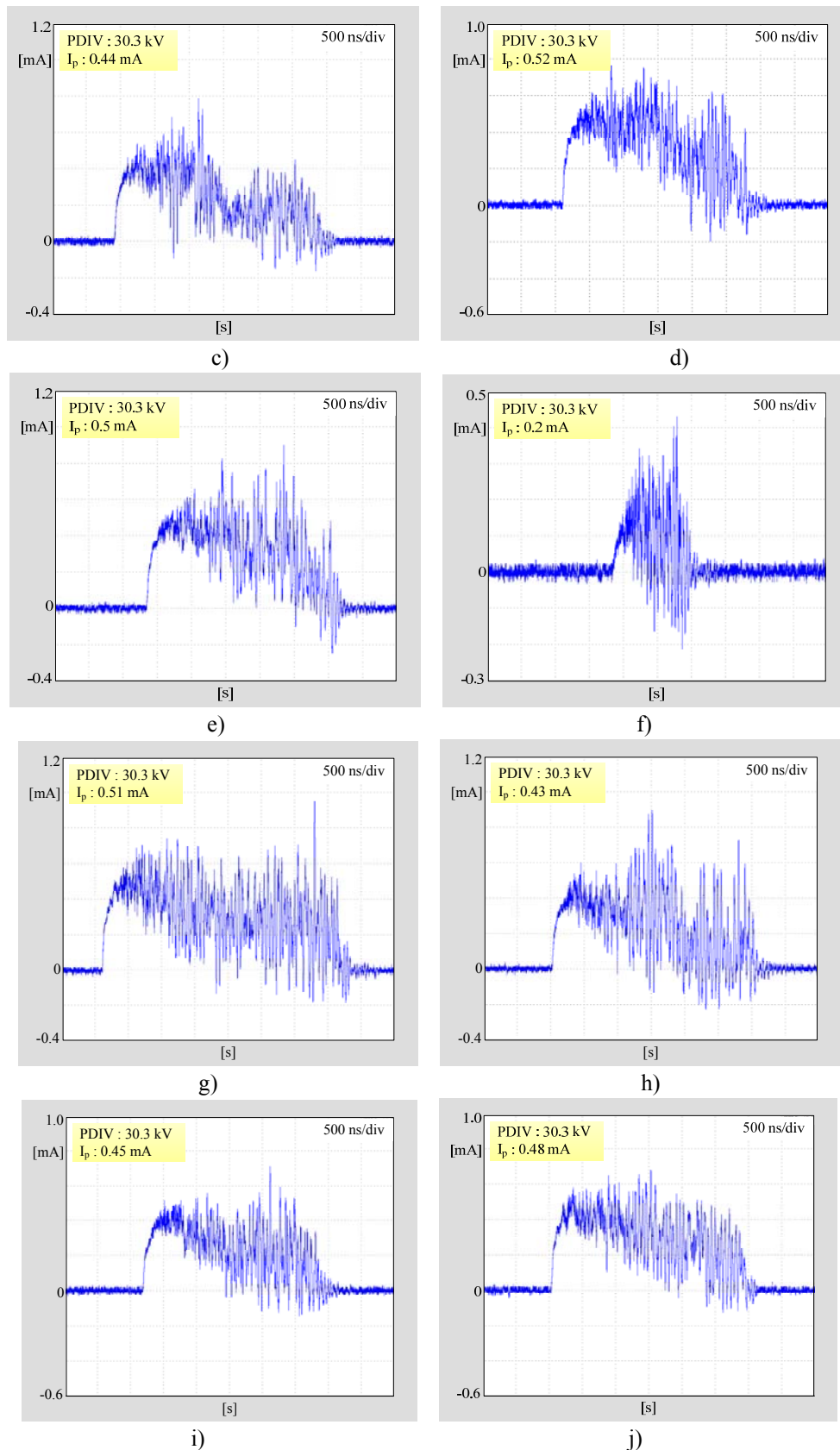


Figure 7.69: 10 PD pulse currents of the mineral oil tested by the $10\ \mu\text{m}$ tip radius needle -75 mm diameter plane electrode system with gap spacing of 50 mm recorded continuously at PDIV level

From the PD pulse current test results, PD pulse currents recorded from both test methods were about 0.2 - 1.3 mA. PD pulse time durations were in the range of 0.6- 9.3 μ s and the rise time were between 40 - 570 ns. The recorded pulse currents illustrated that some discharges might occur after the first discharge happened in the defect of the mineral oil. Normally, the PD pulses were similar in shape but different rise times and time durations which caused also different power and energy of PD pulses dissipated in the mineral oil.

Table 7.23: PD pulse characteristics (pulse current amplitude (mA), pulse duration (μ s) and rise time (ns)) tested by the needle-plane configuration with gap distances of 25 mm and 50 mm at the PDIV level obtained from IEC and the combine PDIV test methods

Parameter	Needle tip radius (μ m)	IEC method				Combine PDIV test method			
		Gap distance 25 mm		Gap distance 50 mm		Gap distance 25 mm		Gap distance 50 mm	
		Plane diameter (mm)		Plane diameter (mm)		Plane diameter (mm)		Plane diameter (mm)	
		50	75	50	75	50	75	50	75
Pulse current	10	0.34-0.69	0.36 -0.69	0.31-0.53	0.20-0.59	0.31-0.43	0.32-0.54	0.17-0.32	0.23-0.37
	20	NA	NA	0.46-0.68	0.61-0.98	0.23-0.61	0.46-0.59	0.32-0.44	0.24-0.51
	40	NA	NA	0.39-1.03	0.54-1.24	0.72-1.08	0.54-0.81	0.32-0.56	0.46-0.63
Pulse duration	10	1.47-3.87	1.04-2.5	1.39-3.69	1.40-3.69	1.51-2.43	0.89-2.03	1.08-2.26	1.07-1.91
	20	NA	NA	2.52-6.63	4.23-5.36	1.32-3.36	1.17-2.30	1.25-2.23	0.93-2.78
	40	NA	NA	2.39-9.30	3.11-9.25	2.64-8.8	1.24-4.65	1.85-3.75	1.90-3.25
Rise time	10	116-264	102 - 234	123 - 236	73-222	99-174	110-168	66-154	52-167
	20	NA	NA	107 - 366	155-315	67-210	93-168	131-188	86-173
	40	NA	NA	74 - 570	210-400	61-173	95-212	109-230	162-276

Table 7.24: PD pulse characteristics (pulse current (mA), pulse duration (μ s) and rise time (ns)) tested by the needle-sphere configurations with gap distances of 25 and 50 mm at the PDIV level obtained from IEC and the combine PDIV test methods

	Current parameter	Needle tip radius (μ m)	IEC method				Combine PDIV test method			
			Sphere diameter (mm)				Sphere diameter (mm)			
			12.7	25.4	50.8	76.2	12.7	25.4	50.8	76.2
Gap distance 25 mm	Pulse current	10	0.32-0.57	0.27-0.64	0.43-0.67	0.35 - 0.70	0.19-0.32	0.25-0.38	0.23-0.44	0.28 - 0.43
		20	NA	NA	NA	NA	0.22-0.51	0.26-0.62	0.35-0.61	0.31 - 0.59
		40	NA	NA	NA	NA	0.33-0.61	0.42-0.83	0.49-0.86	0.31 - 0.78
	Pulse duration	10	1.10-2.97	1.22-3.12	1.41-2.49	1.21 - 2.31	0.68-1.49	0.60-1.68	0.80-1.99	0.67 - 1.54
		20	NA	NA	NA	NA	1.77-2.78	1.16-2.77	1.0-2.45	0.77 - 2.16
		40	NA	NA	NA	NA	1.18-4.53	1.86-4.73	1.57-4.35	1.04 - 3.50
	Rise time	10	91-162	67-162	106 - 185	75 - 223	49 - 126	56 - 115	60 - 166	55 - 153
		20	NA	NA	NA	NA	75 -184	64 - 161	107-227	54 - 200
		40	NA	NA	NA	NA	69 - 216	74 - 257	98-268	68 - 230
Gap distance 50 mm	Pulse current	10	0.27-0.43	0.27-0.51	0.24-0.43	0.19 - 0.51	0.15-0.28	0.18-0.33	0.18-0.36	0.17 - 0.31
		20	NA	0.63 - 1.05	0.46 -0.96	0.38 - 0.97	0.28-0.43	0.35-0.48	0.17-0.47	0.28-0.45
		40	NA	NA	NA	NA	0.25-0.58	0.37-0.65	0.47-0.68	0.38 - 0.69
	Pulse duration	10	1.25-2.81	1.10 - 2.57	1.10-2.30	1.18 - 2.38	0.80-1.74	0.88-1.76	0.93-1.99	0.63 - 1.41
		20	NA	2.93 - 7.64	2.01-6.91	2.37 - 6.41	0.91-2.55	1.34-2.56	1.03-2.94	0.92 - 1.84
		40	NA	NA	NA	NA	1.90-3.62	1.59-5.65	2.62-3.98	1.4 - 4.11
	Rise time	10	61-226	74 - 208	62 - 136	65 - 232	40 - 187	76-167	58-162	47 - 141
		20	NA	49 - 279	86 - 334	61 - 371	45 - 286	78-211	54 - 240	79 - 226
		40	NA	NA	NA	NA	51-273	88-311	106 - 263	124 - 302

In case of different test circuit PDIV experiments, PD pulses obtained from the test circuit number 2 were the negative PD pulses as shown in Fig. 7.70.

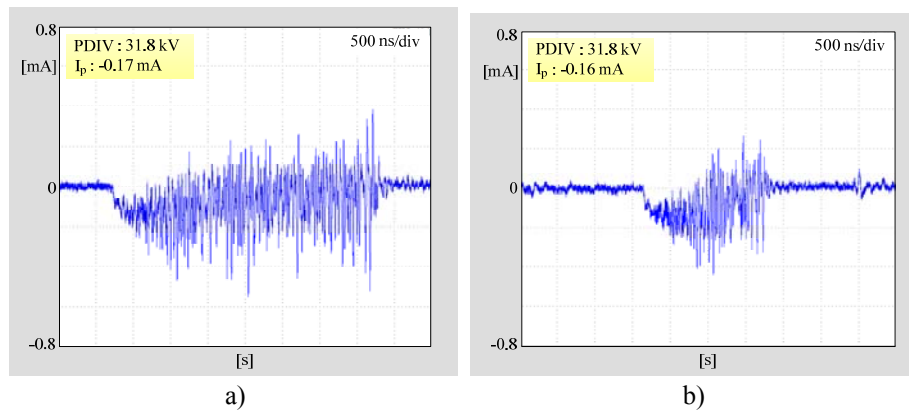


Figure 7.70: PD pulses recorded from test circuit 2 (R shunt connected with coupling capacitor)

7.4.2.2 PD pulse currents from different oil condition experiments

The examples of PD pulse currents at PDIV level under various water contents and oil temperatures are shown in Fig. 7.71 and Fig. 7.72 respectively. The PD pulse characteristics calculated from 10 PD pulses of each study case were represented in Table 7.25.

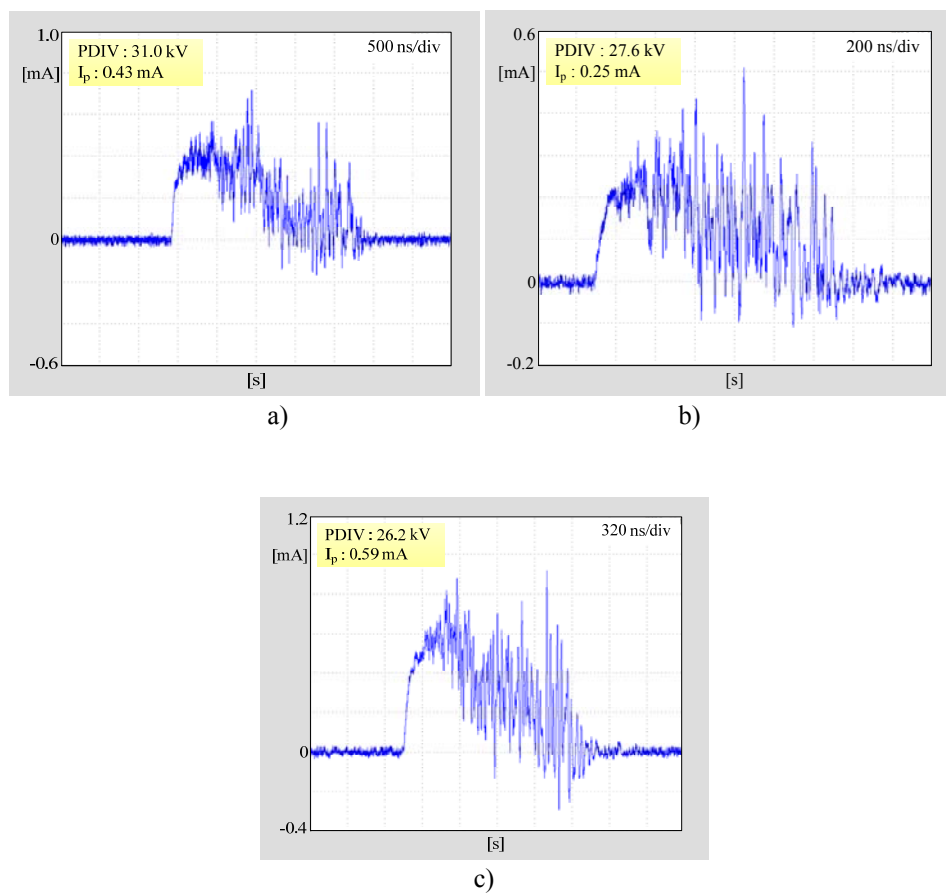


Figure 7.71: PD currents of the mineral oil under room temperature with different water contents at a) 4 ppm b) 20 ppm c) 40 ppm

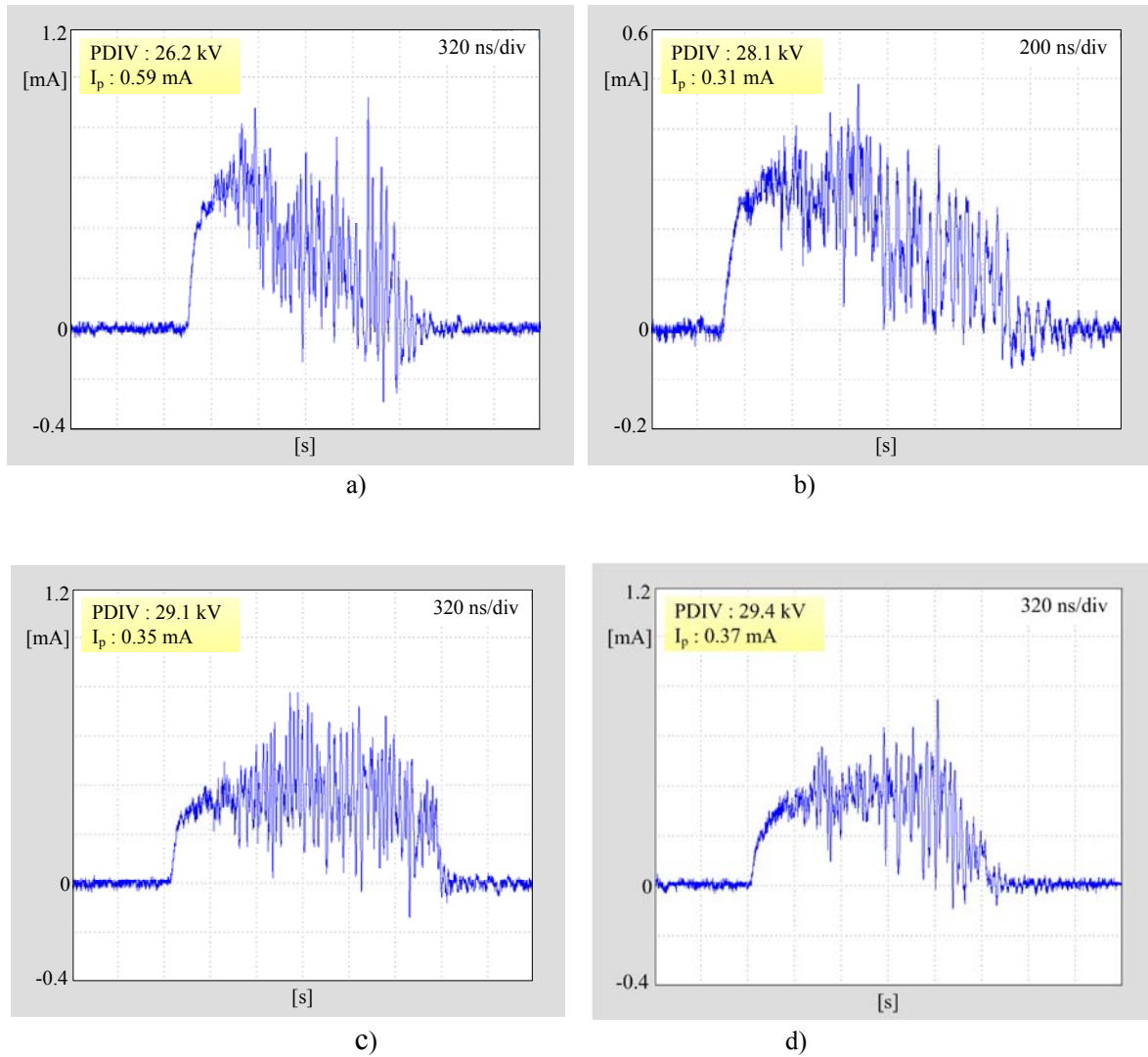


Figure 7.72: PD currents generated in the mineral oil with water content of 40 ppm with different temperatures at

a) at room temperature b) 40°C c) 60°C d) 90°C

Table 7.25: PD pulse characteristics of the mineral oil with different oil conditions

Parameter	Temperature (°C)	Water content		
		4 ppm	20 ppm	40 ppm
Pulse current	RT	0.29-0.61	0.22-0.43	0.22-0.59
	40	0.20-0.53	0.11-0.40	0.26-0.43
	60	0.26-0.52	0.12-0.50	0.28-0.40
	90	0.34-0.60	0.13-0.58	0.30-0.56
Pulse duration	RT	1.22-4.8	0.87-3.47	1.12-3.37
	40	1.23-3.81	0.67-3.00	1.14-3.51
	60	1.40-3.70	0.54-3.31	1.24-3.91
	90	1.57-4.42	0.89-3.42	1.26-3.63
Rise time	RT	91-281	75-298	86-273
	40	100-385	81-421	93-239
	60	97-612	185-512	84-370
	90	94-577	67-667	123-470

The PD pulse peak current was about 0.1 to 0.6 mA which had the rise time of 70 to 670 ns and time duration in the range of 0.5 to 4.8 μ s. The recorded pulse currents illustrated that some discharges might happen after the first discharge happened in the defects of the mineral oil. Furthermore, PD currents at PDIV level were randomly occurred with different rise time and time duration.

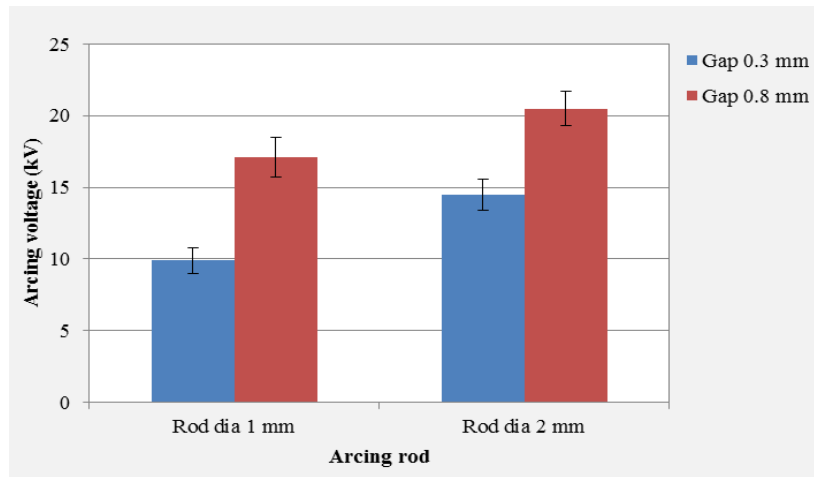
7.5 Preliminary arcing experiment

7.5.1 Arcing voltage and arcing current experiment

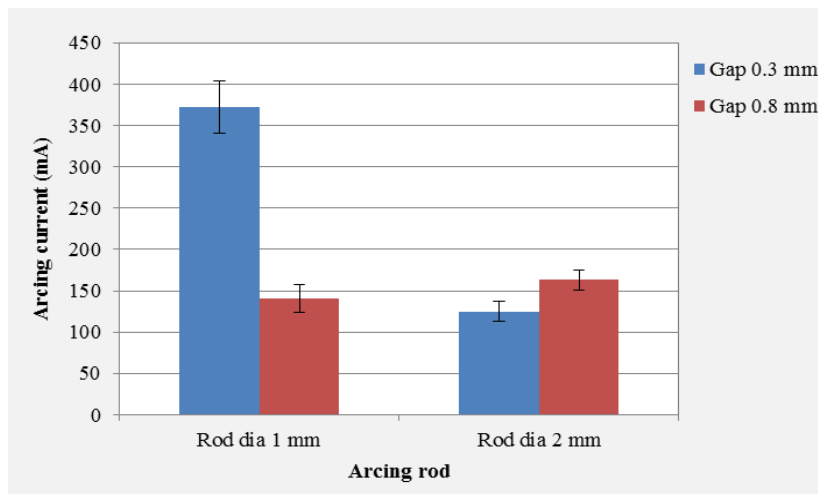
The purpose of this experiment was to study of the arcing phenomena of the mineral oil using a rod – plane electrode configuration. The experimental investigation of the arcing phenomena of the mineral oil, Nynas 4000x, with water content not more than 10 ppm under various tip diameters of the rod-plane electrode arrangements were performed. The tungsten rod electrodes with the tip diameter of 1mm, and 2mm with the curvature of 0.2 mm respectively were used as high voltage electrode, while the brass plane electrode of 75 mm diameter was used as the grounded electrode. The gap distance of the electrode system was set up at 0.3 mm and 0.8 mm respectively. The test experiment was modified from IEC 60156 and performed under room temperature as explained in chapter 6.4. The arcing current, the arcing voltage and the partial discharge pulse current before the arc occurred including the arcing current pulse signal were investigated. The mean value of the arcing voltage (U_{ARC}) and of the arcing current (I_{ARC}) of the mineral oil are illustrated in Table 7.26.

Table 7.26: Mean value U_{arc} and I_{arc} of the mineral oil tested by the rod-plane arrangements, σ_U as voltage standard deviation and σ_I as current standard deviation

Rod diameter (mm)	Gap distance (mm)	Arcing parameters				
		U_{ARC} (kV)	σ_U (kV)	I_{ARC} (mA)	σ_I (mA)	J_{ARC} (A/cm ²)
1	0.3	9.9	0.9	372	32	47.4
	0.8	17.1	1.4	141	17	17.9
2	0.3	14.5	0.9	125	19	3.9
	0.8	20.5	1.2	163	12	5.2



a)

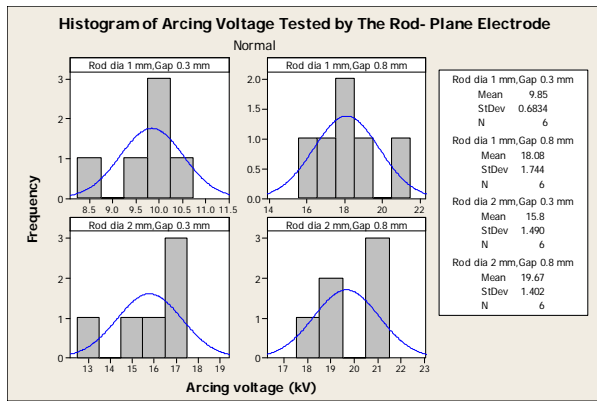


b)

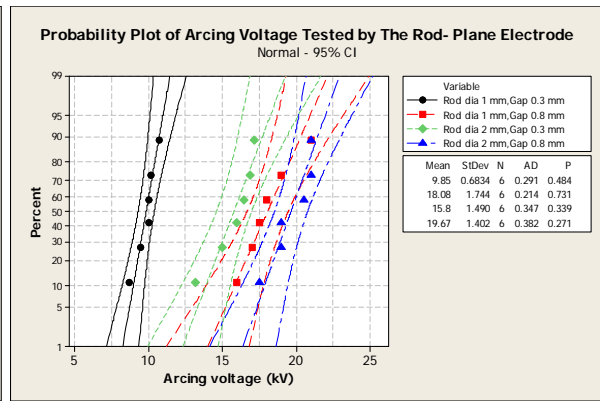
Figure 7.73: Arcing voltage and current from the arcing experiments

a) mean value of arcing voltages from various electrode configurations b) mean value of arcing currents from various electrode configurations

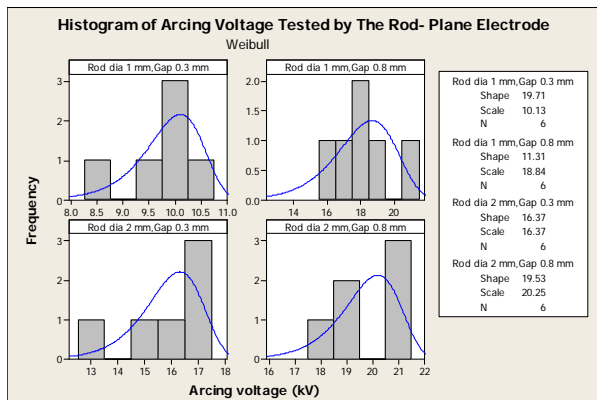
The distribution examples of the arcing voltages and arcing current test results (raw data from rod number 1 of each electrode configuration) were modelled with normal and weibull distributions as shown in Fig. 7.74- Fig. 7.75 respectively.



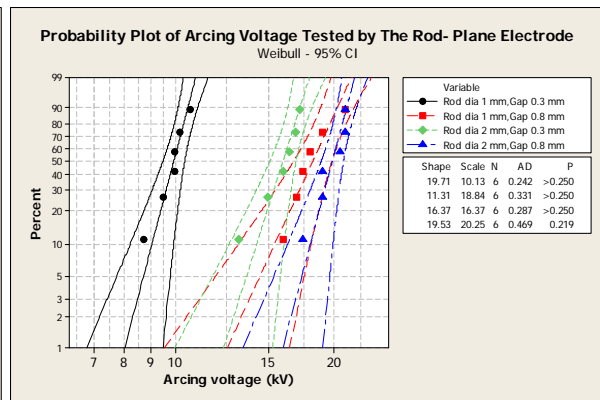
a)



b)



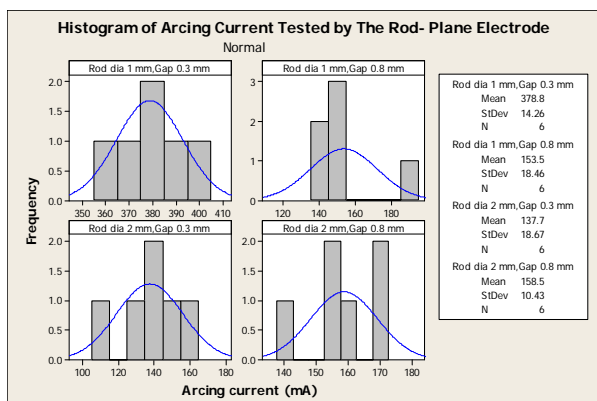
c)



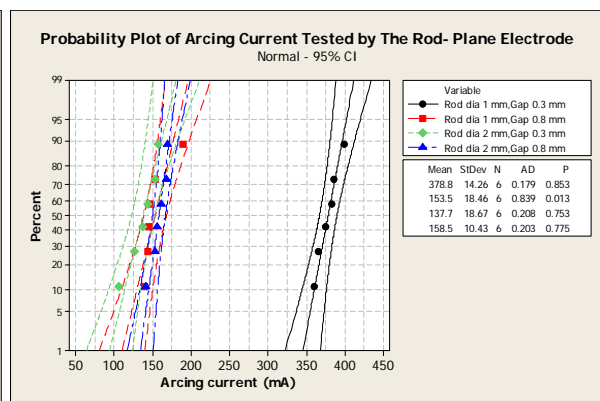
d)

Figure 7.74: Normal and weibull distribution of arcing voltages

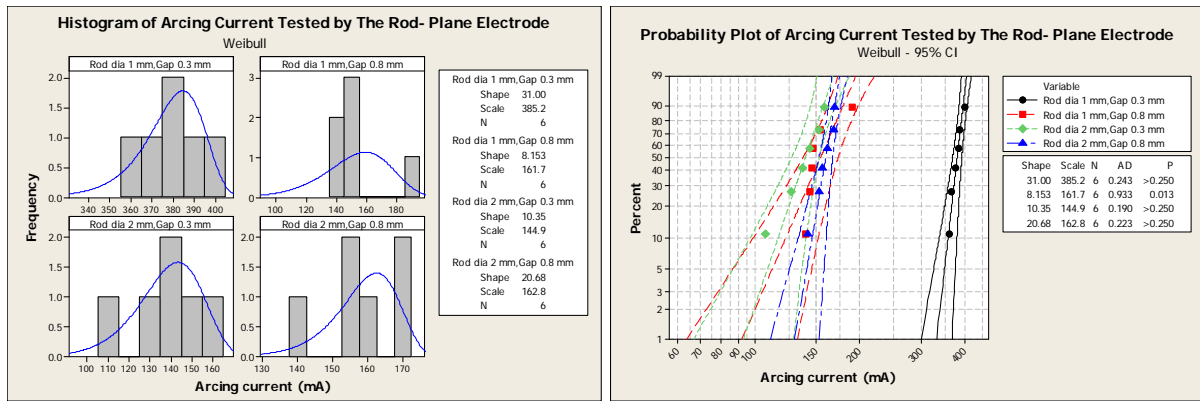
a) histogram with normal distribution plot b) probability plot of normal distribution c) histogram with weibull distribution plot d) probability plot of weibull distribution



a)



b)



c) d)

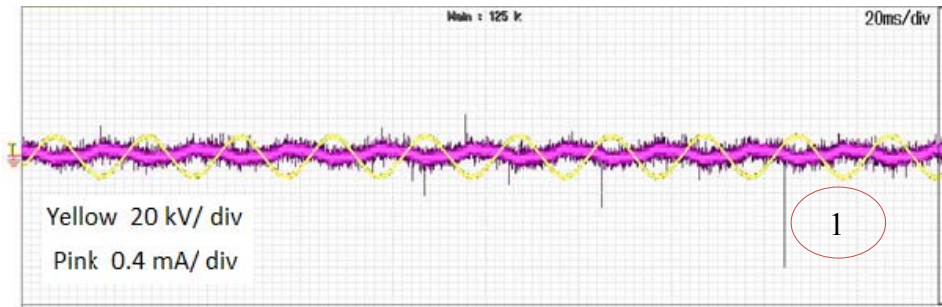
Figure 7.75: Normal and weibull distribution of arcing currents

a) histogram with normal distribution plot b) probability plot of normal distribution c) histogram with weibull distribution plot d) probability plot of weibull distribution

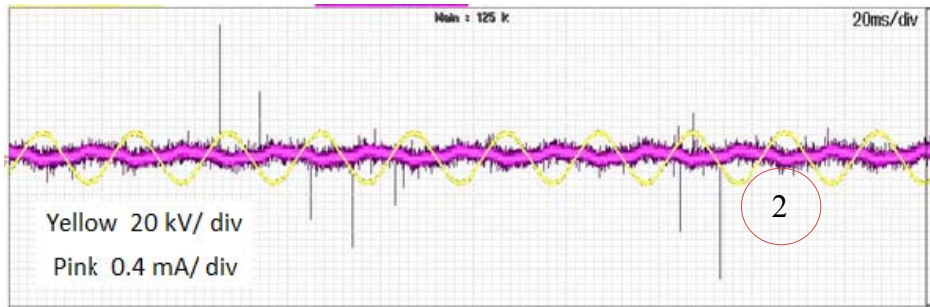
7.5.2 Arcing current pulse train

PD pulse current and arcing pulse current behaviours were detected by the shunt resistor of 50 ohm. The patterns of PD pulse currents of the rod-plane arrangement with gap distance of 0.3 and 0.8 mm were relatively similar. Fig. 7.76 demonstrates the pattern example of PD pulse currents of the rod-plane arrangement with gap distance of 0.3 mm which were recorded from the first stage of PD occurring until a complete arc occurred. The arcing pulse signals is depicted in Fig.7.77. The general development process of PD until the occurrence of arc is as following:

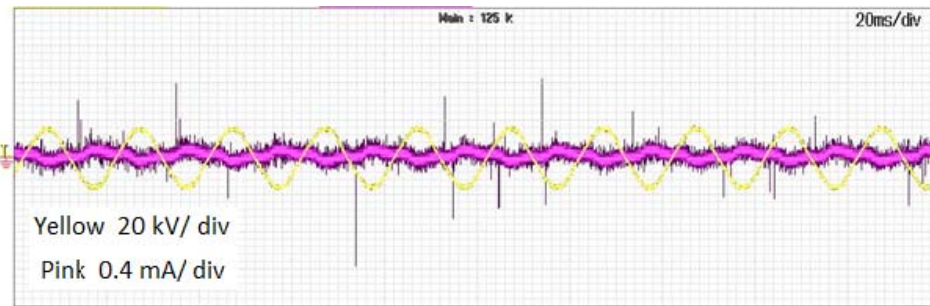
1. The first stage of PD, at this stage PDIV may be detected,
2. PD amplitudes are growing,
3. PD amplitudes and a PD repetition rate are still growing,
4. PD amplitudes and the PD repetition rate are still more and more growing,
5. PD amplitudes and the PD repetition rate a little bit change until completely arcing occurs.



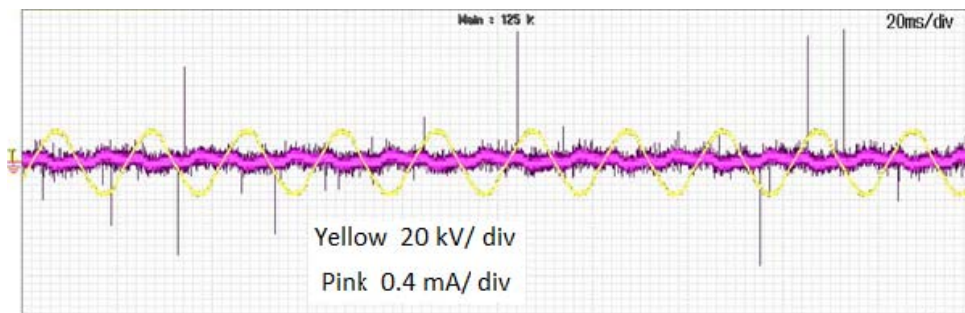
a)



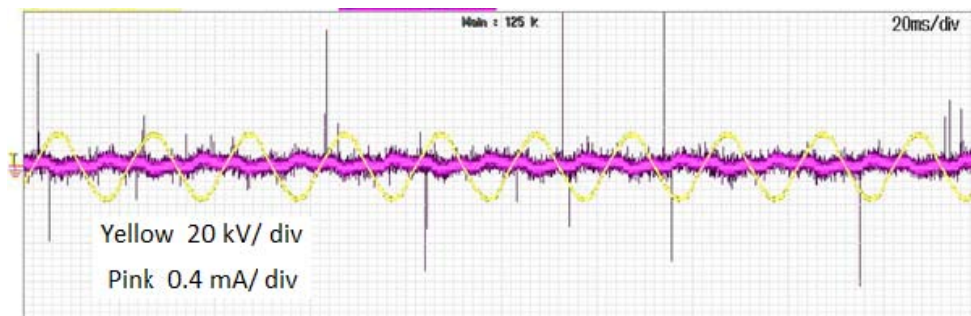
b)



c)



d)



e)

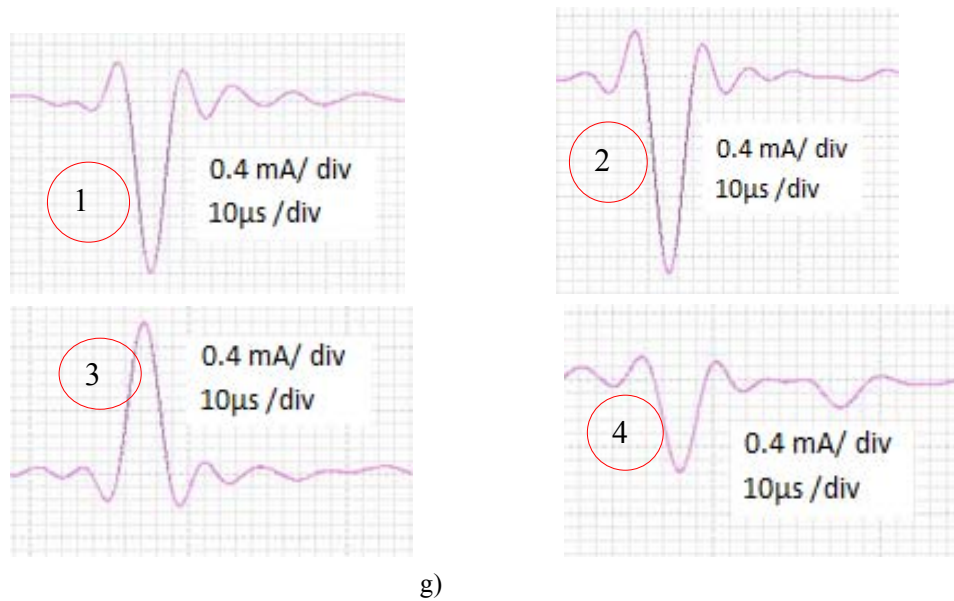
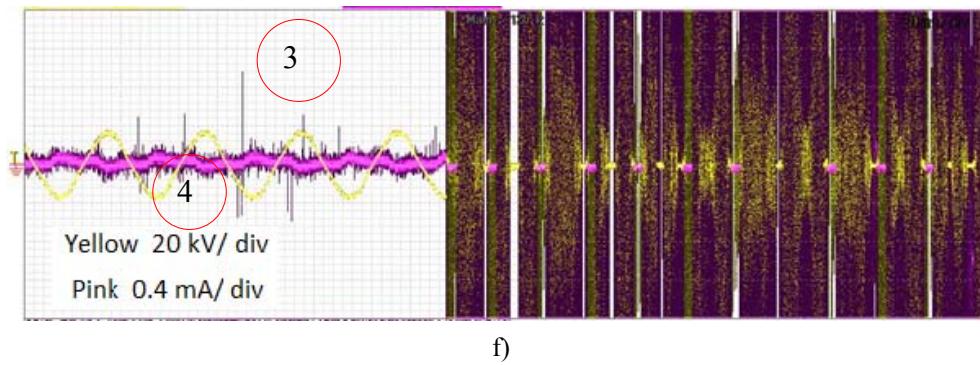


Figure 7.76: PD pulse current behaviors before arcing taking place tested by the rod-plane electrode arrangement, rod diameter of 1mm with gap distance of 0.3 mm, at 11.5 kV, voltage signal: yellow line and current signal: pink line

a) the first stage of PD b) growing of PD amplitudes c) - e) much more growing of PD amplitudes and the PD repetition rates f) PD amplitudes and the PD repetition rates changing a little bit before occurring of the completely arcing g) examples of PD pulse currents before the occurrence of a complete arc at different positions in a)- f) process



a)



b)

Figure 7.77: Arcing current patterns and signals tested by the rod- plane electrode arrangement, rod diameter of 1mm with gap distance of 0.3 mm at 11 kV

a) Arcing current pulse train b) examples of arcing pulse currents

7.5.3 Physical appearance of the mineral oil after arcing test

The occurrence of arcing caused many effects on degradation of the mineral oil and the electrode system. More bubbles including carbon filaments which were generated by arcing might cause the successive breakdown lower. After arcing process was stopped, most bubbles dissolved in the mineral oil, some bubbles moved to stay under or near the supporting electrodes or at top surface of the mineral oil as shown in Fig. 7.78. The carbon filaments formed around the high voltage supporting electrode as well. The carbon filaments and carbon particles caused the degradation of the mineral oil and also caused the change of the mineral oil color. The examples of the forming of carbon filaments forming around the high voltage supporting electrode and the color of the mineral oil after testing are illustrated in Fig.7.79.

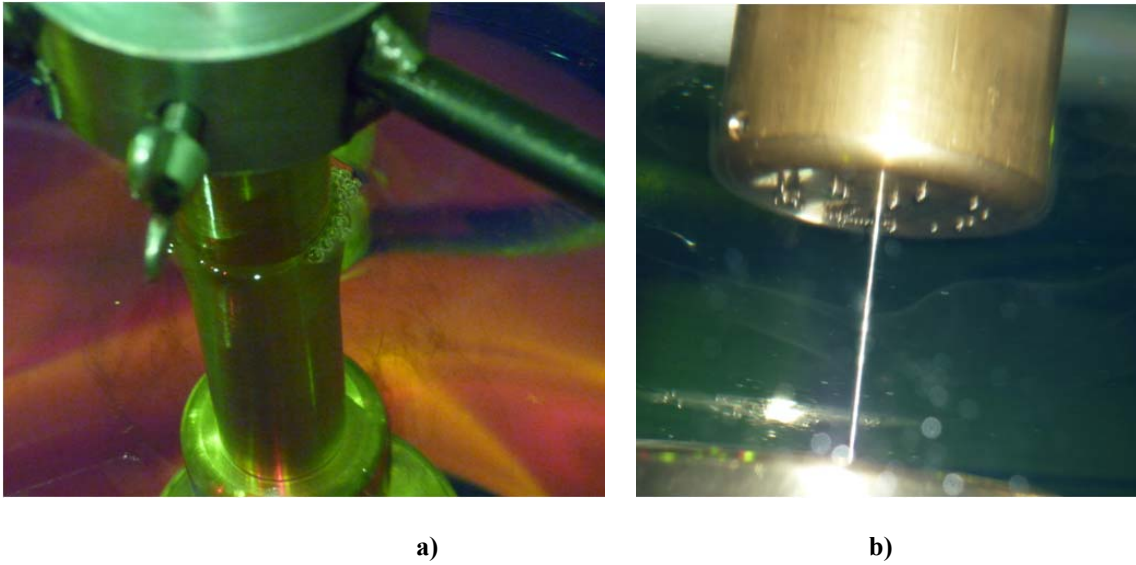


Figure 7.78: Bubbles generated by arcing

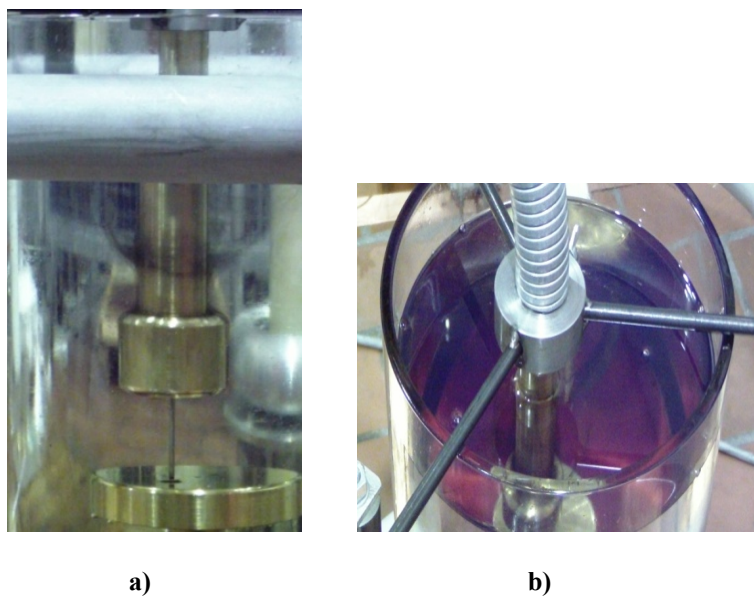


Figure 7.79: Carbon filaments and bubbles generated from the arcing test

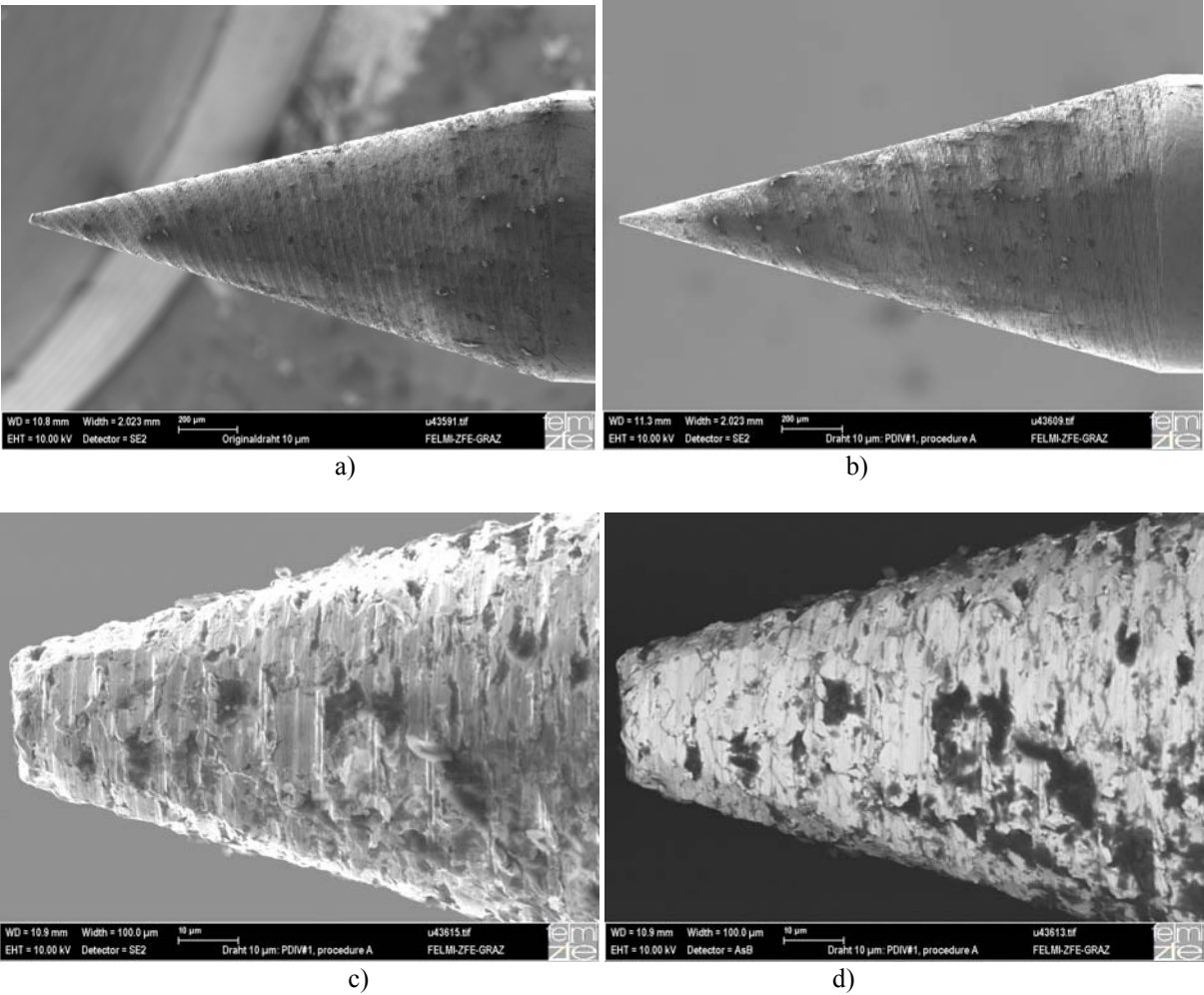
a) carbon filaments setting around the high voltage supporting rod b) bubbles and the color of oil after arcing test

From the experimental test results, the arcing voltage clearly depended on the gap distance. The average arcing voltages tested by the rods with diameter of 1 mm and 2 mm with the curvature of 0.2 mm at both gap distances of 0.3 mm and 0.8 mm were not much different. The average arcing voltage tested by the 2 mm diameter rod was higher than that of the 1 mm diameter rod. In addition, the PD pulse signals and the arcing pulse current signals were relatively similar in shape detected by the low effective bandwidth setting oscilloscope. Moreover, the significant degradation of the mineral oil, such as the oil color appearance, generated bubbles and other particles in oil, could be vividly observed after the arcing test.

7.6 SEM and EDX experiment

7.6.1 SEM and EDX analysis for PDIV electrode systems

SEM and EDX test results of the needles with the tip radius of 10 μ m, 20 μ m, and 40 μ m before and after they were used for PDIV testing of the mineral oil (preliminary PDIV experiment), were relatively similar. The examples of the 10 μ m tip radius needle topography obtained from SE images and the needle morphology acquired from BSE images are illustrated in Fig.7.80.



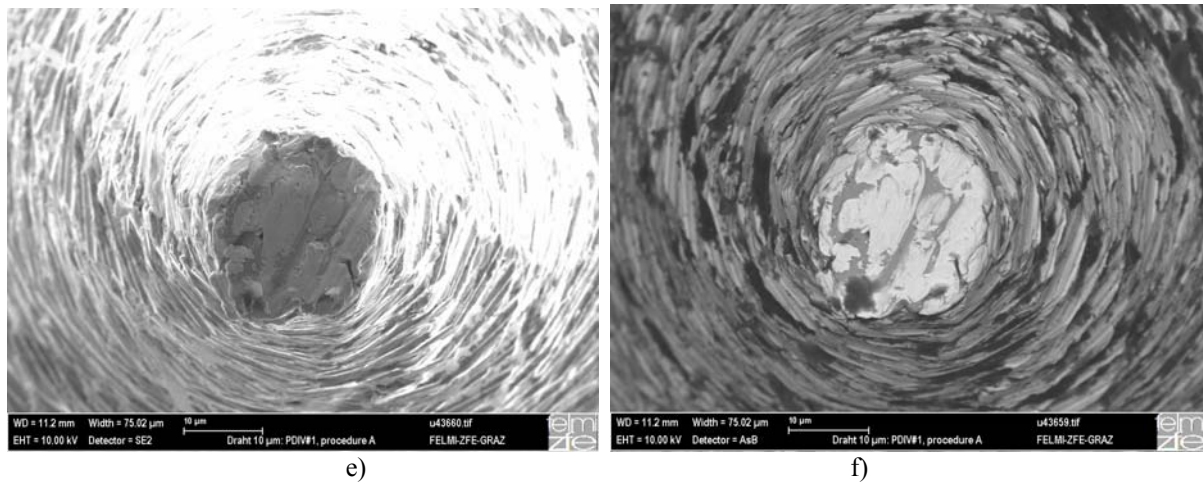


Figure 7.80: SE and BSE images of the 10 μm tip radius needle

- a) SE image: longitudinal view original needle b) SE image: longitudinal view PDIV tested needle
 c) SE image: large scale of PDIV tested needle d) BSE image: large scale of PDIV tested needle
 e) SE image: cross view of PDIV tested needle f) BSE image: cross view of PDIV tested needle

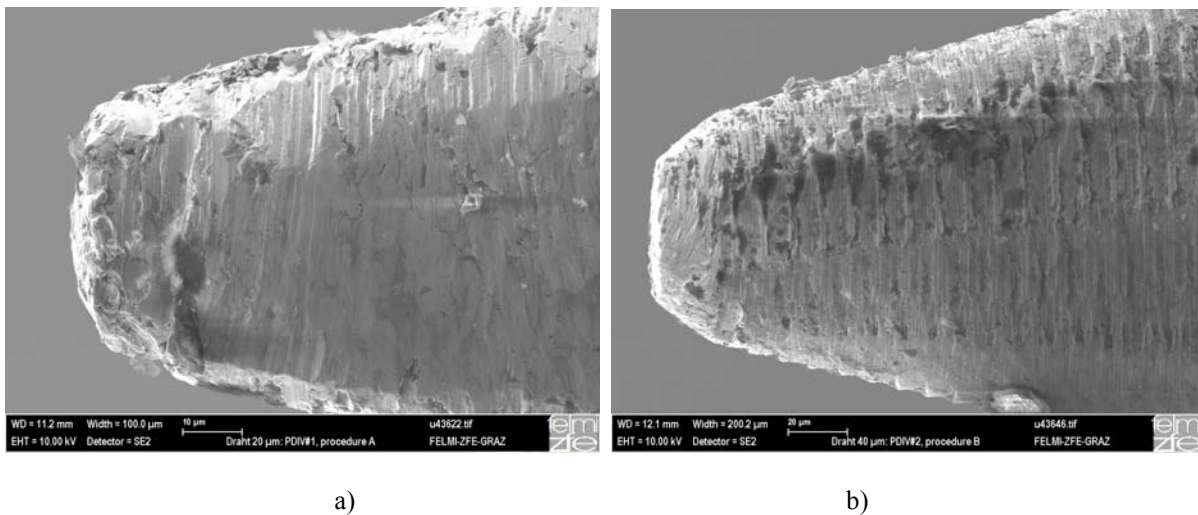
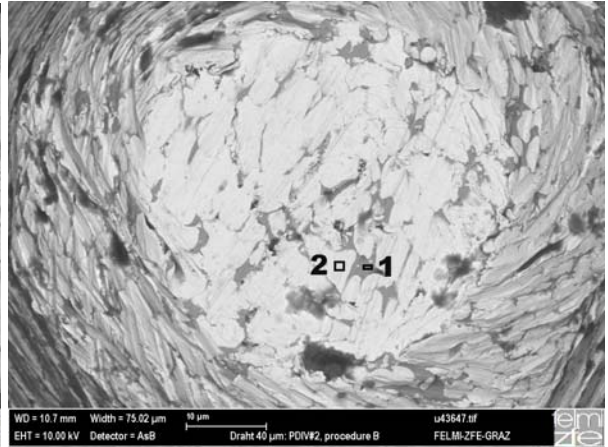
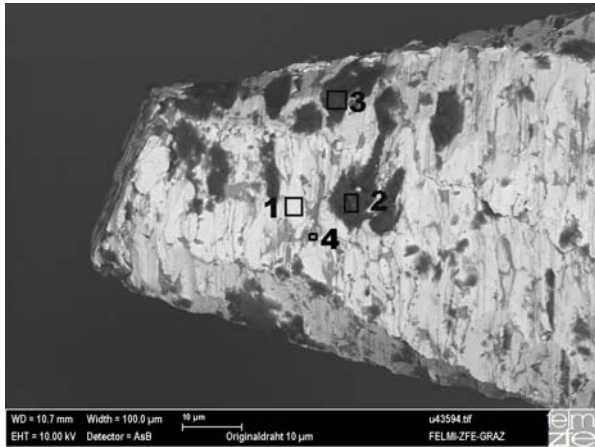


Figure 7.81: SE images: large scale of the PDIV tested needles

- a) the 20 μm tip radius needle b) the 40 μm tip radius needle

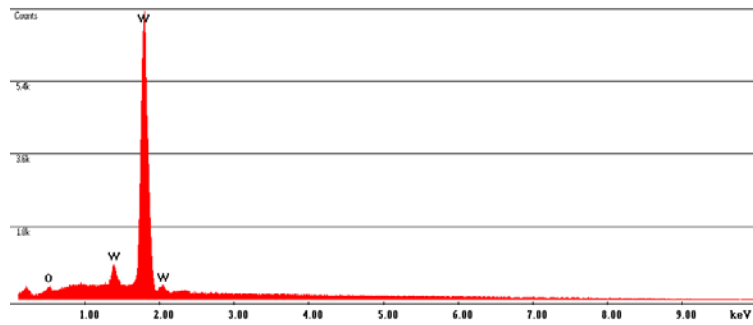
BSE images revealed that both original and PDIV tested needles comprised of at least 2 types of material. To analyze the composition elements, the EDX examination was conducted. EDX spectra generated by the areas near and at the tip of the original needles revealed that tungsten was the major element and carbon was the minor element. The examples of EDX analysis at the tip of the 10 μm tip radius needle is shown in Fig. 7.82. Furthermore, oxygen, sometimes with high count rate, copper, calcium and aluminum were found, as well as silicon and magnesium.



a)

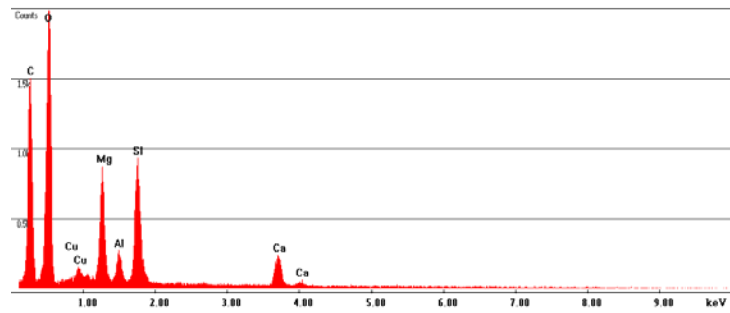
b)

Label A: ux4864: Originaldraht 10microns, u43594 1, 10kV



c)

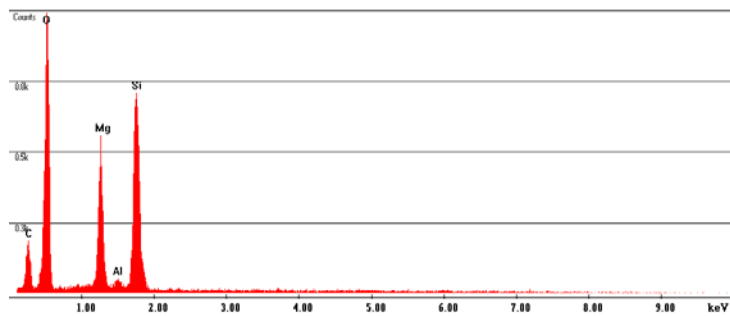
Label A: ux4865: Originaldraht 10microns, u43594 2, 10kV



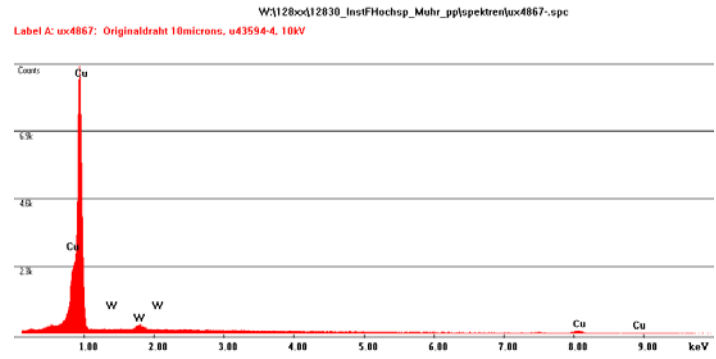
d)

W:\128\ox\12830_InstfHochsp_Muhr_pp\spektr\ux4866.spc

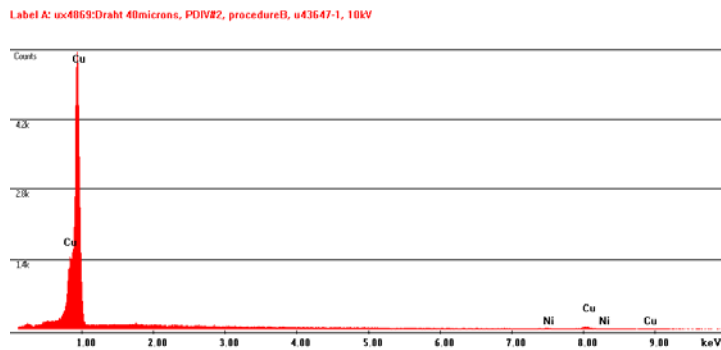
Label A: ux4866: Originaldraht 10microns, u43594 3, 10kV



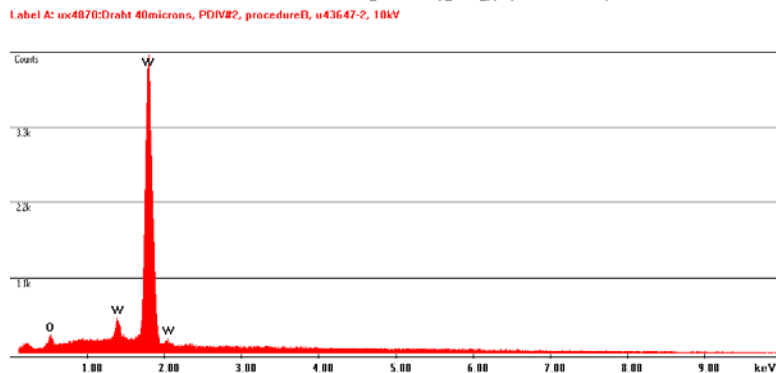
e)



f)



g)

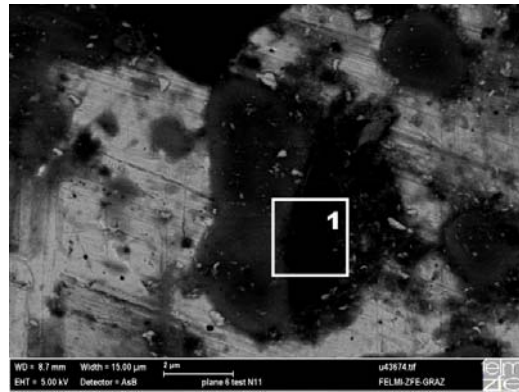


h)

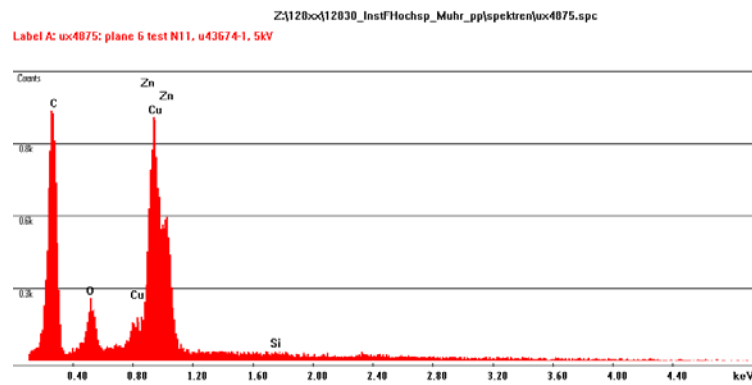
Figure 7.82: BSE images with interested areas and EDX analysis

a) 10 μm tip radius original needle, b) 40 μm PDIV tested needle c) EDX analysis of the interested area 1 of (a) d) EDX analysis of the interested area 2 of (a) e) EDX analysis of the interested area 3 of (a) f) EDX analysis of the interested area 4 of (a) g) EDX analysis of the interested area 1 of (b) h) EDX analysis of the interested area 2 of (b)

SEM and EDX techniques were employed for analysis the plane electrodes as well. The main component of the original plane electrode was copper and zinc. For the PDIV tested plane electrodes, the surface morphology was a bit changed. Carbon, copper and zinc were found with high count rate. Whilst, oxygen was also found with low count rate. However, there was no evidence to show that any part of the tested plane electrodes melted or eroded. Fig. 7.83 represents the BSE image of the PDIV tested plane electrode after 10 time PDIV testing was performed with the 20 μm tip radius needle at 36 kV PDIV level.



a)



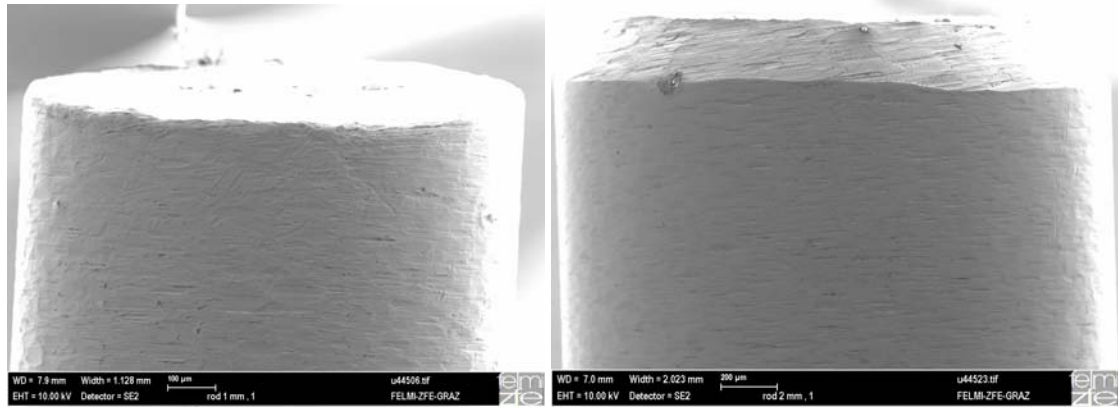
b)

Figure 7.83: SEM and EDX analysis for the tested plane electrode

a) BSE image of the PDIV tested plane electrode after 10 time tests with the 20µm tip radius needle at 36 kV PDIV level (preliminary PDIV experiment) b) EDX-analysis of the interested area 1

7.6.2 SEM and EDX analysis for arcing electrode systems

The SE images and BSE images of the original rods (1 mm dia. and 2 mm dia rod) and the arcing tested rods with the dia.of 1 mm, gap spacing of 0.8 mm, arcing current 132.9 mA, arcing current density 16.93 A/cm² and for gap spacing of 0.3 mm, arcing current 389 mA, arcing current density 49.53 A/cm² are illustrated in Fig. 7.84 and Fig. 7.85 respectively.

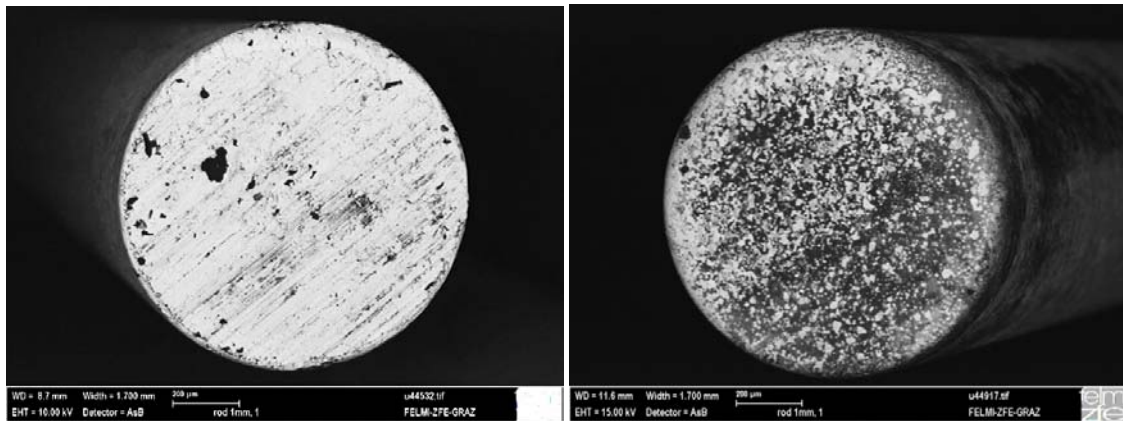


a)

b)

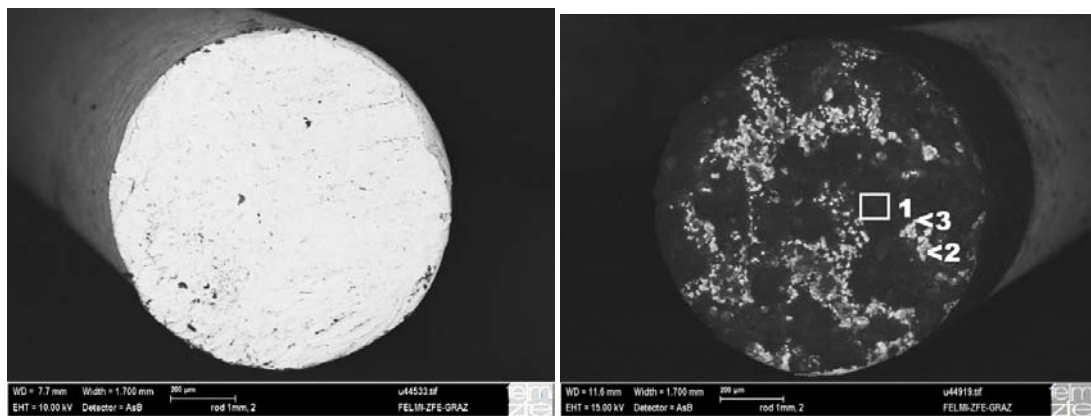
Figure 7.84: SE images of the original rods

a) the 1 mm diameter rod b) the 2 mm diameter rod with the curvature of 0.2 mm



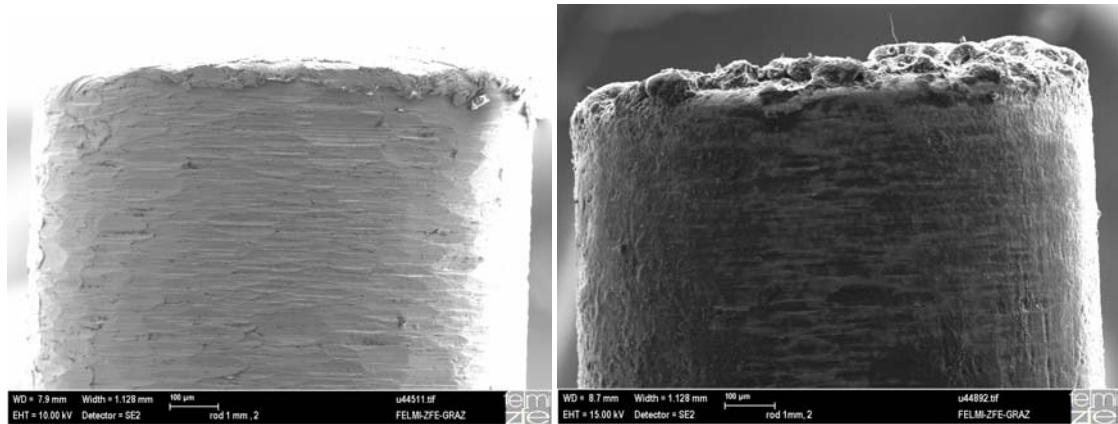
a)

b)



c)

d)



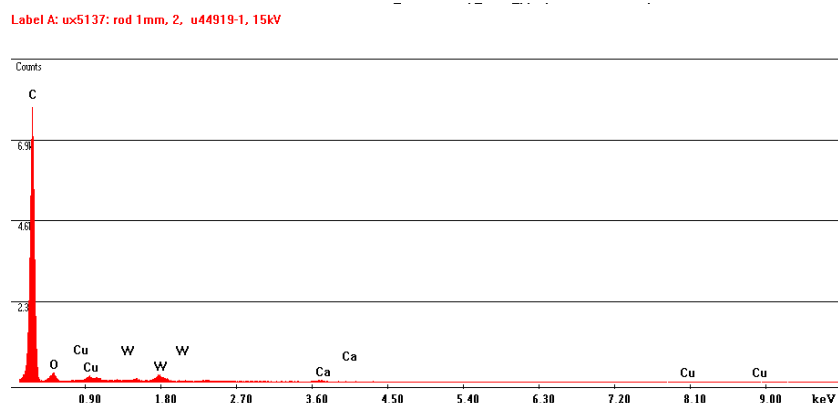
e)

f)

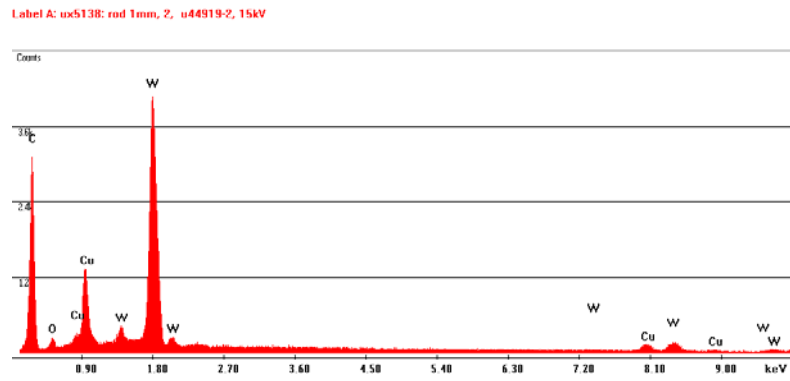
Figure 7.85: BSE image and SE image comparison of the 1 mm diameter rod before and after arcing test with different current densities

a) - b) BSE image and SE image of the rod tested with current density of 16.93 A/cm^2 before and after arcing test c) - f) BSE images and SE images of the rod tested with current density of 49.53 A/cm^2 before and after arcing test

From BSE images, they revealed distinctly that some compositions occurred after the rods were used for arcing test especially at the tip of the rods. The composition density depended on the current density of testing. It was also found that some compositions collected at the lateral surface of the rod with diameter of 1 mm. The topography at the tip of the tested rods illustrated in Fig. 7.85 f) was clearly changed because it was covered by the carbon layer generated from arcing phenomena as represented in EDX analysis in Fig. 7.86. However, for the most arcing rods, there was not much changing in topography before and after they were used for experiment. Fig. 7.86 represents also EDX analysis of other composition elements at the rod tip surface. There is also no evidence to show that any part of the rod melted, tortured or eroded.



a)

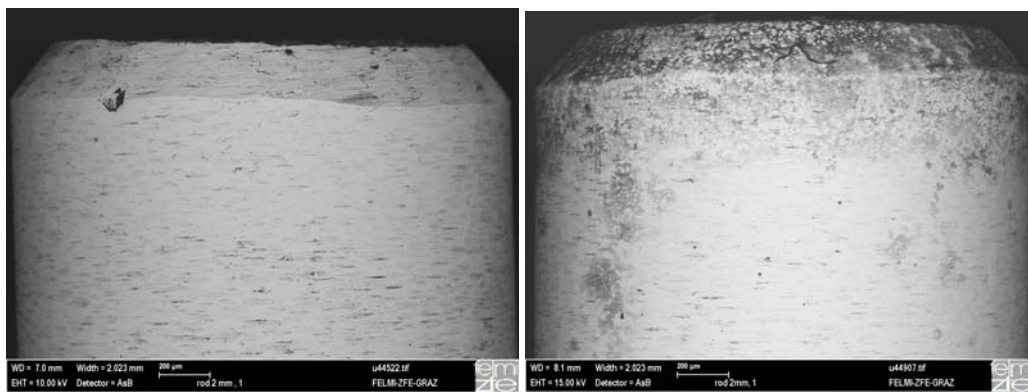


b)

Figure 7.86: EDX analysis of the interested areas of Fig. 7.85

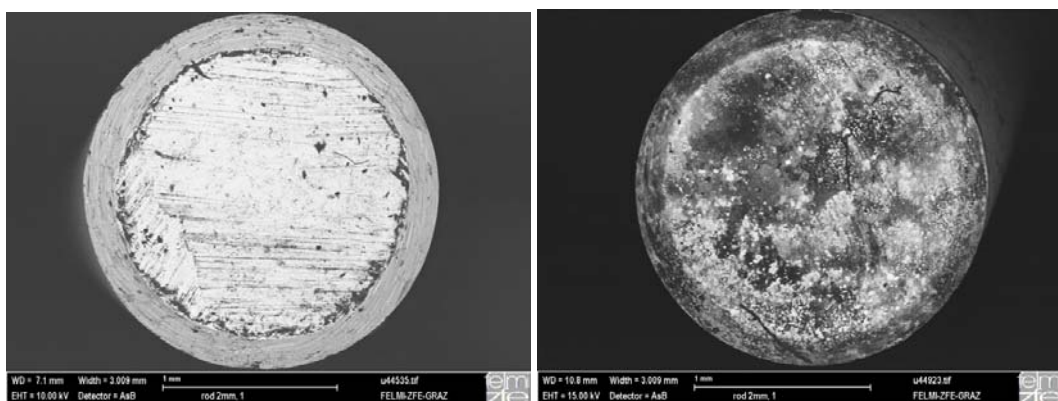
a) area 1 b) area 2

SEM and EDX analysis were utilized to analyze the 2 mm dia arcing rod as shown in Fig. 7.87. The arcing plane electrodes were also analyzed with SEM and EDX techniques, the test results are delineated in Fig. 7.88- Fig. 7.89 respectively.



a)

b)

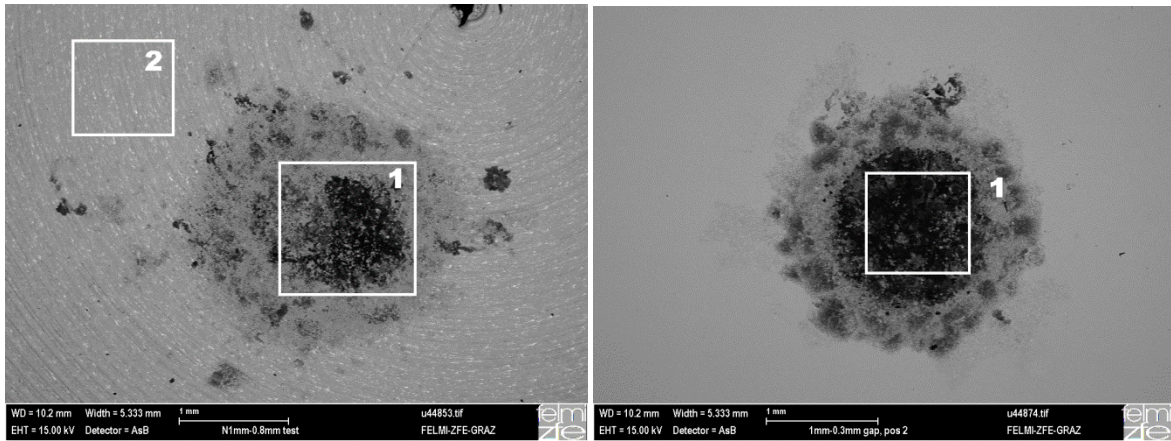


c)

d)

Figure 7.87: BSE image comparison of the 2 mm dia rod with the curvature of 0.2 mm before and after arcing test

a) original rod b) arcing tested rod: longitudinal view c) original rod d) arcing tested rod: cross view



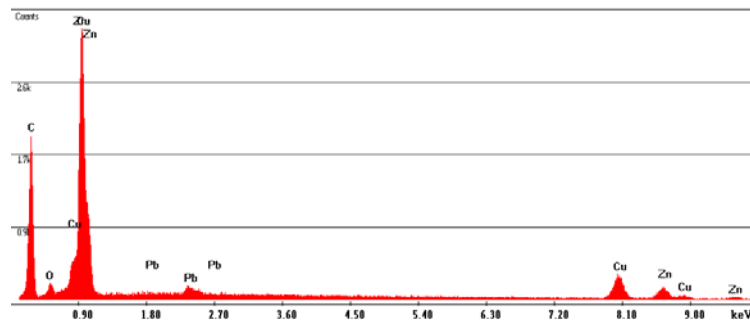
a)

b)

Figure 7.88: BSE images of the arcing tested plane electrodes after testing with the 1 mm diameter rod with

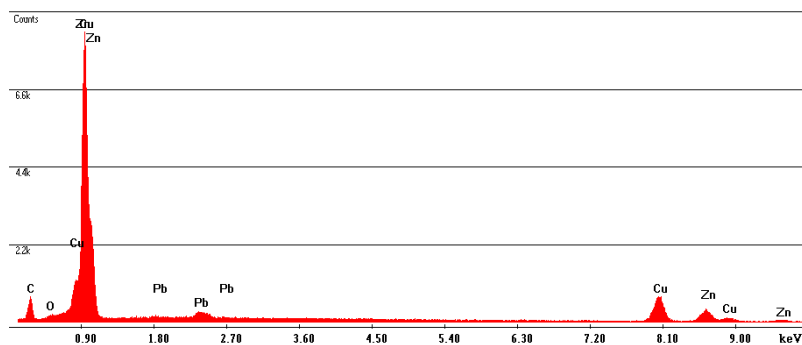
a) gap distance 0.8 mm, arcing current 132.9 mA, arcing current density 16.93 A/cm² b) gap distance 0.3 mm, arcing current 389 mA, arcing current density 49.53 A/cm²

Label A: ux5118: N1mm-0.8mm gap, pos. 1, u44853-1, 15kV



a)

Label A: ux5119: N1mm-0.8mm gap, pos. 1, u44853-2, 15kV



b)

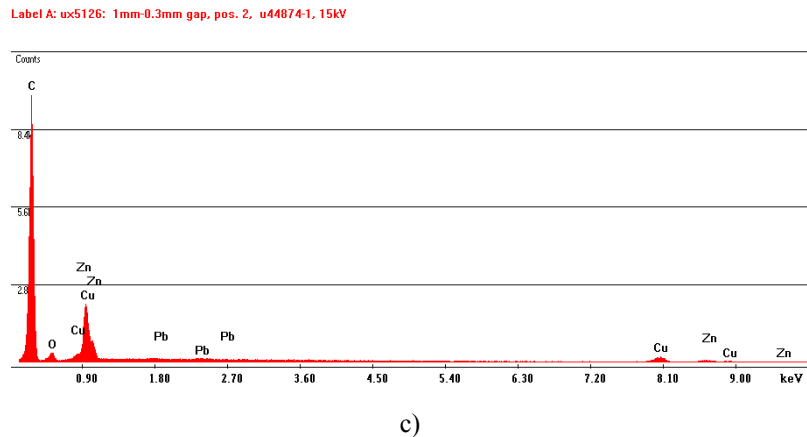


Figure 7.89: EDX analysis of the interested areas of Fig. 7.88

a) area 1 of (a) b) area 2 of (a) c) area 1 of (b)

There were low density compositions covering on the tip of the 2 mm diameter rod after the arcing experiment was performed. In case of SEM and EDX analysis for plane electrodes, the topography of the original and tested plane electrodes was nearly similar. There was also no evidence to show that any part of the plane electrodes melted or eroded. BSE images revealed that the surface of arcing tested plane electrode comprises of at least 3 types of materials. EDX spectra generated by the areas of interest at the arcing points of the plane electrodes as shown in Fig. 7.89 illustrate that the major components consisted of zinc, copper, and carbon. Zinc and copper were the major elements for manufacturing the plane electrode. Carbon was generated from the degradation of the mineral oil during the arcing process. From BSE images, the higher current density arcing rod created more carbon density on the tested plane electrode compared to the carbon produced by the lower current density arcing rod as delineated in Fig. 7.89. Furthermore, the 1 mm diameter arcing rod created more carbon density with a smaller arcing area on the tested plane electrode compared to the carbon produced by the 2 mm diameter arcing rod. Moreover, the quantity of carbon collected at the tested rods was relative to the carbon quantity collected on the tested plane electrodes; in other words, the higher quantity of the carbon on the rods, the higher amount of the carbon is collected on the plane electrodes.

8 Discussion and conclusion

8.1 Effect of electrode configuration on PDIV and PD characteristics of the mineral oil

PDIV depended clearly on electrode configurations related their maximum electric field strength. The electrode configurations especially the needle tip radius and the gap distance had a substantial effect on PDIV value and on the charge value as well. The 10 μ m tip radius needle-plane electrode gave the highest electric field strength compared with other electrode configurations. At the same electrode configuration, the 10 μ m tip radius needle produced the maximum electric field strength higher than the maximum electric field strength generated by the 20 μ m and 40 μ m tip radius needles about 1.7 and 2.9 times respectively. The test results showed that the 10 μ m tip radius needle-75 mm diameter plane electrode provided the lowest PDIV compared with other electrode configurations. This was due to such electrode configuration generated the highest electric field strength. For all investigated electrodes, the PDIV value obtained from the 10 μ m tip radius needle was lower than that value acquired from the 20 μ m and 40 μ m tip radius needles about 1.1-1.4 and 1.3-1.5 times respectively. The PDIV value obtained from the electrode with the gap distance of 50 mm was higher than the PDIV value from the gap distance of 25 mm about 1.1-1.4 times. Moreover, the test methods considerably affected also the PDIV value. IEC test methods provided the PDIV about 1.1-1.4 times higher than the PDIV obtained from the combine PDIV test method. At PDIV level, tested by IEC method, the PD charge amplitudes recorded for 1 minute were higher than 200 pC. PDs occurred between the angles of 35-135 degree of the phase - resolved PD diagram. For combine PDIV test, it produced the PD charge amplitudes recorded for 1 minute in the range of 104-216 pC depending on the gap distances of electrode configurations. Only one or two PDs with lower charge amplitudes occurred nearly or at 90 degree of the phase - resolved PD diagram when the PD activities were examined at the PDIV level obtained from the combine PDIV test method. The combine PDIV test method generated lower PDIV value might due to the longer duration of the mineral oil subjected to the electric field strength. Under high electric field strength with preferable time, the micro bubbles in the mineral oil had high potential to discharge. Furthermore, charge values clearly depended on the needle tip radius. The charge value obtained from the 10 μ m tip radius needle was lower than that value acquired from the 20 μ m and 40 μ m tip radius needles about 1.3-2.0 and 1.8-2.8 times respectively. The charge value obtained from IEC test method was higher than that value acquired from the combine PDIV test method about 1.7-3.1 times. Conversely the PDIV value, the charge value obtained from the electrode with the gap distance of 25 mm was equal or higher than the charge value from the gap distance of 50 mm about 1-1.7 times. To analyze the distribution of the test results,

normal and weibull distribution were proved that they could be used to describe the PDIV and charge test results.

8.2 PD and breakdown mechanism of the mineral oil under PDIV test according to IEC 61294 tested by a needle - plane and a needle - sphere electrode

PDIV diagram is developed to explain PD and breakdown phenomena occurring when the PDIV experiment is performed in accordance with IEC standard. The PDIV diagram is divided into 4 cases as the following; PDIV experiment according to IEC 61294 with a PD level of 100 pC, low probability risk to breakdown, medium probability risk to breakdown, and high probability risk to breakdown.

1. PDIV experiment according to IEC 61294

Considering the PDIV diagram, Fig. 8.1 represents the existence of PD charge when the PDIV measurement is performed. In this process, the tested voltage is applied to the electrode system with a rate of 1kV/sec from zero as shown in the black line until the first PD with the amplitude equal or more than 100 pC happens as illustrated in the red line. The first voltage at $PD \geq 100$ pC is defined and recorded as a PDIV. The PDIV level should be founded before the amplitude of the applied voltage reaches the breakdown zone described in the next section. From the PDIV experiment performed in the laboratory with the new mineral oil with water content below 10 ppm, most PDIV phenomena were found associated with this case.

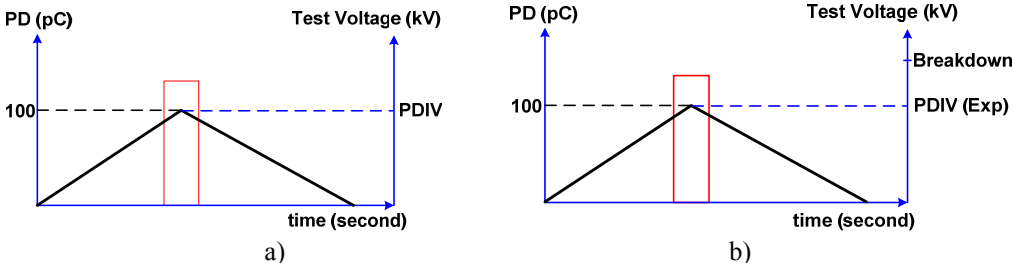


Figure 8.1: PDIV experiment

a) IEC 61294 b) PDIV experiment with breakdown amplitude

2. Low probability risk to breakdown

Another possibly PDIV phenomena can be defined as low probability breakdown risk for PDIV experiment. Observing the testing process, the small PD pulse, $PD < 100$ pC may be found at the low applied voltage level before the specified PD level for PDIV, $PD \geq 100$ pC, is detected as demonstrated in Fig. 8.2 a) by which PDIV(Exp) is defined as the PDIV value obtained from the test experiment. A small PD pulse may be created also after the PDIV level existing as illustrated in Fig. 8.2 b). The presence of one or more small PD pulses does not significantly influence on the subsequent of the PDIV amplitude. However, there are a few cases that the second discharge with the PD amplitude ≥ 100 pC occurs after the PDIV is

found as depicted in Fig. 8.2 c). Generally, the PDIV is detected before the applied voltage reaches the breakdown zone. Therefore, the breakdown cannot happen.

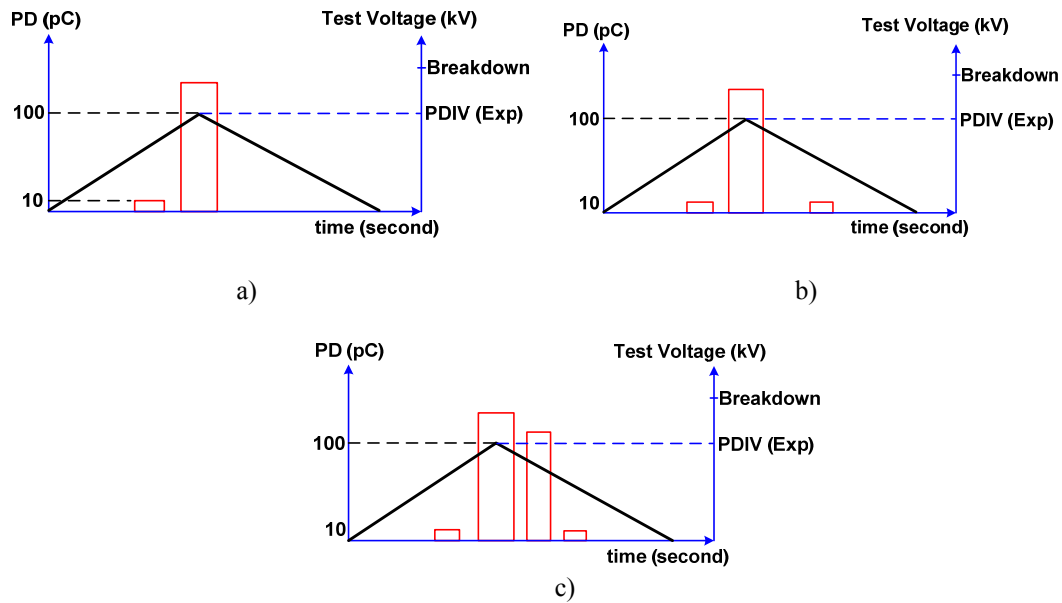


Figure 8.2: Low probability breakdown risk for PDIV experiment

3. Medium probability risk to breakdown

In this case, some small PD pulses are generated. Normally, amplitudes of these small PD pulses depend on the amplitude of applying tested voltage. The existence of small PD pulses directly affects the higher PDIV amplitude (PDIV Exp). This PDIV occurs at a few second time delay compared with the occurring of the first 100 pC PD charge without a small PD (Fig. 8.1) as represented by the red dot line as shown in Fig. 8.3a). Moreover, some discharges with the PD amplitudes which are lower and/or higher than 100 pC may occur after the PDIV is found. This mechanism is depicted in Fig. 8.3 b) and Fig. 8.3 c) respectively.

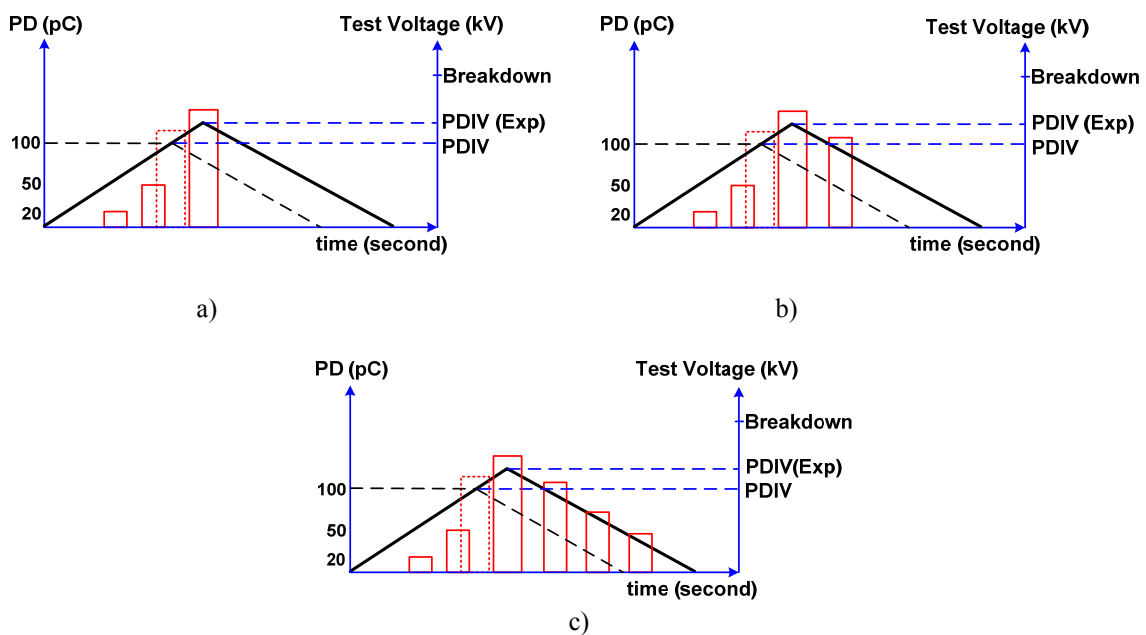


Figure 8.3: High probability breakdown risk for PDIV experiment

4. High risk to breakdown and breakdown event during PDIV test

Normally, the breakdown can happen when PDIV test is carried on as reported in chapter 7. Breakdown events can be categorized based on the time which the breakdown takes place. Two breakdown phenomena may happen; the former breakdown may occur at the same time of finding PDIV; the latter breakdown may take place after PDIV is detected.

4.1 The breakdown happening at the same time of finding PDIV

Fig. 8.4 exhibits the breakdown process which may happen in the PDIV experiment. After the tested voltage is applied to the electrode at a certain voltage level, the small PD pulses are produced in the mineral oil. The higher amplitude of the applied voltage level, the easier generates PD signals as shown in Fig. 8.4 a). The amplitudes of the first and the successive generated PD pulses are still lower than 100 pC as depicted in Fig. 8.4b). The PD activity in a dot red line delineates the first 100 pC PD charge without a small PD. After that, if the tested voltage is still increased to generate the first PD pulse by which $PD \geq 100$ pC, the tested voltage will enter into the breakdown area. Finally, the breakdown happens as shown in Fig. 8.4c).

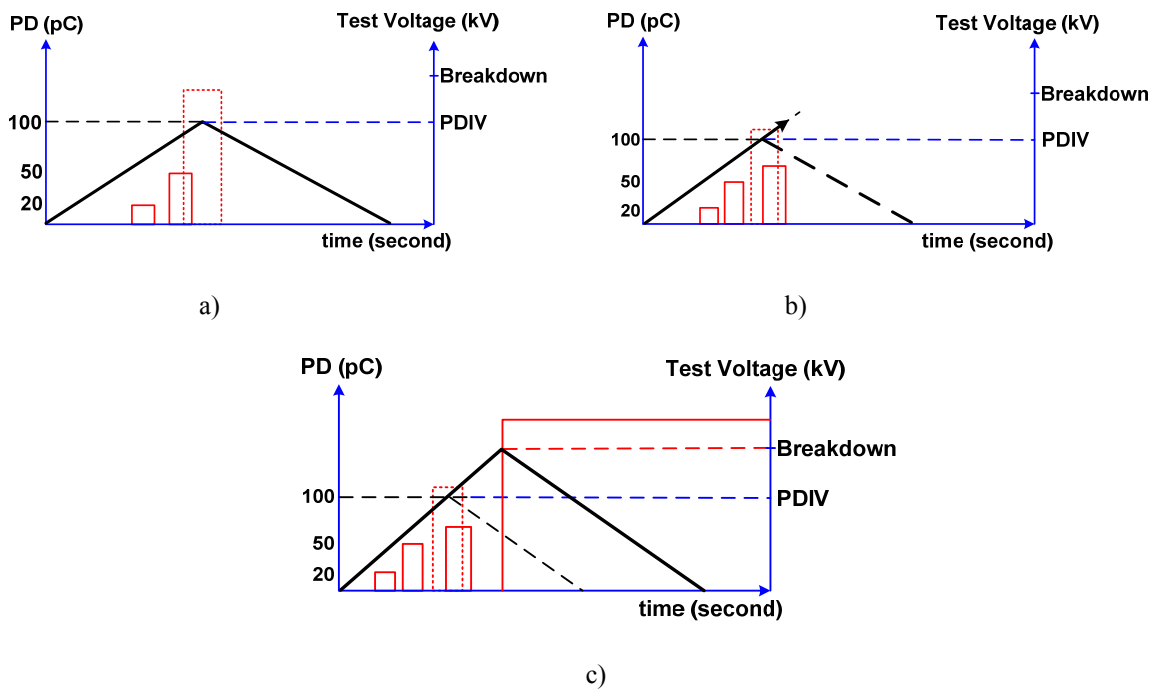


Figure 8.4: PDIV diagram to explain the possibility of breakdown event which can occur when the PDIV experiment is performed according to IEC 61294

4.2 The breakdown happening after PDIV is detected

The PDIV diagram below is utilized to describe another breakdown event which can occur in PDIV test. The first small PD pulse is created at a suitable amplitude of the applied voltage level as presented in Fig. 8.5 a). Then, the bigger PD pulse with its amplitude lower than 100 pC is produced with the increasing applied voltage level as illustrated in Fig. 8.5 b). These small PD pulses cause the successive PD at the PDIV level occurs at the higher applied voltage with a few second time delay. The postponed higher PDIV may cause the breakdown

in the insulation medium after the applied voltage is reduced to a certain voltage level. This breakdown happens after finding PDIV for a few seconds when the defects in the mineral oil get energy enough, the defects will start to discharge; finally the completed breakdown in the insulating medium takes place in a very short time as depicted in Fig. 8.5 c).

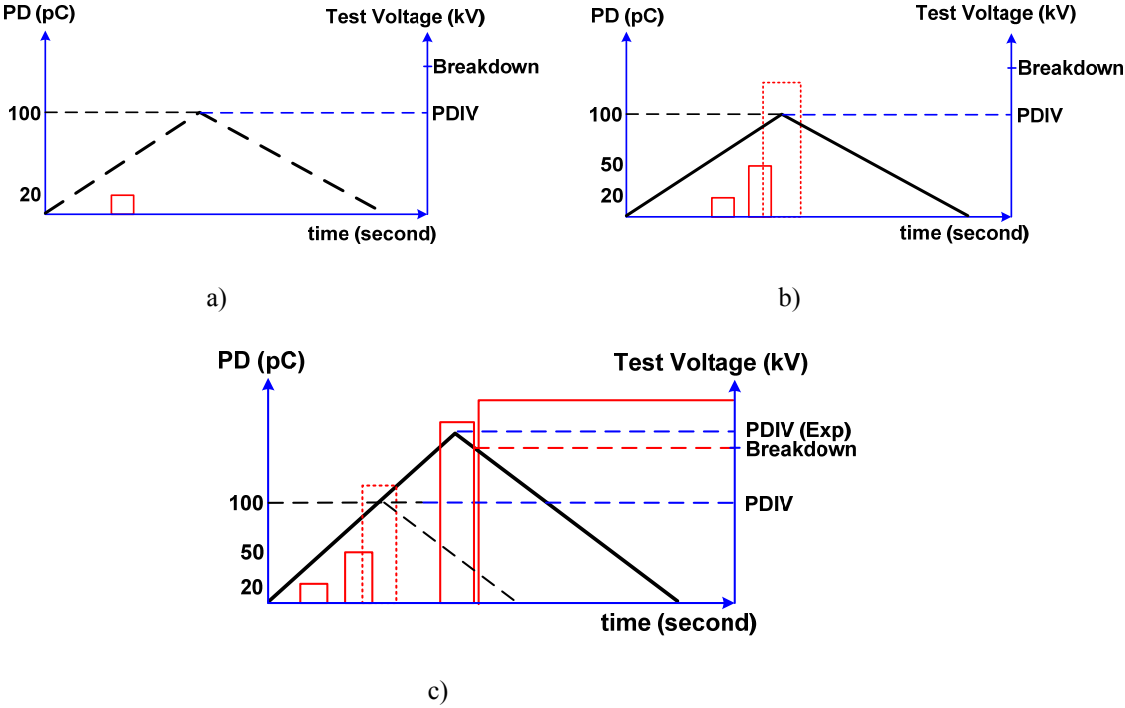


Figure 8.5: PDIV diagram to explain the possibility of breakdown event occurring after PDIV is detected

To avoid the breakdown events during PDIV measurement according to IEC standard, a new PDIV test technique is developed. The developed PDIV test technique is not only preventing the destruction of the PD measuring equipment but also producing the lower PDIV value which nearly approaches the basic idea of PDIV. This PDIV test technique is so called the combine PDIV test technique.

The combine PDIV test technique

This PDIV test technique is composed of IEC test method combined with the step method. The test voltage is applied to the electrode arrangement with a rate of 1 kV/sec from 0% to 70% of the PDIV value (Vs) obtained from the the useful information IEC test method (low probability breakdown risk for PDIV experiment). Then, the tested voltage is increased in steps with 1 kV per step with a step duration of 1 minute until PDIV, the first voltage at PD ≥ 100 pC, is detected. After that, the test voltage is step down to zero. The electrode system is de-energized for 3 minutes. Then, the PDIV experiment is carried out other 4 times in succession. The mean value PDIV of 5 PDIV testings is computed and represented as the PDIV value of the tested insulation. Fig. 8.6 represents the combine PDIV test techniques.

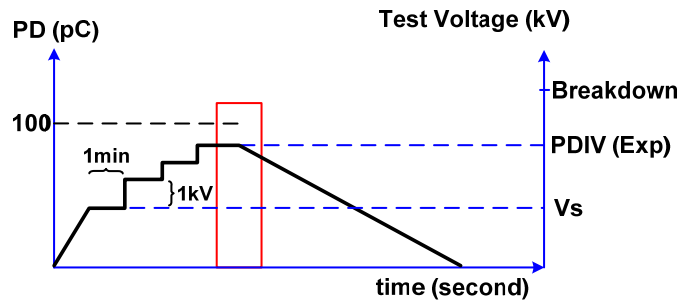
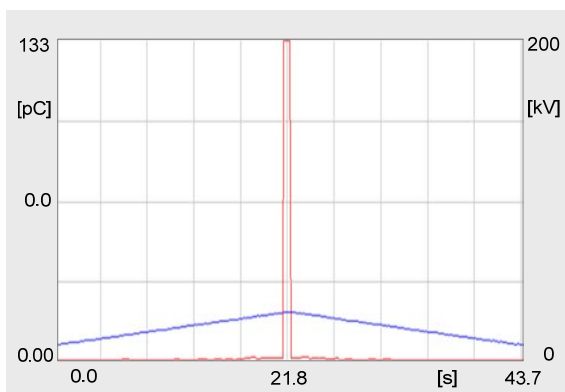


Figure 8.6: Combine PDIV test method

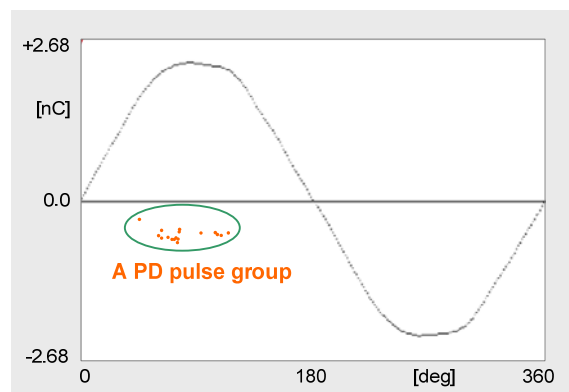
The PDIV level obtained from this test technique should be lower than that PDIV value acquired from IEC test method. This is because the defects of the insulating medium such as moisture or other contaminations have higher probability to discharge with an enough amount PD amplitude due to longer time duration of the tested insulation being under high electric field strength. Table 8.1 compares mean value PDIV, average charge (Q_{IEC}), and peak charge (Q_{PEAK}) obtained from both IEC and combine PDIV test techniques. Fig. 8.7 shows the phase-resolved diagram of both mentioned techniques. All of PDIV test was done with the needle-plane electrode system with various needle tip radii of $10\mu\text{m}$, $20\mu\text{m}$, $40\mu\text{m}$, and the plane electrode of 75 mm diameter with a gap distance of 50 mm.

Table 8.1: Mean value PDIV, average Q_{IEC} and average Q_{peak} obtained from IEC and the combine PDIV test method

PDIV test method	U_{PDIV} (kV)			Q_{IEC} (pC)			Q_{peak} (pC)		
	$10\mu\text{m}$	$20\mu\text{m}$	$40\mu\text{m}$	$10\mu\text{m}$	$20\mu\text{m}$	$40\mu\text{m}$	$10\mu\text{m}$	$20\mu\text{m}$	$40\mu\text{m}$
IEC	30.3	39.1	45.8	270	486	654	675	1217	1633
Combine	25.4	30.0	34.7	133	239	332	331	597	828



a)



b)

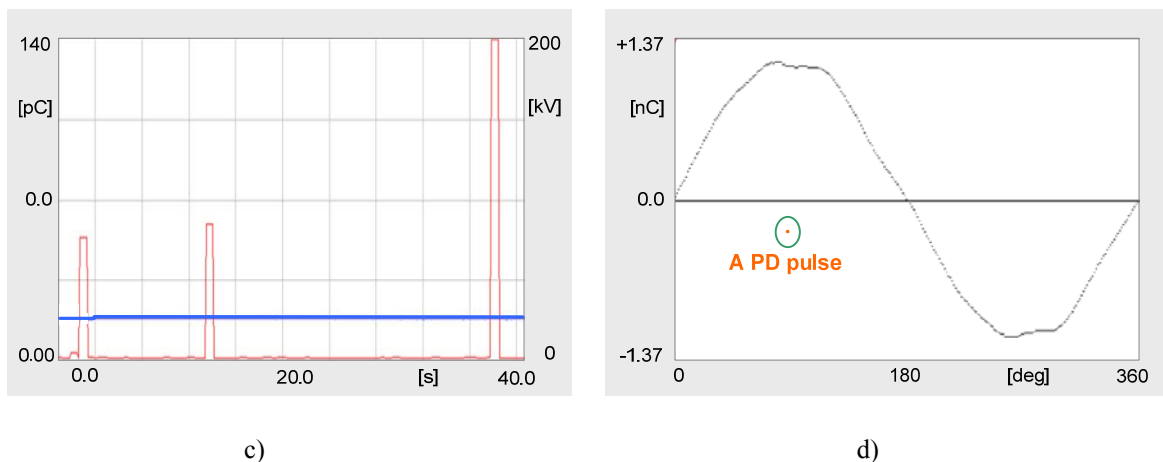
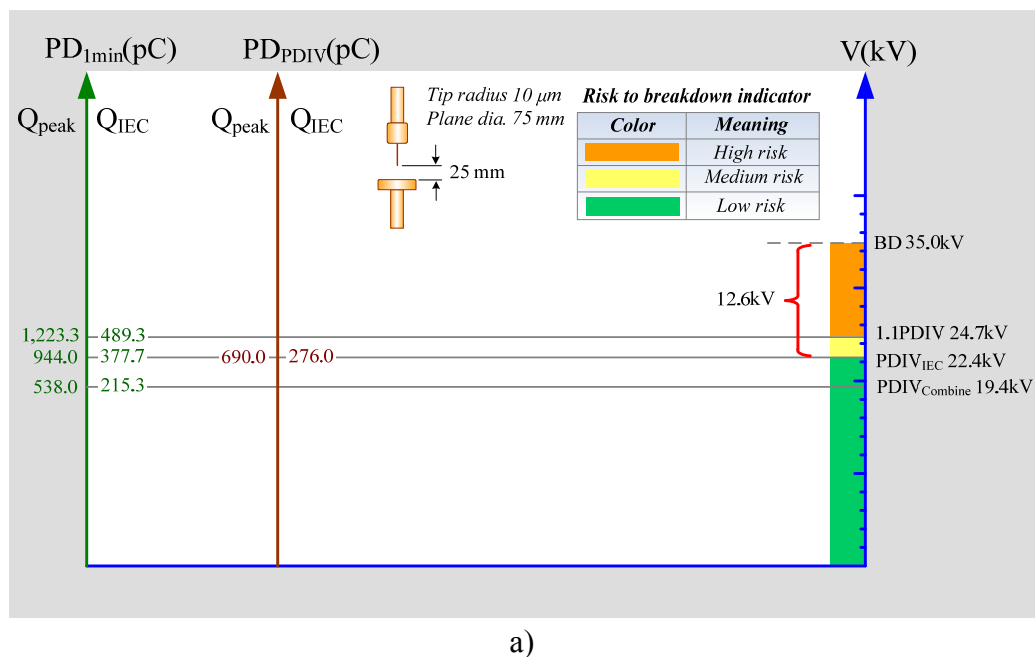
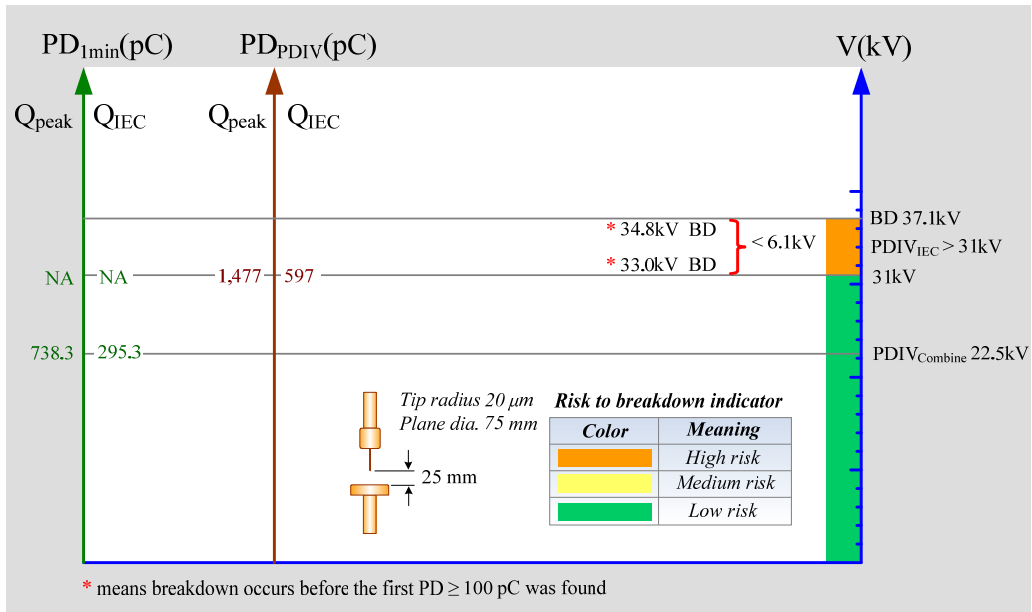


Figure 8.7: Test experiment and phase-resolved diagrams obtained from a)-b) IEC test method c)-d) combine PDIV test method

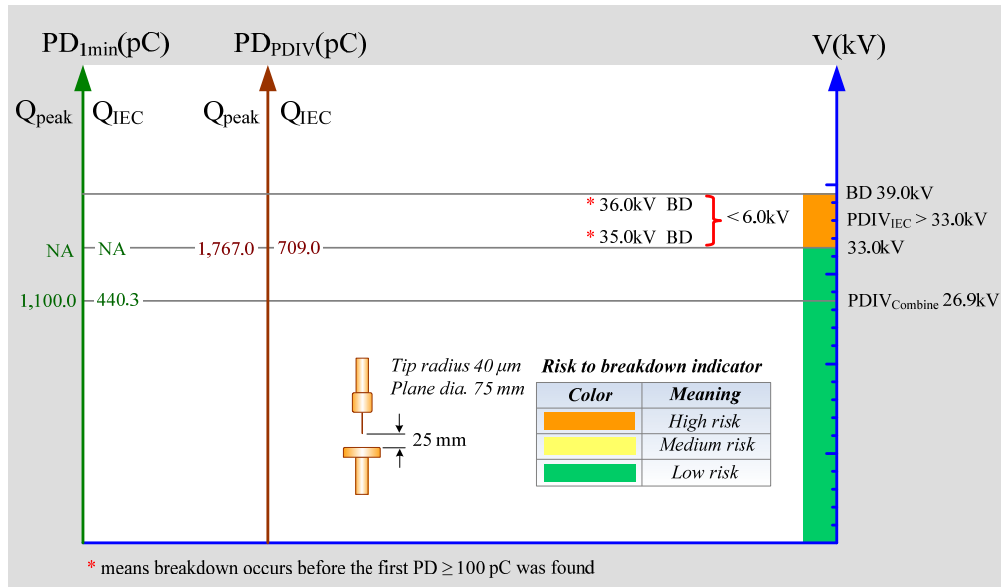
8.3 PDIV and breakdown voltage relationship of the mineral oil tested by the needle- plane electrodes

PDIV and breakdown voltage relationship diagram is developed to explain the risk to breakdown during PDIV experiment is performed. This diagram can be used as a guide to perform PDIV experiment and can apply to select the alternative electrode arrangement for PDIV measurement of liquid insulations especially for mineral oils. PDIV and breakdown voltage diagram tested by the needle- plane electrode with gap spacing of 25 mm and 50 mm are represented in Fig. 8.8 and Fig. 8.9 respectively.





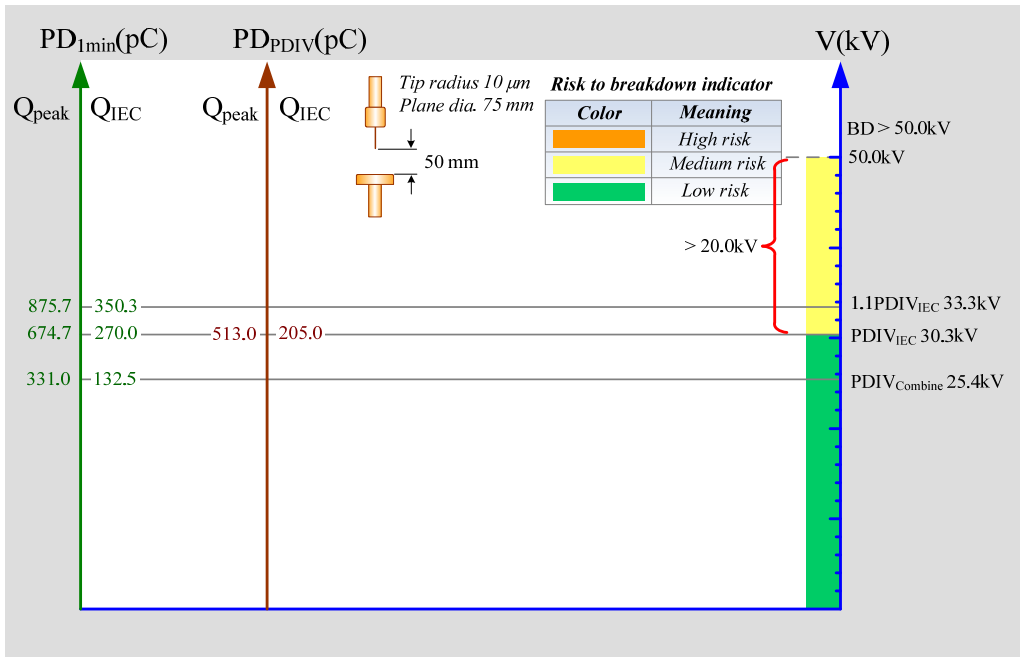
b)



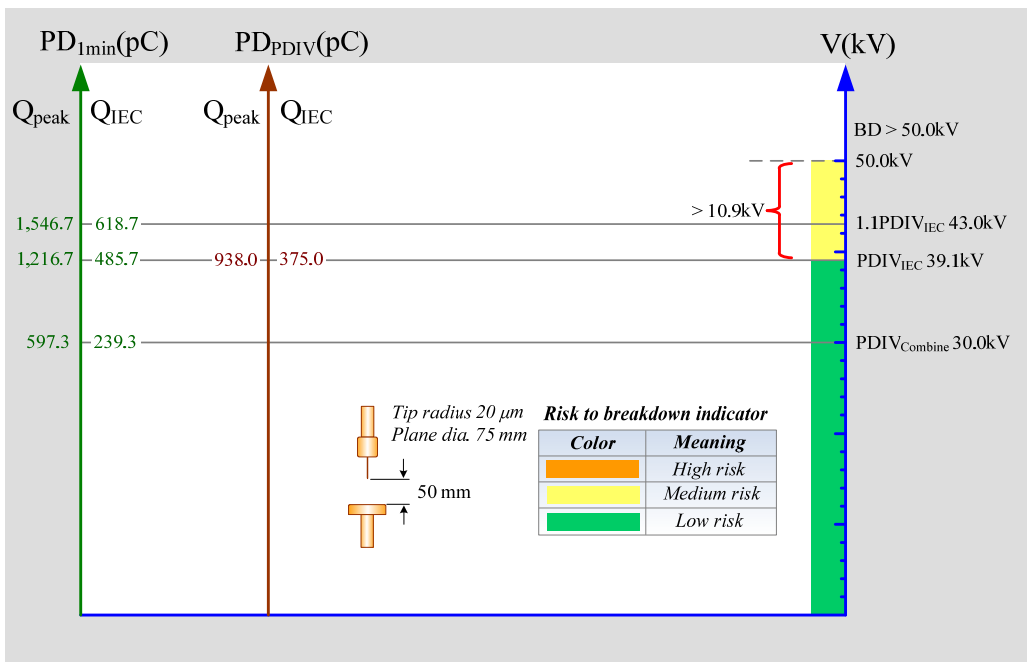
c)

Figure 8.8: PDIV and breakdown voltage diagram of the mineral oil tested by needle- plane electrodes with gap spacing of 25 mm

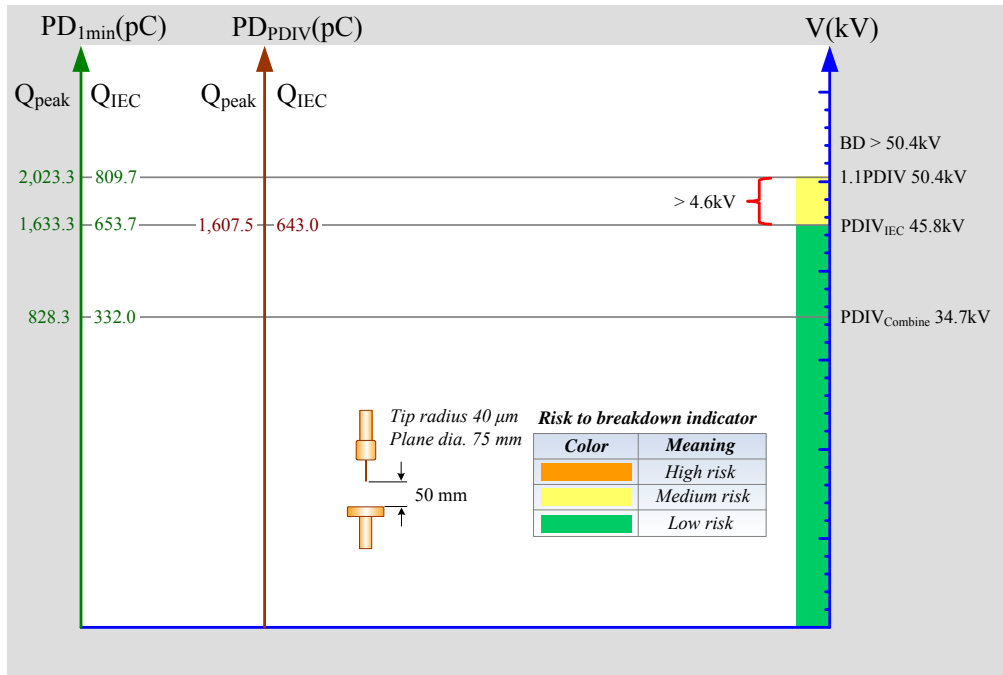
The PDIV and breakdown voltage diagram consists of the breakdown and PDIV levels obtained from IEC and combine PDIV test method. Besides, the charges both Q_{peak} and Q_{IEC} acquired from 1 minute recorded (PD_{1min}) and the first charge value (PD_{PDIV}) at PDIV level are exhibited. Generally, the first charge value at PDIV level is lower than the charge recorded for 1 minute. Moreover, the Q_{IEC} is about 40% of Q_{peak} .



a)



b)



c)

Figure 8.9: PDIV and breakdown voltage diagram tested by needle – plane electrodes with gap spacing of 50 mm

According to Fig. 8.8, only the 10 μ m tip radius needle-75 mm dia. plane electrode provides the medium risk zone for PDIV test of the mineral oil. This electrode configuration has also a biggest voltage range by which the applied voltage can transition from PDIV state to breakdown state. However, there is still risky to perform PDIV experiment using the 10 μ m tip radius needle-75mm dia. plane electrode with gap spacing of 25 mm. The degree of risk considerably relies on the rate of rise of applied voltage for testing as well. There is no medium risk zone for PDIV experiment with the 20 μ m or 40 μ m tip radius needle-75mm dia plane electrode with gap spacing of 25 mm. The breakdown event can immediately develop from PDIV level to breakdown level in a few second of applied voltage if the rate of rise of voltage 1kV/sec according to IEC standard. The longer gap distance of the electrode system can mitigate the degree of risk to breakdown as delineated in Fig.8.9. All electrode configurations have the low risk and medium risk zones. From the experiment, there were no breakdown events for PDIV testing used the needle-plane electrode with gap spacing of 50 mm, even if the experiments were performed at 1.1 PDIV level for observing the PD pulse trains. Another risk to breakdown mitigation technique is applying combine PDIV test method for PDIV experiment. It is obviously demonstrated that the PDIV obtained from the combine PDIV test method is lower than PDIV acquired from IEC test standard.

8.4 Effect of PDIV test methods on PDIV characteristics of the mineral oil

PDIV values were solidly dependent on the PDIV test methods. The PDIV value obtained from IEC test method (M1) gave the highest PDIV by which was higher than the PDIV value from the second test method about 8% - 18%. The PDIV acquired from the third test method was less than the PDIV obtained from the second test method about 5-8%; that meant the PD detection duration in a period of 1 minute and 5 minutes had less impact on the PDIV value if the PDIV measurement was performed by detecting the first voltage that $PD \geq 100$ pC. Therefore, the combine PDIV test method (M2) should be more suitable for PDIV experiment compared with the combine PDIV test method (M3) based on time consumption for testing. The PD detection duration had more influence on the PDIV value in case of measuring the first PD pulse current as M 4 and M 5. The PDIV values acquired from the fourth and fifth test procedures were lower than the PDIV from the standard PDIV test about 21-28% and 37-40% respectively. This was because the minimum detected PD pulse signals obtained from the fourth and the fifth test method were quite low. The PDIV test method M4 and M5 are not recommended for PDIV experiment because noise signals from the testing and measuring system considerably impact on the PDIV value of these PDIV test methods. Moreover, a testing engineer has to make a decision whether the detected signal is PD or not. Therefore, the accuracy of these methods relies on the the experience of the test engineer. The PDIV acquired from the sixth test method tested by the 10 μ m and 20 μ m tip radius needles with plane electrode system was lower than the PDIV from the standard PDIV test about 2-4%. The average result from of 10 time testings was not much different with those obtained from average of 100 time testings. This verified that a 10 time up and down PDIV testings was more or less enough to perform. To analyse the up and down test data for 10,20, and 30 time testings, normal and weibull distribution with confident level 95% could be used to describe. With the 50 time testings or more, normal and weibull distributions with confident level 95% were not suitable to describe the test results.

8.5 Effect of needle lengths on PDIV and PD characteristics of the mineral oil

The maximum electric field strength obtained from the needle-plane electrode was higher than that of the needle- sphere electrode about 1.4-1.5 times. The needle with needle length 45 mm caused the electric field strength higher about 1.15 times than the electric field strength form the needle with needle length 25 mm. According to this reason, the PDIV obtained from the needle with needle length 45 mm was lower a little bit than the PDIV generated by the needle with the needle length 25 mm. The gap distance showed evidently the impact on the PDIV value; the longer gap distance, the higher was PDIV. Furthermore, the PDIV depended apparently on the test methods. At the same needle length and gap distance, the PDIV value acquired from the needle-sphere electrode configuration was higher than the PDIV obtained from needle- plane electrode arrangement about 1.3-1.5 times for IEC test procedure and about 1.2-1.4 times for the combine PDIV test method. The needle length had not much an impact on the PDIV value. To compare the effect of the test methods, the same

electrode system was tested with different test methods. It was revealed that the PDIV value obtained from the IEC test method was higher than the PDIV value acquired from the combine PDIV test method about 1.1-1.3 times. For the charge amplitude and activity, the charge quantity, Q_{IEC} , obtained from the needle-plane electrode configuration was higher than the Q_{IEC} obtained from the needle-sphere electrode arrangement. The increasing of gap distance 2 times reduced the Q_{IEC} about 1.2-1.6 times. PD activity at the PDIV level recorded for 1 minute clearly rested on the test methods. The higher PD repetition rate happened when the PD measurement was performed at the PDIV level obtained from IEC standard test. Whereas, only one or two PDs were found nearly 90 degree of applied voltage when the experiment was performed at the PDIV level obtained from the combine method.

It was evidently demonstrated that the needle - plane electrode system could detect the PDIV value at the lower test voltage and gave the higher Q_{IEC} value compared with testing by the needle - sphere electrode system. The combine method produced the lower PDIV value and the lower Q_{IEC} quantity with much lower PD repetition rate compared with testing by following IEC test method.

8.6 Effect of water contents and temperatures on PDIV and PD characteristics of the mineral oil

Water in mineral oil can produce bubbles when water is heated at the boiling point. Bubble formation may cause by local heating, cavitation or electrical stress. The local heating near the needle tip may cause the forming of the bubbles from the water and then one or more bubbles may discharge because of high electric field. When the mineral oil contains high degree of water content, the formation of bubbles should be higher possibility and then the PDIV of the high water content mineral oil should be lower. From the test results, at room temperature, the water content in the mineral oil influenced more or less on PDIV values. However, at the higher temperature, the PDIV values of the mineral oil with different water contents were relatively the same. The increasing of PDIV value with the increase of temperature might be explained by the water solubility - temperature characteristic. The increase of PDIV value with increasing the temperature was the same as the increasing of breakdown voltage of the mineral oil at higher temperatures. At the higher temperatures, the water solubility of the mineral oil will increase. Therefore, PDIV and breakdown were difficult to take place. The mineral oil expanded when it was heated and it went up to the top of the vessel. Fig. 8.10 represents the mineral oil at the room temperature and at the higher temperatures. The higher temperatures caused the movement of mineral oil and contaminant molecules with higher velocity as depicted in Fig. 8.11. The mineral oil movement direction was clearly observed at the higher temperature. The higher velocity of the mineral oil movement might cause the higher electric field strength of the mineral oil as referred in the literature. Moreover, at 80°C, mineral oil started to evaporate.

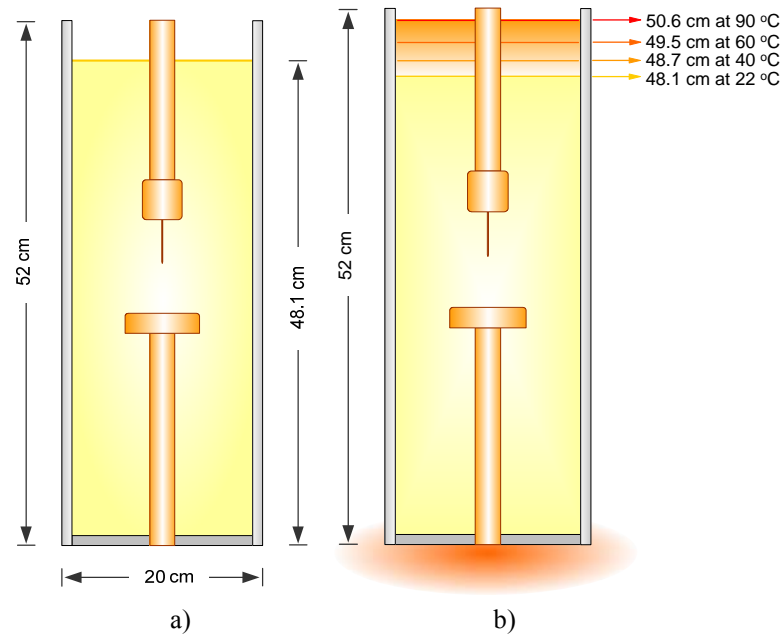
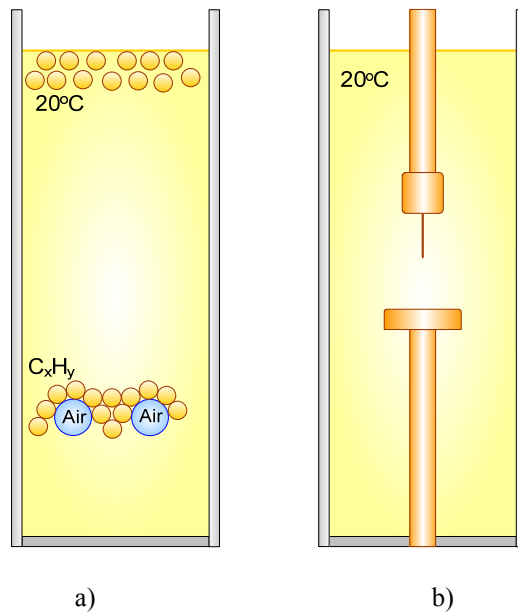


Figure 8.10: Expansion of the mineral oil at the tested temperatures



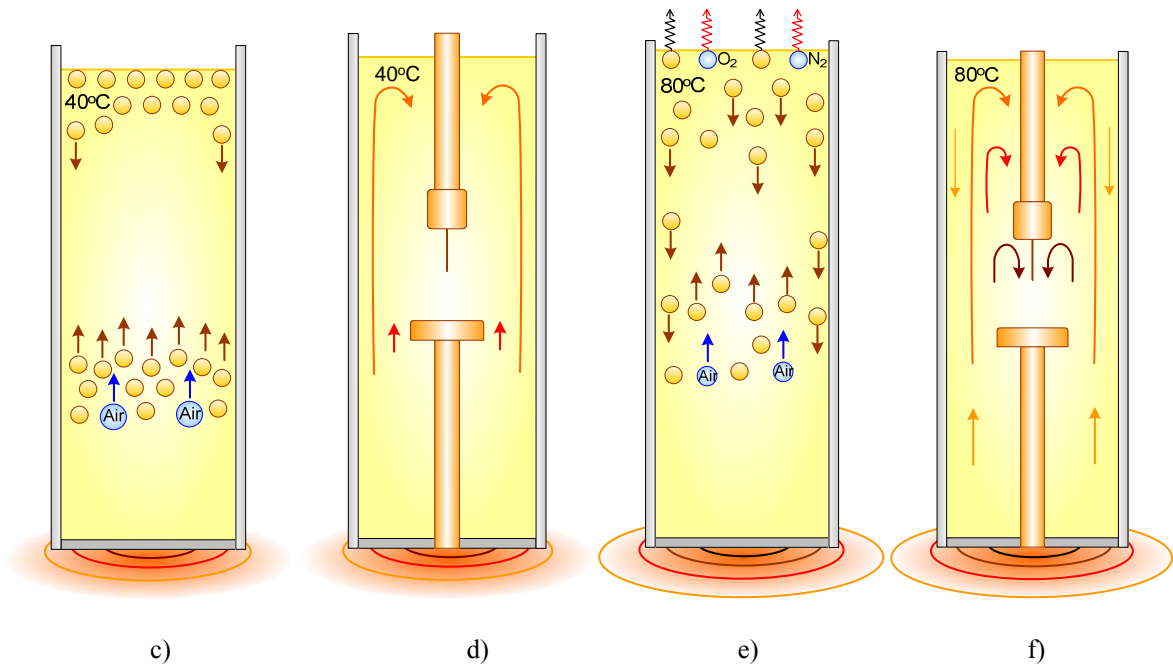


Figure 8.11: Dynamic behaviors of the mineral oil subjected to various temperatures

8.7 PD pulse current behaviors of the mineral oil under PDIV experiment

PD pulse current train behaviors were detected by the shunt resistor of 50 ohm at PDIV level. PD pulse normally took place near or at 90 degree of phase voltage. The patterns of PD pulse train obtained from different tip radius needle-plane electrode configurations were not different. The PD pulse wave forms obtained from PD pulse current train as presented in chapter 7.4.1 was quite smooth because they were measured and displayed with a low effective band width setting oscilloscope to locate their positions in the pulse train. The real PD pulse patterns will be measured and displayed with high effective bandwidth setting oscilloscope as exhibited in chapter 7.4.2.

PD pulse current characteristics obtained from different electrode configurations at room temperature can be concluded as following:

- PD pulse current peak was about 0.2 - 1.3 mA,
- time duration was in the range of 0.6 – 9.3 μ s,
- rise time was about 40 - 570 ns.

The recorded pulse currents illustrated that some discharges might occur after the first discharge happened in the bubble. At the same PDIV level, many PD pulses with different rise times and time durations happened. Normally, the PD pulses were similar in shape but different rise times and time durations which caused different power and energy taking place which dissipated in the mineral oil.

At various oil conditions with different water contents and temperatures, PD pulse current characteristics tested by the 10 μ m tip radius needle -75 mm dia. plane electrode can be summarized as following:

- PD pulse peak current was about 0.1 to 0.6 mA,
- time duration was in the range of 0.5 to 4.8 μ s,
- rise time was approximately 70 - 670 ns.

The maximum values of the peak current and of the current pulse duration decreased when the the mineral oil temperature increased from the room temperature to 40°C. However, the maximum value of peak current and of pulse duration tended to increase when the mineral oil temperature increased from 40°C to 90°C. Besides, the maximum value of PD pulse rise time increased with the increasing of temperatures.

8.8 Effect of electrode configurations on arcing test characteristics of the mineral oil

From the experimental test results, the arcing voltage clearly depended on the gap distance. The average arcing voltages of the rods with diameter of 1 mm and 2 mm with the curvature of 0.2 mm at both gap distances of 0.3 mm and 0.8 mm were not much different. The average arcing voltage of the 2 mm diameter rod was a bit higher than that of the 1 mm diameter rod. The maximum arcing current density was 54.24 A/cm^2 found from the 1 mm diameter rod – plane electrode testing with the gap distance of 0.3 mm. The arcing current magnitude depended on the power rated of the transformers. At the same arcing voltage, the arcing current may be different depending on the power rate of the voltage source. Moreover, the PD pulse signals and the arcing pulse current signals were relatively similar in shape detected by the low effective bandwidth setting oscilloscope. Furthermore, the significant degradation of the mineral oil, such as the oil color appearance, generated bubbles and other particles in oil, could be vividly observed after the arcing test.

8.9 SEM and EDX analysis

The SEM and EDX test results of the needle-plane and the rod-plane electrodes for the PDIV and the arcing test of the mineral oil may be concluded as the following:

1. There was no evidence to show the erosion of the needles and plane electrodes after they were used for PDIV testing. It replies that the tungsten needles with tip radius of $10 \mu\text{m}$, $20 \mu\text{m}$, and $40 \mu\text{m}$ can be used for PDIV testing without the problem of erosion.
2. There was also no evidence to show the erosion of the rods and plane electrodes after they were used for arcing test.
3. Carbon was found at the surface of the needles, rods and plane electrodes especially at the tip of the arcing tested rods and at the arcing point of the tested plane electrode.
4. It was highly possible that carbon comes from the degradation of mineral oil.
5. The intensity of carbon depended on the arcing current density.
6. The collected carbon on the tip of arcing tested rod changed the topography of the arcing test rod which might affect the scattering of breakdown voltage and arcing current of the mineral oil.
7. At low current density most carbon was found at the plane electrodes. With higher current density, carbon was found at the plane electrodes and the rods also.
8. The rod with diameter of 1 mm-75 mm dia. plane electrode can be used for the further arcing research with a gap spacing of 0.3 mm and 0.8 mm with the minimum accepted arcing current density 10 A/cm^2 ; however at a higher current density such as 49 A/cm^2 , it seems to have the problem of the by - product carbon layer generated by the arcing process. The carbon layer which covers the tip of the testing rod may affect the successive breakdown

voltage and the arcing current. In addition, the rod with diameter of 2 mm -75 mm dia. plane electrode with a gap spacing of 0.3 mm may be a choice for the further arcing research if the minimum accepted arcing current density is 10 A/cm².

9. Other compositions such as oxygen, copper, silicon, aluminum and lead were found.

8.10 Conclusion

The main findings of this research are summarized in this part and can be divided into four parts. The first part will explain about the factors affecting the PDIV and PD characteristics of the mineral oil. The second and third parts compose of the proposed electrode configuration and the proposed PDIV test method for PDIV experiment. In the final part the arcing experiment result is described.

1. PDIV and PD characteristics of the mineral oil

PDIV and PD characteristics of the mineral oils depended mainly on three factors composed of the electrode configuration for testing, mineral oil condition and PDIV and PD test techniques.

1.1 Electrode configuration: PDIV and charge values depended apparently on electrode configurations which were related to their maximum electric field strength. The electrode configurations especially the needle tip radius and the gap distance had a considerable effect on the PDIV values and on the charge values as well. The 10 μ m tip radius needle-75 mm dia. plane electrode produced the highest electric field strength compared with other electrode configurations. Therefore, such electrode provided the lowest PDIV. The PDIV values tested by the needle-plane and the needle- sphere electrodes with gap distance of 50 mm was higher than the PDIV values experimented from the gap distance of 25 mm about 1.1-1.4 times. Contrary to the PDIV values, charge values tested with the gap distance of 25 mm was equal or higher than the charge values tested with the gap distance of 50 mm approximately 1-1.7 times. The peak current obtained from the tested electrodes with gap distance of 25 mm was higher than the peak current obtained from testing with the gap distance of 50 mm. Furthermore, the needle with the needle length of 25 mm had a little bit higher PDIV values compared with the PDIV generated from the needle length of 45 mm. This was because the maximum electric field strength generated from both different needle lengths was not much different. In this case, the high voltage supporting rod which was used for support the needle had an impact on the electric field distribution of the electrode system also. Therefore, the impact for the supporting rod has to be considered.

1.2 Mineral oil condition: Two parameters of the mineral oil conditions, water contents and temperatures, were focused on this part. At room temperature, It was found that the degree of water content in the mineral oil influenced more or less on PDIV values. However, at the higher temperatures up to 90°C, the PDIV values of the mineral oil with different water contents, 4 ppm-40 ppm, were relatively the same. The increase of PDIV values with increasing the temperature was comparable with the AC and impulse breakdown characteristics of the mineral oil at higher temperatures. This was because the water solubility of the mineral oil would increase at higher temperatures. Therefore, PDIV and breakdown were difficult to take place. Moreover, the movement of the mineral oil at higher temperatures

caused the higher electric field strength of the mineral oil as referred in the literature. In addition, this research work suggests that PDIV testing was less sensitive to the degree of water contents in the mineral oil compared to AC breakdown testing according to IEC standard. This research also found that the maximum values of the peak current and of the current pulse duration decreased when the the mineral oil temperature increased from the room temperature to 40°C. However, the maximum value of peak current and of pulse duration tended to increase when the mineral oil temperature increased from 40°C to 90°C. Besides, the maximum value of PD pulse rise time increased with the increasing of temperatures.

1.3 PDIV and PD test method: PDIV values were solidly dependent on the PDIV test methods which related to the PDIV definitions. IEC test procedure gave the highest PDIV value compared with other test techniques. The high value of PDIV posed the question that it was the real PDIV or not. Moreover, the IEC test technique had some drawbacks for example, breakdown events could occur when PDIV experiment was performed. The diagram used to explain the breakdown mechanism under PDIV test according to IEC 61294 tested by a needle-plane and a needle-sphere electrode has been developed as illustrated in chapter 8. Furthermore, IEC test technique does not reflect the operation state of high voltage equipment which operates at a nearly constant voltage. The charge values recorded at the PDIV levels obtained from IEC test method was quite high >200 pC. To rectify the disadvantages of IEC test method, the combine PDIV test technique was established. This test technique provided the lower PDIV values and also the lower charge values. The higher PD repetition rate happened when the PD measurement was performed at the PDIV level obtained from IEC standard test. Whereas, only one or two PDs were found nearly 90 degree of applied voltage when the experiment was performed at the PDIV level obtained from the combine method. Additionally, a non-conventional PD measurement by measuring the PD pulse current was proved that it was a powerful PDIV test technique. The detected PD pulse currents provided some important information related to the mineral oil conditions such as the peak current and the current pulse duration. However, there were some points which needed more attention such as the effective setting of the oscilloscope which effected on the detected PD signals. Back ground noise in the testing and measuring system was also needed to pay attention.

These finding parts enhance the understanding of the influence factors on PDIV and PD characteristics of the mineral oil.

2. An alternative electrode configuration for PDIV and PD testing

The 10 μm tip radius tungsten needle-75 mm dia.brass plane electrode showed the high potential ability for PDIV testing of the mineral oil. Using the 10 μm tip radius needle as high voltage electrode was more suitable than employing the 20 μm and the 40 μm tip radius needles for PDIV measurement because the 10 μm tip radius needle provided the lowest PDIV values that meant it had a highest sensitivity to detect PDIV. The standard deviations from such configuration were also low. From the PDIV and breakdown voltage relationship of the needle-plane electrodes with the gap distance of 25 mm, only the 10 μm tip radius needle-plane electrode provided the medium risk zone for PDIV test. This electrode configuration had also a biggest voltage range by which the applied voltage could transition from PDIV state to breakdown state. However, it was better to perform PDIV experiment with gap spacing of 50 mm because there was no breakdown taking place during the PDIV experiment was performed. This electrode arrangement provided bigger transition zone from PDIV to breakdown state compared with testing with gap spacing of 25 mm. Form the

mechanical and thermal characteristic points of views, the electrode system had to withstand high mechanical and thermal stress which might occur during PDIV experiment was performed. This was confirmed by SEM and EDX test results that there was no evidence to show the erosion of the needles and of the plane electrodes after they were used for PDIV testing. Considering the electrode arrangement set up, the setting of the needle- plane electrode was more convenient than setting the needle-sphere electrode by which the needle tip position had to be aligned over the central point of the plane or sphere electrodes with the specified gap distance. Additionally, with the commercial aspect, the lowest PDIV value detection of the proposed electrode causes more possibility to develop such electrode as a commercial product because this electrode does not need a very high voltage source for performing the PDIV experiment.

3. An alternative PDIV test method

The combine PDIV test method was proved that it can be used as an alternative PDIV experiment. It provided bigger transition zone from PDIV to breakdown state compared with testing by IEC test method. The combine PDIV test method can simulate the real operation of the high voltage equipment which operated at a nearly constant voltage. The PDIV values obtained from the combine PDIV test technique were lower than PDIV values from IEC test technique. The lower PDIV test values approached the idea of PDIV testing by which the first voltage level that PD was generated, when the voltage applied to the test object was gradually increased from a lower value at which no PD were observed. Moreover, the charge values obtained from this technique were about 100 pC or more which were high enough to impact on the integrity of the liquid insulation. The charge values obtained from this technique were still lower than the charges from IEC test standard. The repetition rate of PD charge activities from the combine PDIV test technique was quite low; only one or two PD was detected. Besides, this combine PDIV test method provided a test result within the reasonable time of testing.

4. Preliminary arcing experiment:

Preliminary arcing experiment: the experiment revealed that the arcing voltage clearly depended on the gap distance. The average arcing voltages tested by the rods with the diameter of 1 mm was lower a little bit than tested by the 2 mm rod diameter with the curvature of 0.2 mm. The arcing current magnitude relied on the arcing voltage and also the rated power of the high voltage source. With the lower effective bandwidth setting oscilloscope, it was found that the PD pulse current signals and the arcing pulse current signals were relatively similar in shape. Carbon was highly possible generated from the degradation of mineral oil. Carbon was found at the surface of the rods and plane electrodes especially at the tip of the arcing tested rods and at the arcing point of the tested plane electrodes. The intensity of carbon depended on the arcing current density. The collected carbon on the tip of arcing tested rods changed the topography of the tip which might affect the scattering of breakdown voltage and arcing current of the mineral oil. At low current density, most carbon was found at the plane electrodes. With higher current density, carbon was found at the plane electrodes and the rods also. However, there was no evidence to show the erosion of the rods and plane electrodes after they were used for arcing test. Moreover, the significant degradation of the mineral oil, such as the oil color appearance, generated bubbles and other particles in oil, could be vividly observed after the arcing test.

8.11 Resumee

According to the study, the **PDIV and PD characteristics** of the mineral oil depended vigorously on electrode configuration for testing, on the mineral oil condition, and on the PDIV and PD test technique. The **electrode configuration** especially the needle tip radius and the gap distance strongly affected the PDIV and charge values. The 10 μm tip radius tungsten needle-75 mm diameter brass plane electrode produced the lowest PDIV value compared with other electrode configurations. The shorter gap distance of the electrode arrangement caused lower PDIV value but higher charge and current values. For **the oil conditions**, the degree of water contents of 4-40 ppm in the mineral oil more or less impacted on the PDIV values at room temperature. At higher temperatures up to 90°C, the water content levels were found no effect on the PDIV values. PDIV values were substantially dependent on the **PDIV test methods**. IEC test method gave the highest PDIV compared with other five test methods.

The 10 μm tip radius tungsten needle-75 mm diameter brass plane electrode with the gap distance of 50 mm is proposed as **an alternative PDIV testing electrode**. This electrode configuration was proved that it was highly qualified electrode which met any essential requirements as the following: a high sensitivity and high reliability for PDIV and PD measurement, providing a biggest safety zone by which the applied voltage can transition from PDIV state to breakdown state, a high mechanical and thermal stress withstanding, a convenient set up and installation which is preferred for research works. This electrode type has also a highly potential to be developed as a commercial PDIV and PD testing electrode product.

Moreover, this research also found that the PDIV test technique according to IEC standard had some drawbacks especially it allowed the existences of breakdown events during the PDIV tests were performed. The diagram for elucidating the breakdown mechanism under PDIV test according to IEC 61294 tested by a needle-plane and a needle-sphere electrode was established. Furthermore, the PDIV values, charge quantities and charge repetition rates obtained from PDIV testing complied with IEC standard were quite high. The combine PDIV test technique was proposed as **an alternative PDIV test technique** and it was proved that it provided the satisfied test results; lower PDIV and charge values, lower PD repetition rates, and no breakdown event. Furthermore, the non-conventional PD test method by detecting the PD pulse current was proved that it was a powerful PDIV test technique. The detected PD pulse currents provided some important information related to the mineral oil conditions such as the peak currents and the pulse durations.

For the **arcing test of the mineral oil**, the experiment revealed that the arcing voltage clearly depended on the gap distance. The average arcing voltages tested by the tungsten rods with the diameter of 1 mm- 75 mm diameter brass plane electrode was lower than tested by the 2 mm rod diameter with the curvature of 0.2 mm. The arcing current magnitude relied on the arcing voltage and also the rated power of the high voltage source. The arcing current density had strongly effect on by-products such as carbon composition and bubbles. Carbon was found at the surface of the rods and plane electrodes especially at the tip of the arcing tested rods and at the arcing point of the tested plane electrodes. The topography of the arcing tested rod might be changed during arcing test process because of the collected carbon on the tip of the arcing rod. This changing might affect the scattering of breakdown voltage and arcing current of the successive arcing test because of easily bridging of carbon filaments between

the tested electrodes. Besides, there was no evidence to show the erosion of the rods and plane electrodes after they were used for arcing test. Moreover, the significant degradation of the mineral oil, such as the oil color appearance, generated bubbles and other particles in oil, could be apparently observed after the arcing test.

9 Summary

9.1 Summary

Within this work, PDIV and PD characteristics of the mineral oil were investigated. First of all, the patterns of electric field distributions of electrode systems were simulated. It was found that the electric field strength depended mainly on the electrode configuration especially the needle tip radius and gap spacing. The 10 μ m tip radius needle- plane electrode produced the highest electric field strength compared with other electrode configurations. Then, the preliminary PDIV test was performed to investigate the basic parameters for PDIV testing such as the needle tip radius, the test sequence and the PDIV test numbers for one oil samples. The PDIV pulse trains were also measured. The effect of PDIV test method (M1-M6) on PDIV value was also investigated. It was found that PDIV depended clearly on the needle tip radius, the smaller needle tip radius, the lower PDIV level. PDIV was also strongly dependent on the test methods. IEC test technique (M1) provided the highest PDIV level compared with other test methods, while the combine PDIV test technique with the first PD detection (M5) produced the lowest PDIV level. These PDIV experiments were performed by using the tungsten needle electrodes with the tip radius of 10 μ m, 20 μ m, and 40 μ m respectively as the high voltage electrode while the brass plane electrode with 75 mm diameter was used as the grounded electrode. The gap distance of the electrode system was fixed at 50 mm.

After that, **the effect of the electrode configurations** and the mineral oil conditions on PDIV and PD of the mineral oil were examined. The tungsten needle electrode with the tip radius of 10 μ m, 20 μ m, and 40 μ m respectively were used as the high voltage electrode while the brass plane electrode with a diameter of 75 mm as grounded electrode. The gap distance of the electrode system was set up at 25 mm and 50 mm respectively. Two PDIV measurement techniques, IEC and combine PDIV test technique (M1 and M2) were performed. The PDIV value and PD activity at PDIV level including PD pulse currents were recorded. Besides, the plane electrode with diameter of 50 mm and the sphere electrodes with the diameter of 12.7 mm, 25.4 mm, 50.8 mm and 76.2 mm respectively were used as the grounded electrode. According to the study, the PDIV and PD characteristics of the mineral oil depended vigorously on the electrode configuration. The electrode configurations especially the needle tip radius and the gap distance strongly affected the PDIV and the charge values. The 10 μ m tip radius tungsten needle- 75 mm dia. plane electrode produced the lowest PDIV value compared with other electrode configurations. The shorter gap distance of the electrode arrangement caused lower PDIV value but higher charge and current values. Moreover, the effect of needle lengths of 25 mm and 45 mm were investigated also. However, there was no

significant effect of needle lengths on PDIV level. Furthermore, the 10 μm tip radius tungsten needle -75 mm dia. brass plane electrode with the gap distance of 50 mm has been proposed as **an alternative PDIV and PD testing electrode**. This electrode configuration was proved that it was highly qualified electrode which met any essential requirements. The beneficial characteristics of this electrode were based on the assembling body of evidences as the following: a high sensitivity and high reliability for PDIV and PD measurement, a high mechanical and thermal stress withstanding, a convenient set up and installation which was preferred for research works. This electrode type has a highly potential to be developed as a commercial PDIV and PD testing electrode product.

Additionally, this research also found that the PDIV test technique according to IEC standard revealed some drawbacks especially it allowed the existences of breakdown events during the PDIV test. The diagram for elucidating the breakdown mechanism under PDIV test according to IEC 61294 tested by a needle-plane and a needle-sphere electrode was established. The PDIV values, charge quantities and charge repetition rates obtained from PDIV testing complied with IEC standard were quite high. The combine PDIV test technique was proposed as **an alternative PDIV test technique** and it was proved that it provided the satisfied test results; lower PDIV and charge values, lower PD repetition rates, and no breakdown event. In addition, the non-conventional PD test method by detecting the PD pulse current was proved that it was a powerful PDIV test technique. The PD pulse currents were examined and analyzed. PD currents at PDIV level randomly occurred with different rise times and time durations but the patterns of PD pulses were nearly the same. The detected PD pulse currents provided some important information related to the mineral oil conditions such as the peak currents and the pulse durations.

For the oil condition investigation, the mineral oil with water content 4-40 ppm were prepared and investigated at room temperature up to 90°C. It was found that the degree of water contents of the mineral oil more or less impacted on the PDIV values at room temperature. At higher temperatures up to 90°C, the water content levels were found no effect on the PDIV values. The temperatures between 40°C - 90°C had an effect on increasing of the maximum values of the peak PD current, the current time duration and the current rise time. The research work studied also the effect of test circuits on PDIV value. Four PDIV test circuits were arranged and then the PDIV was examined. It was found that four different test circuits provided the relatively similar PDIV values. However, the PDIV patterns were obviously different depending on the position of coupling device connected to the coupling capacitor or the test vessel.

The **preliminary arcing test** of the mineral oil was investigated as well. The tungsten rod electrodes with the tip diameter of 1mm, and 2mm with the curvature of 0.2 mm respectively were used as high voltage electrode, while the brass plane electrode of 75 mm diameter was used as the grounded electrode. The gap distance of the electrode system was set up at 0.3 mm and 0.8 mm respectively. The experiment shown that the electrode configuration had an effect on arcing voltage and arcing current. The PD pulse signals and the arcing pulse current signals were relatively similar in shape. The arcing current density had strongly effect on by-products such as carbon composition and bubbles. Carbon was found at the surface of the rods and plane electrodes especially at the tip of the arcing tested rods and at the arcing points of the tested plane electrodes. The topography of the arcing tested rod might be changed during arcing test process because of the collected carbon on the tip of the arcing rod. This changing might affect the scattering of breakdown voltage and arcing current of the successive arcing test because of easily bridging of carbon filaments between the tested

electrodes. Besides, there was no evidence to show the erosion of the rods and plane electrodes after they were used for arcing test. Therefore, the 1 mm dia. tungsten rod-75 mm dia. plane electrode may be used for the further arcing research. Moreover, the significant degradation of the mineral oil, such as the oil color appearance, generated bubbles and other particles in oil, could be apparently observed after the arcing test. Normal and weibull distributions were proved that they could be used to describe the test data of arcing and also PDIV results.

SEM and EDX was performed to verify the erosion problem which might be occurred after the electrodes, needles, rods and plane electrodes were used for PDIV and arcing investigation. There was no evidence to show the erosion of the needles, rods and plane electrodes after they were used for experiments.

9.2 Further research recommendation

More research in PDIV and PD as well as arcing topics should be done to be clearly understood and applied for industry. The topics are recommended for the further research as following:

1. PDIV characteristics of mineral oil- cellulose insulation under AC applied voltage,
2. PDIV application for online monitoring,
3. PDIV characteristics of alternative oils,
4. PDIV characteristics of insulating liquids under DC applied voltage and under mix AC- DC applied voltage,
5. New PDIV definition and PDIV test technique may be required to established,
6. Arcing characteristic of mineral oil and its application for evaluation the integrity of mineral oil.

List of Figures

3.1 Energy and electrical consumptions for next twenty years.....	4
3.2 Failure causes for transformers	5
4.1 A possible molecular structure of the mineral oils.....	16
4.2 Development of mineral oil characteristics and the increasing of transformer capacity....	17
4.3 Polarization phenomena	20
4.4 A circuit of a dielectric	21
4.5 Dielectric constant as a function of frequency and temperature of a transformer oil	22
4.6 Different kinds of polarization mechanisms	23
4.7 Variation of different types of polarization with relaxation time under a step-function electric field	24
4.8 Dissipation factor against frequency at 90°C.....	25
4.9 Conduction mechanism in dielectric liquids.....	26
4.10 Conduction current.....	27
4.11 DC conductivity of an insulating oil respected to the time of applied voltage	27
4.12 Ion concentration and temperature relationship at 1 kHz of the mineral oils with the approximately equivalent viscosity.....	28
4.13 Influence of water content in the mineral oil	29
4.14 Relationship between the saturation water content and the oil temperature	30
4.15 Temperature effect	31
4.16 Temperature effect on breakdown characteristic of the mineral oil	32
4.17 Temperature effect on air solubility.....	33
4.18 Relationship between dielectric breakdown and the relative oil-dissolved air density for the mineral oil.....	33

4.19 Relationship between breakdown strength of the mineral oil with different contents and temperatures	34
4.20 Moisture effect on breakdown strength of the mineral oil at room temperature with different concentrations.....	37
4.21 Electric double layers	42
4.22 Charge generations.....	43
4.23 Sequence of events when discharge occurs in the liquid dielectric	43
4.24 Positive and negative streamers of the mineral oils (top and bottom) experimented with the needle-plane electrode system, the streamer modes from left to right.....	46
4.25 Positive streamer and negative streamer propagation of the tested electrode	47
4.26 Streamer appearance frequency against applied voltage	48
4.27 AC breakdown voltage of the transformer oil in divergent fields against gap distance (average of 10 measurements).....	49
4.28 Basic PD test circuit	50
4.29 Coupling device in series with the coupling capacitor.....	50
4.30 Coupling device in series with the test object.....	51
4.31 Calibration circuits	51
4.32 PD pulse current.....	52
4.33 PD pulse current and apparent charge characteristic	53
4.34 Typical positive pulse currents.....	54
4.35 PD pulse currents in the mineral oil.....	56
4.36 PD pulse bursts at PDIV and above PDIV level	58
4.37 Paschen's law diagram.....	58
4.38 Electrode configurations for PDIV measurement	59
4.39 Streamer inception field strength and voltage versus tip radius in cyclohexane	60
4.40 Relationship between positive streamer characteristics with the streamer inception voltage and needle tip radius.....	61
4.41 Variation of streamer structures versus tip radius.....	61
4.42 Needle profiles	62

4.43 Streamer inception.....	63
4.44 Oil condition effect on PDIV	65
4.45 Experiment for fiber-bridge formation in the insulating liquid	67
4.46 Elongation under an AC field of a water globule in silicone fluid	68
4.47 Breakdown of a liquid dielectric (silicone fluid) due to instability of a water globule above the critical field	68
4.48 Mineral oil breakdown test results	71
4.49 Voltage-current characteristic of the DC electrical discharge	72
4.50 A schematic drawing of the visual characteristics and voltage distribution along the axis of an arc discharge.....	73
4.51 Two configurations of the free-burning arc	73
4.52 Time variations of current, voltage, and temperature for a 50 Hz, 10 A arc, 3 mm long, in air between copper electrodes.....	74
4.53 Gas bubbles produced by an arc surrounded by mineral oil	75
4.54 Diagram of erosion process of arcing tested electrode	76
4.55 Needle erosion.....	77
4.56 Structure details of SEM and EDX	79
4.57 Beam specimen interaction signals caused by the electron beam (primary beam).....	80
4.58 Beam specimen interactions.....	80
4.59 X-ray spectrum of copper showing K-series and L-series X-ray peaks and the continuous X-ray spectrum (bremsstrahlung or continuum) obtained from a Si(Li) EDS detector with an ultrathin (diamond) X-ray window	81
4.60 X-ray spectrum of an aluminum tungsten oxide on a carbon foil supported on a copper grid	81
5.1 Electrodes for PDIV experiment.....	87
5.2 Needle - plane electrode test cell	88
5.3 Needle - sphere electrode test cell.....	89
5.4 Diagram of the needle - plane electrode test cell for water content and temperature effect on PDIV value experiment.....	89
5.5 Mineral oil for PDIV experiment.....	90

5.6 Water content measurement	91
5.7 Basic mineral oil characteristic measurement.....	91
5.8 Test circuit diagram for PDIV experiment.....	92
5.9 Test circuit setup	92
5.10 Test circuit diagrams for PDIV experiments.....	94
5.11 Arcing electrodes	95
5.12 Test circuit diagram for arcing test	96
5.13 Test set up for arcing test	96
5.14 Mesh generation for electric field simulation	97
6.1 PDIV standard test procedure(IEC)	100
6.2 Combine PDIV test method with 100 pC charge detection	101
6.3 Combine PDIV test method with the first PD detection	102
6.4 Up and down PDIV test method with 100 pC charge detection	103
6.5 Arcing test diagram.....	104
7.1 Electric field magnitude line distributions of the needle- plane electrode systems	105
7.2 Electric field magnitude line distributions near the needle tips of the needle-plane electrode systems with different gap distances	106
7.3 Electric field magnitude line distributions near the needle tips of the needle-sphere electrode systems with different gap distances	107
7.4 Maximum electric field magnitude of the electrode systems with different needle tip radii, different electrode shapes and gap distances	109
7.5 Electric field magnitude line distributions of the needle-plane and of the needle-sphere electrode systems with different needle lengths.....	110
7.6 Comparison of maximum electric field magnitude of the electrode systems with different needle lengths.....	110
7.7 Electric field magnitude line distributions of the rod-plane electrode systems	111
7.8 Electric field magnitude line distributions of the arcing rod-plane electrode systems	112
7.9 Comparison of the mean value PDIV as a function of needle tip radius with σU as standard deviation in kV obtained from test experiment A and B.....	114

7.10 Probability plot of PDIV raw data obtained from the needle (number 1)- plane electrode configuration	115
7.11 Histogram and the probability plot for PDIV raw data.....	116
7.12 Histogram and the probability plot for PDIV experiment A.....	117
7.13 Histogram and the probability plot for PDIV experiment B.....	118
7.14 Comparison of the average charge values as a function of the needle tip radius obtained from test experiment A and B	119
7.15 Histogram and the probability plot of the average charge values from experiment A.....	119
7.16 Histogram and the probability plot of the average charge values from experiment B .	120
7.17 PD activities at the PDIV test level.....	120
7.18 PD activities at the PDIV test level 31.8 kV from the experiment A; blue line is the tested voltage and the red line is PD activity	121
7.19 Mean value PDIV of the 10 μm tip radius needle-plane electrode configuration as a function of the test methods	122
7.20 Mean value PDIV of the 20 μm tip radius needle-plane electrode configuration as a function of the test methods	122
7.21 Mean value PDIV of the 40 μm tip radius needle-plane electrode configuration as a function of the test methods	123
7.22 Mean value PDIV obtained from different PDIV test methods tested by the needle-plane electrode arrangement with 50 mm gap spacing.....	124
7.23 Normal and weibull distribution of the PDIV test data obtained from the 10 μm tip radius needle(needle 1) - plane electrode configuration as a function of test methods	124
7.24 Mean value PDIV obtained from up and down PDIV test as a function of number of testing	126
7.25 Normal and weibull distribution of up and down PDIV value obtained from the 10 μm tip radius needle (needle 1) -75 mm diameter plane electrode configurations	126
7.26 Normal and weibull distribution of up and down PDIV value obtained from 100 time testings of various tip radius needles (needle 3) – plane electrode configurations.....	127
7.27 Mean value PDIV obtained from different PDIV test methods tested by the 10 μm tip radius needle with various grounded electrode systems	129
7.28 Average charge quantities obtained from different PDIV test methods tested by the 10 μm tip radius needle with various grounded electrode systems.....	130

7.29 Mean value PDIV obtained from the combine PDIV test method of the electrode systems	130
7.30 Average charge quantities obtained from the combine PDIV test method of the electrode systems	131
7.31 Normal and weibull distribution of PDIV value obtained from the 10 μm tip radius needle- 75 mm diameter plane electrode (a-b) and obtained from various tip radius needles-75 mm diameter plane electrode(c-d) tested according to IEC test method....	132
7.32 Normal and weibull distribution of PDIV value obtained from various tip radius needles -5 mm diameter plane electrode tested according to the combine PDIV test method ...	133
7.33 Normal and weibull distribution of PDIV value obtained from the 10 μm tip radius needle-12.7 mm diameter sphere electrode tested according to IEC test method	133
7.34 Normal and weibull distribution of PDIV value obtained from various tip radius needles - 12.7 mm diameter sphere electrode tested according to the combine PDIV test method	134
7.35 Phase-resolved PD and ϕ -q-n PD characteristic recorded for one minute tested by the 10 μm tip radius needle -75 mm diameter plane electrode with gap distance of 50 mm.	135
7.36 Average first charge quantity at PDIV level of the needle- plane electrode systems	136
7.37 The first charge behaviors at PDIV level obtained from the 10 μm tip radius needle – 75 mm diameter plane electrode configuration.....	137
7.38 Normal and weibull distribution of the average first charge at PDIV level.....	138
7.39 Breakdown events during PDIV measurement recorded by ICM and the oscilloscope	140
7.40 Mean value PDIV obtained from different needle lengths and PDIV test techniques..	143
7.41 Relationship between charge values of each electrode configuration	143
7.42 Normal and weibull distribution of PDIV value obtained from the needle-plane electrode systems tested according to IEC test method	144
7.43 Normal and weibull distribution of PDIV value obtained from the needle-plane electrode sytems tested according to the combine PDIV test method	145
7.44 Normal and weibull distribution of PDIV value obtained from the needle-sphere electrode systems tested according to IEC test method	145
7.45 Normal and weibull distribution of PDIV value obtained from the needle-sphere electrode sytems tested according to the combine PDIV test method	146
7.46 Normal and weibull distribution of PDIV value obtained from the needle-sphere electrode systems and the needle-plane electrode sytems tested according to IEC test method.....	147

7.47 Normal and weibull distribution of PDIV value obtained from the needle-sphere electrode system and the needle-plane electrode system tested according to the combine PDIV test method.....	147
7.48 Phase- resolved PD characteristics recorded for one minute at the PDIV value tested by the needle-plane electrode system with the needle length of 25 mm and the gap distance of 25 mm	148
7.49 Phase-resolved PD characteristics recorded for one minute at the PDIV value tested by the needle- plane electrode with the needle length of 45 mm and the gap distance of 50 mm.....	148
7.50 Phase-resolved PD characteristics recorded for one minute at the PDIV value tested by the needle- sphere electrode with the needle length of 45 mm and the gap distance of 50 mm.....	149
7.51 Mean value PDIV of the mineral oil with different water contents as function of oil temperatures	152
7.52 Comparison average charge values of the mineral oil with different water contents as function of oil temperatures	153
7.53 Mean value PDIV of the mineral oil with different water contents as function of oil temperatures	153
7.54 Comparison mean value PDIV of the mineral oil with different water contents as function of oil temperatures tested by IEC test method and the combine PDIV test method.....	154
7.55 Normal and weibull distribution of PDIV value obtained from the 10 μ m tip radius needle - 75 mm diameter plane electrode of the mineral oil with water content of 4 ppm at various oil temperatures (IEC test method).....	155
7.56 Normal and weibull distribution of PDIV values obtained from the 10 μ m tip radius needle- 75 mm diameter plane electrode of the mineral oil with various oil temperatures and water contents (IEC test method)	155
7.57 Normal and weibull distribution of PDIV value obtained from the 10 μ m tip radius needle –75 mm diameter plane electrode of the mineral oil with various oil temperatures (the combine PDIV test method).....	156
7.58 Breakdown voltage and mean value PDIV at room temperature with different water contents.....	157
7.59 PD phase-resolved diagram of the mineral oil with water content 4 ppm at different oil temperatures recorded for 1 minute at the PDIV levels obtained from IEC test method	158
7.60 PD phase-resolve diagram of the mineral oil under room temperature with different water contents recorded for 1 minute at the PDIV levels obtained from IEC test method	158

7.61 Relative permittivity of the mineral oil with different water contents and temperatures	159
7.62 Loss factor of the mineral oil with different water contents and temperatures.....	159
7.63 Mean value PDIV of different PDIV test circuits.....	161
7.64 Normal and weibull distribution of PDIV value obtained from different test circuits .	162
7.65 Normal and weibull distribution of PDIV value obtained from different test circuits .	162
7.66 PD phase-resolved diagram recorded for 1 minute at PDIV level of different test circuits	163
7.67 PD pulse train of the mineral oil tested by the needle-plane electrode arrangement, needle tip radius of 20 μm , N11, at PDIV of 37.9 kV in preliminary PDIV experiment	166
7.68 PD pulse currents of the mineral oil tested by the 10 μm tip radius needle-75 mm diameter plane electrode and tested by the 10 μm tip radius needle-12.7 mm diameter sphere electrode, gap spacing of 50 mm at PDIV level	167
7.69 10 PD pulse currents of the mineral oil tested by the 10 μm tip radius needle -75 mm diameter plane electrode system with gap spacing of 50 mm recorded continuously at PDIV level.....	168
7.70 PD pulses recorded from test circuit 2 (R shunt connected with coupling capacitor)...	171
7.71 PD currents of the mineral oil under room temperature with different water contents .	171
7.72 PD currents generated in the mineral oil with water content of 40 ppm with different temperatures	172
7.73 Arcing voltage and current from the arcing experiments.....	175
7.74 Normal and weibull distribution of arcing voltages.....	176
7.75 Normal and weibull distribution of arcing currents	177
7.76 PD pulse current behaviors before arcing taking place tested by the rod-plane electrode arrangement, rod diameter of 1mm with gap distance of 0.3 mm, at 11.5 kV.....	179
7.77 Arcing current patterns and signals tested by the rod- plane electrode arrangement, rod diameter of 1mm with gap distance of 0.3 mm at 11 kV	180
7.78 Bubbles generated by arcing	181
7.79 Carbon filaments and bubbles generated from the arcing test	181
7.80 SE and BSE images of the 10 μm tip radius needle.....	183
7.81 SE images: large scale of the PDIV tested needles.....	183

7.82 BSE images with interested areas and EDX analysis	185
7.83 SEM and EDX analysis for the tested plane electrode	186
7.84 SE images of the original rods	187
7.85 BSE image and SE image comparison of the 1 mm diameter rod before and after arcing test with different current densities	188
7.86 EDX analysis of the interested areas of Fig. 7.85	189
7.87 BSE image comparison of the 2 mm dia rod with the curvature of 0.2 mm before and after arcing test	189
7.88 BSE images of the arcing tested plane electrodes after testing with the 1 mm diameter rod	190
7.89 EDX analysis of the interested areas of Fig. 7.88	191
8.1 PDIV experiment	193
8.2 Low probability breakdown risk for PDIV experiment	194
8.3 High probability breakdown risk for PDIV experiment	194
8.4 PDIV diagram to explain the possibility of breakdown event which can occur when the PDIV experiment is performed according to IEC 61294	195
8.5 PDIV diagram to explain the possibility of breakdown event occurring after PDIV is detected	196
8.6 Combine PDIV test method	197
8.7 Test experiment and phase- resolved diagrams	198
8.8 PDIV and breakdown voltage diagram of the mineral oil tested by needle – plane electrodes with gap spacing of 25 mm	199
8.9 PDIV and breakdown voltage diagram tested by needle – plane electrodes with gap spacing of 50 mm	201
8.10 Expansion of the mineral oil at the tested temperatures	204
8.11 Dynamic behaviors of the mineral oil subjected to various temperatures	205

List of Tables

3.1 Use of insulating liquids.....	7
3.2 Relative cost of insulating liquids.....	7
4.1 Mineral oil composition.....	11
4.2 N- butane and isobutane characteristic comparison.....	12
4.3 Molecular structures of hydrocarbon components.....	14
4.4 Effect of compositions on mineral oil properties.....	15
4.5 Physical characteristics of mineral oils.....	18
4.6 Chemical characteristics of mineral oils.....	18
4.7 Electrical characteristics of mineral oils.....	19
4.8 Physical characteristic testing of mineral oils.....	38
4.9 Chemical characteristic testing of mineral oils.....	39
4.10 Electrical characteristic testing of mineral oils.....	40
4.11 Streamer propagation modes of the mineral oils.....	46
4.12 Electrode configurations of ASTM and IEC standards for oil breakdown testing.....	70
4.13 Short circuit current of power supply and circuit interrupting time of oil testing international standards.....	76
4.14 Softening and melting temperatures for contact materials.....	78
5.1 Electrode systems utilized for PDIV experiment.....	86
5.2 Zoom of the tip profiles of the example needles.....	87
5.3 Electrode systems for arcing experiment.....	95
7.1 Maximum electric field magnitude of the electrode systems for preliminary PDIV test as a function of needle tip radii.....	106
7.2 Maximum electric field magnitude of the electrode systems with different needle tip radii, different electrode shapes and gap distances.....	108

7.3	Maximum electric field magnitude of the electrode systems with different needle lengths	110
7.4	Maximum electric field magnitude of the experimented rod-plane electrode systems ..	112
7.5	Mean value PDIV from 10 time testings of each needle-plane arrangement as a function of needle tip radius with σ_u as standard deviation in kV obtained from the preliminary PDIV experiment A	113
7.6	Mean value PDIV from 10 time testings of each needle – plane arrangement as a function of needle tip radius with σ_u as standard deviation in kV obtained from the preliminary PDIV experiment B	114
7.7	Comparison of the mean value PDIV from preliminary PDIV experiment A and B ...	114
7.8	PDIV raw data obtained from the needle (number 1)-plane electrode configuration....	115
7.9	Average charge quantity from PDIV experiment A and B	118
7.10	Mean value PDIV obtained for different PDIV test methods tested by the needle- plane electrode arrangements with 50 mm gap spacing	123
7.11	Mean value PDIV obtained form up and down experiment.....	125
7.12	Mean value PDIV (kV) and average PD charge quantity (pC) of the mineral oil as function of electrode configurations with the gap distance of 25 and 50 mm.	129
7.13	Average value of the first PD charge at PDIV level	136
7.14	Breakdown cases during performing the PDIV experiments according to IEC test method	139
7.15	Needle configurations before and after breakdown occurring	141
7.16	Mean value PDIV and average charge quantity at PDIV level of the electrode arrangements as a function of needle lengths, gap distances and test methods	143
7.17	Mean value PDIV of the mineral oil with different oil conditions obtained from different test methods.....	151
7.18	Average charge quantity of the mineral oil with different oil conditions obtained from different test methods	151
7.19	Breakdown voltage value of the mineral oil with different water contents.	157
7.20	Mineral oil characteristics with different water contents and temperatures	160
7.21	Mean value PDIV obtained form different PDIV test circuits.....	161
7.22	Breakdown voltage compared with PDIV of the needle- plane electrode configurations	164

7.23 PD pulse characteristics (pulse current amplitude (mA), pulse duration (μs) and rise time (ns)) tested by the needle-plane configuration with gap distances of 25 mm and 50 mm at the PDIV level obtained from IEC and the combine PDIV test methods 169

7.24 PD pulse characteristics (pulse current (mA), pulse duration (μs) and rise time (ns)) tested by the needle-sphere configurations with gap distances of 25 and 50 mm at the PDIV level obtained from IEC and the combine PDIV test methods 170

7.25 PD pulse characteristics of the mineral oil with different oil conditions 173

7.26 Mean value U_{arc} and I_{arc} of the mineral oil tested by the rod-plane arrangements, σ_U as voltage standard deviation and σ_I as current standard deviation 174

8.1 Mean value PDIV, average Q_{IEC} and average Q_{peak} obtained from the IEC and the combine PDIV test method 197

References

- [1] R. Bartnikas, *Engineering Dielectrics, Electrical Insulating Liquids*, Vol. III, 1997: ASTM, pp 25- 322.
- [2] CIGRÉ Working Group A 2.35, CIGRÉ brochure 436, *Experiences in service with new insulating liquids*, October, 2010.
- [3] G.C.Montanari, “Insulation diagnosis of high voltage apparatus by partial discharge investigation”, 8th International Conference on Properties and Applications of Dielectric Materials, 2006, Bali, Indonesia, pp.1-11.
- [4] A. Cavallini, G. C. Montanari, and F. Puletti, “Partial discharge analysis and asset management: experiences on monitoring of power apparatus”, Transmission & Distribution Conference and Exposition, 2006, Latin America, pp.1-6.
- [5] Barry H. Ward, “A survey of new techniques in insulation monitoring of power transformers”, IEEE Electrical Insulation Magazine, 2001, pp.16-23.
- [6] X. Wang and Z. D. Wang, “Insulating liquids-determination of the partial discharge inception voltage(PDIV)-test procedure”, presented in 11th INSUCON International Electrical Insulation Conference, 2009, Birmingham, UK.
- [7] E. Kuffel, W.S. Zaengl and J. Kuffel, *High Voltage Engineering,- fundamentals*, second edition, 2000, Newnes Press, pp. 385-392 and 423-447.
- [8] U.S. Energy Information Administration, *The International Energy Outlook 2011*, 2011, Washington, DC.
- [9] Corporate Headquarters, *2012 The Outlook for Energy: A View to 2040*, 2012.
- [10] R. Baehr, “Transformer technology state-of-the art and trends of future development”, CIGRÉ ELECTRA, No.198, pp.13-19.
- [11] CIGRÉ Working Group 12.18, CIGRÉ brochure 227, *Guidelines for life management techniques for power transformers*, January, 2003.
- [12] CRO Forum, *Risk Management Options: Emerging Risk Initiative*, in *Power Blackout Risks 2011*: Amsterdam, Netherlands.
- [13] I.A. Metwally, “Failures, monitoring and new trends of power transformers”, IEEE Potentials, Vol.30, No.3, 2011, pp. 36-43.
- [14] *IEEE recommended practice for the design of reliable industrial and commercial power systems - redline*, IEEE Std 493-2007 (Revision of IEEE Std 493-1997) - Redline, 2007.

-
- [15] CIGRÉ Task Force D1.01.10, CIGRÉ brochure 323, *Ageing of cellulose in mineral-oil insulated transformers*, October, 2007.
- [16] Weidman System International, *Weidmann Electrical Technology Compendium*, version 1.1e/d.
- [17] D.F.Binns, A.B. Crompton and A. Jaberansari, “Economic design of a 50 kVA distribution transformer, part 1: the use of liquids of low flammability”, IEE Proceedings C: Generation, Transmission and Distribution, Vol.133, No.7, 1986, pp. 445-450.
- [18] A.C.M. Wilson, *Insulating Liquids: their uses, manufacture and properties*, 1980, The Institution of Electrical Engineers, pp. 1-90.
- [19] M.M. Hirschler, *Electrical Insulating Materials: International Issues*, 2000: ASTM International.
- [20] IEC 60422, *Supervision and maintenance guide for mineral insulating oils in electrical equipment*, 1989.
- [21] I. Fofana et al, “Ageing behaviour of mineral oil and ester liquids: a comparative study”, *Electrical Insulation and Dielectric Phenomena*, 2008, CEIDP 2008. Annual Report Conference, 2008, pp.87-90.
- [22] I.L. Hosier et al, “An ageing study of blends of dodecylbenzene and mineral oil”, *IEEE Transactions on Dielectrics and Electrical Insulation*, Vol.16, No 6, 2009, pp. 1664-1675.
- [23] M.A.G. Martins, “Vegetable oils, an alternative to mineral oil for power transformers- experimental study of paper aging in vegetable oil versus mineral oil”, *IEEE Electrical Insulation Magazine*, Vol.26, No.6, 2010, pp. 7-13.
- [24] G.K. Frimpong, T.V. Oommen and R. Asano, “A survey of aging characteristics of cellulose insulation in natural ester and mineral oil”, *IEEE Electrical Insulation Magazine*, Vol.27, No.5, 2011, pp. 36-48.
- [25] H.P. Gasser et al, “Aging of pressboard in different insulating liquids”, *ICDL 2011, IEEE International Conference on Dielectric Liquids*, 2011, pp.1-5.
- [26] S.M. Islam, T. Wu and G. Ledwich, “A novel fuzzy logic approach to transformer fault diagnosis”, *IEEE Transactions on Dielectrics and Electrical Insulation*, Vol. 7, No.2, 2000, pp. 177-186.
- [27] Q. Su, L.L. Lai and P. Austin, “A fuzzy dissolved gas analysis method for the diagnosis of multiple incipient faults in a transformer”, *Advances in Power System Control, Operation and Management*, 2000, APSCOM-00, 2000 International Conference, 2000, Vol.2, pp. 344-348.
- [28] R.J. Liao et al, “Fuzzy information granulated particle swarm optimisation-support vector machine regression for the trend forecasting of dissolved gases in oil-filled transformers”, *IET Electric Power Applications*, Vol. 5, No.2, 2011, pp. 230-237.
-

-
- [29] H. Moulai, A. Nacer and A. Beroual, "Dissolved gases analysis in relation to the energy of electrical discharges in mineral oil", *IEEE Transactions on Dielectrics and Electrical Insulation*, Vol.19, No.2, 2012, pp. 498-504.
- [30] R. Eberhardt et al, "Partial discharge behaviour of an alternative insulating liquid compared to mineral oil", *Power Modulator and High Voltage Conference (IPMHVC), 2010 IEEE International Conference*, 2010, pp. 426-429.
- [31] V. Dang, A. Beroual, and C. Perrier, "Comparative study of statistical breakdown in mineral, synthetic and natural ester oils under AC voltage", *ICDL 2011, IEEE International Conference on Dielectric Liquids*, 2011, pp.1-4.
- [32] J. Dai and Z.D. Wang, "A comparison of the impregnation of cellulose insulation by ester and mineral oil", *IEEE Transactions on Dielectrics and Electrical Insulation*, Vol.15, No.2, 2008, pp. 374-381.
- [33] C. Perrier and A. Beroual, "Experimental investigations on insulating liquids for power transformers: mineral, ester, and silicone oils", *IEEE Electrical Insulation Magazine*, Vol.25, No.6, 2009, pp. 6-13.
- [34] L. Ruijin et al, "A comparative study of physicochemical, dielectric and thermal properties of pressboard insulation impregnated with natural ester and mineral oil", *IEEE Transactions on Dielectrics and Electrical Insulation*, Vol.18, No.5, 2011, pp. 1626-1637.
- [35] O. Lesaint and T.V. Top, "Streamer initiation in mineral oil, part I: electrode surface effect under impulse voltage", *IEEE Transactions on Dielectrics and Electrical Insulation*, Vol. 9, No.1, 2002, pp. 84-91.
- [36] T.V. Top and O. Lesaint, "Streamer initiation in mineral oil, part II: influence of a metallic protrusion on a flat electrode", *IEEE Transactions on Dielectrics and Electrical Insulation*, Vol.9, No.1, 2002, pp. 92-96.
- [37] Torshin Yu, "The universal discharge mechanism in mineral oil and possible estimation of its breakdown voltage", *ICDL 2002, IEEE International Conference on Dielectric Liquids*, 2002, pp. 107-110.
- [38] P.E. Frayssines et al, "Prebreakdown and breakdown phenomena under uniform field in liquid nitrogen and comparison with mineral oil", *IEEE Transactions on Dielectrics and Electrical Insulation*, Vol.10, No.6, 2003, pp. 970-976.
- [39] A.B. Eriksson, R. Liu and C. Tornkvist, "Differences in streamer initiation and propagation in ester fluids and mineral oil", *ICDL 2011, IEEE International Conference on Dielectric Liquids*, 2011, pp.1-4.
- [40] O. Lesaint and T.V. Top, "Streamer inception in mineral oil under ac voltage", *Dielectric Liquids (ICDL), 2011 IEEE International Conference*, 2011, pp.1-5.
- [41] J.G. Hwang et al, "Effects of nanoparticle charging on streamer development in transformer oil-based nanofluids", *Journal of Applied Physics*, Vol.107(1), 2010, pp. 014310-1 - 014310-17.
-

-
- [42] D. Yue-fan et al, "Effect of TiO₂ nanoparticles on the breakdown strength of transformer oil", *Electrical Insulation (ISEI), Conference Record of the 2010 IEEE International Symposium*, 2010, pp.1-3.
- [43] P. Aksamit, D. Zmarzly and T. Boczar, "Electrostatic properties of aged fullerene-doped mineral oil", *IEEE Transactions on Dielectrics and Electrical Insulation*, Vol.18, No.5, 2011, pp.1459-1462.
- [44] L. Yu-zhen et al, "Experimental investigation of breakdown strength of mineral oil-based nanofluids", *ICDL 2011, IEEE International Conference on Dielectric Liquids*, 2011, pp.1-3.
- [45] R. Liu et al, "Fundamental research on the application of nano dielectrics to transformers", *Electrical Insulation and Dielectric Phenomena (CEIDP), 2011 Annual Report Conference*, 2011, pp 423-427.
- [46] Zhou Jian-quan et al, "AC and lightning breakdown strength of transformer oil modified by semiconducting nanoparticles", *Electrical Insulation and Dielectric Phenomena (CEIDP), 2011 Annual Report Conference*, 2011, pp.652-654.
- [47] D. Yue-fan et al, "Effect of semiconductive nanoparticles on insulating performances of transformer oil", *IEEE Transactions on Dielectrics and Electrical Insulation*, Vol.19, No.3, 2012, pp.770-776.
- [48] F. Scatiggio et al, "Corrosive sulfur in insulating oils: its detection and correlated power apparatus failures", *IEEE Transactions on Power Delivery*, Vol.23, No.1, 2008, pp. 508-509.
- [49] R. Maina et al, "Corrosive sulfur effects in transformer oils and remedial procedures", *IEEE Transactions on Dielectrics and Electrical Insulation*, 2009, Vol.16, No.6, pp. 1655-1663.
- [50] S. Okabe et al, "Analysis methods of sulfide and sulfoxide compounds in mineral insulating oil for diagnosis on electrostatic charging of power transformers", *IEEE Transactions on Dielectrics and Electrical Insulation*, Vol.19, No.1, 2012, pp. 181-187.
- [51] R. Shuangzan et al, "Research on streaming electrification of insulation mineral oil", *Properties and Applications of Dielectric Materials, 2009, ICPADM 2009, IEEE 9th International Conference*, 2009, pp. 988-991.
- [52] S. Okabe, M. Kohtoh and T. Amimoto, "Diagnosis on increase in electrostatic charging tendency of mineral insulating oil for power transformers due to aging", *IEEE Transactions on Dielectrics and Electrical Insulation*, Vol.17, No.3, 2010, pp. 953-963.
- [53] S. Okabe, M. Kohtoh and T. Amimoto, "Investigation of electrostatic charging mechanism in aged oil-immersed transformers", *IEEE Transactions on Dielectrics and Electrical Insulation*, Vol.17, No. 1, 2010, pp. 287 -293.
- [54] IEC 60270, *High-voltage test techniques-partial discharge measurements*, 2001.
-

-
- [55] IEC 61294, *Insulating Liquids – determination of the partial discharge inception voltage (PDIV) – test procedure*, 1993.
- [56] Philippe Mallet, “Characterization of dielectric liquid by measurement of the partial discharge inception voltage”, ICDL1990, IEEE International Conference on Dielectric Liquids, 1990, pp.529-534.
- [57] C. Mazzetti, M. Pompili and O. Foster, “A study of partial discharge measurements in dielectric liquids”, IEEE Transactions on Electrical Insulation, Vol.27, No.3, 1992, pp. 445-450.
- [58] M. Pompili et al, “The effect of the definition used in measuring partial discharge inception voltages”, IEEE Transactions on Electrical Insulation, Vol.28, No.6, 1993, pp.1002-1006.
- [59] M. Pompili, C. Mazzetti and R. Bartnikas. “Testing, evaluation and standardisation of transformer oils”, ICDL2005, IEEE International Conference on Dielectric Liquids, 2005, pp.361-364.
- [60] Z.D.Wang et al, “Discussion on possible additions to IEC 60879 and IEC 61294 for insulating liquid tests”, IET Electric Power Applications, Vol.5, No.6, 2011, pp.486-493.
- [61] O. Lesaint and R. Tobazeon, “Streamer generation and propagation in transformer oil under AC divergent field conditions”, IEEE Transactions on Electrical Insulation, Vol.23, No.6, 1988, pp.941-954.
- [62] M. Pompili, “Partial discharge development and detection in dielectric liquids”, IEEE Transactions on Dielectrics and Electrical Insulation, Vol.16, No.6, 2009, pp.1648-1654.
- [63] E. Gockenbach, H. Borsi and B. Dolata, *Research project on the comparison of electric and dielectric properties of natural ester fluid with a synthetic ester and a mineral based transformer oil*, University of Hannover, September-November 2005.
- [64] N. Pattanadech et al, “The influence of the test methods on the partial discharge inception voltage value of the mineral oil using the needle- plane electrode configuration”, Condition Monitoring and Diagnosis (CMD), 2012 International Conference, 2012, pp.597-600.
- [65] BS ISO 1998-1:1998, *Petroleum industry, terminology, raw materials and products*. 1998.
- [66] Andreas K uchler, *Hochspannungstechnik: grundlagen-technologie-anwendungen*, Springer, 1996, pp. 210-233 and 319-322.
- [67] Manfred Beyer et al, *Hochspannungstechnik: theoretische und praktische grundlagen*, Springer- Verlag, 1986, pp.145-162.
- [68] Sami Matar and Lewis F. Hatch, *Chemistry of Petrochemical Process*, Second edition, Gulf Publishing Company, Houston, Texas, 2000, pp 11- 42.
- [69] Nynas, *Base Oil Handbook*, www.nynas.com/naphtenics, pp. 1-46.
-

-
- [70] Ravindra Arora and Wolfgang Mosch, *High Voltage Insulation Engineering :behaviour of dielectrics, their properties and applications*, Wiley Eastern Limited,1995, pp. 198 -234.
- [71] Francis A. Carey, *Organic Chemisty*, fourth edition, McGraw- Hill, 2000, pp. 53-80 and 398-400.
- [72] R. Lewis and W. Evans, *Chemistry*, Third edition, Palgrave Macmillan, 2006, pp. 307-327.
- [73] J. Truong, *McGraw-Hill Ryerson Chemistry 11*, McGraw-Hill, 2011, pp. 544-563.
- [74] J. Truong, *McGraw-Hill Ryerson Chemistry 12*, McGraw-Hill 2011, pp. 12-19.
- [75] William C. Lyons, *Standard Handbook of Petroleum and Natural Gas Engineering*, volume 1, Gulf Publishing Company, Houston, Texas, 1996, pp. 300-321.
- [76] Markus Zahn, *Conduction and Breakdown in Dielectric Liquids* in *Wiley Encyclopedia of Electrical and Electronics Engineering*, Wiley&Son, 1999, pp. 89 - 123.
- [77] Juan Martinez-Vega, *Dielectric Materials for Electrical Engineering*, John Wiley& Sons, 2010, pp. 352-355.
- [78] George E. totten, Steven R. Vestbrook, and Rajesh J. Shah, *Fuels and Lubricants Handbook :Technology, Properties, Performance and Testing*, ASTM Manual series,2003, pp. 575-578.
- [79] Maria Eklund, “Mineral insulating oils: functional requirements, specifications and production”, 2006 IEEE International Symposium on Electrical Insulation, pp.68-72.
- [80] *VDEW-Ölbuch: Band 2 :Isolierflüssigkeiten*, 1996, pp.11 -20.
- [81] Andrzej Sierota and Juris Rungis, “Electrical Insulating oils part I: characterization and pre- treatment of new transformer oils”, IEEE Electrical Insulation Magazine, Vol. 11, No.1, 1995, pp. 8-20.
- [82] M. Khalifa and H. Anis, *Insulating Liquids*, in *High Voltage Engineering: theory and practice*, second edition, revised and expanded, Marcel Dekker, 2000, pp. 207-231.
- [83] Steve Krawiec, “Review of recent change of mineral oil specifications”, 2009 IEEE electrical insulation conference, Montreal,QC, Canada, 31 may-3 June 2009, pp.363-367.
- [84] Nynas,*Transformer Oil Handbook*, www.nynas.com/naphtenics, pp. 1-51.
- [85] S.Bisnath et al, *Theory, Design, Maintenance and Life Management of Power Transformer*, Power series, Johannesburg, South Africa, April 2008, pp. 93-194.
- [86] Paul Gill, *Electrical Power Equipment Maintenance and Testing*, Marcel Dekker, 1998, pp. 135-170.
-

-
- [87] Frank M. Clark, *Insulating Materials for Design and Engineering Practice*, John Wiley & Sons, 1962, pp. 39- 49.
- [88] BS EN 60296: *Fluids for electrotechnical applications-unused mineral insulating oils for transformers and switchgears*, 2012.
- [89.] ASTM D 2864-02: *Standard terminology relating to electrical insulating liquids and gases*, June 2002.
- [90] A. R. Blythe, *Electrical Properties of Polymer*, Cambridge University Press, 1980, pp. 15-45.
- [91] J.C. Anderson, *Dielectrics*, Reinhold Publishing Corporation, 1964, pp. 15-19.
- [92] P.J. Harrop, *Dielectrics*, London Butterworths, 1972, pp. 3-8.
- [93] J.A. Kok, *Electrical Breakdown of Insulating Liquids*, Philips Technical Library, 1961, pp. appendix III.
- [94] K.C. Koa, *Dielectric Phenomena in Solids: with emphasis on physical concepts of electronic process*, Elsevier Academic Press, 2004, pp. 52 -90.
- [95] W.F. Schmidt, *Conduction Mechanisms in Liquids*, in *Electrical Insulating Liquids*, R. Bartnikas; editor, Vol. III, 1997: ASTM, pp. 147 -210.
- [96] T.Takashima et al, "I-V characteristics and liquid motion in needle to plane and razor blade to plane configurations in transformer oil and liquid nitrogen", *IEEE Transactions on Electrical Insulation*, Vol. 23, No.4, 1988, pp. 645-658.
- [97] Ravindra Arora and Wolfgang Mosch, *High Voltage and Electrical Insulation Engineering*, Wiley, 2011, pp. 275-317.
- [98] Maik Koch, *Reliable Moisture Determination in Power Transformers*, Dissertation, Universität Stuttgart, 2008, pp. 17-19.
- [99] CIGRÉ Working Group A2.30, CIGRÉ brochure 349, *Moisture equilibrium and moisture migration within transformer insulation systems*, June 2008.
- [100] I.Fotana, H.Borsi and E. Gockenbach, "Fundamental investigations on some transformer liquids under various outdoor conditions", *IEEE Transactions on Dielectrics and Electrical Insulation*, Vol.8, No.6, December, 2001, pp.1040-1047.
- [101] Y.Du et al, "Moisture solubility for differently conditioned transformer oils", *IEEE Transactions on Dielectrics and Electrical Insulation*, Vol.8, No.5, October, 2001, pp. 805-811.
- [102] S. Jayaram, "Effects of thermal and viscous drag forces on AC breakdown characteristics of transformer oil", CEIDP 1993, Conference on Electrical Insulation and Dielectric Phenomena, 17-20, October 1993, pp. 396-401.

-
- [103] Imad –U- khan, Zhongdong Wang and Ian Cotton, “ Dissolved gas analysis of alternative fluids for power transformers”, IEEE Electrical Insulation Magazine, Vol. 23, No.5, September/October 2007, pp. 5-14.
- [104] F.M. Clark, “Dielectric strength of mineral oils”, Transactions of The American Institute of Electrical Engineers, January 1935, pp. 50 -55.
- [105] Vasily Y. Ushakov et al, *Impulse Breakdown of Liquids*, Spinger -Verlag Berlin Heidelberg, 2007, pp. 263 -314.
- [106] S. Okabe et al, “Influence of diverse compounds on electrostatic charging tendency of mineral insulation oil used for power transformer insulation”, IEEE Transactions on Dielectrics and Electrical Insulation, Vol.16, No.3, June 2009, pp. 900-908.
- [107] S. Krawiec, “Production of corrosive sulphur free transformer fluids”, Electrical Insulation Conference and Electrical Manufacturing Expo 2007, October 2007, Nashville, TN, pp.76-79.
- [108] F. Scatiggio et al, “Corrosive sulfur induced failures in oil-filled electrical power transformers and shunt reactors”, IEEE Transactions on Power Delivery, Vol. 24, No.3, July 2009, pp. 1240-1248.
- [109] CIGRÉ Working Group A2.32, CIGRÉ brochure 378, *Copper sulphide in transformer insulation*, April 2009.
- [110] V. Tumiatti et al, “Corrosive in mineral oils:its detection and correlated transformer failures”, 2006 IEEE International Symposium on Electrical Insulation, 2006, pp. 400-402.
- [111] R. M. De Carlo et al, “Copper contaminated insulating mineral oils- testing and investigations”, IEEE Transactions on Dielectrics and Electrical Insulation, Vol.20, No.2, April 2013, pp. 557-563.
- [112] T. Amimoto et al, “Concentration dependence of corrosive sulfur on copper-sulfide deposition on insulating paper used for power transformer insulation”, IEEE Transactions on Dielectrics and Electrical Insulation, Vol. 16, No. 5, October 2009, pp.1489-1495.
- [113] M. Levin, “Interaction between insulating paper and transformer oil: bacterial content and transport of sulfur and nitrogen compounds”, IEEE Electrical Insulation Magazine, Vol.24, No.4, July/ August 2008, pp. 41-46.
- [114] T.V. Oommen and E. M. Petrie, “Particle contamination levels in oil-filled large power transformers”, IEEE Transactions on Power Apparatus and Systems, Vol. PAS -102, No.5, May 1983, pp. 1459 -1465.
- [115] Michalis G. Danikas, “Particles in transformer oil, technical report”, IEEE Electrical Insulation Magazine, Vol.7, No.2, March/April 1991, pp. 39-40.
- [116] CIGRÉ Working Group 17 of Study Committee 12, *Effect of particles on transformer dielectric strength*, June 2000.
-

-
- [117] M. Krins, H. Borsi, and E. Gockenbach, "Influence of carbon particles on the breakdown and partial discharge inception voltage of aged mineral based transformer oil", 7th International Conference on Dielectric Material Measurements & Applications, 23-26 September 1996, pp. 251 -254.
- [118] X. Wang and Z.D. Wang, "Particle effect on breakdown voltage of mineral and ester based transformer oils", 2008 Annual Report Conference on Electrical Insulation Dielectric Phenomena, pp. 598-602.
- [119] W.G. Chadband, "The electrical breakdown of insulating oil", Power Engineering Journal, March 1992, pp. 61 - 67.
- [120] F. Carraz, P. Rain and R. Tobazeon, "Particles- initiated breakdown in a quasi - uniform field in transformer oil", IEEE Transactions on Dielectrics and Electrical Insulation, Vol.2, No.6, December 1995, pp. 1052-1063.
- [121] L. E. Lundgaard, D. Linhjell and G. Berg, "Streamer/leaders from a metallic particle between parallel plane electrodes in transformer oil", IEEE Transactions on Dielectrics and Electrical Insulation, Vol. 8, No.6, December 2001, pp. 1054- 1063.
- [122] Kamal Miners, "Particles and moisture effect on dielectric strength of transformer oil using VDE electrodes", IEEE Transactions on Power Apparatus and Systems, Vol. PAS -101, No.3, March 1982, pp.751 -756.
- [123] CIGRÉ Working Group D1.33, CIGRÉ brochure 366, *Guide for partial discharge measurements in compliance to IEC 60270*, December 2008.
- [124] D. König and Y. N. Rao, *Partial Discharges in Electrical Power Apparatus*, VDE-Verlag, 1993. pp. 17 -23.
- [125] Rainer Patsch and Farhad Berton, "Pulse sequence analysis -a diagnostic tool based on the physics behind partial discharge", J. Phys. D: Appl. Phys.35, 2002, pp 25-32.
- [126] A. Pedersen, G. C. Crichton and I. W. McAllister, "The theory and measurement of partial discharge transients", IEEE Transactions on Electrical Insulation, Vol. 26, No. 3, June 1991, pp. 487 -497.
- [127] E. Lemke, "A critical review of partial - discharge models", IEEE Transactions on Electrical Insulation, Vol.28, No.6, Nov/Dec 2012, pp. 11-16.
- [128] Rainer Patsch, Johannes Menzel and Djamel Benzerouk, "Partial discharge analysis to monitor the condition of oils", EIC'07, Nashville, Tennessee, USA, 2007, pp. 63-66.
- [129] A. Denat, "High field conduction and prebreakdown phenomena in dielectric liquids", IEEE Transactions on Dielectrics and Electrical Insulation, Vol.13, No.3, June 2006, pp. 518-525.
- [130] T.J. Lewis, "Basic electrical processes in dielectric liquids", IEEE Transactions on Dielectrics and Electrical Insulation, Vol.1, No.4, August 1994, pp. 630 - 643.

-
- [131] R. Kattan, A. Denat and N. Bonifaci, "Formation of vapor bubbles in non-polar liquids initiated by current pulses", IEEE Transactions on Electrical Insulation, Vol. 26, No.4, August 1991, pp.656 -662.
- [132] Alfredo Contin and Stefano Pastore, "Classification and separation of partial discharge signals by means of their auto-correlation function evaluation", IEEE Transactions on Dielectrics and Electrical Insulation, Vol.16, No.6, pp. 1609-1622.
- [133] S.M. Strachen et al, "Knowledge- based diagnosis of partial discharges in power transformers", IEEE Transactions on Dielectrics and Electrical Insulation, Vol.15, No.1, February 2008, pp. 259 - 268.
- [134] H.Borsi and U.Schröder, "Initiation and formation of partial discharges in mineral-based insulating oil", IEEE Transactions on Dielectrics and Electrical Insulation, Vol.1, No.3, June 1994, pp.419-425.
- [135] Yu.V.Torshin, "On the existence of leader discharges in mineral oil", IEEE Transactions on Dielectrics and Electrical Insulation, Vol.2, No.1, February 1995, pp. 167- 179.
- [136] J. George Hwang et al, "Modeling streamers in transformer oil: the transitional fast 3rd mode streamer", 9th International Conference on Properties and Applications of Dielectric Materials, July 19-23,2009, Harbin, China, pp. 573-578.
- [137] A. Beroual et al, "Propagation and structure of streamers in liquid dielectrics", IEEE Electrical Insulation Magazine, Vol.14, No.2, March/April 1998, pp. 6-17.
- [138] P. Biller, "A simple qualitative model for the different types of streamers in dielectric liquids", ICDL1996, IEEE International Conference on Dielectric Liquids ,1996, pp. 189-192.
- [139] W. G. Chadband, "The ubiquitous positive streamer", IEEE Transactions on Electrical Insulation", Vol.23, No.4, August 1988, pp. 697-706.
- [140] D. Linhjell et al, "Streamers in long point-plane gaps in cyclohexane with and without additives under step voltage", ICDL2001, IEEE International Conference on Dielectric Liquids ,2001, pp.1-5.
- [141] P. Rain and O. Lesaint, "A comparison of prebreakdown phenomena in mineral oil under step and ac voltages in divergent fields at large distances", ICDL1993, IEEE International Conference on Dielectric Liquids ,1993, pp. 259-263.
- [142] P.Rain and O. Lesaint, " Prebreakdown phenomena in mineral oil under step and ac voltage in large gap divergent field", IEEE Transactions on Dielectrics and Electrical Insulation, Vol.1, No.4, August 1994, pp. 692-701.
- [143] H. Okubo, N. Hayakawa and A. Matsushita, "The relationship between partial discharge current pulse waveforms and physical mechanisms", IEEE Electrical Insulation Magazine, Vol.18, No.3, May/June, 2002, pp. 38-43.
-

-
- [144] H.Moulai, A. Nacer and A. Beroual, "Correlation between current, emitted light, electric field and propagation velocity of positive streamers in liquid dielectrics under ac voltage", ICDL2011, IEEE International Conference on Dielectric Liquids ,2011, pp.1-4.
- [145] H. Okubo and N. Hayakawa, "A novel technique for partial discharge and breakdown investigation based on current pulse waveform analysis", IEEE Transactions on Dielectrics and Electrical Insulation, Vol. 12, No. 4, August 2005, pp. 736-744.
- [146] H.Borsi and U.Schröder,"Fundamental investigations concerning the behavior of partial discharges (PD) in dielectric liquids", ICDL1990, IEEE International Conference on Dielectric Liquids ,1990, pp. 490-494.
- [147] M. Pompili, C. Mazzetti and R. Bartnikas, "Early stages of negative PD development in dielectric liquids", IEEE Transactions on Dielectrics and Electrical Insulation, Vol. 2, No.4, August 1995, pp. 602-613.
- [148] B. Fallou et al,"Development of criteria for the selection of liquid dielectrics", International Conference on Large High Voltage Electric System, 31st session 1986, CIGRÉ Paris, Vol.1, 15-10, pp. 1-10.
- [149] M. Pompili, "Partial discharge measurement in dielectric liquids", ICDL2008, IEEE International Conference on Dielectric Liquids ,2008, pp.1-7.
- [150] C. Mazzetti et al,"A comparison of streamer and partial discharge inception voltages in liquid dielectrics", Dielectric Materials, Measurements and Application 1992, Sixth International Conference, pp. 93 -95.
- [151] M. Pompili, C. Mazzetti and R. Bartnikas, "Comparative PD pulse burst characteristics of transformer type natural and synthetic ester fluids and mineral oils", IEEE Transactions on Dielectrics and Electrical Insulation, Vol.16, No. 6,December 2009, pp.1511 -1518.
- [152] M. Pompili, C. Mazzetti and R. Bartnikas, "Partial discharge pulse sequence patterns and cavity development times in transformer oils under ac conditions ", IEEE Transactions on Dielectrics and Electrical Insulation, Vol.12, No. 2, April 2005, pp. 395 -403.
- [153] M. Pompili, C. Mazzetti and R. Bartnikas, "Characteristics of the partial discharge pulse burst in transformer and switchgear oils", ICDL2002, IEEE International Conference on Dielectric Liquids ,2002, Graz, Austria, July 7 -12, 2002 , pp.87 -90.
- [154] M. Pompili, C. Mazzetti and R. Bartnikas, "Simultaneous ultrawide and narrowband detection of PD pulses in dielectric liquids", IEEE Transactions on Dielectrics and Electrical Insulation, Vol.5, No.3, June 1998, pp. 402-407.
- [155] M. Pompili, C. Mazzetti and R. Bartnikas, "PD pulse burst characteristics of transformer oils", IEEE Transactions on Power Delivery, Vol. 21, No.2, April 2006, pp. 689 -698.

-
- [156] M. Pompili, C. Mazzetti and R. Bartnikas, "Partial discharge pulse epoch distribution in dielectric liquids and impregnated papers under AC conditions", ICDL1999, IEEE International Conference on Dielectric Liquids ,1999, Nara, Japan, July 20 - 25, 1999, pp. 215 - 218.
- [157] Pompili, C. Mazzetti and E.O. Forster, "Partial discharge distributions in liquid dielectrics", IEEE Transactions on Electrical Insulation, Vol.27, No.1, February 1992, pp. 99-105.
- [158] Carl Ejnar Sölver, *Discharge Pulses in Transformer Oil at Alternating Voltage; Pulse Shape and Partial Discharge Measurements*", Technical report No. 54, School of Electrical Engineering, Chalmers University of Technology, Göteborg, Sweden, January 1975, pp. 67-81.
- [159] Knut Dumke, *Untersuchungen an einer Esterflüssigkeit als Isolierstoff für Transformatoren*, Dissertation, Fachbereich Elektrotechnik und Informationstechnik der Universität Hannover, pp. 16-19.
- [160] Chathan Cooke and Wayne Hagman, "Nondestructive breakdown test for insulating oils", EPRI Substations Diagnostic Conf. III, New Orleans, Nov. 1994.
- [161] M. Pompili and R. Bartnikas, "On partial discharge measurement in dielectric liquids", IEEE Transactions on Dielectrics and Electrical Insulation", Vol.19, No.5, October 2012, pp.1476 -1481.
- [162] R.Coelho and J.Debeau, "Properties of the tip- plane configuration", J.Phys.D: Appl. Phys., 1971, Vol. 4. pp. 1266-1280.
- [163] W. Pfeiffer et al, "About the dimensioning of a needle plane electrode arrangement for comparative investigations of partial discharges in air", Proceedings: Electrical Insulation Conference and Electrical Manufacturing & Coil Winding Conference, Rosemont, Illinois, September 22-25, 1997, pp. 301 -307.
- [164] O. Lesaint, "Streamer in liquids: relation with practical high voltage insulation and testing of liquids", ICDL2008, IEEE International Conference on Dielectric Liquids ,2008, pp. 1-6.
- [165] H. Yamashita, K. Yamazawa and Y. S. Wang, "The effect of tip curvature on the prebreakdown streamer structure in cyclohexane", IEEE Transactions on Dielectrics and Electrical Insulation, Vol. 5, No.3, June 1998, pp. 396- 401.
- [166] T. M. Do, J. L. Auge and O. Lesaint, "A study of parameters influencing streamer inception in silicone oil", IEEE Transactions on Dielectrics and Electrical Insulation, Vol.16, No. 3, June 2009, pp. 893-899.
- [167] O. Lesaint and P.Gournay, "On the gaseous nature of positive filamentary streamers in hydrocarbon liquids I: influence of the hydrostatic pressure on the propagation", J.Phys. D:Appl. Phys.27,1994, pp. 2111-2116.

-
- [168] H. Yamashita et al, "The effect of tip curvature on the prebreakdown density change streamer in cyclo- hexane", ICDL1996, IEEE International Conference on Dielectric Liquids ,1996, Roma, Italy, July 15 -19, 1996, pp. 226 -229.
- [169] P. Rain et al, "Behavior of streamers under divergent ac fields in transformer oils at large gaps", IEEE Transactions on Electrical Insulation, Vol.26, No.4, August 1991, pp. 715 -725.
- [170] R.Kattan, A. Denat and N. Bonifaci, "Formation of vapor bubbles in non-polar liquids initiated by current pulses", IEEE Transactions on Electrical Insulation, Vol. 26, No. 4, August 1991, pp. 656 -662.
- [171] S. Patrissi et al, "A study of the effect of electrical breakdown in dielectric liquids on the needle point structure", ICDL1993, IEEE International Conference on Dielectric Liquids ,1993, Baden-Dättwil, Switzerland, July 19-23, 1993, pp. 376-382.
- [172] E. O. Forster, "Partial discharges and streamers in liquid dielectrics: the significance of the inception voltage", IEEE Transactions on Electrical Insulation, Vol. 28, No. 6, December 1993, pp. 941-946.
- [173] H.Borsi and U. Schröder, "Initiation and formation of partial discharges in mineral-based insulating oil", IEEE Transactions on Dielectrics and Electrical Insulation, Vol.1, No.3, June 1994, pp. 419-425.
- [174] T. Van Top and O. Lesaint, "Effect of electrode geometry and cellulose particles on streamer initiation in oil under divergent AC field", Proceedings of the 5th International Conference on Properties and Applications of Dielectric Materials, May 25-30,1997, Seoul, Korea, pp. 178-181.
- [175] Ruben D. Garzon, *High Voltage Circuit Breakers: design and applications*, second edition, Marcel Dekker Inc, 2002, chapter 5.
- [176] M.S. Naidu and V. Kamaraju, *High Voltage Engineering*, second edition, McGraw-hill, pp. 33-35 and 49-63.
- [177] J Reece Roth, *Industrial Plasma Engineering Volume 1: Principles*, Department of Electrical and Computer Engineering, University of Tennessee, Knoxville, Institute of Physics Publishing, Bristol and Philadelphia, 2000, chapter 10.
- [178] A. H. Sharbaugh, J. C. Devins and S. J. Rzasz, "Progress in the field of electric breakdown in dielectric liquids", IEEE Transaction on Electrical insulation, Vol. EI - 13, No.4, August 1978, pp. 249- 276.
- [179] Dieter Kind and Kurt Feser, *Hochspannungs – Versuchstechnik*, Vieweg, pp.176-177.
- [180] Z. Krasucki, "Breakdown of liquid dielectrics", Proceeding of The Royal Society of London, series A, Mathematical and Physical Sciences, Vol.294, No.1438, Oct 4,1966, pp. 393-404.

-
- [181] C.G.Gaton and Z.Krasucki, "Bubble in insulating liquids: stability in an electric field", Proceeding of The Royal Society of London, series A, Mathematical and Physical Sciences, Vol.280, No.1381,Jul 21, 1964, pp. 211-226.
- [182] H.M.Jones and E.E.Kunhardt, "Development of pulsed dielectric breakdown in liquids", J. Phys. D: Appl. Phys. 28, 1995, pp. 178-188.
- [183] W. R. Wilson, "A fundamental factor controlling the unit dielectric strength of oil", Transactions of The American Institute of Electrical Engineers, Part III: Power Apparatus and System, Vol.72, No. 2, February 1953, pp. 68-74.
- [184] W. F. Schmidt, "Elementary process in the development of the electrical breakdown of liquids", IEEE Transaction on Electrical Insulation, Vol.EI -17, No. 6, December 1982, pp. 478- 483.
- [185] P.K.Watson and J. B. Higham, "Electric breakdown of transformer oil", Proceedings of The IEE- Part IIA: Insulating Materials, Vol.100, No.3, 1953, pp.168- 174.
- [186] T. J. Lewis , "Electric breakdown in organic liquids", Proceedings of the IEE- Part IIA: Insulating Materials, Vol.100, No.3, 1953, pp.141- 148.
- [187] ASTM D877, *Standard test method for dielectric breakdown voltage of insulating liquids using disk electrodes.*
- [188] ASTM D1816, *Standard test method for dielectric breakdown voltage of insulating oils of petroleum origin using VDE electrodes.*
- [189] IEC 60156, *Insulating liquids – determination of the breakdown voltage at power frequency – test method.*
- [190] Teach corner, <http://sdmyers.com/techcorner/index.html>
- [191] W. Lick, G.J. Pukel and H. M. Muhr, "New test method for dielectric breakdown voltage of insulating oils", Electrical Insulating Materials,2005 (ISEIM 2005), Proceedings of 2005 International Symposium,Vol.3, pp. 853 -856.
- [192] C.Vincent, C. Benoit and R. Oliver, "Comparative evaluation of parameters of the dielectric breakdown test on transformer oil", ICDL1996, IEEE International Conference on Dielectric Liquids ,1996, Roma, Italy, July 15 -19, 1996, pp. 337- 341.
- [193] M. Khalifa and M. Abdel- Salam, *Arc Discharge in High Voltage Engineering: theory and practice*, second edition, revised and expanded, Marcel Dekker, 2000, pp. 185-204.
- [194] Kazou Bekki, Taro Yamamoto and Koichiro Sawa, "Breaking arc in dielectric liquids", Electrical Contacts 1990, Proceedings on The Forty -Second IEEE Holm Conference Joint with The 18th International Conference on Electrical Contacts 1996, pp. 252-261.
- [195] Gordon W. Mills, "The mechanisms of the showering arc", IEEE Transaction on Parts, Materials and Packaging, Vol. PMP-5, No.1, March 1969, pp. 47-55.
-

-
- [196] J.H. Tortai, N. Bonifaci and A. Denat, "Insulation properties of some liquids after an electric arc", IEEE Transaction on Dielectrics and Electrical Insulation, Vol. 9, No.1, February 2002, pp. 2-9.
- [197] G. St-Jean et al, "Comparative performance of paraffinic and naphthenic insulating oils under arc-quenching conditions", IEEE Transaction on Power Apparatus and System, Vol. PAS-99, No.6, Nov/Dec 1980, pp. 2439-2447.
- [198] R. Musil, M. Baur and W. Pfister, "Testing practices for the AC breakdown voltage testing of insulation liquids", IEEE Electrical Insulation Magazine, Vol. 11, No. 1. Jan/Feb 1995, pp.21-26.
- [199] G. Fodor and M. Baur, "Progress of AC breakdown voltage test devices of insulating liquids", ICDL2002, IEEE International Conference on Dielectric Liquids, 2002, Graz, Austria, July 7- 12, 2002, pp. 333-336.
- [200] Thomas Schoenemann, "Comparing investigations of the erosion phenomena on selected electrode materials in air and sulfurhexafluoride", Electrical Contacts 1990, Proceedings on The Forty -Second IEEE Holm Conference Joint with The 18th International Conference on Electrical Contacts 1996, pp. 115-120.
- [201] Kejian Wang and Qiping Wang, "Erosion of silver-base material contacts by breaking arcs", IEEE Transaction on Components, Hybrids, and Manufacturing Technology, Vol.14, No.2, June 1991, pp. 293-297.
- [202] John J. Shea, "High current AC break arc contact erosion", Electrical Contacts 2008, Proceedings on the 54th IEEE Holm Conference, pp. xxii -xlvi.
- [203] X. Zhou and J. Heberlien, "An experimental investigation of factors affecting arc-cathode erosion", J. Phys. D: Appl. Phys. 31,1998, pp.2577 -2590.
- [204] W.R. Wilson, "High-current arc erosion of electric contact materials", Transactions of The American Institute of Electrical Engineers, Part III: Power Apparatus and System, Vol.74, No.3, August 1955, pp. 657-664.
- [205] Joseph I. Goldstein et al, *Scanning Electron Microscopy and X Ray Microanalysis*, Third edition, Kluwer Academic/Plenum Publishers,2003, pp. 1-17 and 271-323.
- [206] Instrumentation, <http://www4.nau.edu/microanalysis/Microprobe-SEM/Instrumentation.html>
- [207] Bob Hafner, "Scanning electron microscopy primer", http://www.charfac.umn.edu/instruments/sem_primer.pdf
- [208] Åsa Kassman Rudolphi, "Scanning electron microscopy (SEM) and scanning probe microscopy (SPM)", http://www.cb.uu.se/~ewert/SEM_SPM_bildanalys.pdf
- [209] Introduction to electron microscopy, accessible at caur.uga.edu/ppt/EMintro.pptx
- [210] Scanning electron microscopy (SEM) imaging modes, Cobham Technical Services, reliability and failure analysis, www.cobham.com/technicalservices
-

-
- [211] Scanning electron microscope, accessible at caur.uga.edu/ppt/SEM_Fan.ppt
- [212] Energy-dispersive X-ray spectroscopy, http://en.wikipedia.org/wiki/Energy-dispersive_X-ray_spectroscopy
- [213] Bob Hafner, "Energy dispersive spectroscopy on the SEM: a primer", http://www.charfac.umn.edu/instruments/eds_on_sem_primer.pdf
- [214] Electron microscopy, http://www.microscopy.ethz.ch/xray_spectrum.htm
- [215] BS EN 61649: *Weibull analysis*, 2008.
- [216] W. Rungseevijitprapa, *Influence of Dry Ageing on The Breakdown Behavior of XLPE Insulated High Voltage Cables*, Dissertation, University of Hannover, 2001, pp.31-32.
- [217] IEEE Std 930™-2004, *IEEE Guide for The Statistical Analysis of Electrical Insulation Breakdown Data*, 2004.
- [218] Warwick Manufacturing Group, "Weibull analysis", Section 8, University of Warwick.
- [219] Minitab User's Guide 2, distribution analysis, <http://www.math.ntnu.no/~bo/TMA4275/Download/15.Distribution.Analysis.pdf>
- [220] Lou Johnson, "Modeling non-normal data using statistical software", R&D magazine, August 2007, www.rdmag.com, pp. 26-27.
- [221] Anthony J. Hayter, *Probability and Statistics for Engineers and Scientists*, third edition, Thomson Brooks/Cole, 2003, pp. 343-347.
- [222] William Mendenhall, Robert J. Beaver and Barbara M. Beaver, *Introduction to Probability and Statistics*, eleventh edition, Thomson Brooks/Cole, 2003, pp.327-329.
- [223] Computer Systems/Software, "Identifying the distribution of data is key to analysis", www.engineerlive.com
- [224] L.A. Dissado, "Theoretical basis for the statistics of dielectric breakdown", *J. Phys. D: Appl. Phys.* 23, 1990, pp.1582-1591.
- [225] L.A. Dissado et al, "Weibull statistics in dielectric breakdown; theoretical basis, application and implications", *IEEE Transactions on Electrical Insulation*, Vol. EI-19, No.3, June 1984, pp. 227-233.
- [226] C. Chauvet and C. Laurent, "Weibull statistics in short-term dielectric breakdown of thin polyethylene films", *IEEE Transactions on Electrical Insulation*, Vol.28, No.1, February 1993, pp. 18-29.
- [227] D. Martin and Z. D. Wang, "Statistical analysis of the AC breakdown voltages of ester based transformer oils", *IEEE Transactions on Dielectrics and Electrical Insulation*, Vol.15, No.4, August 2008, pp.1044-1050.

-
- [228] A. Contin, M. Cacciari and G.C. Montanari, "Estimation of weibull distribution parameters for partial discharge inference", *Electrical Insulation and Dielectric Phenomena*, 1994, CEIDP 1994, pp.71-78.
- [229] M. Cacciari, A. Contin and G.C. Montanari, "Use of a mixed – weibull distribution for the identification of PD phenomena", *IEEE Transactions on Dielectrics and Electrical Insulation*, Vol. 2, No.6, December 1995, pp. 1166-1179.
- [230] R. Schifani and R. Candela, "A new algorithm for mixed weibull analysis of partial discharge amplitude distribution", *IEEE Transactions on Dielectrics and Electrical Insulation*, Vol.6, No.2, April 1999, pp. 242-249.

Appendices

A: List of publications

- [1] N. Pattanadech et al, “Partial discharge characteristics in oil of different electrode systems”, ISH 2011, 17th International Symposium on High Voltage Engineering, August 22-26, 2011, Hannover, Germany.
- [2] N. Pattanadech et al, “The study of partial discharge characteristics of mineral oil using needle-plane electrode configuration”, ICHVE 2012: The 2012 International Conference on High Voltage Engineering and Application, Sept. 17-20, 2012, China.
- [3] N. Pattanadech et al, “The study of partial discharge characteristics of mineral oil using needle-plane electrode configuration base on partial discharge pulse current measurement”, ICHVE 2012: The 2012 International Conference on High Voltage Engineering and Application, Sept. 17 - 20, 2012, China.
- [4] N. Pattanadech et al, “SEM and EDX analysis of the needle-plane and the rod-plane electrodes for the partial discharge inception voltage measurement and the arcing test of the mineral oil”, CMD 2012: 2012 IEEE International Conference on Condition Monitoring, Sept. 23-27, 2012, Bali, Indonesia, pp. 353-356.
- [5] N. Pattanadech et al, “The influence of the test methods on the partial discharge inception voltage value of the mineral oil using the needle-plane electrode configuration”, CMD 2012: 2012 IEEE International Conference on Condition Monitoring, Sept. 23-27, 2012, Bali, Indonesia, pp. 597-600.
- [6] N. Pattanadech et al, “The study of the arcing phenomena of the mineral oil using the rod-plane electrode configuration”, CMD 2012: 2012 IEEE International Conference on Condition Monitoring, Sept. 23-27, 2012, Bali, Indonesia, pp. 1059-1062.
- [7] N. Pattanadech et al, “The partial discharge characteristics of mineral oil using needle-plane and needle-sphere electrode configuration base on pulse current measurement”, CEIDP 2012: Electrical Insulation and Dielectric Phenomena(CEIDP 2012), Oct. 14-17, 2012, Montreal, Quebec, Canada, pp. 64-67.
- [8] N. Pattanadech et al, “SEM and EDX analysis of the electrode system for the partial discharge inception voltage measurement and arcing test of the mineral oil”, International Journal on Electrical Engineering and Informatics, Volume 4, Number 4, December, 2012, pp. 633-645.
- [9] N. Pattanadech et al, “Effect of mineral oil condition on partial discharge inception voltage characteristics”, ISH 2013, 18th International Symposium on High Voltage Engineering, August 25-30, 2013, Seoul, Korea.

-
- [10] N. Pattanadech et al, "Partial discharge inception voltage characteristics of mineral oil of different electrode arrangement", ISH 2013, 18th International Symposium on High Voltage Engineering, August 25-30, 2013, Seoul, Korea.
- [11] N. Pattanadech et al, "The possibility of using a needle-plane electrode for partial discharge inception voltage measurement", CEIDP 2013: Electrical Insulation and Dielectric Phenomena (CEIDP 2013), Oct. 20-23, 2013, Shenzhen, China.

B: Investigated material

Material data sheet: Nynas Nytro 4000x

PRODUCT DATA SHEET
Nytro 4000X

PROPERTY	UNIT	TEST METHOD	SPECIFICATION LIMITS		TYPICAL DATA
			MIN	MAX	
1 - Function					
Viscosity, 40°C	mm ² /s	ISO 3104		12.0	9.1
Viscosity, -30°C	mm ² /s	ISO 3104		1800	850
Pour point	°C	ISO 3016		-40	-57
Water content	mg/kg	IEC 60814		30	<20
Breakdown voltage					
- Before treatment	kV	IEC 60156	30		40-60
- After treatment	kV	IEC 60296	70		>70
Density, 20°C	kg/dm ³	ISO 12185		0.895	0.868
DDF at 90°C		IEC 60247		0.005	<0.001
2 - Refining/stability					
Appearance		IEC 60296	Clear, free from sediment		complies
Acidity	mg KOH/g	IEC 62021		0.01	<0.01
Interfacial tension	mN/m	EN 14210	40		49
Total sulphur content	%	ISO 14596		0.05	<0.01
Corrosive sulphur		DIN 51353	non-corrosive		non-corrosive
Potentially corrosive sulphur		IEC 62535	non-corrosive		non-corrosive
Corrosive sulphur		ASTM D 1275 B	non-corrosive		non-corrosive
DBDS	mg/kg	IEC 62697-1		not detectable	not detectable
Antioxidant	wt %	IEC 60666	0.34	0.40	0.38
Metal passivator additives	mg/kg	IEC 60666		not detectable	not detectable
2-Furfural and related compounds content	mg/kg	IEC 61198		0.05	<0.05
Aromatic content	%	IEC 60590			4
3 - Performance					
Oxidation stability at 120°C, 500 h		IEC 61125 C			
Total acidity	mg KOH/g			0.30	<0.01
Sludge	wt %			0.05	<0.01
DDF at 90°C				0.050	<0.010
4 - Health, safety and environment (HSE)					
Flash point, PM	°C	ISO 2719	135		146
PCA	wt %	IP 346		3	<3
PCB		IEC 61619	not detectable		not detectable

Nytro 4000X is an inhibited insulating oil with extremely good electrical and excellent ageing properties meeting IEC 60296 Ed. 4 (2012), special applications.

Severely Hydrotreated Insulating Oil
Issuing date: 2013-05-24

This data sheet is available at
https://nyport.nynas.com/Apps/1112.nsf/wnpds/Nytro_4000X_IEC/SFile/PDS_Nytro_4000X_EN.pdf

C: High water content mineral oil preparation

Equipment and material need for preparation the high water content mineral oil

1. 4 tin cans and 2 glass boxes
2. 1 liter distilled water and 17 liter low water content mineral oil
3. A temperature controlled heater and a heating blanket 110 volt
4. A stainless steel hose
5. A voltage controlled ac source 0 -220 volt, 10 ampere

High water content mineral oil preparation procedure

1. Pour 1 liter of distilled water in the tin can #1.
2. Prepare 17 liters of the mineral oil from the oil retreat machine. Normally, the mineral oil from the oil retreat machine contains water content about 3-4 ppm.
3. Divide the mineral oil into two parts; the first part about 9 liters is poured into the test vessel, the second part was divided into two tin cans, tin can #3 and tin can #4, 4 liters of the mineral oil for each tin can, which are used to prepare for high water content mineral oil.
4. Connect the tin can #1 with the empty tin can #2 via the stainless steel hose.
5. Boil the distilled water in the tin can #1 at 150°C for about 10 minutes until the water is changed to be the steam which can be observed from the vapour going out from the small hole of the empty tin can #2.
6. Replace the tin can #2 with the tin can #3.
7. Heat the mineral oil in the tin can #3 with temperature about 40°C - 60°C.
8. Let the steam from the tin can #1 go into the mineral oil tin can #3 for 10 minutes, steam vapour goes to mix with the mineral oil.
9. Let the mineral oil with vapour in the tin can #3 naturally cool down for about 1 hour.
10. Measure the water content of the mix steam-mineral oil, high water content mineral oil, which is between 40 ± 2 ppm.
11. Let the high water content mineral oil in the tin can #3 naturally cools down for further 15 hours.
12. Transfer the high water content mineral oil about 3.5 liters from the tin can #3 to the glass box via a plastic pipe to avoid the free water droplets which have condensed in the high water content mineral oil and normally stay at the bottom of the tin can go into the glass box. High water content mineral oil can be kept for 2-3 days for PDIV testing.
13. Do the same procedures from 4 -12 with the mineral oil in the tin can #4.
14. Pour the high water content mineral oil into the low water content mineral oil in the test vessel. Now the total mineral oil in the test vessel is about 16 liters.
15. Heat the test vessel by using the heating blanket at the oil temperature about 50 degree for 1 hour.
16. Let the mix mineral oil naturally cool down.

17. Check the final water content of the mineral oil in the test vessel which should be about 18 -22 ppm.
18. Mineral oil which has the water content about 20 ± 2 ppm is ready to test.
19. For 40 ppm water content of the mineral oil preparation, the distilled water is boiled. Then, the steam is mixed with the low water content mineral oil in the tin can #3 about 30 minutes. The water content in the mineral oil after it is naturally cooled down is about 100-120 ppm. The high water content mineral oil is prepared about 6 liters to mix with the 10 liter low water content mineral oil to get the 16 liter mineral oil with water content about 40 ± 2 ppm.

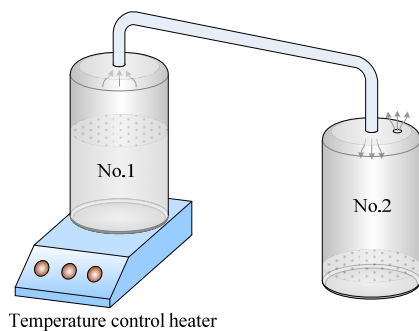


Figure C.1: Steam transferring from the boiling distilled water can go into the empty can

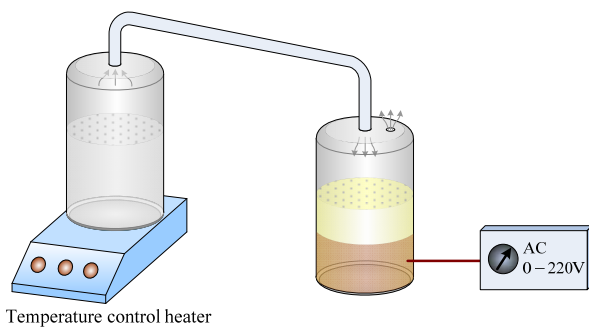


Figure C.2: Steam transferring from the boiling distilled water can go into the mineral oil can, while the mineral oil can is heated by the heating blanket about $40^{\circ}\text{C} - 60^{\circ}\text{C}$

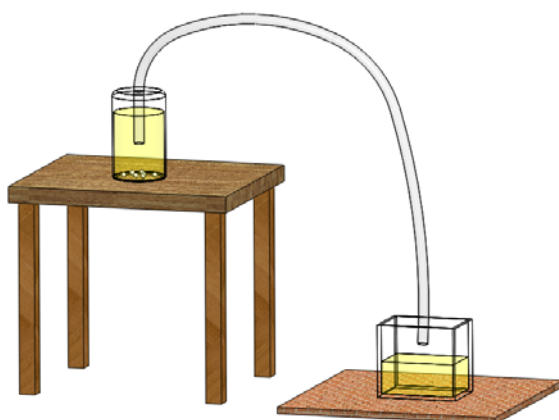


Figure C.3: Transferring the room temperature high water content mineral oil from the tin can to keep in the glass box before pouring into the test vessel for PDIV experiment

D: Temperature control of the mineral oil

Equipment and material need for controlling the temperature of the mineral oil

1. A heating blanket and a bottom heater
2. A voltage controlled ac source 0-220 volt for the heating blanket and a voltage controlled ac source 0-220 volt for the bottom heater
3. A temperature sensor and a temperature display
4. A thermometer and an infrared thermometer gun

Temperature control procedure

1. The heating blanket is equipped cover the glass wall of the test vessel and the bottom heater is firmly attached with the bottom of the test vessel. Besides, the temperature sensor is also installed at the bottom inside the test vessel. The temperature of the mineral oil is displayed by the temperature display.
2. The aim of using the heating blanket is to reduce time consumption to heat up the mineral oil at room temperature to the specified temperature. The heating blanket is also used to maintain the temperature of 90 ± 2 °C of the mineral oil.
3. To control the oil temperature at 40°C, 60°C, and 90°C, the heating blanket and the bottom heater are operated with different applied voltage sources.
4. To control the mineral oil temperature at 40°C, the heating blanket is operated

with

- the applied voltage about 80-85 volts and the bottom heater is operated with the applied voltage 220 volts at the room temperature. When the mineral oil temperature is about 40°C, the heating blanket is turned off. Only the bottom heater is operated with the applied voltage about 120 volts-140 volts to maintain the oil temperature at 40 ± 2 °C.
5. To control the mineral oil temperature at 60 °C, the heating blanket is operated with the apply voltage about 80-85 volts and the bottom heater is operated with the apply voltage 220 volts at the room temperature. When the mineral oil temperature is about 60 °C, the heating blanket is turned off. Only the bottom heater is operated with the applied voltage 220 volts to maintain the oil temperature at 60 ± 2 °C.
 6. To control the mineral oil temperature at 90°C, the heating blanket is operated with the apply voltage about 80-85 volt and the bottom heater is operated with the apply voltage 220 volts at the room temperature until the mineral oil temperature is up to 90 °C. The heating blanket is still operated with the applied voltage about 60-80 volt and the bottom heater is also operated with the applied voltage 220 volts to maintain the oil temperature at 90 ± 2 °C.



Figure D.1: Heating blanket and bottom heater



Figure D.2: Voltage controlled ac sources



Figure D.3: Temperature display

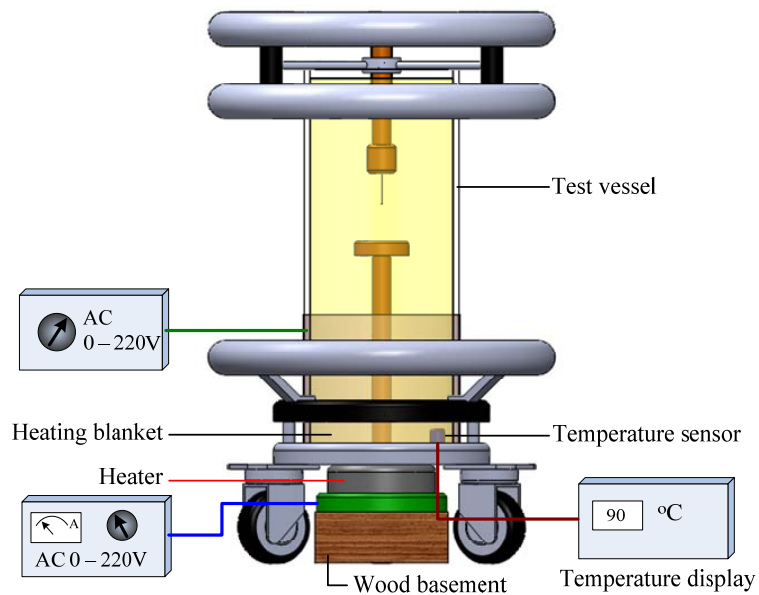


Figure D.4: Test vessel equipped with the heating blanket and the bottom heater including the temperature sensor and the temperature display

E: Summarized lists of equipment

E.1: Test vessel

Test cell for PDIV and PD experiment used in this research

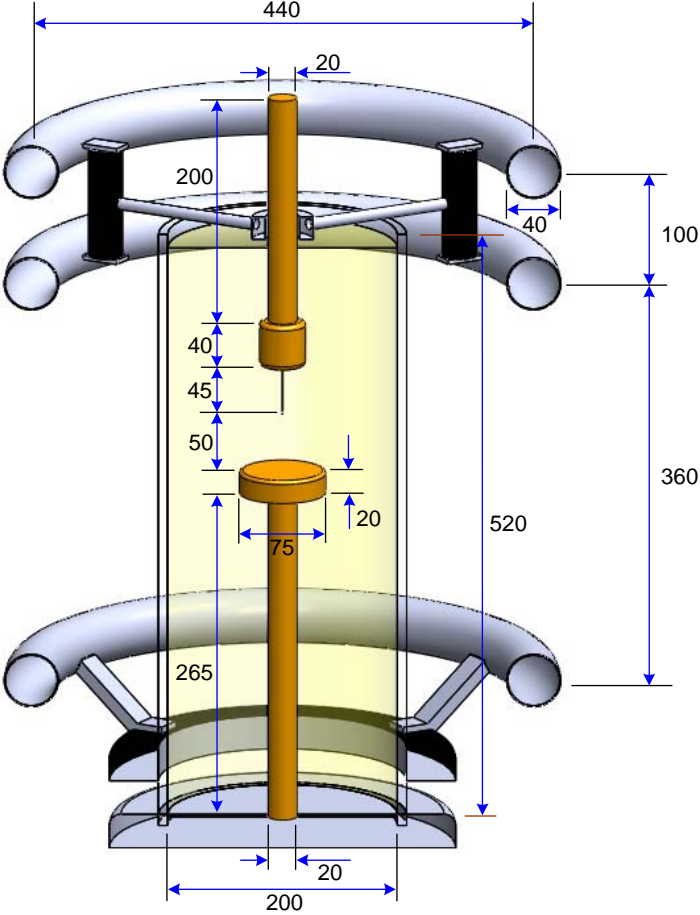


Figure E.1: Test cell drawing diagram

E.2: Needle-plane and needle-sphere electrodes

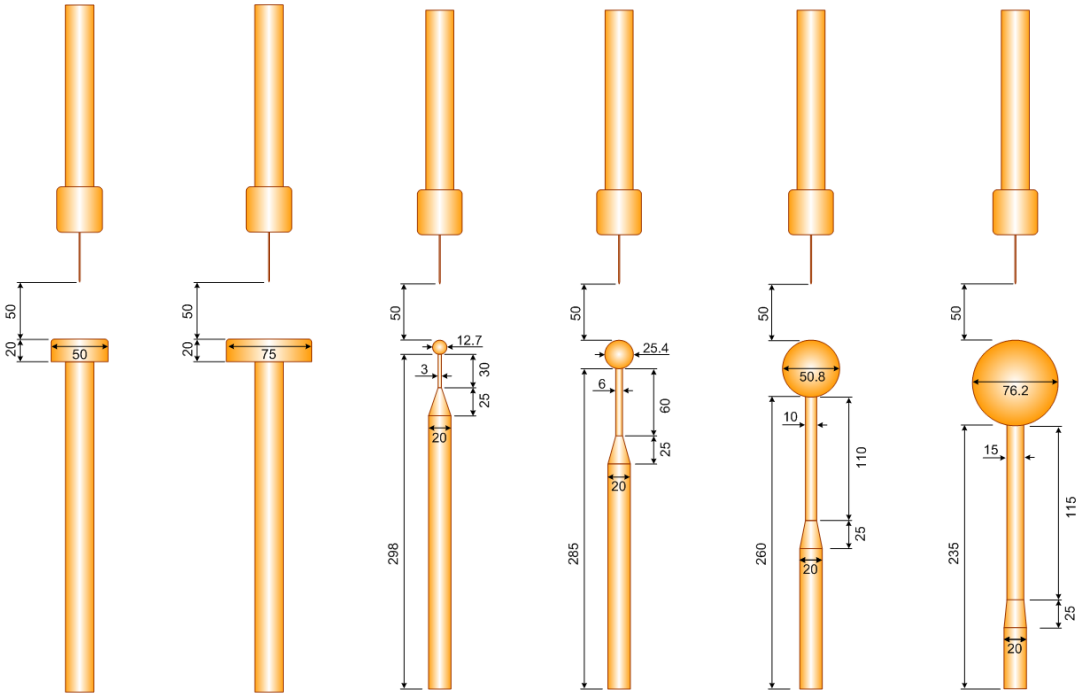


Figure E.2: Needle-plane and needle-sphere electrode diagram

E.3: Shunt resistor

1. 50 ohm shunt resistor: 50 ohm shunt resistor comprises of 4 pieces in parallel of 200 ohm non inductive caddock resistors

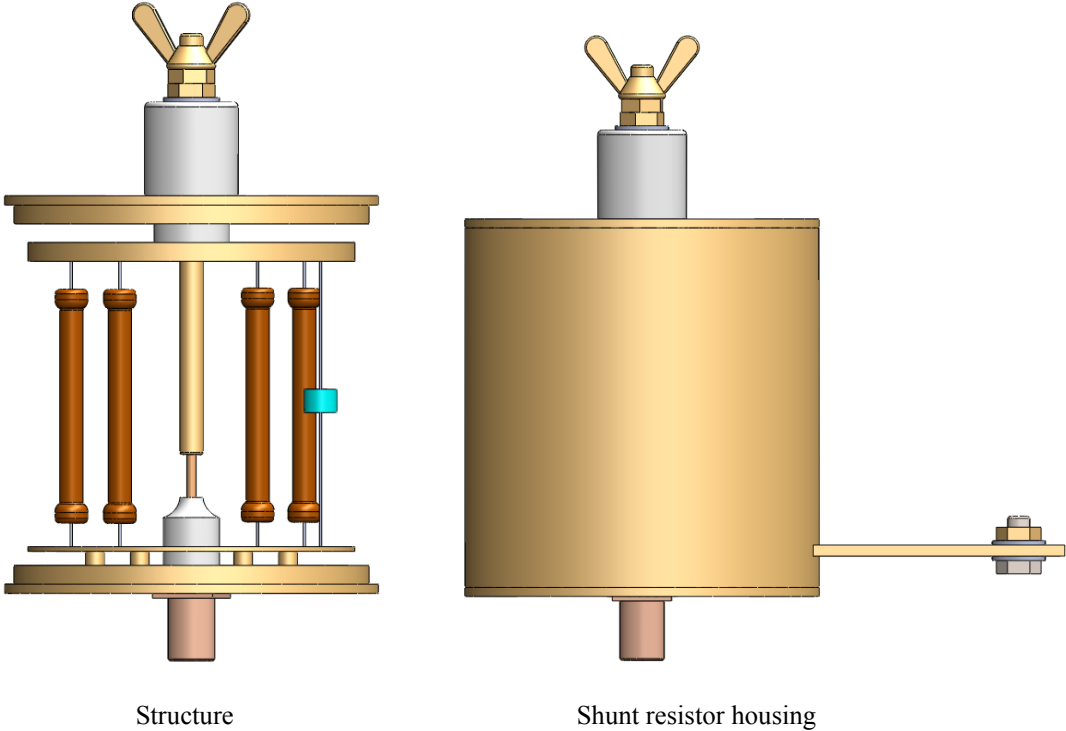


Figure E.3.1: 50 ohm shunt resistor for PD current detection

2. Matching impedance

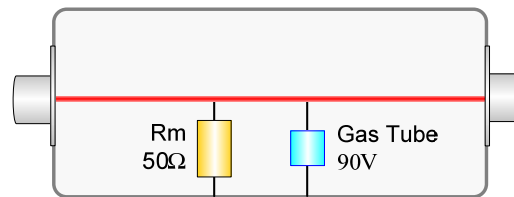


Figure E.3.2: Matching impedance

E.4: Apparatus

High Voltage test transformer

Type: Single phase transformer
Voltage input rating: 0 – 220/440 Volt
Voltage output rating: 0 – 50/100 kV
Impedance: 4%
Power Capacity: 5 kVA
Frequency: 50 Hz

High Voltage test transformer for arcing experiment

Type: Single phase transformer
Voltage input rating: 0 – 220V
Voltage output rating: 0 – 8 kV/16 kV/ 32 kV

Limiting resistor

Resistance: 50 k Ω
Max. power dissipation: 60 Watt

Capacitive voltage divider

Ratio: 2,000 : 1
Total capacitance (C_n): 100 pF
Voltage rating: 200 kV
Capacitance (C_2): 200 nF
Frequency: 50 Hz,
BIL: 500 kV

Coupling Capacitor

Capacitance: 100 pF
Voltage rating: 100 kV

Coupling device

Impedance 10k Ω /5 pF
Voltage limit: 90 V

PD Monitoring Instrument

Brand: Power Diagnostix – ICM
Bandwidth: 40 – 800 kHz

Oscilloscope

Brand: Yokogawa

Type: DLM2054

Bandwidth: 2.5 GS/s, 500 MHz

Input channel: 4 Channels

Digital multimeter

Brand: DM9C

Maximum current 10 A

Maximum voltage 600 V

Curriculum vitae

Norasage Pattanadech

received B.Eng and M.Eng degree in electrical engineering from King mongkut's institute of technology ladkrabang (KMITL) in 1998 and Chulalongkorn university in 2002 respectively. He joined Mahanakom university of technology in 2002-2004 before working at King mongkut institute of technology ladkrabang, Bangkok, Thailand until now. In 2007, he has been promoted as an assistant professor at electrical engineering department, king mongkut institute of technology ladkrabang. Since February 2010, he has started for Ph.D. study in the Institute of High Voltage Engineering and System Management, Graz University of Technology, Austria. His research activities have been mainly involved partial discharge in insulating liquids, solid insulator characteristics, high voltage testing and equipment.